

**Establishing the fast-growing bacterium
Vibrio natriegens as a next-generation chassis for
synthetic biology**

Kumulative Dissertation

zur Erlangung des Grades eines

Doktor der Naturwissenschaften

(Dr. rer.nat.)

des Fachbereichs Biologie der Philipps-Universität Marburg

Vorgelegt von

Daniel Stukenberg

Aus Bad Pyrmont

Marburg an der Lahn, 2024

Originaldokument gespeichert auf dem Publikationsserver der
Philipps-Universität Marburg
<http://archiv.ub.uni-marburg.de>



Dieses Werk bzw. Inhalt steht unter einer
Creative Commons
Namensnennung
4.0 Deutschland Lizenz.

Die vollständige Lizenz finden Sie unter:
<https://creativecommons.org/licenses/by/4.0/legalcode.de>

Die vorliegende Dissertation wurde von Dezember 2019 bis Dezember 2023 am LOEWE-Zentrum für Synthetische Mikrobiologie (SYNMIKRO) in Marburg unter der Leitung von Frau Prof. Dr. Anke Becker durchgeführt.

Vom Fachbereich Biologie der Philipps-Universität Marburg
(Hochschulkennziffer 1180) als Dissertation angenommen: 18.03.2024

Erstgutachter(in): Prof. Dr. Anke Becker

Zweitgutachter(in): Prof. Dr. Victor Sourjik

Tag der Disputation: 22.03.2024

Die in dieser Arbeit vorgestellten Ergebnisse sind im Rahmen folgender Artikel in Fachzeitschriften veröffentlicht oder zur Publikation eingereicht worden:

Daniel Stukenberg, Josef Hoff, Anna Faber, Anke Becker. **NT-CRISPR, combining natural transformation and CRISPR-Cas9 counterselection for markerless and scarless genome editing in *Vibrio natriegens***. *Communications Biology*, 5(1), 265 (2022)

Lea Ramming*, Daniel Stukenberg*, María del Carmen Sánchez Olmos, Anke Becker, Daniel Schindler. **DNA replication is not a limiting factor for rapid growth of *Vibrio natriegens***. *bioRxiv*, doi: <https://doi.org/10.1101/2023.05.26.541695>. (2023), *in revision at Communications Biology*

(* = shared first authorship)

Daniel Stukenberg, Anna Faber, Anke Becker. **graded-CRISPRi, a novel tool for tuning the strengths of CRISPRi-mediated knockdowns in *Vibrio natriegens* using gRNA libraries**. *bioRxiv*, doi: <https://doi.org/10.1101/2024.01.29.577714> (2024), *submitted to ACS Synthetic Biology*

Des Weiteren wurde ein zentraler Aspekt des Forschungsgebiets in folgendem, ebenfalls in einer Fachzeitschrift veröffentlichten Übersichtsartikel behandelt. Die Arbeit an diesem Artikel begann bereits vor Beginn des Promotionsprojektes unter Leitung von Dr. Georg Fritz und wurde im Verlauf dieser Promotion abgeschlossen.:

Josef Hoff*, Benjamin Daniel*, Daniel Stukenberg*, B W. Thuronyi, Torsten Waldminghaus, Georg Fritz. ***Vibrio natriegens*: an ultrafast-growing marine bacterium as emerging synthetic biology chassis**. *Environmental Microbiology*, 22(10), p. 4394-4408 (2020)

(* = shared first authorship)

Table of Contents

Table of Contents	4
Zusammenfassung	5
Summary	7
Abbreviations.....	9
1. Introduction.....	10
1.1. Synthetic biology and the concept of chassis organisms	10
1.2. <i>V. natriegens</i> , a fast-growing marine organism	11
1.3. DNA replication in <i>Vibrionaceae</i>	13
1.4. Natural transformation.....	16
1.5. CRISPR-Cas.....	19
2. Aims of this work: Establishing <i>V. natriegens</i> as a next-generation SynBio chassis	23
3. Results	24
3.1. NT-CRISPR, combining natural transformation and CRISPR-Cas9 counterselection for markerless and scarless genome editing in <i>Vibrio natriegens</i>	24
3.2. DNA replication is not a limiting factor for rapid growth of <i>Vibrio natriegens</i>	63
3.3. graded-CRISPRi, a novel tool for tuning the strengths of CRISPRi-mediated knockdowns in <i>Vibrio natriegens</i> using gRNA libraries	89
4. Discussion	137
4.1. Does <i>V. natriegens</i> have the right properties for a new SynBio chassis?	137
4.2. Do we already have the tools for ambitious SynBio projects with <i>V. natriegens</i> ?	138
4.3. Advantages and limitations of NT-CRISPR compared to other genome engineering methods for <i>V. natriegens</i>	140
4.4. Future directions for improvement of NT-CRISPR	141
4.5. Developing a CRISPRi-based tool leading to different knockdown strengths	143
4.6. Metabolic burden in experiments with CRISPRi.....	147
4.7. Potential mechanistic causes for the high susceptibility of <i>V. natriegens</i> towards metabolic burden	148
4.8. Possible strategies to solve the metabolic burden susceptibility.....	150
4.9. synSC1.0 as a platform strain for future projects	151
4.10. Which tools are still missing to fully establish <i>V. natriegens</i> as a next-generation SynBio chassis?.....	153
5. Conclusion	155
6. References	157
Erklärung	168
Danksagung	169
Curriculum vitae	170

Zusammenfassung

Vibrio natriegens ist der bislang am schnellsten wachsende bekannte Organismus mit einer Verdopplungszeit von unter zehn Minuten unter optimalen Bedingungen. Wegen dieser interessanten Eigenschaft und wegen der Fähigkeit eine große Spanne von Kohlenstoffquellen zu nutzen, wurde *V. natriegens* als neuer Chassis Organismus für die Synthetische Biologie und Biotechnologie gehandelt. Jedoch sind Berichte über erfolgreiche Anwendungen von *V. natriegens* in diesen Bereichen bislang selten. Dies liegt vermutlich an dem Fehlen von effizienten und zuverlässigen genetischen Werkzeugen. Außerdem ist bislang das Wissen über die Biologie von *V. natriegens* sehr begrenzt, was zu unvorhersehbaren Herausforderungen bei der Nutzung führen kann. In Kombination haben diese beiden Gründe bislang die breite Anwendung von *V. natriegens* in der Synthetischen Biologie verhindert.

In dieser kumulativen Dissertation beschreibe ich meinen Beitrag dazu, diese Einschränkungen zu beheben.

Im Rahmen dieser Dissertation wurden zwei CRISPR-Cas9-basierte Werkzeuge zu dem Set an verfügbaren Methoden für *V. natriegens* hinzugefügt.

Das erste Werkzeug ist NT-CRISPR. Diese Methode wurde entwickelt, um unsere Fähigkeit zu verbessern das Genom von *V. natriegens* modifizieren zu können. NT-CRISPR basiert auf der Fähigkeit von *V. natriegens* freie DNA aus der Umwelt aufzunehmen. Dieser Prozess wird natürliche Transformation genannt. Natürliche Transformation kann benutzt werden, um eine breite Spanne an genetischen Modifikationen einzubringen, wie Deletionen, Integration von fremder DNA oder der Erzeugung von Punktmutationen. In einem nachgeschalteten Schritt wird CRISPR-Cas9 aktiviert. Dadurch werden selektiv nicht modifizierte Zellen getötet, um die Effizienz der Methode zu erhöhen. Es konnte gezeigt werden, dass verschiedene Arten von genomischen Modifikationen mit hoher Effizienz durchgeführt werden können. Weiterhin war die gleichzeitige Deletion von drei Sequenzen möglich.

Zusätzlich zu NT-CRISPR, welches zu einer permanenten genetischen Veränderung führt, wurde graded-CRISPRi entwickelt für eine induzierbare Repression von Genen in *V. natriegens*. Durch die Nutzung von zwei verschiedenen induzierbaren Promotoren konnte ein streng reguliertes System entwickelt werden. Dieses zeigte keine Aktivität in Abwesenheit der Induktoren. Außerdem wurden gRNA-Varianten mit verschiedenen Längen und mit Fehlern zur

Zielsequenz verwendet, um abgestufte Knockdowns zu ermöglichen. Dieses Konzept wurde außerdem auf vier verschiedene Reportergene angewendet, um eine Vielzahl an Expressionsleveln bei mehreren Zielgenen zu erzeugen. Abschließend wurde graded-CRISPRi gegen native Gene gerichtet, um den Zusammenhang zwischen der Proteinmenge und dem Wachstumsverhalten zu untersuchen.

Zusätzlich zur Entwicklung von genetischen Werkzeugen wurden Fortschritte im Verständnis des schnellen Wachstums von *V. natriegens* erzielt. Wie fast alle Stämme der *Vibrionaceae* Familie, hat auch *V. natriegens* eine zweigeteilte Genomkonfiguration. Die beiden Chromosomen wurden fusioniert um den Stamm synSC1.0 zu erzeugen, der ein einzelnes Chromosom besitzt. Eine phänotypische Charakterisierung im Vergleich zum Ausgangsstamm zeigte keine auffälligen Unterschiede gibt. Dies führte zu der Schlussfolgerung, dass die zweigeteilte Genomkonfiguration von *V. natriegens* keine Voraussetzung für das schnelle Wachstum ist.

Summary

Vibrio natriegens is the fastest-growing organism known to date with a minimal doubling time of less than ten minutes under optimal conditions. Due to this exciting property and also because of its capability to use a wide range of carbon sources, it was proposed as a novel chassis for Synthetic Biology and Biotechnology. However, so far reports about successful applications of *V. natriegens* are scarce. This is likely due to the lack of efficient and reliable genetic tools. Furthermore, the knowledge about the biology of *V. natriegens* is still limited, which leads to unforeseeable challenges for its application. In combination, these two reasons have prevented the widespread application of *V. natriegens* in Synthetic Biology so far.

In this cumulative thesis I describe my contribution to tackling these limitations.

Within the scope of this thesis, two CRISPR-Cas9-based tools were added to the set of available methods for *V. natriegens*.

The first tool is NT-CRISPR. This method was developed to improve our ability to perform genomic modifications in *V. natriegens*. NT-CRISPR relies on *V. natriegens*' ability to take up free DNA from the environment in a process called natural transformation. This can be used to introduce a wide range of genomic modifications, such as deletions, integration of foreign DNA or the introduction of point mutations. In a subsequent step, CRISPR-Cas9 is activated to selectively kill non-modified cells, thereby drastically increasing the efficiency of genome modification by natural transformation. It was demonstrated that genome engineering can be performed with high efficiencies for various types of modifications, as well as for the simultaneous deletion of three sequences.

In addition to NT-CRISPR, which leads to permanent genetic modifications, graded-CRISPRi was developed as a tool for the inducible repression of genes in *V. natriegens*. By using two different inducible promoters, a tightly regulated system was created, which does not show any activity in the absence of the inducers. Furthermore, libraries with gRNAs of different lengths and mismatches to the target sequence were used to generate graded knockdown strengths. This concept was applied to four different reporter genes to demonstrate that graded-CRISPRi can be used to generate various expression levels of multiple targets in *V. natriegens*. Lastly, graded-CRISPRi was targeted against native genes to study the relationship between protein abundance and growth behavior.

In addition to developing genetic tools, some progress has been made regarding the understanding of the rapid growth of *V. natriegens*. Like almost all strains of the *Vibrionaceae* family, *V. natriegens* has a bipartite genome configuration. The two chromosomes were fused to generate the monopartite strain synSC1.0. A phenotypic characterization in comparison to the parental strain revealed that synSC1.0 did not show any major difference. This led to the conclusion that the bipartite genome configuration of *V. natriegens* is not a requirement for its rapid growth.

Abbreviations

5' UTRs	5' untranslated regions
aa	amino acids
Acr	anti-CRISPR proteins
ATc	anhydrotetracycline
bp	base pair
cAMP	cyclic AMP
Cas	CRISPR-associated
Chr1	Chromosome 1
Chr2	Chromosome 2
CRISPR	clustered regularly interspaced short palindromic repeats
CRISPRi	CRISPR interference
CRP	cAMP receptor protein
<i>crtS</i>	Chr2 triggering site
C-terminus	carboxy-terminus
dCas9	catalytically inactive (dead) Cas9
DHBA	dihydroxybenzoic acid
<i>dif</i>	deletion-induced filamentation
DNA	Deoxyribonucleic acid
dsDNA	double stranded DNA
DUE	DNA unwinding element
gRNA	single guide RNA, guide RNA
IPTG	Isopropyl β -D-1-thiogalactopyranoside
KOPS	FtsK-orientating polar sequences
MAGE	multiplex automated genome engineering
MuGENT	Multiplex Genome Editing by Natural Transformation
Ori	origin of replication
Ori1	Ori of chromosome 1
Ori2	Ori of chromosome 2
Ori _{Ec}	Ori of <i>E. coli</i>
PAM	protospacer adjacent motif
PCR	Polymerase chain reaction
RNA	Ribonucleic acid
rRNA	ribosomal RNA
ssDNA	single stranded DNA
SynBio	Synthetic biology
tDNA	transforming DNA
Ter	terminus region
tracrRNA	trans-activating CRISPR RNA
tRNA	transfer RNA

1. Introduction

1.1. Synthetic biology and the concept of chassis organisms

Synthetic biology (SynBio) is a relatively new field of biology which originated around the turn of the millennium (Cameron et al., 2014), although the term was already used by the French chemist Stéphane Leduc in 1912 in his book “*La biologie synthétique*” (Leduc, 1912). Analogous to mechanical and electrical engineering, SynBio is often described as the engineering discipline of biology (Andrianantoandro et al., 2006; Cheng and Lu, 2012). The underlying idea behind SynBio is that specific functions can be engineered into existing biological systems (Raman et al., 2021). Furthermore, SynBio is based on several engineering principles, such as standardization, modularity and abstraction (Garner, 2021). These principles are implemented through the famous design-build-test-learn cycle, which visualizes the stepwise improvement of an initial design through construction, experimental characterization, and the analysis of the generated data to decide on modifications for an improved version of the design (Garner, 2021).

Another important concept of SynBio is the chassis (De Lorenzo et al., 2021). The term chassis is derived from the French word *châssis*, meaning frame or container (De Lorenzo et al., 2021). In car engineering, the chassis is the structural body, which gives stability to the final product. The chassis further serves to carry other important components of a car, e.g. the engine or the passenger seats (De Lorenzo et al., 2021). In the field of SynBio, the term chassis is less well-defined but usually refers to an organism, which is capable of hosting and replicating recombinant DNA (De Lorenzo et al., 2021). However, the term chassis was also used to describe non-living systems, e.g. a partially self-replicating cell-free *in vitro* reactions (Libicher et al., 2020).

Historically, only few organisms were used as chassis for SynBio, such as *Escherichia coli* or *Saccharomyces cerevisiae* (Cameron et al., 2014). Obviously, these organisms were chosen as they represent the most studied and therefore best understood organisms of the prokaryotes and eukaryotes, respectively. In recent years, scientists have started to explore less studied organisms as novel chassis for SynBio (Kim et al., 2016). Each organism possesses a unique combination of characteristics. The required properties of a chassis organism depend on the specific application (Adams, 2016). The chassis with optimal properties for the development

of a living biosensor for heavy metals in wastewater might not have the ideal properties for the commercial production of high-value chemicals in large-scale bioreactors and vice versa. It is therefore crucial to know the strengths and weaknesses of an organism to identify suitable use cases.

One organism, which possesses some intriguing features for the development of a novel chassis for SynBio is *Vibrio natriegens*.

1.2. *V. natriegens*, a fast-growing marine organism

V. natriegens was first isolated in 1958 by William J. Payne from salt marsh mud on the Atlantic coast of Georgia in the USA (Payne, 1958) and was later also found in other ecological niches, including in symbiosis with other organisms (Benbouzid-Rollet et al., 1991; Mehbub et al., 2018). In 1961, the fast growth of *V. natriegens*, was first described with a doubling time below ten minutes (Eagon, 1961). This measurement was also confirmed more recently (Hoffart et al., 2017).

V. natriegens is a gram-negative bacterium and belongs to the *Harveyi* clade, which also comprises several other fast-growing species within the *Vibrio* genus (Sawabe et al., 2013) (**Figure 1**). Unlike other member of the *Vibrio* genus, *V. natriegens* is not known to be a pathogen and does not possess known *Vibrio* toxins (Lee et al., 2016; Weinstock et al., 2016). Therefore, *V. natriegens* was suggested as a potential future fast-growing model organism and as a new chassis for SynBio (Hoff et al., 2020; Hoffart et al., 2017; Lee et al., 2016; Weinstock et al., 2016).

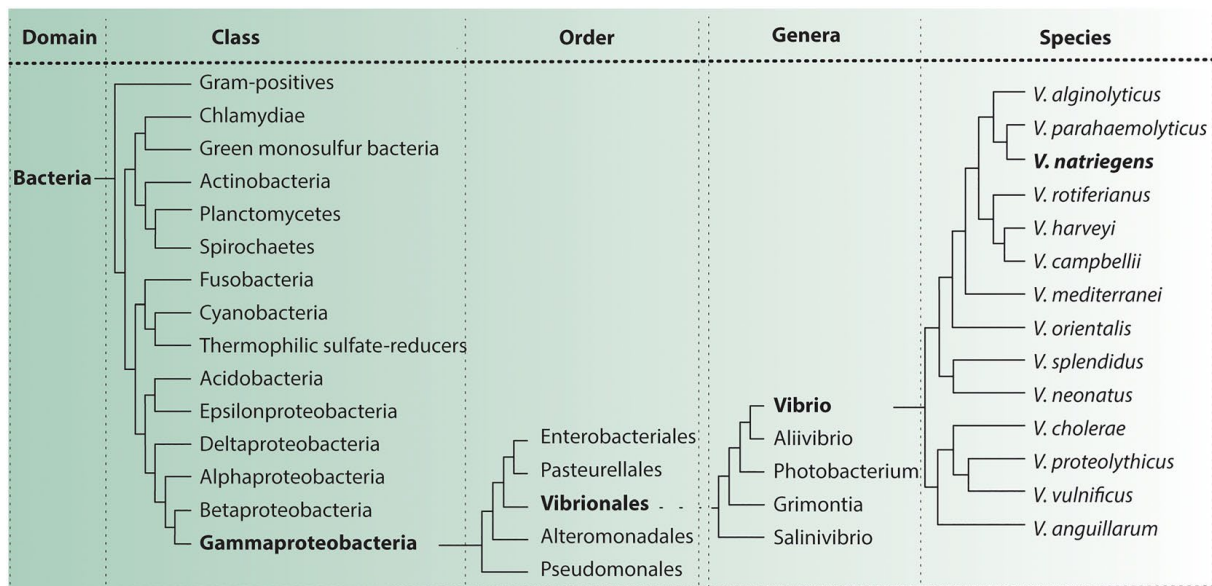


Figure 1: Cladogram of *V. natriegens*.

V. natriegens belongs to the domain bacteria, the class Gammaproteobacteria, the order Vibrionales, the family *Vibrionaceae* (not shown), and the genus *Vibrio*. Lengths of lines does not represent evolutionary distance (Hoff et al., 2020).

In the last decade, the genome of *V. natriegens* was sequenced (Maida et al., 2013; Wang et al., 2013), and a comprehensive set of genetic parts (Stukenberg et al., 2021; Tietze et al., 2022; Tschirhart et al., 2019), as well as a first generation of genome engineering methods (Dalia et al., 2017; Lee et al., 2017; Weinstock et al., 2016) were developed. This allowed the first application-oriented projects, demonstrating the potential of *V. natriegens* for its use in biotechnology (Dalia et al., 2017; Thoma et al., 2022; Wang et al., 2020).

Some studies have contributed hints regarding possible mechanisms leading to the fast growth of *V. natriegens*. Several studies found a very active metabolism. For example, a high glucose uptake rate was described (Hoffart et al., 2017; Long et al., 2017), as well as a more than two-fold higher ATP generation per biomass (Long et al., 2017). Interestingly, the structure of the central metabolism does not differ qualitatively from *E. coli* (Coppens et al., 2023; Long et al., 2017), which is consistent with the finding that ATP generation per mol of glucose is very similar (Long et al., 2017). The authors of a publication describing a whole-genome metabolic model even concluded: “These simulations suggest that *V. natriegens* holds no obvious intrinsic metabolic advantage when compared to *E. coli*” (Coppens et al., 2023).

Conflicting reports can be found regarding the translational machinery of *V. natriegens*. Aiyar et al. estimated that *V. natriegens* possesses about 115,000 ribosomes per cell at a growth rate

1. Introduction

of 4^h, compared to 70,000 ribosomes in fast-growing *E. coli* cells (Aiyar et al., 2002). However, the higher number of ribosomes in *V. natriegens* compared to *E. coli* could not be confirmed by analyzing the total proteome of both organisms (Coppens et al., 2023).

V. natriegens has a bipartite genome configuration with a larger main chromosome (Chr1, ~ 3.2 Mbp) and a smaller secondary chromosome (Chr2, ~ 1.9 Mbp) (Lee et al., 2019). *V. natriegens* carries 11 rRNA operons, 129 tRNA genes, and 4578 predicted open reading frames (Lee et al., 2019). A set of essential genes was identified and most of them were found to be located on Chr1 (Lee et al., 2019). Many duplicates of essential genes were additionally found on Chr2 (Lee et al., 2019).

The bipartite genome configuration is a distinct feature of *V. natriegens* compared to the most commonly used bacterial model organisms, such as *E. coli* or *Bacillus subtilis* (Blattner et al., 1997; Kunst et al., 1997). A solid understanding of the mechanisms permitting this atypical genome configuration is necessary to assess potential chances and challenges for the use of *V. natriegens* as a novel chassis.

1.3. DNA replication in *Vibrionaceae*

Almost all sequenced genomes from strains belonging to the *Vibrionaceae* family show a bipartite genome configuration (Okada et al., 2005) with just a few naturally occurring or synthetically generated single chromosome strains (Sozhamannan and Waldminghaus, 2020; Val et al., 2014, 2012; Xie et al., 2017).

The human pathogen *Vibrio cholerae* has become a model organism for the regulation of DNA replication in bacteria with a multipartite genome (see Ramachandran, Jha and Chatteraj, 2014 and Espinosa, Barre and Galli, 2017 for excellent reviews). In contrast, there is almost no information regarding DNA replication in *V. natriegens* and whether there are any mechanistic differences compared to *V. cholerae*. However, many components of the replication machinery are highly conserved within the *Vibrionaceae* (Fournes et al., 2021; Kemter et al., 2018) and therefore it is likely that DNA replication in *V. natriegens* functions mechanistically similar to *V. cholerae*. Therefore, I will briefly review the chromosome replication and segregation mechanisms of *V. cholerae* in the following paragraphs.

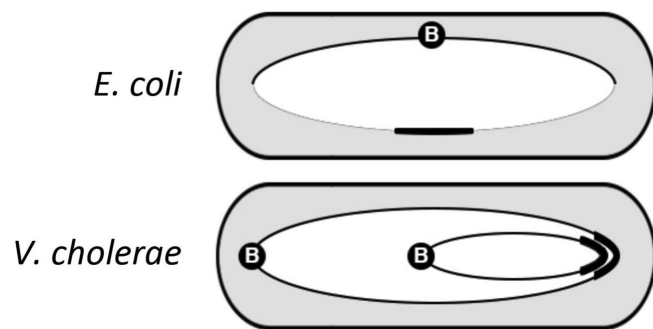
Each chromosome of *V. cholerae* harbors a single origin of replication (Ori), which initiates a bi-directional replication of that chromosome. The replication forks move along both arms of

1. Introduction

the chromosomes (the replicohores) and meet approximately opposite of the Ori in the terminus region (Ter) (Espinosa et al., 2017). Both chromosomes of *V. cholerae* show a longitudinal orientation, which is in contrast to *E. coli* which has a transversal chromosome arrangement. The Ori of Chr1 (Ori1) is located at the old pole and the Ter of Chr1 at the new pole (Ramachandran et al., 2014). The Ori of chromosome 2 (Ori2) is positioned in the middle of the cell with its Ter also located at the new pole (Ramachandran et al., 2014) (**Figure 2**).

Figure 2: Chromosome organization of *E. coli* and *V. cholerae*.

The chromosome of *E. coli* shows a transversal arrangement with Ori (B) and Ter (thick lines) both positioned at mid cell. *V. cholerae* has a longitudinal chromosome arrangement with Ori of Chr1 and Ter at the other pole. In case of Chr2, the Ori is located at mid cell.



(Modified from Ramachandran et al. 2014).

The initiation of replication is mechanistically different for both chromosomes. Replication initiation of Chr1 functions similarly to the chromosome of *E. coli*. DnaA binds to DnaA binding sites and thereby triggers the opening of an AT-rich region, the DNA unwinding element (DUE). This allows the assembly of the replisome and consequently the start of DNA replication. The high similarity between Ori1 of *V. cholerae* and the Ori of *E. coli* (Ori_{EC}) even allows the functional replacement of Ori_{EC} with Ori1 (Koch et al., 2010).

Replication of Chr2 mechanistically resembles the replication of iteron-based plasmids like the *E. coli* F-plasmid or of the P1-phage (Konieczny et al., 2014). In addition to DnaA, Ori2 requires a second initiator protein for the melting of the DUE and consequently for the start of DNA replication (Fournes et al., 2021). This protein is RctB, which is highly conserved in *Vibrionaceae* (Fournes et al., 2021). RctB triggers unwinding of DUE by binding to 11-12mers in the Ori2 region, which allows formation of the replisome and thereby the start of DNA replication.

It was shown that replication of both chromosomes has evolved for termination synchrony (Kemter et al., 2018). In *Vibrionaceae*, Chr2 is smaller than Chr1. Therefore, Chr2 replication has to start with a delay relative to Chr1 (Kemter et al., 2018; Val et al., 2016). The exact timing

1. Introduction

of Chr2 replication is achieved through a sophisticated and still not fully understood mechanism. In early studies, it was shown that Ori2 replication starts after a specific sequence on Chr1 is replicated (Baek and Chatteraj, 2014). This sequence was called *crtS* (Chr2 triggering site) (Baek and Chatteraj, 2014). Binding of RctB to *crtS* triggers a change in binding affinity of RctB towards the 11-12mers at Ori2. (Baek and Chatteraj, 2014; de Lemos Martins et al., 2018; Fournes et al., 2021). Binding of RctB to *crtS* is dependent on the transcriptional regulator Lrp (Doan et al., 2023). When the copy number of *crtS* is increased immediately after its replication, or when additional copies of *crtS* are present at ectopic sites, more RctB is activated for binding to the 11-12mers, eventually triggering replication of Chr2 (Ramachandran et al., 2018).

During replication, both chromosomes are actively segregated to ensure that both daughter cells inherit one copy of the replicated chromosomes (Ramachandran et al., 2014). This is achieved through one ParABS system per chromosome. Both ParABS systems are orthogonal but work mechanistically similar (Espinosa et al., 2017). *parS* is a DNA sequence on the respective chromosome, which is bound specifically by their cognate ParB (David et al., 2014; Possoz et al., 2022). ParB interacts with the ATPase ParA (Hui et al., 2010). ParA is most abundant close to the cell poles and pulls the *parS* bound ParB towards the poles by retraction of ParA by an ATP-dependent mechanism (Possoz et al., 2022).

The Ter of both chromosomes is located close to mid-cell before cell division (Srivastava et al., 2006). To ensure proper segregation, both chromosomes possess FtsK-orientating polar sequences (KOPS), whose purpose is to load the FtsK protein onto the DNA (Bigot et al., 2005). FtsK is a membrane-bound DNA translocase, which interacts with other cell division proteins, e.g. FtsZ, and is therefore located at the newly forming cell division septum (Zorrilla et al., 2021). FtsK actively translocates the chromosomes into the daughter cells (Stouf et al., 2013). Directionality of this translocation is achieved through the directionality of FtsK loading through the KOPS sequences (Bigot et al., 2005). As the final step of DNA replication, chromosome dimers are resolved through the site-specific recombinase complex XerCD. XerCD recognizes *dif* (deletion-induced filamentation) sites, which are located in the Ter of both chromosomes (Val et al., 2008).

1.4. Natural transformation

One crucial characteristic of a chassis is the ability to introduce foreign DNA to express heterologous genes or to modify its genetic information. *V. natriegens* is capable of natural transformation, which can be a useful route for the uptake of plasmid DNA (Specht et al., 2023) or for genome engineering (Dalia et al., 2017).

Natural transformation was first described in the famous Griffith experiment, where it was shown that non-pathogenic strains of *Streptococcus pneumoniae* could gain pathogenicity when incubated with heat-inactivated cells of a pathogenic *S. pneumoniae* strain (Griffith, 1928). At the time it was not known what mechanism was responsible for this phenotypic change. Later, research by Avery *et al.* demonstrated that the uptake of DNA, rather than proteins, is responsible for the observed phenotypic change (Avery et al., 1944). Since then, natural transformation was experimentally confirmed in over 80 different species (Johnston et al., 2014), including important model organisms, such as *Bacillus subtilis* (Anagnostopoulos and Spizizen, 1961) and *V. cholerae* (Meibom et al., 2005).

In the following paragraphs I will review natural transformation in *Vibrionaceae*, with a special emphasis on the best-studied member of that family *V. cholerae*, as well as on the available knowledge about *V. natriegens* as the main organism of this thesis. Natural transformation in *V. cholerae* is well studied and summarized in several excellent review articles (Johnsborg et al., 2007; Johnston et al., 2014; Seitz and Blokesch, 2013).

Natural transformation starts with the recognition of extracellular double stranded DNA (dsDNA) by the tip of a type IV pilus (Ellison et al., 2018). The dsDNA is pulled into the periplasmic space through the PilQ transmembrane pore by retraction of the type IV pilus (Ellison et al., 2018; Weaver et al., 2020). Once a portion of the dsDNA arrives in the periplasm, it is bound by ComEA (Seitz et al., 2014). Sequential binding of stretches of the incoming dsDNA by ComEA eventually leads to the complete import of the DNA through a Brownian ratchet mechanism, which allows stepwise diffusion through the PilQ pore into the periplasm but no reverse diffusion towards the extracellular space (Seitz et al., 2014). The next step is the transport from the periplasm into the cytoplasm by the transmembrane protein ComEC (Silale et al., 2021). In this translocation process, one strand of the DNA is degraded so that single stranded DNA (ssDNA) arrives in the cytoplasm (Silale et al., 2021). In the cytoplasm, the ssDNA is bound by ssDNA binding proteins DprA and Smf, which promote loading of RecA onto the

1. Introduction

ssDNA by direct protein-protein interaction (Mortier-Barrière et al., 2007). RecA then completes the natural transformation process by integrating the ssDNA into the host genome through homologous recombination (Mortier-Barrière et al., 2007). Interestingly, *V. cholerae* does not show a preference for DNA of related strains and species (Suckow et al., 2011), which is in contrast to other organisms (Dai et al., 2018; Hamilton and Dillard, 2006).

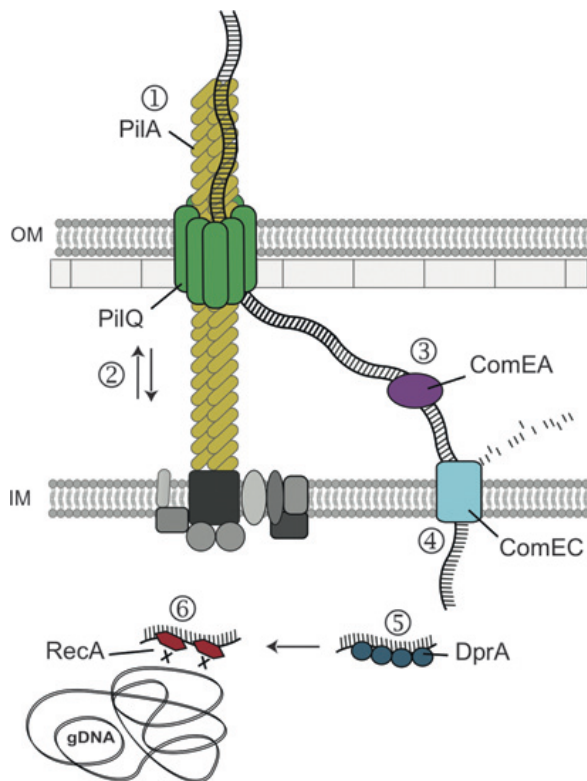


Figure 3: Model for DNA uptake through natural transformation in *V. cholerae*.

dsDNA is recognized by a pilus composed of PiliA subunits. Once the dsDNA is imported into the periplasm through a PilQ pore, it is bound by ComEA. In a next step, ComEC translocates the DNA into the cytoplasm as a single strand, while degrading the second strand. The ssDNA in the cytoplasm is recognized by the ssDNA binding protein DprA. Homologous recombination into the host chromosome is mediated by RecA.

(Modified from Seitz and Blokesch 2013)

Natural transformation is controlled by several intertwined regulatory pathways (**Figure 4**) to ensure the activation of natural competence only under the right conditions (Seitz and Blokesch, 2013). One major player is the competence master regulator TfoX, which is responsible for the upregulation of many necessary components for natural transformation, especially for the DNA uptake machinery (Meibom et al., 2005). TfoX in *V. cholerae* is induced in the presence of chitin, which suggests that *V. cholerae* is performing natural transformation mostly in its aquatic habitat when the cells are associated with chitinous exoskeletons of crustaceans (Huq et al., 1983; Meibom et al., 2005). On a molecular level, the presence of chitin oligomers in the cytoplasm is sensed by the membrane-bound transcriptional regulator TfoS, which can then activate transcription of the small RNA TfoR (Dalia et al., 2014). TfoR binds to the mRNA of *tfoX*, thereby changing its secondary structure and promoting translation (Yamamoto et al., 2011). On the transcriptional level, *tfoX* expression is directly activated by

1. Introduction

the cyclic AMP (cAMP) receptor protein (CRP) in the presence of cAMP. This links the activation of natural transformation to the general nutritional status of the cell (Wu et al., 2015).

In contrast to *V. cholerae*, growth on chitin does not lead to natural competence in *V. natriegens* (Dalia et al., 2017). However, overexpression of *tfoX* from either *V. cholerae* or *V. natriegens* through an inducible promoter can be used to facilitate natural transformation and therefore circumvent the natural regulatory cascade (Dalia et al., 2017).

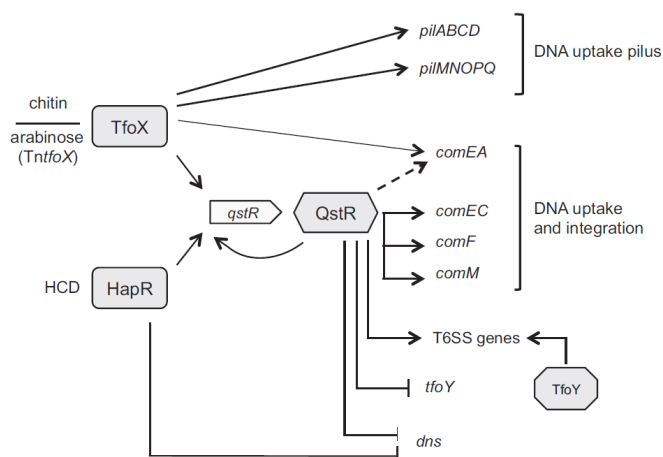


Figure 4: Overview about regulation of natural competence in *V. cholerae*.

TfoX activates expression of genes for DNA uptake and of *qstR*. HapR directly represses expression of *dns* and activates expression of *qstR*. QstR upregulates multiple *com* genes. Abbreviations: arabinose TntfoX = plasmid derived expression of *tfoX* with an arabinose inducible promoter, HCD = high cell density (Jaskólska et al., 2018).

The second key player in the regulation of natural transformation in *V. cholerae* is QstR. QstR is a transcriptional regulator that is necessary for the expression of many competence genes, e.g. ComEC and ComEA (Jaskólska et al., 2018). *qstR* expression is dependent on TfoX (Lo Scudato and Blokesch, 2013) and on the additional transcription factor HapR (Jaskólska et al., 2018). HapR is produced at high cell density in response to the quorum sensing signal CAI-1.

In summary, *V. cholerae*'s natural competence is dependent on the two master regulators TfoX and QstR, which together activate the genes necessary for natural transformation. TfoX is induced in the presence of chitin (via TfoS and TfoR) and under conditions of carbon starvation (via CRP-cAMP). QstR is produced at high cell density, dependent on the quorum sensing signal

CAI-1. HapR also represses expression of *dns*, an endonuclease, which likely prevents degradation of the incoming DNA (Blokesch and Schoolnik, 2008).

A single study investigated the regulation behind natural competence in *V. natriegens* based on a machine-learning-based analysis of a large set of transcriptomic data (Shin et al., 2023). The general regulatory pattern behind natural competence in *V. natriegens* appears to be similar to *V. cholerae*. Shin *et al.* found that the genes for the regulators described above, *tfoX*, *qstR*, and *hapR* all show increased expression under competence-inducing conditions (Shin et al., 2023). Also most, but not all, competence genes seem to be regulated by the same transcription factors as in *V. cholerae* (Shin et al., 2023). The authors also compared the essentiality of competence-related genes for natural transformation between different *Vibrio* species and found some genes that are essential in some *Vibrios* but not in others (Shin et al., 2023).

In summary, it is very likely that the main regulatory pathways for establishing natural competence, as well the mechanistic steps in uptake and integration of the extracellular DNA are conserved between different *Vibrio* species, including *V. natriegens* (Shin et al., 2023). However, there are also crucial differences, e.g. the failure of *V. natriegens* to induce natural competence in response to chitin (Dalia et al., 2017).

1.5. CRISPR-Cas

Establishing an organism as a novel chassis for synthetic biology requires efficient tools for genome engineering. These can be used to enhance beneficial or to mitigate disadvantages properties of the organism. Over the last decade, CRISPR-Cas has become a versatile tool for genome engineering in a wide range of organisms. CRISPR-Cas should therefore be considered as the basis for the development of tools for potential new chassis organisms such as *V. natriegens*.

In 1987 Ishino *et al.* by chance found an interesting region in the chromosome of an *E. coli* strain, which they reported as follows: “Five highly homologous sequences of 29 nucleotides were arranged as direct repeats with 32 nucleotides as spacing” (Ishino et al., 1987). This is the first report about a locus, which would later be identified as a CRISPR array. The term CRISPR is an abbreviation for “clustered regularly interspaced short palindromic repeats” and was coined by Jansen *et al.* (2002). They also found that specific genes are located in the

1. Introduction

proximity of CRISPR loci in different species, which they termed CRISPR-associated (*cas*) genes (Jansen et al., 2002). At the time, the physiological role of these CRISPR loci and the *cas* genes was not known. In 2005, several groups found that the “spacers” between the directed repeats often share homology with sequences from phages or conjugative plasmids (Bolotin et al., 2005; Mojica et al., 2005; Pourcel et al., 2005). A first hint towards a possible role of CRISPR-Cas systems in phage defense was found by Mojica *et al.*, who observed that many strains of *Sulfolobus solfataricus* carry a prophage integrated into their chromosome (Mojica et al., 2005). A single exception was a strain, which carried a spacer homologous to a sequence of that exact prophage, suggesting that the CRISPR system prevented infection by that phage (Mojica et al., 2005).

Later, it was shown that mutants of *Streptococcus thermophilus*, which survived exposure to virulent bacteriophages, had acquired new spacers homologous to sequences from the phages they were exposed to (Barrangou et al., 2007). This finding demonstrated the main role of CRISPR-Cas systems in the defense against bacteriophages (Barrangou et al., 2007).

The exact steps leading to the acquisition of new spacers and the defense mechanisms against intruding phages differ between different classes and types of CRISPR-Cas systems. A recent hierarchical classification groups all known CRISPR-Cas systems into classes, types, and branches (Makarova et al., 2020). The tools developed within the scope of this thesis are derived from the CRISPR-Cas system of *Streptococcus pyogenes* (Stukenberg et al., 2022, **Chapter 3.1**; Stukenberg et al., 2024, **Chapter 3.3**). Therefore, in this chapter, I will focus on this system.

The used CRISPR-Cas system belongs to class 2, type II and subtype A (Le Rhun et al., 2019). This type II-A system is composed of a CRISPR array with repeats and spacers and four *cas* genes, namely *cas1*, *cas2*, *csn2*, and *cas9*. Also, there is a trans-activating CRISPR RNA (*tracrRNA*) encoded within the CRISPR locus (Le Rhun et al., 2019). Cas1, Cas2, Csn2, and Cas9 form a super complex, which allows the acquisition of new spacers by capturing a short DNA fragment of invading phages and subsequent integration into the CRISPR array of the host (Jakhanwal et al., 2021; Ka et al., 2018; Wilkinson et al., 2019).

The CRISPR array is then fully transcribed as a pre-CRISPR RNA (*crRNA*), which base-pairs with the unprocessed *tracrRNA*. This complex is subsequently co-processed by Cas9 and the host-encoded RNase III (Deltcheva et al., 2011). Eventually a complex between Cas9, *crRNA*, and

tracrRNA forms, which can cleave target DNA sequences thereby preventing successful infection by an incoming bacteriophage (Jinek et al., 2012).

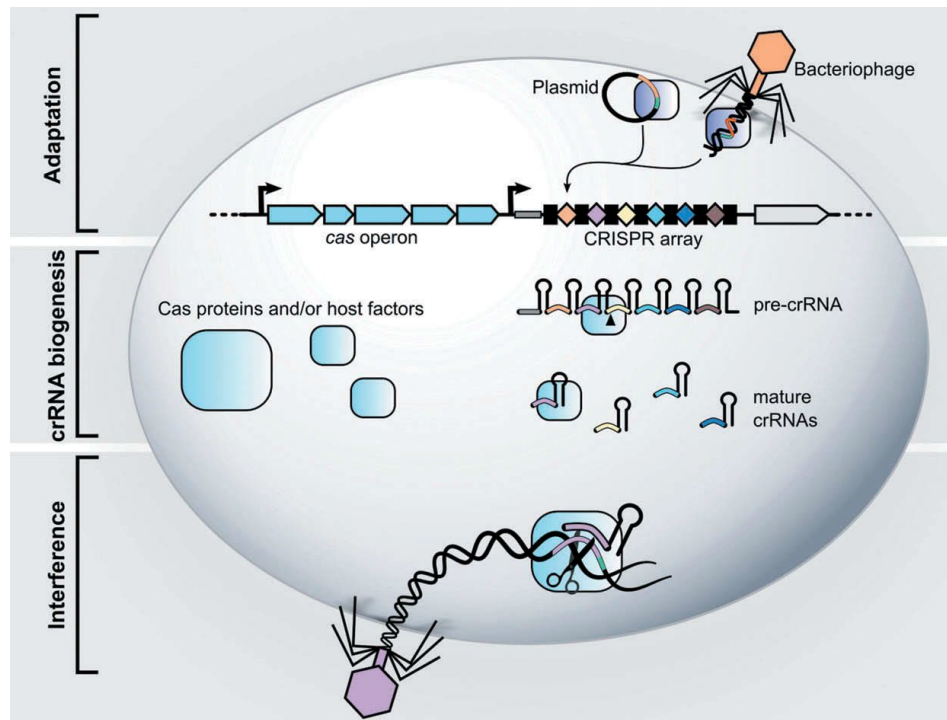


Figure 5: Steps in the phage defense through the type II-A CRISPR-Cas system of *S. pyogenes* DNA sequences from an infecting phage or a plasmid is integrated into the CRISPR array. The CRISPR array is then transcribed into a pre-crRNA, which is processed by Cas proteins and host factors into mature crRNAs. These crRNAs bind to a Cas protein to generate the interference complex, which can degrade incoming DNA from a related bacteriophage species (Le Rhun et al., 2019).

A synthetic chimera of crRNA and tracrRNA was developed and termed single guide RNA or just guide RNA (gRNA) to simplify the use of CRISPR-Cas as a tool (Jinek et al., 2012).

A necessary sequence motif for target recognition is the protospacer adjacent motif (PAM) (Jinek et al., 2012), which is recognized by the Cas9 protein independent of the sequence of the associated RNAs (Anders et al., 2014). In case of the type II-A system of *S. pyogenes*, the PAM is NGG (Mojica et al., 2009) and to a lower extent NAG (Jiang et al., 2015). Cas9 possesses two nuclease domains, HNH and RuvC, which each cleave one strand of the target DNA (Jinek et al., 2012). Cleavage of the DNA target occurs as a blunt double-strand-break three nucleotides upstream of the PAM (Gasiunas et al., 2012).

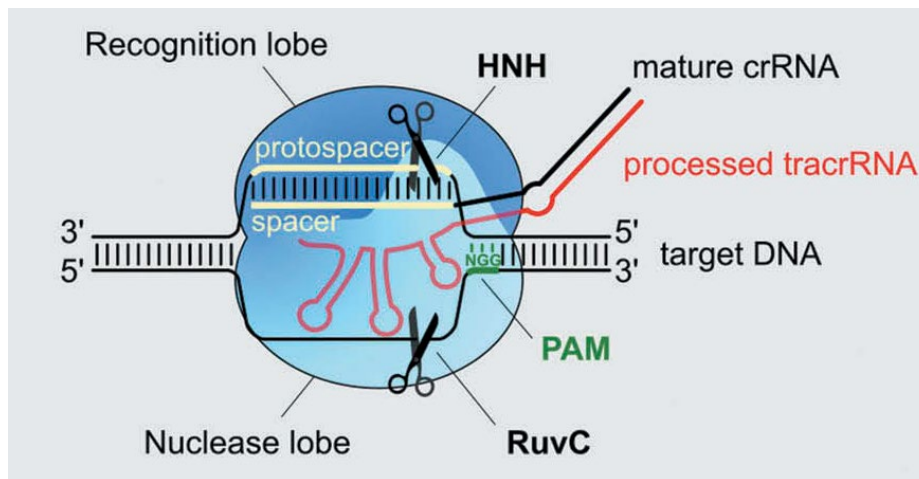


Figure 6: DNA cleavage by Cas9.

The mature crRNA, together with the processed tracrRNA form a complex with Cas9 (blue object). The crRNA carries the spacer sequence, which recognizes the protospacer sequence on the target DNA. The PAM is directly recognized by the Cas9 protein. Two nuclease domains, HNH and RuvC, cleave the target DNA three bp upstream of the PAM (Modified from Le Rhun et al., 2019).

CRISPR-Cas systems prevent the infection of bacterial cells by viruses. Those viruses therefore have a strong selection pressure to evolve measures to counteract CRISPR-Cas systems (Pawluk et al., 2018). Many phages were found to encode specific anti-CRISPR proteins (Acr), which allow infection of bacterial cells, although they possess an active CRISPR-Cas system (Bondy-Denomy et al., 2013; Pawluk et al., 2018, 2014). AcrIIA4 is one Acr able to inhibit the Cas9 from *S. pyogenes* and is encoded by a *Listeria monocytogenes* prophage (Rauch et al., 2017). AcrIIA4 binds directly to the Cas9 protein at residues essential for PAM binding and therefore inhibits binding of the Cas9-RNA ribonucleoprotein to the target DNA and consequently prevents DNA cleavage (Yang and Patel, 2017). Acrs have been used before to modulate the activity of CRISPR-Cas-based tools (Aschenbrenner et al., 2020; Bubeck et al., 2018; Hoffmann et al., 2019; Shin et al., 2017).

2. Aims of this work: Establishing *V. natriegens* as a next-generation SynBio chassis

V. natriegens is a fascinating bacterium, mainly because of its ability to grow rapidly under a wide range of conditions. Therefore, it has the potential to be developed into a next-generation chassis organism for SynBio. However, reports about successful applications of *V. natriegens* are still limited, presumably because of the lack of efficient and well-characterized genetic tools. Therefore, **the first aim of this work was to expand the range of molecular tools for *V. natriegens*.**

I first approached this task through the development of NT-CRISPR. The idea behind this method is to combine natural transformation for genomic modification with a subsequent CRISPR-Cas9-based counterselection step (Stukenberg et al., 2022, **Chapter 3.1**). As a second tool, I envisioned graded-CRISPRi as a novel tool to control the expression of native genes. This tool is based on CRISPR interference (CRISPRi) and is expected to allow additional use cases where a permanent deletion of a gene is not possible or not desired (Stukenberg et al., 2024, **Chapter 3.3**).

Beyond the availability of efficient tools, our limited understanding of the biology of *V. natriegens* limits its applicability. Therefore, in addition to the development of novel tools, **the second aim of this work is to gather insights into the mechanisms underlying the rapid growth of *V. natriegens*.**

As the bipartite genome configuration of *V. natriegens* is atypical for bacteria, we wanted to explore if this is a requirement for its rapid growth. This was achieved by fusing both chromosomes of *V. natriegens* to generate a strain with a monopartite chromosome configuration. Characterization of its growth behavior in comparison to the parental strain revealed that the bipartite configurations is not necessary for rapid growth of *V. natriegens* (Ramming et al., 2023, **Chapter 3.2**).

3. Results

The work described in this thesis was performed in collaboration with other scientists and the result was already published or submitted to different scientific journals. In this chapter, I will briefly summarize these publications and specify my exact contribution. After each summary, the respective publication is shown in full. Associated datasets are available at the publisher's website of the respective publications.

3.1. NT-CRISPR, combining natural transformation and CRISPR-Cas9 counterselection for markerless and scarless genome editing in *Vibrio natriegens*

Daniel Stukenberg, Josef Hoff, Anna Faber, Anke Becker

Communications Biology, 5(1), p. 265

In this publication, we describe the development and characterization of a novel genome engineering tool for *V. natriegens*, which we termed NT-CRISPR. NT-CRISPR functions in two temporally distinct steps. First, the desired genomic modification is performed through natural transformation. Second, CRISPR-Cas9-based counterselection kills non-modified cells, thereby drastically increasing the overall editing efficiency.

In the NT-CRISPR method, genome engineering through natural transformation is activated by the production of TfoX, the master regulator for natural competence. This transcription factor is encoded on a plasmid and its production is induced by Isopropyl β -D-1-thiogalactopyranoside (IPTG). The exact genomic modification is determined by the sequence of the transforming DNA (tDNA), which is usually prepared in a PCR and carries sequences homologous to the region surrounding the target gene. Depending on the tDNA sequence, natural transformation leads to the deletion of a genomic region, integration of foreign DNA or the introduction of point mutations.

Counterselection through CRISPR-Cas9 is achieved by targeting a DNA sequence present in wild type but not in correctly edited cells. The target of CRISPR-Cas9 is defined through the spacer sequence of the gRNA. Due to the absence of non-homologous end joining in *V. natriegens*, introduction of a DNA double-strand-break through CRISPR-Cas9 leads to cell death. To achieve sufficient control over the activity of CRISPR-Cas9 prior to induction, we

3. Results

added the sequence coding for the anti-CRISPR protein AcrIIA4 under control of a weak constitutive promoter to the plasmid design. This allowed the transformation with plasmids carrying both a *cas9* sequence and a *gRNA* with a spacer directed against a chromosomal target, which was not possible before. All components for CRISPR-Cas9-based counterselection are encoded on the same plasmid as *tfoX*, leading to a single plasmid design.

To quantitatively characterize different aspects of the tool, we targeted the gene *wbfF*. Strains with deletion of *wbfF* form almost transparent colonies, which allowed us to calculate editing efficiencies based on the ratios of colonies with the $\Delta wbfF$ and wild type morphologies. With this readout, we tested different amounts of tDNAs, as well as different length of homologous flanks. Furthermore, we tested the killing efficiency with different gRNAs and found that up to 99.999% of cells could be killed upon CRISPR-Cas9 induction.

After these initial benchmarking experiments, we applied NT-CRISPR for the deletion of several genomic regions. We found that almost all colonies resulting from the NT-CRISPR procedure carried the desired modification. This was also true for larger deletions, e.g. of the flagellar gene cluster or the prophages *vnp1* or *vnp2*, with sizes between 30 kbp and 40 kbp. We selected genes and groups of genes as examples for deletions based on the expectation that their loss might improve plasmid transformation efficiency. Unfortunately, none of these mutations was beneficial.

Beyond deletions, we demonstrated the capability of NT-CRISPR for the integration of foreign DNA into the chromosome of *V. natriegens*. As a test case, we created translation fusions of several genes with the fluorescent reporter mScarlet-I. We selected genes expected to be regulated depending on the growth phase, which we could confirm by measuring fluorescence in parallel to a growth curve.


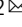
We showed that NT-CRISPR can be used to introduce point mutations by altering single nucleotides in genes required for the utilization of alternative carbon source leading to premature stop codons. This allowed us to use the failure to grow on minimal media with the respective carbon source as an indication for successful modification. In some cases, we only succeeded in generating point mutations when an additional silent mutation was introduced. This was likely necessary to evade the DNA mismatch repair system.

The modular design of the NT-CRISPR within the framework of the Marburg Collection (Stukenberg et al., 2021) allowed us to build NT-CRISPR plasmids with multiple gRNAs, each targeting one gene. This allowed us to perform up to three deletions in single round of editing. Especially for integrations and point mutations, the requirement of the Cas9 for an NGG PAM sequence might limit applicability of NT-CRISPR. We could demonstrate the compatibility of the near PAM-less variant SpG Cas9, which requires only NGN as a PAM (Walton et al., 2020), with NT-CRISPR.

Personal contribution

I conceived the NT-CRISPR method with input from Anke Becker. I constructed all plasmids, based on previously built basic parts. The inducible promoters used to control expression of *tfoX*, *cas9* and *gRNA* were built and characterized by Anna Faber. I performed all experiments, apart from the characterization of the plasmid transformation efficiency, which was done by Josef Hoff. I wrote the first draft of the manuscript, which was later improved based on feedback from all other authors.

NT-CRISPR, combining natural transformation and CRISPR-Cas9 counterselection for markerless and scarless genome editing in *Vibrio natriegens*

Daniel Stukenberg^{1,2,3}, Josef Hoff^{1,2,3}, Anna Faber^{1,2} & Anke Becker^{1,2}  

The fast-growing bacterium *Vibrio natriegens* has recently gained increasing attention as a novel chassis organism for fundamental research and biotechnology. To fully harness the potential of this bacterium, highly efficient genome editing methods are indispensable to create strains tailored for specific applications. *V. natriegens* is able to take up free DNA and incorporate it into its genome by homologous recombination. This highly efficient natural transformation is able to mediate uptake of multiple DNA fragments, thereby allowing for multiple simultaneous edits. Here, we describe NT-CRISPR, a combination of natural transformation with CRISPR-Cas9 counterselection. In two temporally distinct steps, we first performed a genome edit by natural transformation and second, induced CRISPR-Cas9 targeting the wild type sequence, and thus leading to death of non-edited cells. Through cell killing with efficiencies of up to 99.999%, integration of antibiotic resistance markers became dispensable, enabling scarless and markerless edits with single-base precision. We used NT-CRISPR for deletions, integrations and single-base modifications with editing efficiencies of up to 100%. Further, we confirmed its applicability for simultaneous deletion of multiple chromosomal regions. Lastly, we showed that the near PAM-less Cas9 variant SpG Cas9 is compatible with NT-CRISPR and thereby broadens the target spectrum.

¹Center for Synthetic Microbiology, Philipps-Universität Marburg, Marburg, Germany. ²Department of Biology, Philipps-Universität Marburg, Marburg, Germany. ³Max-Planck Institute for Terrestrial Microbiology, Marburg, Germany. ✉email: anke.becker@synmikro.uni-marburg.de

V*ibrio natriegens* is a fast-growing marine bacterium with a doubling time of <10 min^{1,2}. It has become a promising chassis organism due to its interesting properties, such as a wide substrate range, lack of pathogenicity and a highly active translational machinery^{3–6}. A crucial factor for the utility of an organism is the availability of efficient and reliable methods for genome engineering for both basic research and application-oriented projects. In case of the primary prokaryotic model organism *Escherichia coli*, large scale genome engineering projects have led to both fundamental physiological insights^{7,8} and to platform strains for biotechnological applications^{9,10}. Examples for this are genome reduction projects^{7,8} or recoding of the *E. coli* genome by replacing all amber stop codons¹¹. In addition to single strains with multiple modifications, a library of strains each carrying a deletion of a single non-essential gene, known as the Keio Collection¹², has proven to be a highly valuable resource for basic research in *E. coli*. So far, such ambitious projects with *V. natriegens* are still distant prospects and require the establishment of genome engineering methods matching those available for *E. coli* in terms of efficiency and ease of use^{13–15}.

In recent years, first steps have been made to turn *V. natriegens* into a genetically accessible model organism. Its genome, consisting of two chromosomes, was sequenced and published in 2013^{16,17}. Moreover, protocols for transformation with plasmids and first genome engineering methods have been developed by either taking inspiration from tools developed for *E. coli*^{5,18,19} or by harnessing organism-specific advantages of *V. natriegens*. The latter is the case for multiplex genome editing by natural transformation (MuGENT)²⁰. Natural transformation describes the uptake of free DNA from the environment by a host-encoded multicomponent machinery, and sequential integration of this DNA into the genome by RecA mediated homologous recombination²¹. This capability is widespread among *Vibrio* species and many other phylogenetically unrelated bacteria²². Natural transformation was harnessed in the MuGENT method for genome engineering in *V. natriegens* by plasmid-based overproduction of the competence master regulator TfoX²⁰. This way, the need to identify the natural inducer for natural transformation, which is chitin for *Vibrio cholerae* but unknown for *V. natriegens*, was circumvented²⁰. While MuGENT showed a stunning efficiency with up to 10% of the cells carrying a deletion, this method relies on integration of an antibiotic resistance marker into a chromosomal locus for the selection of modified clones²⁰. As a result, subsequent removal of the antibiotic resistance marker is required through additional laborious steps or the marker remains in the genome, thereby preventing future use of the respective antibiotic for selection.

A different strategy to efficiently discriminate between edited and non-edited cells has been developed in a wide range of organisms through the CRISPR-Cas9 system^{14,23,24}. The endonuclease Cas9 is directed to a defined genomic locus through an easily adaptable guide RNA (gRNA), thus providing remarkable flexibility²⁵. Cleavage through the Cas9/gRNA complex introduces a DNA double-strand break (DSB)²⁶ which is lethal to most prokaryotic bacteria due to the absence of the non-homologous end joining (NHEJ) pathway²⁷. If CRISPR-Cas9 is designed to target the wild type sequence, non-edited cells can be efficiently killed, while the edited cells are immune to Cas9 cleavage and survive. When performed after application of the editing method, CRISPR-Cas9-based counter selection can greatly increase the fraction of modified cells and hence the apparent editing efficiency^{14,23,24}. Cell death of *V. natriegens* as a result of Cas9-mediated DNA cleavage has been confirmed recently, suggesting the absence of NHEJ²⁸.

Here, we report the NT-CRISPR method combining the highly efficient genome editing through natural transformation with a

CRISPR-Cas9-based counter selection strategy. We achieved editing efficiencies of up to 100% for deletions, integrations and point mutations, and demonstrated multiplexed deletions of three genomic target regions. The NT-CRISPR method obviates the integration of antibiotic resistance markers and thereby allows for scarless and markerless genome engineering in *V. natriegens*.

Results and discussion

Design of and rationale behind NT-CRISPR. For NT-CRISPR, we envisioned a one-plasmid design to achieve a convenient and fast workflow. One necessary component of the NT-CRISPR system is the master regulator for natural competence *tfoX*. Similar to a previous approach²⁰, we use the *tfoX* gene from *Vibrio cholerae* under the control of the isopropyl β-D-1-thiogalactopyranoside (IPTG) inducible P_{tac} promoter. In addition, our design requires the components of the CRISPR-Cas9 system, namely *cas9* and *gRNA*, both driven by the anhydrotetracycline (ATc) inducible P_{tet} promoter (Fig. 1a). In our construct, we used improved variants of P_{tac} and P_{tet}²⁹. We found that simultaneously maintaining the coding sequences for Cas9 and a gRNA targeting a genomic sequence to be a major challenge in *V. natriegens*. A possible reason was trace production of Cas9 and gRNA through leaky promoter activity which was probably sufficient to introduce DNA DSBs and consequently causes cell death. This problem persisted even when a weak ribosome binding site was used and the strongest available SsrA-derived protein degradation tag (M0050)³⁰ was fused to Cas9 to reduce cellular abundance of this protein. Previously, it had been shown that by these two measures, the Cas9 and gRNA coding sequences could be established together in *E. coli* cells¹⁴. However, when *V. natriegens* cells were transformed with the plasmid carrying all CRISPR-Cas9 components, we obtained only very few colonies carrying a wide range of deleterious mutations in the plasmid, rendering the CRISPR-Cas9 system non-functional. In contrast, the same plasmid with a non-binding control gRNA could be easily introduced to this host.

The final solution to the strong toxicity of Cas9 and gRNA produced at basal levels was the expression of the anti-CRISPR protein-encoding gene *acrIIA4* under control of the constitutive promoter J23106. *AcrIIA4* shows a high affinity to Cas9 and the Cas9-gRNA complex, efficiently inhibiting Cas9-gRNA from binding to the DNA target and consequently preventing the introduction of DSB^{31,32}. Anti-CRISPR proteins have been used in eukaryotes to reduce off-target effects^{33,34} or to achieve spatiotemporal control over CRISPR-Cas9 activity, for example through an optogenetic approach³⁵ or by selective expression in certain cell types³⁶. Moreover, anti-CRISPR proteins were used in the prokaryotic species *Clostridium acetobutylicum* to enable cells to carry *cas9* and *gRNA* simultaneously without toxic effects³⁷. In a similar fashion, we used constitutive expression of *acrIIA4* to compensate for the basal production of Cas9 and gRNA. After adding *acrIIA4* to our design, we were finally able to transform *V. natriegens* with a plasmid carrying both *cas9* and a gene coding for a chromosome targeting gRNA. The full plasmid design is shown in Fig. 1a.

The first step after transformation of the NT-CRISPR plasmid (Fig. 1a) is the natural transformation, which requires the addition of IPTG to induce production of the master regulator TfoX. For a simple deletion, a transforming DNA (tDNA), with sequences homologous to the regions flanking the target sequence to be deleted, is added to the cells (Fig. 1b). Only a minority of cells in the population will be modified, while the vast majority of cells will still have the wild type sequence. The last step in the workflow is the CRISPR-Cas9 mediated counterselection (Fig. 1c). Therefore, ATc is added to induce expression of both *cas9* and the

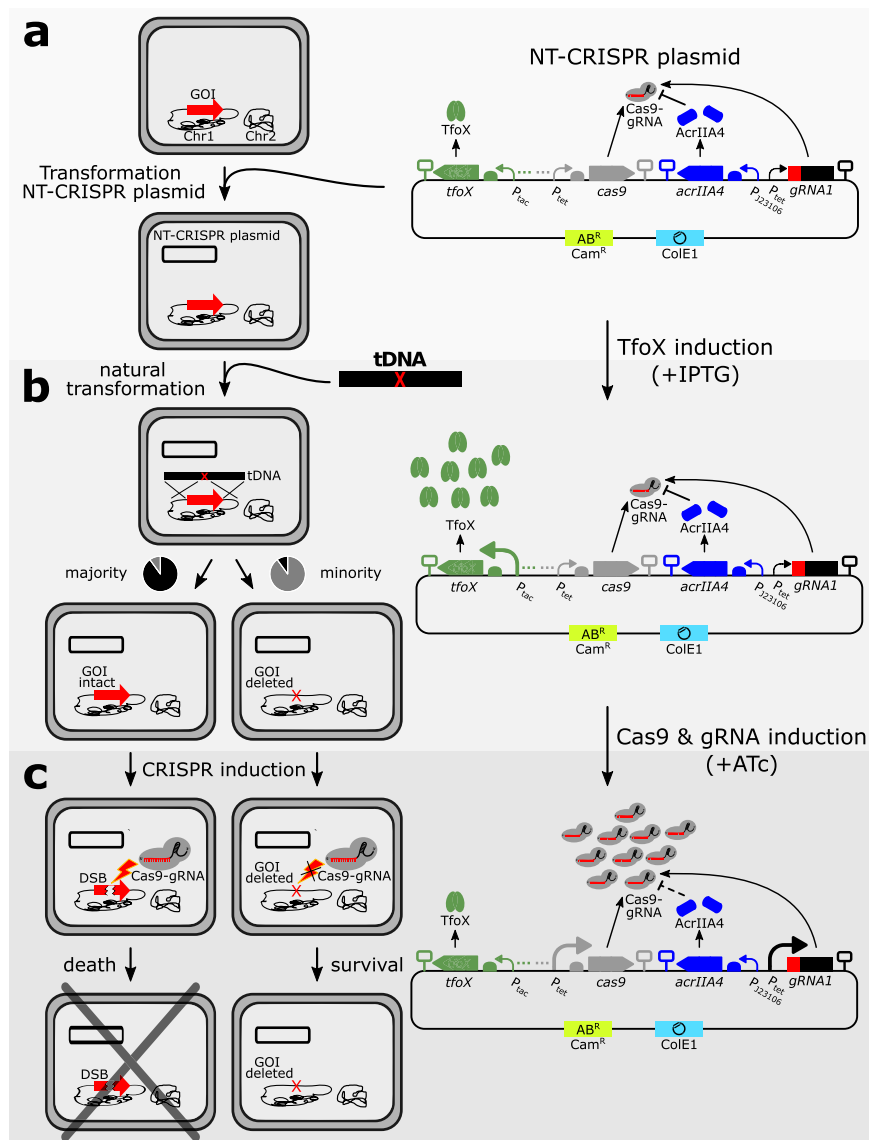


Fig. 1 Overview of the NT-CRISPR workflow. NT-CRISPR plasmid carries *tfoX* (P_{tac} , green), *cas9* (P_{tet} , gray), *acrIIA4* (J23106, blue) and gRNA, consisting of gRNA spacer (red) and scaffold (black), controlled by P_{tet} . The backbone carries a chloramphenicol resistance marker (Cam^R) and a ColE1 origin of replication. Increasing abundance and size of promoter indicate increased expression. SBOL symbols for omitted detail (three dots) represent the transcriptional unit for the regulatory proteins *Lacl* and *TetR* for P_{tac} and P_{tet} , respectively. **a** *V. natriegens* cells are transformed with the NT-CRISPR plasmid. The gene of interest (GOI) is indicated with a red arrow on chromosome 1 (black). **b** Expression of *tfoX* is induced by IPTG and tDNA is introduced. The tDNA is homologous to the sequences flanking the GOI. The majority of cells are not modified and the GOI stays intact, while a minority loses the GOI (red X). **c** Production of Cas9 and gRNA is induced by ATc. A DSB is introduced in wild type cells (discontinued red arrow) by Cas9-gRNA, leading to cell death. No DSB is introduced in genome edited cells, permitting survival.

gRNA gene to overcome the *acrIIA4* threshold causing DSB and cell death in cells with the wild type sequence. In contrast, modified cells are immune to CRISPR-Cas9 counterselection because the target sequence is no longer present in the genome (Fig. 1c). As a result, the counterselection step enriches successfully edited cells.

Inducible cell killing by CRISPR-Cas9. As described above, it is crucial for the NT-CRISPR method to tightly control CRISPR-Cas9 and induce cell death only upon induction. We reasoned that the ratio between *acrIIA4* and *cas9* expression strength is important. Expression of *acrIIA4* that is too weak might not be sufficient to compensate for the leaky *cas9* and *gRNA* gene expression, still leading to premature cell death. On the other hand, *acrIIA4* expression that is too strong, could prevent

efficient counterselection despite a full induction of the CRISPR-Cas9 system. To test a range of *acrIIA4* and *cas9* expression strengths, we created twelve plasmids representing the combinatorics of four different ribosome binding sites (RBS) for *acrIIA4* with three distinct RBS for *cas9*. The RBS used differ in their expression strengths which were recently quantified in *V. natriegens* with fluorescent reporter experiments³⁰. These variants were tested for their ability to trigger cell death upon addition of ATc as the inducer of Cas9 and gRNA production. We used a gRNA targeting the non-essential *wbfF* gene, which is involved in capsule polysaccharide biosynthesis³⁸. Combinations of different RBS for *cas9* and *acrIIA4* were tested to identify translation rates and consequently a protein stoichiometry which leads to efficient inducible cell killing. As a simple experiment, we cultivated cells in microplates and continuously measured OD₆₀₀ to track growth

of the cultures. To induce expression of *cas9* and the *gRNA* gene, ATc was added in a final concentration of 200 ng/mL to exponentially growing cells 1 h after the start of the batch cultivation. We observed a reduction in OD_{600} , indicating cell death about 1.5 h after ATc-mediated induction of *cas9* and the *gRNA* gene with ATc for all strains carrying plasmids using the moderately strong RBS B0032³⁰ for *acrIIA4* (Supplementary Fig. S1a). While the choice of the RBS for *acrIIA4* and consequently its expression strength, apparently has a strong impact on the inducibility of the CRISPR-Cas9 system, we found no difference between the three tested RBS for *cas9*, neither in this growth experiment in liquid culture (Supplementary Fig. S1a) nor in a separate agar plate-based assay which yielded counterselection efficiencies similar to those obtained applying the actual NT-CRISPR editing workflow (Supplementary Fig. S1b). Of the three variants that showed inducible cell killing in the growth experiment, we proceeded with plasmid pST_116, which carries the strongest of the three tested RBS for *cas9* B0033³⁰.

Dependence of gene deletion efficiencies on tDNA amount and homologous sequence length. We chose *wbfF* as a first target to demonstrate gene deletion by our NT-CRISPR-based approach in *V. natriegens* since deletion mutants of this gene show an almost transparent colony morphology²⁰. This phenotype allows for distinction between wild type and *wbfF* mutant colonies to conveniently calculate gene deletion efficiencies. We reproduced this phenotype by our approach using tDNA comprising 3 kb homologous sequences flanking the designed deletion of the *wbfF* coding sequence (1734 bp) (Fig. 2a). Subsequently, we characterized the genome editing efficiency dependent on the amount of tDNA supplied (1 ng, 10 ng or 100 ng) and on the induction state of the CRISPR-Cas9 system (Fig. 2b). We obtained almost 100% of all colonies with the transparent $\Delta wbfF$ morphology for all three DNA amounts tested when CRISPR-Cas9 was induced. This suggests a remarkably high editing efficiency of NT-CRISPR, even when just 1 ng of tDNA was used. However, in absence of counterselection we observed a decrease in the fraction of positive colonies with decreasing tDNA amounts (Fig. 2b). This is in accordance with a previous study describing natural transformation for genome engineering in *V. natriegens*²⁰. This trend also became apparent through the absolute number of positive colonies (CFU/ μ L) which decreased with lower amounts of tDNA for both the induced and uninduced samples (Supplementary Fig. S2a, b). With 100 ng of added tDNA and without counterselection, we still obtained ~20% of positive colonies (Fig. 2b), further supporting the potential of natural transformation for genome engineering in *V. natriegens*.

In a second experiment, we investigated the impact of different lengths of the homologous sequences of the tDNA on the success of genome editing with NT-CRISPR (Fig. 2c). When CRISPR-Cas9 was induced, we again obtained high editing efficiencies of at least 90% for all tested fragment lengths, with exception of the samples with 50 bp homologous flanks. More than 98% editing efficiency was achieved for 3000 bp and 1000 bp homologous flanks. However, a dependency of the efficiency of natural transformation on the length of the tDNAs is suggested by the fact that a lower absolute number of colonies with $\Delta wbfF$ mutant morphology (given as CFU/ μ L) was obtained for tDNAs with shortened homologous flanks. This was observed both with and without CRISPR-Cas9-based counterselection (Supplementary Fig. S2c, d). Decreases in putative $\Delta wbfF$ CFU/ μ L by ~40 fold and ~4 fold were observed when reducing the flanks from 3000 to 1000 bp and 1000 to 500 bp, respectively (Supplementary Fig. S2c). Further shortening the flanks down to 100 bp did not result in considerable additional drops in the number of putative $\Delta wbfF$ colonies (given as CFU/ μ L) (Supplementary

Fig. S2c). Note that a decreasing length of tDNAs correlates with an increasing number of molecules for 100 ng mass of tDNA. An almost constant number of colonies obtained for fragments with homologous flanks of 500 bp, 200 bp and 100 bp suggests that a possible reduction in uptake or recombination efficiency of shorter fragments is partly compensated by a higher concentration of tDNA molecules. Another result with potential practical implications is the high editing efficiency of ~90% obtained by NT-CRISPR with an asymmetric tDNA fragment with 3000 bp and 50 bp homologous sequence surrounding the deletion (Fig. 2c). This fragment can be easily generated in one PCR by adding the short 50 bp arm as an overhang to one of the PCR primers used to amplify the long arm. Applying such an asymmetric DNA fragment for natural transformation-mediated locus exchange by homologous recombination was successfully established for *V. cholerae*, but required the deletion of at least two ssDNA exonucleases to achieve reasonable editing efficiencies²⁰. If deletion of the orthologous ssDNA exonucleases in *V. natriegens* could even further increase the editing efficiency with short tDNA fragments remains unknown. Nonetheless, due to the highly efficient counterselection, asymmetrical tDNA fragments with one short arm might represent a convenient approach to introduce single gene deletions.

Collectively, the initial characterizations suggest that combining natural transformation with efficient, targeted CRISPR-Cas9-mediated counterselection considerably increases genome editing frequencies in *V. natriegens*. Moreover, even low amounts of tDNA like 1 ng and homologous flanks as short as 100 bp are sufficient to produce more than 90% correct colonies.

NT-CRISPR proof-of-concept for generating deletions of different lengths, point mutations and integrations in a set of target genes.

Inspired by these promising results, we sought to apply CRISPR-NT for various types of genome edits and to expand the set of chromosomal target sequences for our proof-of-concept study in *V. natriegens*. We assembled NT-CRISPR plasmids with 15 different gRNAs targeting a range of different sequences, both on chromosome 1 and 2. The reason behind selecting these genes is described below. In order to quantify the “killing efficiency” of the respective gRNAs, we performed the NT-CRISPR protocol without addition of tDNA. Samples were either induced with ATc to induce CRISPR-Cas9-based counterselection or remained uninduced. The ratios of the resulting CFU/ μ L allows for calculation of killing efficiency in the NT-CRISPR workflow. The shown gRNAs resulted in killing efficiencies within a narrow range between 99.9999% (*malQ*) and 99.964% (*vnp1*) (Fig. 2d). The value of the strongest tested gRNA that targeted *malQ* translates to the survival of just one out of 100,000 cells. A non-targeting gRNA was included as a control and resulted in a slight reduction of cells upon Cas9 and gRNA induction, possibly due to unspecific toxicity or protein production burden. An empty plasmid control ruled out negative effects of the inducer ATc at the applied concentration.

In the NT-CRISPR method, editing through natural transformation and CRISPR-Cas9-based counterselection occur in two temporally distinct steps. Consequently, with knowledge of the killing efficiency, it is possible to calculate the apparent editing efficiency from the initial editing efficiency before counterselection. The apparent editing efficiency is defined as the fraction of positive cells after counterselection. With a highly efficient gRNA even an initial editing efficiency of just 10^{-6} (one edited cell out of one million) was computed to result in 10^{-1} or 10% of all remaining cells being correct after counterselection (Fig. 2e). With the weakest shown gRNA, an initial editing efficiency of 10^{-3} (0.1%), which is far below the values obtained for simple deletions without counterselection (Fig. 2b), was calculated to be sufficient for

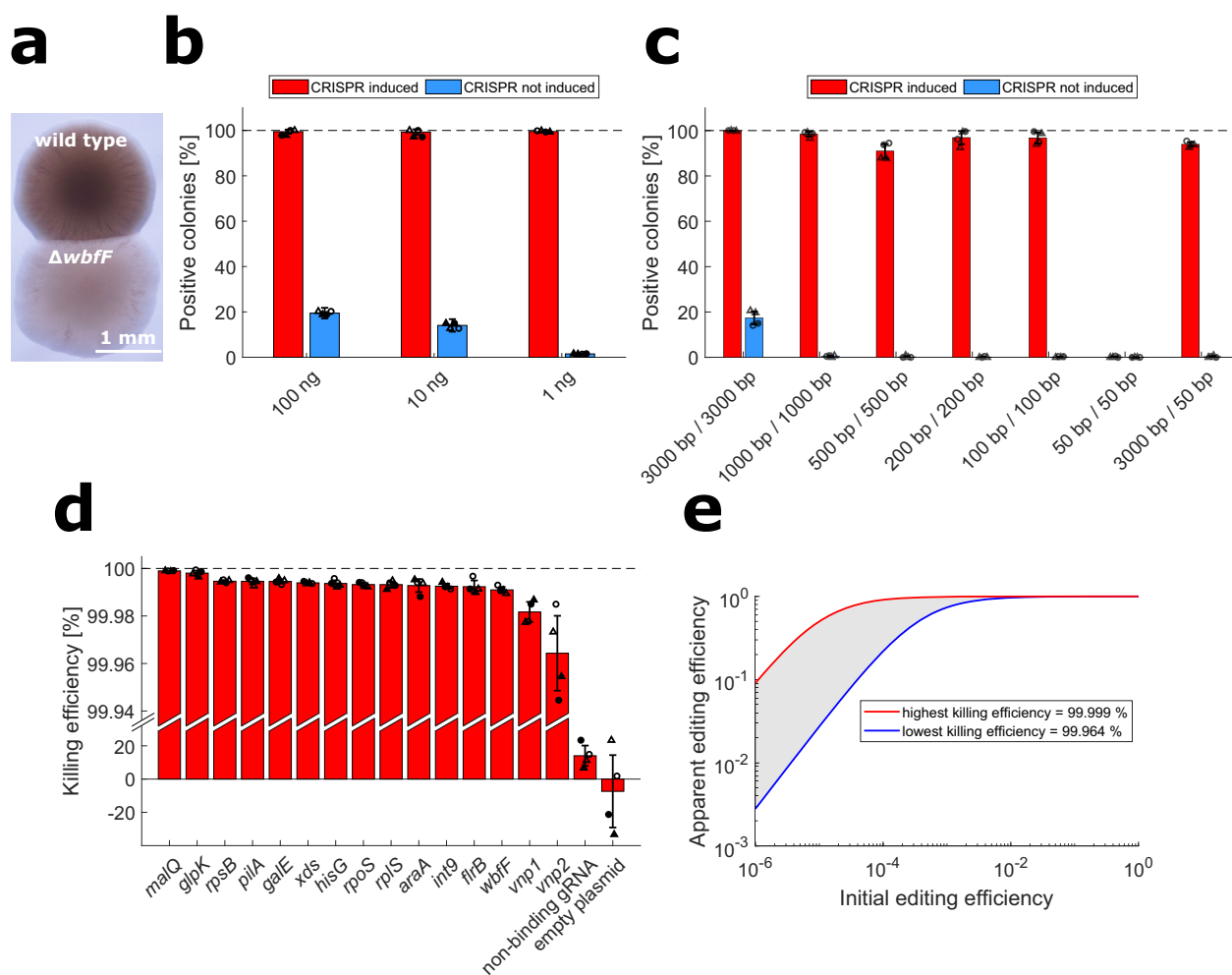


Fig. 2 Quantitative characterization of NT-CRISPR and killing efficiencies with different gRNAs. **a** Different morphologies of wild type and $\Delta wbff$ colonies. Image acquired with transmission light. **b** NT-CRISPR with different amounts of tDNA, targeting *wbff*. This experiment was performed with the indicated amount of tDNA with symmetrical 3 kb flanks upstream and downstream of the target sequence. Red and blue bars show results for samples with and without CRISPR-based counterselection, respectively. $n = 4$ replicates, representing two independent biological replicates (circle or triangle) and two independent experiments (filled or open symbols). Underlying colony counts are provided in Supplementary Fig. S2a and b. **c** NT-CRISPR with different tDNA fragment lengths, targeting *wbff*. Red and blue bars show results for samples with and without CRISPR-based counterselection, respectively. This experiment was performed with 100 ng of tDNA and the respective fragment length. With the exception of the last bar, tDNA fragments are symmetrical with the same length for the upstream and downstream homologous sequence. $n = 4$ replicates, representing two independent biological replicates (circle or triangle) and two independent experiments (filled or open symbols). Underlying colony counts are provided in Supplementary Fig. S2c,d. **d** Results of killing assay for different gRNAs. Killing efficiency is calculated as follows: $\text{Killing efficiency}[\%] = 1 - \frac{\text{CFU}/\mu\text{L with counterselection}}{\text{CFU}/\mu\text{L without counterselection}} * 100$. $n = 4$ replicates, representing two independent biological replicates (circle or triangle) and two independent experiments (filled or open symbols). **b-d** Bars show the mean of all replicates and error bars indicate standard deviation of the mean. The dashed line indicates the highest possible value. **e** Calculation of apparent editing efficiency from initial editing efficiency. Initial editing efficiency describes a theoretical value, assuming no enrichment through counterselection against non-modified cells. Apparent editing efficiency provides the expected fraction of correct colonies after counterselection. The red and blue curves use the highest (*malQ*) and lowest (*vnp2*) killing efficiencies observed in Fig. 2d.

achieving apparent editing efficiencies of almost 100% through robust counterselection. Different gRNAs for the same gene should not influence the initial natural transformation-dependent editing step but might yield different counterselection efficiencies. Since we observed a very narrow range of killing efficiencies for the different gRNAs shown (Fig. 2d), we do not expect screening of gRNAs for enrichment of certain genetic modifications to be necessary, as long as the used gRNA is in principle functional and yields a killing efficiency approximately within the reported range.

Deletions. To demonstrate the applicability of NT-CRISPR for deletions, we selected single genes and groups of genes as targets whose loss might lead to an increased plasmid transformation

efficiency. So far, the tremendous potential of *V. natriegens* as a fast-growing strain for the selection and propagation of in vitro assembled plasmids is still hampered due to transformation efficiencies that are much lower than the ones observed for highly engineered *E. coli* strains³⁰. We targeted the two prophage regions *vnp1* and *vnp2*, as their removal leads to increased survival under osmotic stress conditions³⁹ which might be experienced by the cells during preparation of chemically competent cells. In addition, we chose *galE*, encoding an enzyme which provides precursors for the synthesis of lipopolysaccharides, because an increased plasmid transformation efficiency was reported for *galE* mutants of some Gram-negative bacteria, presumably due to the loss of cell surface structures which might impair plasmid uptake^{40,41}. Along the same line, we reasoned

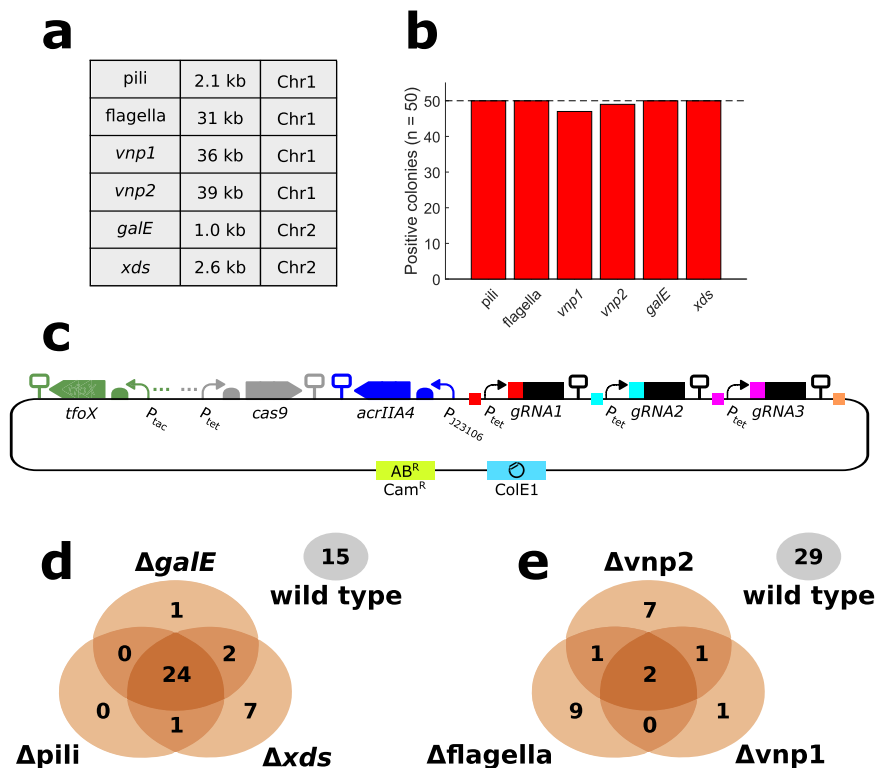


Fig. 3 Results of single and multiple deletions with NT-CRISPR. a Table providing information about deleted sequence. Locus tags of deleted genes are as follows: Pili (PN96_01310 - PN96_01315), flagella (PN96_02540 - PN96_02685), vnp1 (PN96_04290 - PN96_04520), vnp2 (PN96_06880 - PN96_07085), galE (PN96_22140), xds (PN96_19285). Chr1 = Chromosome 1, Chr2 = Chromosome 2. **b** Efficiency of deletions. Positive colonies were identified by PCR assays ($n = 50$ colonies). The dashed line indicates the highest possible value. **c** Visualization of NT-CRISPR plasmid carrying three gRNAs. Colored squares indicate matching fusion sites used for construction of this plasmid using Golden Gate Assembly. More details regarding the assembly of a multi gRNA NT-CRISPR plasmid is provided in Supplementary Fig. S5a,b. SBOL symbols for omitted detail (three points) represent the transcriptional unit for the regulatory proteins LacI and TetR for P_{tac} and P_{tet} , respectively. **d, e** Venn diagrams to visualize results of multigene deletions. Note that areas of ellipses and intersections are not proportional to the displayed values. Colonies of cells carrying none of the deletions are indicated with a separate ellipsis (gray). Results were obtained by PCR assays ($n = 50$ colonies). Plasmids used are pST_138 (**d**) and pST_137 (**e**).

that removal of other surface structures, namely the flagella and pili, could also contribute to increased transformation efficiency. Lastly, we included the gene coding for the extracellular nuclease Xds⁴², which could degrade the incoming plasmid DNA similarly to the Dns nuclease. Deletion of *dns* was already confirmed to drastically increase the plasmid transformation efficiency of chemically competent cells^{5,30}.

The target sequences for deletion described above span a wide range in size from 1.0 kb (*galE*) up to the prophage region of *vnp2* with 39 kb and are located on either chromosome 1 or chromosome 2 (Fig. 3a). To quantify the editing efficiency of each of these deletions, we analyzed 50 colonies by colony PCR. For all targets, except for the two prophage regions, all screened colonies were correct including the deletion of a flagellar gene cluster of 31 kb. Also, the prophage regions were deleted with 47 and 49 colonies out of 50 being correct, a remarkably high efficiency considering the size of 36 kb and 39 kb, respectively (Fig. 3b). We sequenced the target regions for four colonies per target and found the desired sequence in all clones, with a single exception. In case of *vnp1*, one clone missed four bp directly adjacent to the deleted sequence (Supplementary Fig. S3a). It was shown previously that the prophages are activated spontaneously at low frequencies³⁹. It is tempting to speculate that this deviation from the desired sequence is the result of a spontaneous loss of the prophage region, which would still confer resistance to the CRISPR-based counterselection, rather than the targeted deletion by natural transformation.

As described above, the targets for deletion were selected because we hoped that their deletion would improve plasmid

transformation efficiency of *V. natriegens*. We tested all single deletions but did not see any significant increase in transformation efficiency (Supplementary Fig. S4).

One feature of CRISPR-based systems is its inherent modularity. Simultaneous targeting of multiple sequences is possible by simply including multiple gRNAs (Fig. 3c). Assembly of a plasmid harboring all required components to target three different loci is achieved by firstly constructing the gRNA expression cassette and secondly by integrating them into a plasmid already carrying all remaining components (Supplementary Fig. S5a). We tested this approach by simultaneously deleting three of the genomic regions which could be efficiently removed individually. We obtained striking results for the simultaneous deletion of the pili operon, *xds* and *galE*, with 24 out of 50 tested colonies carrying all three deletions (Fig. 3d). As an even bigger challenge, we successfully deleted the flagellar gene cluster and both prophage regions simultaneously in two out of 50 colonies (Fig. 3e). The deleted regions sum up to 106 kb, equaling ~2% of the *V. natriegens* genome. We obtained these results using just 10 ng of each tDNA. For the simultaneous deletion of the pili operon, *xds* and *galE*, increasing the amount of tDNA to 100 ng for each target resulted in 44 out of 50 colonies (88%) carrying all three deletions (Supplementary Fig. S6). The killing efficiency with three gRNAs was found to be similar or slightly higher than that with the individual gRNAs (Supplementary Fig. S7), suggesting that undesired recombination events within the sequences identical in all gRNA expression cassettes (P_{tet} and gRNA scaffold) did not occur at perturbing frequencies. The current design allows construction of NT-CRISPR plasmids with two to five gRNAs (Supplementary Fig. S5b), even

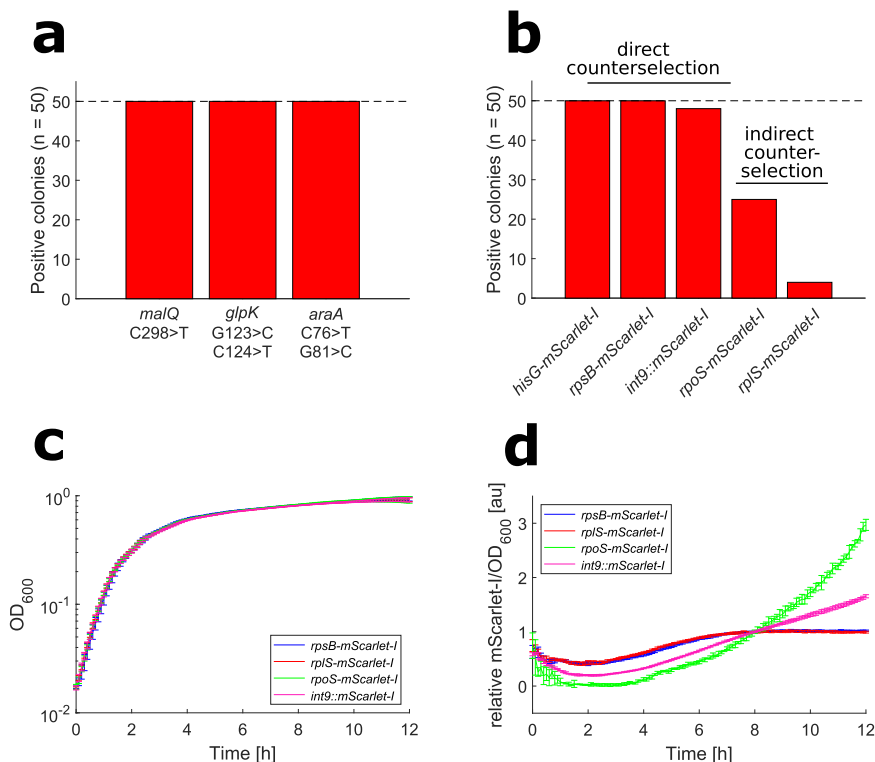


Fig. 4 Results of point mutations and integrations introduced by NT-CRISPR. a Efficiency of introducing point mutations. Targeted genes are *malQ* (PN96_15600, Chr1), *glpK* (PN96_01955, Chr1) and *araA* (PN96_16040, Chr2). Positive colonies refer to the ability to grow on the respective carbon source ($n = 50$ colonies). G > C mutation introduces a stop codon and C > T mutation (for *glpK* and *araA*) introduces a silent mutation as a C-C mismatch to evade mismatch repair. **b** Integration of mScarlet-I. mScarlet-I fused to 3' end of *hisG* (PN96_07800), *rpsB* (PN96_02260), *rpoS* (PN96_01115) and *rplS* (PN96_01280) and the integration of mScarlet-I with a constitutive promoter into one intergenic region between genes with locus tags PN96_06135 and PN96_06140, all on chromosome 1. Positive colonies were identified by PCR assays ($n = 50$ colonies). "Direct counterselection" describes counterselection through a gRNA overlapping the integration site, while "indirect counterselection" refers to the selection through a silent point mutation ~300 bp upstream of the integration site. **c** Growth curves of translational fusions and strain with integrated constitutive mScarlet-I cassette. $n = 8$ replicates, representing four independent biological replicates and two independent experiments. Curves show the mean of all replicates and error bars indicate standard deviation of the mean. **d** Normalized mScarlet-I signal. mScarlet-I/OD₆₀₀ was normalized by value at timepoint 8 h to compensate for different mScarlet-I signals. Underlying data without normalization is shown in Supplementary Fig. S9. $n = 8$ replicates, representing four independent biological replicates and two independent experiments. Curves show the mean of all replicates and error bars indicate standard deviation of the mean.

though we note that successful deletion of more than three loci was not demonstrated within the scope of this study.

Point mutations. In addition to deletions, we tested NT-CRISPR for the introduction of point mutations. The three genes, *malQ*, *araA* and *glpK*, involved in catabolism of the alternative carbon sources maltose, arabinose and glycerol, respectively, were chosen as proof-of-concept targets for the introduction of point mutations. The introduction of a premature stop codon by a single point mutation can be easily identified because this prevents *V. natriegens* from growing on minimal medium with the respective carbon source. In case of *malQ*, we randomly selected 50 colonies yielded by the NT-CRISPR approach and tested them for their ability to grow on M9 minimal medium with maltose as the sole carbon source. None of the tested colonies could grow indicating successful genome modification (Fig. 4a). Subsequently, the target sequence of four colonies was sequenced and the introduction of the desired point mutation was confirmed for all tested colonies. In case of *araA* and *glpK*, a first attempt to introduce a point mutation was not successful and resulted in very few colonies, none of them carrying the desired edit (Supplementary Fig. S8a, b). High editing efficiency of 100%, based on the inability of cells from the tested colony to grow on minimal medium with the respective carbon source, could be achieved by introducing a second silent point mutation, leading to a C-C mismatch (G>C mutation) (Fig. 4a). It

was shown previously that *V. natriegens* has an active methyl-directed mismatch repair (MMR) pathway, preventing the efficient introduction of point mutations by natural transformation²⁰. It is known that C-C mismatches inhibit MMR in a wide range of other organisms^{43–45}. Our data suggest that this is also the case in *V. natriegens*. The approach to introduce a C-C mismatch in addition to the desired mutation can serve as a convenient solution when MMR hinders successful introduction of certain point mutations. Again, we confirmed the point mutations as well as the additional C-C mismatch by sequencing the target regions of *glpK* and *araA* (Supplementary Fig. S3b, c).

Integrations. Lastly, we wanted to test if NT-CRISPR is also applicable for integrations into the genome. The approach presented here could be a powerful tool to fuse fluorescent reporter genes to any gene of interest to study their expression or the localization of their gene product. We selected genes that are expected to differ in expression during different growth phases in a batch culture to follow their expression dynamics by measuring the reporter signal. We fused the coding region of the red fluorescent protein mScarlet-I⁴⁶ to the 3' end of four genes which are known to be differentially regulated during transition into and in the stationary phase of *E. coli*. As candidates for genes with high expression level in the exponential growth phase, we chose two ribosomal protein-encoding genes. We picked *rpsB* and *rplS* because fusion of

fluorescent reporter proteins to the respective ribosomal proteins was possible in *E. coli* without noticeable detrimental effects on growth or ribosome assembly⁴⁷. We chose *hisG*, involved in histidine biosynthesis⁴⁸, and *rpoS*, encoding the stress sigma factor σ^{38} ⁴⁹, as candidates for genes upregulated in stationary phase. A control strain was generated by first creating an mScarlet-I transcription unit with a strong constitutive promoter (J23111) and a strong RBS (B0030). Then this construct was integrated into an intergenic region with neighboring genes in convergent orientation (int9).

Counterselection for successful integration can be performed through a gRNA, which overlaps the integration site so that successful modification disrupts the gRNA binding sequence and thereby confers resistance against CRISPR-based counterselection. In case of *rpoS* and *rplS*, no suitable PAM sequence was available at the desired integration site. As a workaround, we introduced a silent point mutation 300 bp from the integration site. This point mutation was used for the counterselection, expecting the integration of mScarlet-I when the silent point mutation was present. For each integration, 50 randomly selected colonies were screened by colony PCR. When a gRNA was available for direct counterselection at the integration site, we reliably obtained high editing efficiencies with almost all tested colonies being correct (Fig. 4b). In contrast, for *rpoS* and *rplS*, editing efficiencies were drastically lower with just 25 and four out of 50 colonies carrying the desired mScarlet-I integration, respectively. Sequencing DNA from four colonies each, which were negative in the PCR screening, revealed that all clones carried the selected silent point mutation, suggesting that not the full-length tDNA fragment was incorporated through homologous recombination. It remains to be investigated if introduction of the silent point mutation closer to the actual integration site than the 300 bp tested here, might lead to a higher editing efficiency. We additionally note that the size of the integrated sequence is relatively short with ~700 bp and ~1300 bp for the translational fusions with mScarlet-I and the integration of the constitutive expression cassette, respectively. Within the scope of this project, we did not evaluate if larger sequences, e.g., sequences encoding full metabolic pathways, can be integrated with similar efficiencies. The generated constructs were tested for their growth behavior and mScarlet-I signal. No growth

difference was observed between all tested strains (Fig. 4c). This is also the case for the two strains carrying mScarlet-I fusions to the essential ribosomal genes *rpsB* and *rplS*²⁸, which is in accordance with similar experiments in *E. coli*⁴⁷. The mScarlet-I signal of the tested strains showed the expected growth phase dependency. The *rpsB*-mScarlet-I and *rplS*-mScarlet-I strains displayed almost identical courses of fluorescent signal, suggesting a very similar regulation of both ribosomal protein genes. Both strains showed a steady increase in reporter-mediated fluorescence signal in the time window between 2 and 6 h, before reaching a plateau. In contrast, the *rpoS*-mScarlet-I strain showed an increasing signal after 4 h with an even steeper rise after 6 h. A constant increase from the onset of the stationary phase (~2 h) and throughout the stationary phase was observed for the strain carrying the constitutively expressed mScarlet-I cassette (Fig. 4d). The data are shown as relative mScarlet-I/OD₆₀₀ to account for strong differences in the absolute signal strength (Supplementary Fig. S9). Unfortunately, the signal mediated by *hisG*-mScarlet-I was hardly measurable and did not allow for quantitative characterization (Supplementary Fig. S10a, b). The results presented here serve as an example of how NT-CRISPR can be used for the construction of reporter strains to study the regulation of important physiological processes.

Overcoming PAM dependency with engineered Cas9. The use of Cas9 is limited by the availability of the PAM sequence, NGG (*N* = any nucleotide) in case of the commonly used Cas9 from *Streptococcus pyogenes*. While there are always plenty of possible gRNAs available for larger deletions, introduction of specific point mutations or genomic integrations into a desired locus might be restricted when no PAM can be found nearby, thus requiring inefficient workaround solutions (see generation of *rpoS*-mScarlet-I and *rplS*-mScarlet-I above). In recent years, substantial progress has been made in developing new Cas9 variants with a wider PAM spectrum^{50–52}. We tested the near-PAMless Cas9 variant SpG Cas9⁵¹ with the PAM requirement being NGN. In theory, each G and C nucleotide in the genome can serve as a PAM, thereby largely expanding the number of available gRNAs.

We introduced the described mutations into the *cas9* sequence in the NT-CRISPR plasmid and tested it with gRNAs targeting *wbfF* with all possible PAM doublet pairs (NGG, NGA, NGC and

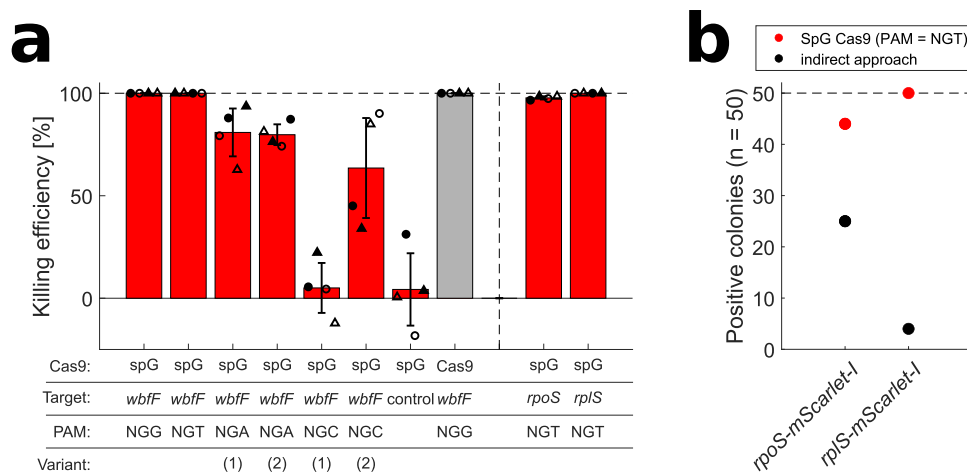


Fig. 5 Testing compatibility of near PAM less spG Cas9 in NT-CRISPR. a Killing efficiency with spG Cas9 with all possible PAM sequences. Cas9 with NGG PAM is shown as a reference in gray. Killing efficiency is calculated as follows: Killing efficiency[%] = $1 - \frac{\text{CFU}/\mu\text{L with counterselection}}{\text{CFU}/\mu\text{L without counterselection}} * 100$. *n* = 4 replicates, representing two independent biological replicates (circle or triangle) and two independent experiments (filled or open symbols). Bars show the mean of all replicates and error bars indicate standard deviation of the mean. The dashed line indicates the highest possible value. **b** Efficiency for integration of mScarlet-I using either SpG Cas9 with a NGT PAM sequence or using the indirect approach described above. Integration of mScarlet-I was identified by PCR assays (*n* = 50 colonies).

NGT). The *wbfF* gRNA with a NGG PAM showed similar killing efficiencies when used with Cas9 and SpG Cas9, confirming the general compatibility of SpG Cas9 with NT-CRISPR. The tested gRNAs with alternative PAM sequences showed a wide range of killing efficiencies from 99.993% (NGT) and no significant effect for (NGC) (Fig. 5a). We note that other determinants, apart from the PAM sequence, can influence the killing efficiency and the limited number of tested gRNAs does not allow for formulation of general claims about the applicability of SpG Cas9 with alternative PAMs in the framework of NT-CRISPR in *V. natriegens*. However, it appears as if the killing efficiencies were far lower than the obtained values for the many gRNAs tested before with NGG PAMs in our study (cf. Figure 2d), except for the tested gRNA using NGT as a PAM. Based on the high killing efficiency which we observed with a gRNA using NGT as a PAM, we designed two additional gRNAs overlapping the 3' end of *rpoS* and *rplS* and also measured high killing efficiencies for these (Fig. 5a). Thereafter, we used SpG Cas9 together with these two gRNAs for the integration of *mScarlet-I* at the 3' end of *rpoS* and *rplS*. For 50 randomly selected colonies, successful *mScarlet-I* integration was confirmed for 44 and 50 colonies for *rpoS* and *rplS*, respectively, compared to 25 and 4 for the indirect approach described above (Fig. 5b). In conclusion, the killing efficiency with SpG Cas9 and alternative PAM sequences tends to be lower than Cas9 with NGG PAMs. Nevertheless, our results suggest that applying SpG Cas9 together with gRNAs using NGT as a PAM could be a suitable strategy for the integration of sequences when no gRNA with NGG is available at the desired target sequence.

Conclusion

In this study, we developed NT-CRISPR which builds on the previous application of natural transformation for genome engineering in *V. natriegens*²⁰ by adding a CRISPR-Cas9-based counterselection step. With killing efficiencies of up to 99.999%, most genomic modifications, including deletions, integrations and point mutations, can be performed with almost 100% efficiency. As one highlight, we demonstrate the simultaneous deletion of multiple genes through the expression of multiple gRNAs directed against different target sequences. The NT-CRISPR workflow can be performed in a standard working day. The full process, including preparation of tDNAs and cloning of gRNAs as well as curing of the NT-CRISPR plasmid after successful genome modification, can be achieved in one week (Fig. 6a). The efficiency of plasmid curing is extremely high with an average of ~95% of colonies consisting of cells which have lost the NT-CRISPR plasmid after plating the culture from a single cultivation step in antibiotic free medium (Fig. 6b). Edits with this method can be performed with single-base precision, without the — transient or permanent — integration of antibiotic resistance markers, and do not leave any undesired scars in the genome. The major limitation of this method is its PAM dependency which might restrict access to some sequences for modifications. We present two approaches to close this gap by either introducing a silent, selectable point mutations or by using SpG Cas9⁵¹ with alternative PAM sequences.

We are confident that this method will provide the growing *V. natriegens* community with a convenient and highly efficient

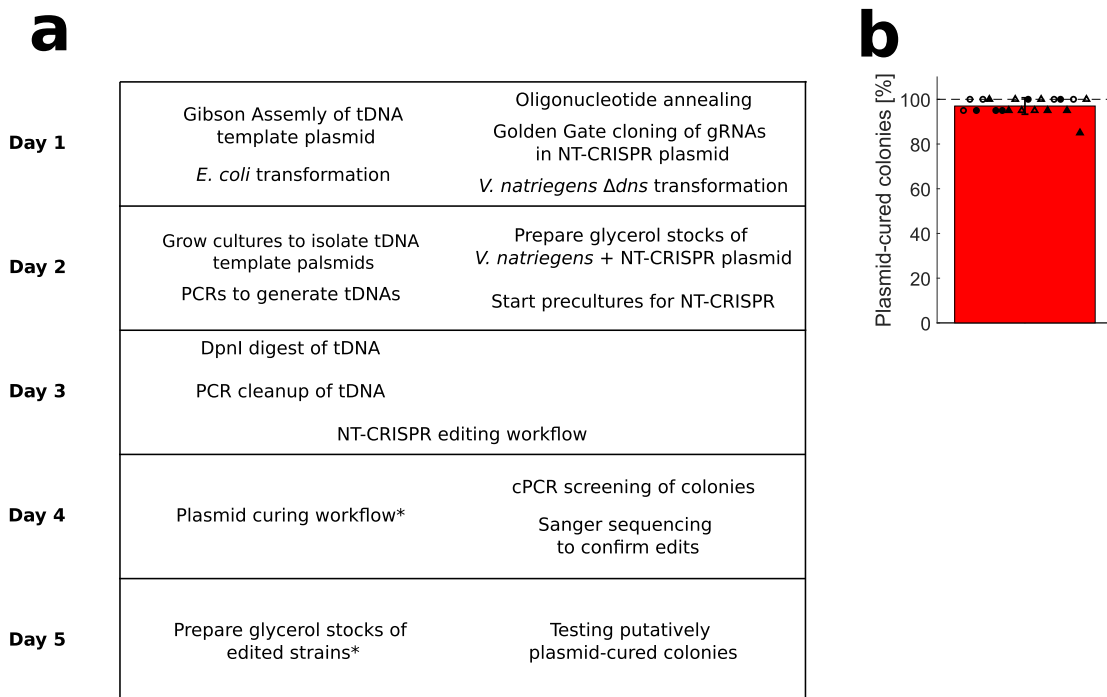


Fig. 6 Timetable of full NT-CRISPR procedure and plasmid curing. **a** Under ideal conditions, eight to ten hours per day are sufficient to go from preparation of tDNAs and cloning of gRNAs into the NT-CRISPR plasmid to a plasmid-cured edited strain in one week (Monday to Friday). Steps marked with asterisks (verification of edits by cPCR and Sanger sequencing, as well as the confirmation of plasmid loss after plasmid curing) can be performed in parallel with the next steps. To increase success rate, multiple colonies can be used for the consecutive step and later be discarded if verification yields negative results. Details for all individual steps can be found in the Method sections. **b** Plasmid curing efficiency. The workflow was performed as described in the Method sections with colonies resulting from deletion of *wbfF* with NT-CRISPR. $n = 20$ replicates, representing five *wbfF* deleted colonies of two transformants of the NT-CRISPR plasmid (circle or triangle) and two independent experiments (filled or open symbols). The bar shows the mean of all replicates and the error bar indicates the standard deviation of the mean. The reported fraction of plasmid-cured colonies is the result of streaking 20 colonies of each replicate on LBv2 agar plates with and without chloramphenicol. Colonies resulting in growth on LBv2 agar plates without but not with chloramphenicol were considered to consist of cells that have lost the NT-CRISPR plasmid. Fotos of streaked colonies are shown in Supplementary Fig. S11.

genome engineering tool. It sets the foundation for sophisticated strain engineering projects to exploit the fascinating properties of *V. natriegens* for academic and industrial applications in the future.

Furthermore, natural transformation is a commonly used strategy for genome engineering in a wide range of biotechnologically and clinically relevant bacteria, e.g., *Bacillus subtilis*⁵³, *Vibrio cholerae*⁵⁴, *Vibrio fischeri*⁵⁵, *Streptococcus thermophilus*⁵⁶, and *Streptococcus mutans*⁵⁷. The NT-CRISPR method described here for *V. natriegens* could serve as a blueprint to upgrade existing natural transformation approaches with CRISPR-Cas9-based counterselection to accelerate research in these important organisms.

Methods

Bacterial strains and culture conditions. The *V. natriegens* strain used for this study is a derivative of ATCC14048 with deletion of the *dns* gene, constructed in a previous project for increased plasmid transformation efficiency³⁰. *V. natriegens* was routinely grown in LBv2⁵ medium with added chloramphenicol if appropriate. Chloramphenicol was added with a final concentration of 4 µg/mL for liquid and 2 µg/mL for solid medium.

Strains were prepared for long term storage at -80 °C by growing cultures for 6–8 h at 37 °C and mixing 700 µL of grown cultures with 700 µL of 50% glycerol. We found that the additional washing step reported previously^{19,30} is not required when cultures are not grown into deep stationary phase (e.g., overnight at 37 °C).

Preparation of chemically competent *V. natriegens* cells and heat-shock transformation.

Preparation of chemically competent cells and heat-shock transformation was performed as described before³⁰. A preculture of *V. natriegens* ATCC14048 Δdns was inoculated from a glycerol stock and grown overnight at 37 °C and 220 rpm. At the next day 125 mL of preheated LBv2 medium (37 °C) was inoculated with the overnight culture to a final OD₆₀₀ of 0.01 in a 1 L baffled shake flask. This culture was grown at 200 rpm (37 °C) until an OD₆₀₀ between 0.5 and 0.7 was reached. The culture was then transferred to pre-cooled 50 mL falcon tubes and incubated on ice for 10 min, followed by centrifugation for 10 min at 3000 × g at 4 °C. The supernatant was discarded, and the pellets were resuspended in 40 mL cold TB buffer per 125 mL bacterial culture (TB buffer: 10 mM Pipes, 15 mM CaCl₂, 250 mM KCl, pH adjusted to 6.7 with KOH, then add 55 mM MnCl₂, filter sterilized). The cells were again incubated on ice for 10 min and further centrifuged for 10 min at 3000 × g at 4 °C. The supernatant was removed and pellets were resuspended in 5 mL cold TB buffer per 125 mL starting culture and consolidated in a single falcon tube, before adding 350 µL dimethyl sulfoxide. After another 10 min incubation on ice, 50 µL aliquots were prepared in 1.5 mL tubes and snap frozen in liquid nitrogen. Aliquots were stored at -80 °C until further use.

Chemically competent *V. natriegens* ATCC14048 Δdns cells were transformed by adding DNA to an aliquot of competent cells and incubated on ice for 30 min. After 30 min, cells were heat shocked in a water bath at 42 °C for 45 s then immediately incubated on ice for 10 min before recovery. The cells were recovered in 1 mL warm LBv2 medium, shaking at 37 °C for 1 h at 700 rpm. After recovery, the cells were pelleted by centrifugation at 3000 × g for 1 min, the supernatant was decanted and the pellet was resuspended in the remaining ~50 µL residual medium. The whole volume was plated on 37 °C warm LBv2 plates containing the appropriate antibiotic and incubated overnight at 37 °C.

Construction of NT-CRISPR plasmids. Plasmids were constructed within the framework of the Marburg Collection, a recently published Golden Gate-based cloning toolbox for *V. natriegens*³⁰. Part sequences and detailed description of plasmid assembly are provided in Supplementary Data and Supplementary Table 1, respectively. Assembly of the plasmids was performed in *E. coli* NEB Turbo, with the exception of the exchange of gRNA spacer sequences, as the resulting plasmids are intended for experiments in *V. natriegens*. Adaptation for different target sequences was achieved by replacing a sfGFP dropout fragment with the gRNA spacer sequence by annealing two complementary oligonucleotides. If not indicated otherwise, pST_116 was used for plasmids carrying single gRNAs with Cas9 and pST_140 whenever spG Cas9 was used. Annealing reaction was set up by mixing 1.5 µL of each oligonucleotide (100 µM) with 5 µL T4-DNA ligase buffer (Thermo Scientific) in a total reaction volume of 50 µL. Reactions are incubated in a heat block at 95 °C for 15 min, before switching off the heat block for slowly cooling down the samples to room temperature (~1 h). Cloning reaction with the NT-CRISPR plasmids was set up with ~200 ng of the respective plasmid, 3 µL annealed oligonucleotides, 0.5 µL of T4-DNA Ligase (5 Weiss U/µL, Thermo Scientific) and BsaI (10 U/µL) and 1 µL T4-DNA ligase buffer in a total reaction volume of 10 µL. Reactions were run in a thermocycler with 30 cycles of 37 °C (2 min) and 16 °C (5 min), followed by a final digestion step at 37 °C for 30 min and an enzyme denaturation step at 80 °C for 10 min. Transformation of *V. natriegens* was performed with 5 µL of the cloning reactions by heat-shock transformation. Sequences

of oligonucleotides are provided in Supplementary Data. Two colonies from each transformation plate were used as biological replicates in each experiment. In case of NT-CRISPR plasmids carrying multiple gRNA sequences, each gRNA expression cassette was first constructed individually on plasmids carrying a kanamycin resistance marker. A range of these plasmids is available representing the available positions in a level 2 plasmid in the framework of the Marburg Collection³⁰. For this, the oligonucleotides for the respective spacers were annealed and the cloning reaction was set up as described for the NT-CRISPR plasmid above with the difference that ~70 ng of plasmid DNA was used. In a second step, those gRNA cassettes were integrated into plasmid pST_119, carrying all remaining components in a Golden Gate reaction performed as described above but with Esp3I (10,000 U/mL, NEB) instead of BsaI. The assembly of NT-CRISPR plasmids with multiple gRNAs is visualized in Supplementary Fig. S5a and b. The assembly of the separate gRNA expression cassettes as well as the multi gRNA NT-CRISPR plasmid were performed using *E. coli* as a chassis: The sequence was confirmed by Sanger sequencing and the plasmids were finally introduced into *V. natriegens* by heat-shock transformation.

Selection of gRNAs. gRNAs for NT-CRISPR were mostly designed using the in-built feature “Find CRISPR sites” in Geneious Prime (Version 2021.2.1.), which uses the algorithm described by Doench et al. 2014⁵⁸. Of the predicted gRNAs, the ones with a high predicted activity score were selected. gRNAs for three targets, namely *flrB* (flagella), *pilA* (pili) and *xds*, were initially designed for CRISPR interference applications, using the algorithm described by Calvo-Vallmañan et al. 2020⁵⁹. Those gRNAs yielded similar results in terms of killing efficiency (Fig. 2d) and editing efficiency (Fig. 3b) compared to gRNAs designed using Geneious Prime. This suggests that sufficiently efficient gRNAs for NT-CRISPR can be obtained through different algorithms. We note that two out of 17 gRNAs tested within the scope of this work did not appear to lead to CRISPR-based counterselection (Sequences for two *rhaA* targeting gRNAs in Supplementary Data).

Preparation of tDNAs. The tDNAs used for the natural transformation were prepared by first assembling a tDNA template plasmid using Gibson Assembly⁶⁰ and then use this plasmid in a PCR to generate the tDNA fragments. All tDNA template plasmids were generated with 3 kb homologous sequences. The part entry vector of the Marburg Collection, pMC_V_01 was used as a vector for most tDNA template plasmids. In some cases, we observed a strong toxicity of the cloned sequences and used the plasmid pMC_V_11, a low-to-medium copy derivative of pMC_V_01 with p15A instead of ColE1 as the origin of replication. All primer sequences used for assembly of the tDNA template plasmids and the subsequent PCR reactions are provided in Supplementary Data. The template was eliminated after the PCR reactions by addition of 1 µL DpnI (10,000 U/mL, NEB) to 25 µL PCR reactions and incubation at 37 °C for at least 1 h. Lastly, a PCR cleanup was performed with the E.Z.N.A Cycle Pure Kit (Omega Bio-Tex), according to manufacturer's instructions.

Natural Transformation with CRISPR-Cas9 counterselection (NT-CRISPR workflow).

Natural transformation was performed largely as described previously for *V. natriegens*²⁰ with the addition of an additional step for CRISPR-Cas9 mediated counterselection. Precultures were grown overnight (16–17 h) at 30 °C and 200 rpm in 5 mL LBv2 with 4 µg/mL chloramphenicol and 100 µM IPTG (Roth, CAS: 367-93-1) to induce *tfoX* expression. The natural transformation was started by adding 3.5 µL of the precultures (OD₆₀₀ ~9–11) to 350 µL sea salt medium (28 g/L (Sigma, S9883)) with 100 µM IPTG in a 1.5 mL reaction tube. Unless indicated otherwise, 10 ng of tDNA with 3 kb homologous flanks was added. Samples were briefly vortexed and then incubated statically at 30 °C for 5 h. In a subsequent step, 1 mL LBv2 without antibiotics was added to the cells. For CRISPR-Cas9 induction, 200 ng/mL ATc (Alfa Aesar, 13803-65-1) was added to the LBv2 medium. Tubes were mixed by inversion and incubated at 300 rpm and 30 °C for 1 h. 100 µL of appropriate dilutions (e.g., 10⁻³ for single deletions or 10⁻⁴ for uninduced controls) were plated on LBv2 agar plates with 2 µg/mL chloramphenicol. For CRISPR-Cas9 induction, 200 ng/mL ATc was added to the agar plates. For experiments without CRISPR-Cas9 induction, ATc was omitted from both the liquid medium and the agar plates. All experiments were performed with two biological replicates obtained from transformation of the gRNA cloning reaction in *V. natriegens* or the re-transformation of the multi-gRNA NT-CRISPR plasmid, previously assembled using *E. coli*.

Quantification of killing efficiencies in the NT-CRISPR workflow. Samples for assessing killing efficiencies were prepared as described above for the NT-CRISPR workflow but without addition of tDNAs. For each strain, two 1.5 mL reaction tubes were run in parallel, with and without CRISPR-Cas9 counterselection. To one tube, 200 ng/mL ATc was added to the LBv2 medium and for the preparation of LBv2 agar plates and the second tube was run in parallel without any ATc. The ratio between the obtained CFU/µL from these two samples was used to calculate the killing efficiency.

Verification of edits after NT-CRISPR. The approach used for the verification of colonies after NT-CRISPR differed between mutation types. For the quantitative

characterization of NT-CRISPR (Fig. 2b, c) with *wbfF* as the target, colonies with different morphologies were counted and used to calculate editing efficiencies. For all other targets, we tested 25 colonies from each biological replicate, resulting in 50 analyzed colonies. All deletions, apart from *wbfF*, were verified by PCR with one primer slightly outside of the homologous flank and the other primer binding at the junction of the deletion, bridging the gap between the upstream and downstream sequence flanking the deleted region. Integrations were screened using one primer outside of the homologous flanks and a second primer binding inside the mScarlet-I sequence. For increased throughput, PCRs were performed in 96-well plates. For this, colonies were used to inoculate 100 μ L LBv2 in 96-well round bottom plates and incubated at 1000 rpm in a 96-well plate shaker for 5–6 h to obtain densely grown cultures. Cells were harvested by centrifugation at 3000 \times g for 10 min. Medium was aspirated and cell pellets were resuspended in 100 μ L water. Cell lysis was achieved by floating the 96-well plate on a 95 $^{\circ}$ C water bath for 15 min. Lastly, 96-well plates were centrifuged again at 3000 \times g for 10 min and 1 μ L of the supernatant was used in 12.5 μ L PCR reactions with Taq polymerase (NEB) according to manufacturer's instructions. Point mutations were confirmed phenotypically by streaking the obtained colonies on M9 minimal medium agar plates with either glucose or the alternative carbon source. Colonies resulting in growth on M9 agar plates with glucose but not on plates with the respective secondary carbon source were considered as successfully edited. M9 agar plates were prepared (for 100 mL) by autoclaving H₂O (35.7 mL) together with 1.5 g agarose. Subsequently all remaining components were prewarmed to 60 $^{\circ}$ C and added to the autoclaved components as follows: 50 mL 2 \times M9 salts (Na₂HPO₄ (17 g/L), KH₂PO₄ (6 g/L), NaCl (1 g/L), NH₄Cl (2 g/L), sterile filtered), 10 mL NaCl (20 %), 4 mL carbon source (10 %), 200 μ L MgSO₄ (1 M), 100 μ L (CaCl₂). For all mutations, PCR results and phenotypic characterizations were confirmed by Sanger sequencing. Four colonies were used for each deletion, integration or point mutation. Sequencing was performed through Microsynth SeqLab using PCR fragments and a primer binding ~500 bp upstream of the respective modification. Primers used for PCR verification and sequencing are provided in Supplementary Data.

Plasmid curing. After verification of the modifications, the NT-CRISPR plasmid was cured. For this, colonies yielded by the NT-CRISPR method were used to inoculate 5 mL of antibiotic free LBv2 and grown at 37 $^{\circ}$ C for 6–7 h. To obtain single colonies, we plated 100 μ L of a 10⁻⁷ dilution, prepared in LBv2, on antibiotic free LBv2 agar plates. After overnight incubation at 37 $^{\circ}$ C, colonies were patched on LBv2 with and without 2 μ g/mL chloramphenicol to check for plasmid loss. Colonies growing on the antibiotic free agar plates but not on agar plates containing chloramphenicol were considered to consist of plasmid-cured cells. Glycerol stocks of plasmid-cured strains were prepared as described above.

Quantification of mScarlet-I signal of *V. natriegens* reporter strains. Quantitative reporter experiments were performed largely as described before for the characterization of genetic parts³⁰. First, material from glycerol stocks was resuspended in 50 μ L LBv2 and 5 μ L of the resulting suspension was used to inoculate 95 μ L of LBv2 in a flat bottom 96-well plate. Cells were incubated as precultures for 5.5–6 h (equating an overnight culture in similar workflows for *E. coli*) and then diluted 1:100 in fresh LBv2 to start the experiment in a Biotek Synergy H1 micro plate reader. Measurements were taken in 6 min intervals with a 3 min shaking step in double orbital mode and maximum speed occurring between measurements. The OD₆₀₀ was measured in “normal” mode with eight measurements per data point and 100 ms delay after plate movement. mScarlet-I fluorescence was measured with a focal height of 6.5 mm, excitation and emission wavelength of 579 nm and 616 nm, respectively, and a gain of 90. Strains were used after curing of the NT-CRISPR plasmid. Sample data were first corrected by subtracting the mean of four blank wells (LBv2 medium) from the sample measurements. Growth curves were computationally synchronized by aligning the first data point of each well with OD₆₀₀ > 0.015 and the mean of the OD₆₀₀ values of the aligned growth curves of all tested replicates and independent experiments was plotted. The relative mScarlet-I/OD₆₀₀ values were obtained by dividing all mScarlet-I/OD₆₀₀ values by the value of the respective sample at timepoint 8 h, to compensate for different absolute mScarlet-I signals.

Testing inducible cell killing in liquid medium in a micro plate reader. Material from glycerol stocks was first resuspended in 50 μ L LBv2 with chloramphenicol (4 μ g/mL). Subsequently, 95 μ L of medium in a 96-well plate was inoculated with 5 μ L from the resuspended glycerol stock material. This plate was incubated for 5–6 h at 37 $^{\circ}$ C. To begin the experiment, the precultures were diluted 1:1000 in fresh LBv2 medium with chloramphenicol with a final volume of 100 μ L per well. ATC was added to a final concentration of 200 ng/mL after 1 h of cultivation and the measurement was resumed. Experiments were performed in a Biotek Synergy H1 micro plate reader as described above but without measurement of fluorescence. Sample data were corrected by subtracting the mean of four blank wells (LBv2 medium) from the sample measurements.

Statistics and reproducibility. Biological replicates represent different levels within the NT-CRISPR workflow. Biological replicates of the 1st level represent independent colonies obtained after transformation of the NT-CRISPR plasmid and biological replicates of the 2nd level represents colonies obtained after successful genome modification with NT-CRISPR. Two 1st level replicates were used to characterize parameters of the NT-CRISPR method, namely editing efficiencies with different DNA amounts or

fragment lengths as well as to characterize killing efficiencies in liquid cultures and within the editing workflow. These experiments were repeated twice on different days to ensure biological and experimental reproducibility. Proof-of-concept experiments for deletions, point mutations and integrations were performed with two 1st level biological replicates and 25 colonies (2nd level) were screened for each replicate, resulting in a total of 50 tested colonies. Phenotypic characterization of strains with integration of mScarlet-I (translational fusion and constitutively expressed transcription unit) was performed with two colonies (2nd level) from each biological replicate of NT-CRISPR plasmid transformation (1st level), resulting in a total of four biological replicates. This experiment was repeated twice on different days to ensure biological and experimental reproducibility. Plasmid curing was quantified with five colonies after *wbfF* deletion (2nd level) from each biological replicate of NT-CRISPR plasmid transformation (1st level). This experiment was repeated twice on different days to ensure biological and experimental reproducibility.

Reporting summary. Further information on research design is available in the Nature Research Reporting Summary linked to this article.

Data availability

Genetic part sequences and descriptions of plasmid assemblies are provided in Supplementary Data and Supplementary Table 1, respectively. Sequences of all oligonucleotides used in this study are provided in Supplementary Data. All data used to generate the figures shown in this publication are provided as Supplementary Data. Additional source data are deposited in the figshare repository (<https://doi.org/10.6084/m9.figshare.17297132.v3>). Plasmid maps of NT-CRISPR plasmids and plasmids carrying the separate gRNA expression cassettes for assembly of multi-gRNA NT-CRISPR plasmids are available as Supplementary Data. Plasmids were submitted to Addgene (plasmid IDs 179332 to 179342) and are available from the authors upon reasonable request. Any other relevant data are available from the corresponding author upon reasonable request.

Code availability

Custom MATLAB Scripts used for data analysis and preparation of figures shown in this publication are provided as Supplementary Software 1. All MATLAB Scripts were confirmed to run on MATLAB version 2021b.

Received: 12 August 2021; Accepted: 8 February 2022;

Published online: 25 March 2022

References

- Eagon, R. G. Generation Time of Less Than 10 min *J. Bacteriol.* **83**, 736–737 (1962).
- Payne, W. J. Studies on bacterial utilization of uronic acids. III. Induction of oxidative enzymes in a marine isolate. *J. Bacteriol.* **76**, 301–307 (1958).
- Hoff, J. et al. *Vibrio natriegens*: an ultrafast-growing marine bacterium as emerging synthetic biology chassis. *Environ. Microbiol.* **22**, 4394–4408 (2020).
- Hoffart, E. et al. High substrate uptake rates empower *Vibrio natriegens* as production host for industrial biotechnology. *Appl. Environ. Microbiol.* **83**, 1–10 (2017).
- Weinstock, M. T., Heseck, E. D., Wilson, C. M. & Gibson, D. G. *Vibrio natriegens* as a fast-growing host for molecular biology. *Nat. Methods* **13**, 849–851 (2016).
- Aiyar, S. E., Gaal, T. & Gourse, R. L. rRNA promoter activity in the fast-growing bacterium *Vibrio natriegens*. *J. Bacteriol.* **184**, 1349–1358 (2002).
- Kato, J. & Hashimoto, M. Construction of consecutive deletions of the *Escherichia coli* chromosome. *Mol. Syst. Biol.* **3**, 132 (2007).
- Pósfai, G. et al. Emergent Properties of Reduced-Genome *Escherichia coli*. *Sci. (80-)*. **312**, 1044 LP–1041046 (2006).
- Lee, J. H. et al. Metabolic engineering of a reduced-genome strain of *Escherichia coli* for L-threonine production. *Microb. Cell Fact.* **8**, 2 (2009).
- Selas Castiñeiras, T., Williams, S. G., Hitchcock, A. G. & Smith, D. C. *E. coli* strain engineering for the production of advanced biopharmaceutical products. *FEMS Microbiol. Lett.* **365**, fny162 (2018).
- Isaacs, F. J. et al. Precise Manipulation of Chromosomes in Vivo Enables Genome-Wide Codon Replacement. *Sci. (80-)*. **333**, 348 LP–348353 (2011).
- Baba, T. et al. Construction of *Escherichia coli* K-12 in-frame, single-gene knockout mutants: the Keio collection. *Mol. Syst. Biol.* **2**, 2006.0008–2006.0008 (2006).
- Jiang, Y. et al. Multigene Editing in the *Escherichia coli* Genome via the CRISPR-Cas9 System. *Appl. Environ. Microbiol.* **81**, 2506 LP–2502514 (2015).
- Reisch, C. R. & Prather, K. L. J. The no-SCAR (Scarless Cas9 Assisted Recombineering) system for genome editing in *Escherichia coli*. *Sci. Rep.* **5**, 15096 (2015).

15. Wang, H. H. et al. Programming cells by multiplex genome engineering and accelerated evolution. *Nature* **460**, 894–898 (2009).
16. Maida, I. et al. Draft Genome Sequence of the Fast-Growing Bacterium *Vibrio natriegens* Strain DSMZ 759. *Genom. Announc.* **1**, e00648–13 (2013).
17. Wang, Z., Lin, B., Hervey, W. J. 4th & Vora, G. J. Draft Genome Sequence of the Fast-Growing Marine Bacterium *Vibrio natriegens* Strain ATCC 14048. *Genom. Announc.* **1**, e00589–13 (2013).
18. Lee, H. H., Ostrov, N., Gold, M. A. & Church, G. M. Recombineering in *Vibrio natriegens*. *bioRxiv* 130088 (2017) <https://doi.org/10.1101/130088>.
19. Lee, H. H. et al. *Vibrio natriegens*, a new genomic powerhouse. *bioRxiv* 58487 (2016) <https://doi.org/10.1101/058487>.
20. Dalia, T. N. et al. Multiplex Genome Editing by Natural Transformation (MuGENT) for Synthetic Biology in *Vibrio natriegens*. *ACS Synth. Biol.* **6**, 1650–1655 (2017).
21. Seitz, P. & Blokesch, M. Cues and regulatory pathways involved in natural competence and transformation in pathogenic and environmental Gram-negative bacteria. *FEMS Microbiol. Rev.* **37**, 336–363 (2013).
22. Johnsborg, O., Eldholm, V. & Håvarstein, L. S. Natural genetic transformation: prevalence, mechanisms and function. *Res. Microbiol.* **158**, 767–778 (2007).
23. Aparicio, T., de Lorenzo, V. & Martínez-García, E. CRISPR/Cas9-enhanced ssDNA recombineering for *Pseudomonas putida*. *Microb. Biotechnol.* **12**, 1076–1089 (2019).
24. Penewit, K. et al. Efficient and Scalable Precision Genome Editing in *Staphylococcus aureus* through Conditional Recombineering and CRISPR/Cas9-Mediated Counterselection. *MBio* **9**, e00067–18 (2018).
25. Jiang, W., Bikard, D., Cox, D., Zhang, F. & Marraffini, L. A. RNA-guided editing of bacterial genomes using CRISPR-Cas systems. *Nat. Biotechnol.* **31**, 233–239 (2013).
26. Cui, L. & Bikard, D. Consequences of Cas9 cleavage in the chromosome of *Escherichia coli*. *Nucleic Acids Res.* **44**, 4243–4251 (2016).
27. Shuman, S. & Glickman, M. S. Bacterial DNA repair by non-homologous end joining. *Nat. Rev. Microbiol.* **5**, 852–861 (2007).
28. Lee, H. H. et al. Functional genomics of the rapidly replicating bacterium *Vibrio natriegens* by CRISPRi. *Nat. Microbiol.* **4**, 1105–1113 (2019).
29. Meyer, A. J., Segall-Shapiro, T. H., Glassey, E., Zhang, J. & Voigt, C. A. *Escherichia coli* ‘Marionette’ strains with 12 highly optimized small-molecule sensors. *Nat. Chem. Biol.* **15**, 196–204 (2019).
30. Stukenberg, D. et al. The Marburg Collection: a Golden Gate DNA Assembly Framework for Synthetic Biology Applications in *Vibrio natriegens*. *ACS Synth. Biol.* (2021) <https://doi.org/10.1021/acssynbio.1c00126>.
31. Kim, I. et al. Solution structure and dynamics of anti-CRISPR AcrIIA4, the Cas9 inhibitor. *Sci. Rep.* **8**, 3883 (2018).
32. Yang, H. & Patel, D. J. Inhibition Mechanism of an Anti-CRISPR Suppressor AcrIIA4 Targeting SpyCas9. *Mol. Cell* **67**, 117–127.e5 (2017).
33. Aschenbrenner, S. et al. Coupling Cas9 to artificial inhibitory domains enhances CRISPR-Cas9 target specificity. *Sci. Adv.* **6**, eaay0187 (2020).
34. Shin, J. et al. Disabling Cas9 by an anti-CRISPR DNA mimic. *Sci. Adv.* **3**, e1701620 (2017).
35. Bubeck, F. et al. Engineered anti-CRISPR proteins for optogenetic control of CRISPR-Cas9. *Nat. Methods* **15**, 924–927 (2018).
36. Hoffmann, M. D. et al. Cell-specific CRISPR-Cas9 activation by microRNA-dependent expression of anti-CRISPR proteins. *Nucleic Acids Res.* **47**, e75 (2019).
37. Wasels, F., Chartier, G., Hocq, R. & Lopes Ferreira, N. A CRISPR/Anti-CRISPR Genome Editing Approach Underlines the Synergy of Butanol Dehydrogenases in *Clostridium acetobutylicum* DSM 792. *Appl. Environ. Microbiol.* **86**, e00408–e00420 (2020).
38. Bik, E. M., Bunschoten, A. E., Willems, R. J. L., Chang, A. C. Y. & Mooi, F. R. Genetic organization and functional analysis of the otn DNA essential for cell-wall polysaccharide synthesis in *Vibrio cholerae* O139. *Mol. Microbiol.* **20**, 799–811 (1996).
39. Pfeifer, E. et al. Generation of a Prophage-Free Variant of the Fast-Growing Bacterium *Vibrio natriegens*. *Appl. Environ. Microbiol.* **85**, e00853–19 (2019).
40. Van Die, I. M., Zuidweg, E. M., Bergmans, J. E. N. & Hoekstra, W. P. M. Transformability of *galE* variants derived from uropathogenic *Escherichia coli* strains. *J. Bacteriol.* **158**, 760–761 (1984).
41. Bursztyn, H., Sgaramella, V., Ciferri, O. & Lederberg, J. Transfectability of rough strains of *Salmonella typhimurium*. *J. Bacteriol.* **124**, 1630–1634 (1975).
42. Blokesch, M. & Schoolnik, G. K. The Extracellular Nuclease Dns and Its Role in Natural Transformation of *Vibrio cholerae*. *J. Bacteriol.* **190**, 7232 LP–7237240 (2008).
43. Su, S. S., Lahue, R. S., Au, K. G. & Modrich, P. Mispair specificity of methyl-directed DNA mismatch correction in vitro. *J. Biol. Chem.* **263**, 6829–6835 (1988).
44. Detloff, P., Sieber, J. & Petes, T. D. Repair of specific base pair mismatches formed during meiotic recombination in the yeast *Saccharomyces cerevisiae*. *Mol. Cell. Biol.* **11**, 737 LP–737745 (1991).
45. Meier, P. & Wackernagel, W. Impact of *mutS* inactivation on foreign DNA acquisition by natural transformation in *Pseudomonas stutzeri*. *J. Bacteriol.* **187**, 143–154 (2005).
46. Bindels, D. S. et al. mScarlet: a bright monomeric red fluorescent protein for cellular imaging. *Nat. Methods* **14**, 53–56 (2017).
47. Nikolay, R. et al. Validation of a fluorescence-based screening concept to identify ribosome assembly defects in *Escherichia coli*. *Nucleic Acids Res.* **42**, e100–e100 (2014).
48. Cavanagh, A. T., Chandransu, P. & Wassarman, K. M. 6S RNA regulation of *relA* alters ppGpp levels in early stationary phase. *Microbiology* **156**, 3791–3800 (2010).
49. Jaishankar, J. & Srivastava, P. Molecular Basis of Stationary Phase Survival and Applications. *Front. Microbiol.* **8**, 2000 (2017).
50. Kleinstiver, B. P. et al. Engineered CRISPR-Cas9 nucleases with altered PAM specificities. *Nature* **523**, 481–485 (2015).
51. Walton, R. T., Christie, K. A., Whittaker, M. N. & Kleinstiver, B. P. Unconstrained genome targeting with near-PAMless engineered CRISPR-Cas9 variants. *Sci. (80-.)* **368**, 290 LP–290296 (2020).
52. Hu, J. H. et al. Evolved Cas9 variants with broad PAM compatibility and high DNA specificity. *Nature* **556**, 57–63 (2018).
53. Vojcic, L., Despotovic, D., Martinez, R., Maurer, K.-H. & Schwaneberg, U. An efficient transformation method for *Bacillus subtilis* DB104. *Appl. Microbiol. Biotechnol.* **94**, 487–493 (2012).
54. Dalia, A. B., McDonough, E. & Camilli, A. Multiplex genome editing by natural transformation. *Proc. Natl Acad. Sci.* **111**, 8937 LP–8938942 (2014).
55. Visick, K. L., Hodge-Hanson, K. M., Tischler, A. H., Bennett, A. K. & Mastrodomenico, V. Tools for Rapid Genetic Engineering of *Vibrio fischeri*. *Appl. Environ. Microbiol.* **84**, e00850–18 (2018).
56. Blomqvist, T., Steinmoen, H. & Håvarstein, L. S. Natural genetic transformation: a novel tool for efficient genetic engineering of the dairy bacterium *Streptococcus thermophilus*. *Appl. Environ. Microbiol.* **72**, 6751–6756 (2006).
57. Morrison, D. A., Khan, R., Junges, R., Åmdal, H. A. & Petersen, F. C. Genome editing by natural genetic transformation in *Streptococcus mutans*. *J. Microbiol. Methods* **119**, 134–141 (2015).
58. Doench, J. G. et al. Rational design of highly active sgRNAs for CRISPR-Cas9-mediated gene inactivation. *Nat. Biotechnol.* **32**, 1262–1267 (2014).
59. Calvo-Villamañán, A. et al. On-target activity predictions enable improved CRISPR-dCas9 screens in bacteria. *Nucleic Acids Res.* **48**, e64–e64 (2020).
60. Gibson, D. G. et al. Enzymatic assembly of DNA molecules up to several hundred kilobases. *Nat. Methods* **6**, 343–345 (2009).

Acknowledgements

We thank Prof. Ankur B. Dalia for supplying plasmid pMMB-TfoX and Prof. Christopher A. Voigt for the Marionette Sensor Collection which was supplied through Addgene (Addgene Kit #100000137). Lastly, we thank Dr. Patrick Sobetzko and Marc Teufel for intense discussions throughout the project.

Author contributions

D.S., and A.B. conceived the design of this project. D.S. performed the majority of experiments. J.H. characterized transformation efficiency of mutant strains and A.F. constructed and tested inducible promoters used in the NT-CRISPR plasmid. D.S. analyzed the data. D.S. and A.B. wrote the paper. A.B. supervised the study. This work was funded by the State of Hesse (Germany) through the LOEWE research cluster MOSLA and the European Union through the BioRoboost project (H2020-NMBP-TR-IND-2018-2020/BIOTEC-01-2018 (CSA), Project ID 210491758). D.S. received funding through the International Max Planck Research School for Environmental, Cellular, and Molecular Microbiology (IMPRS-Mic).

Funding

Open Access funding enabled and organized by Projekt DEAL.

Competing interests

The authors declare no competing interests.

Additional information

Supplementary information The online version contains supplementary material available at <https://doi.org/10.1038/s42003-022-03150-0>.

Correspondence and requests for materials should be addressed to Anke Becker.

Peer review information *Communications Biology* thanks Dominik Niopek and the other, anonymous, reviewers for their contribution to the peer review of this work. Primary Handling Editors: Audrone Lapinaite and Caitlin Karniski.

Reprints and permission information is available at <http://www.nature.com/reprints>

Publisher's note Springer Nature remains neutral with regard to jurisdictional claims in published maps and institutional affiliations.



Open Access This article is licensed under a Creative Commons Attribution 4.0 International License, which permits use, sharing, adaptation, distribution and reproduction in any medium or format, as long as you give appropriate credit to the original author(s) and the source, provide a link to the Creative Commons license, and indicate if changes were made. The images or other third party material in this article are included in the article's Creative Commons license, unless indicated otherwise in a credit line to the material. If material is not included in the article's Creative Commons license and your intended use is not permitted by statutory regulation or exceeds the permitted use, you will need to obtain permission directly from the copyright holder. To view a copy of this license, visit <http://creativecommons.org/licenses/by/4.0/>.

© The Author(s) 2022

NT-CRISPR, combining natural transformation and CRISPR-Cas9 counterselection for markerless and scarless genome editing in *Vibrio natriegens*

Daniel Stukenberg^{1,2,3}, Josef Hoff^{1,3}, Anna Faber^{1,2}, and Anke Becker^{1,2*}

¹Center for Synthetic Microbiology, Philipps-Universität Marburg, Marburg, Germany

²Department of Biology, Philipps-Universität Marburg, Marburg, Germany

³Max-Planck Institute for Terrestrial Microbiology, Marburg, Germany

*For correspondence: anke.becker@synmikro.uni-marburg.de

Contents

Supplementary Figure S1 - Stoichiometry of Cas9 and AcrIIA4 is essential for inducible cell killing.

Supplementary Figure S2 - Underlying CFU/ μ L for Figure 2B and 2C

Supplementary Figure S3 - Sequencing results of $\Delta vnp1$ strains

Supplementary Figure S4 - Transformation efficiency of deletion strains

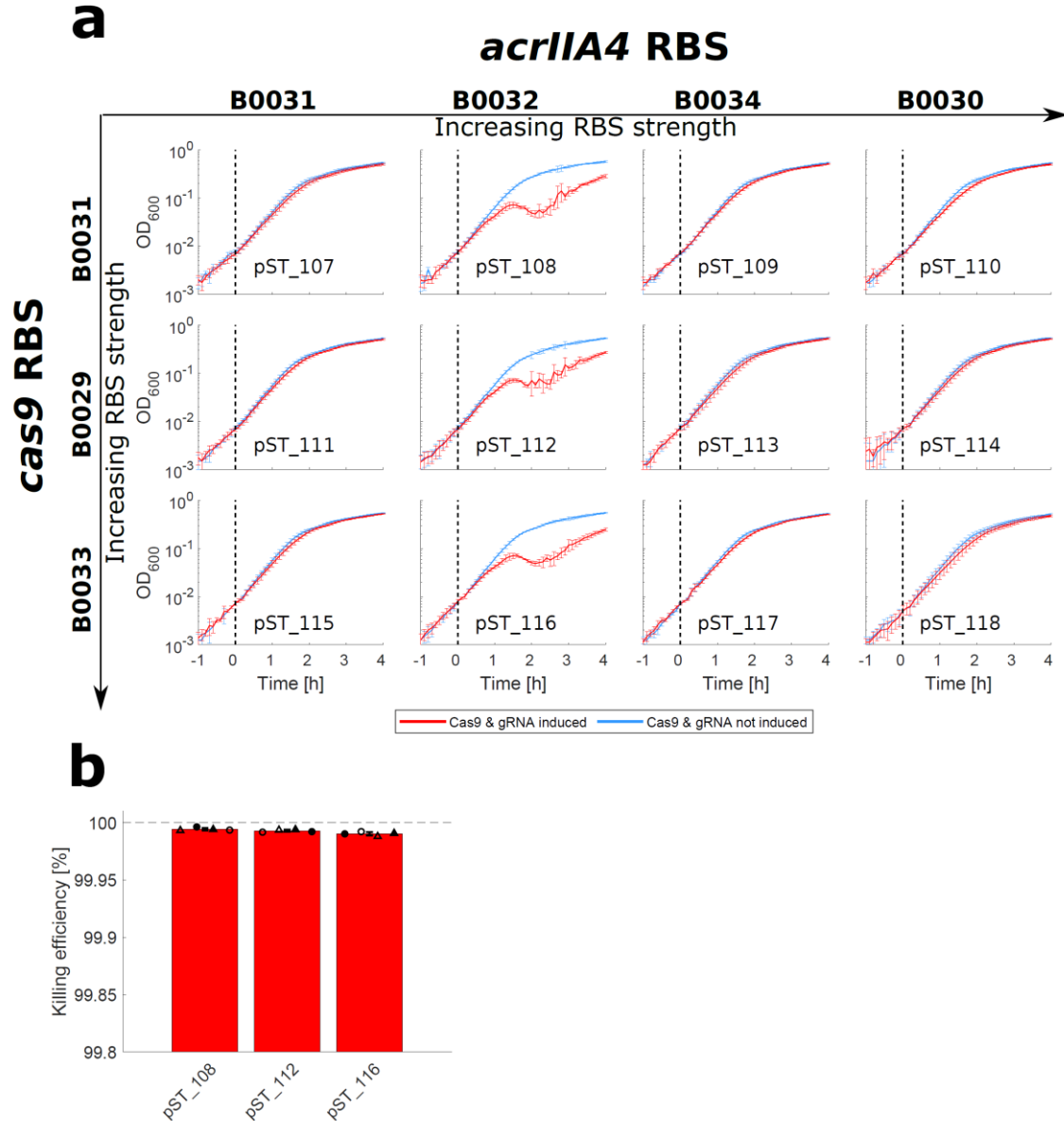
Supplementary Figure S5 - Assembly of NT-CRISPR plasmid with multiple gRNAs

Supplementary Figure S6 - Killing assay with strains carrying plasmids with three gRNAs

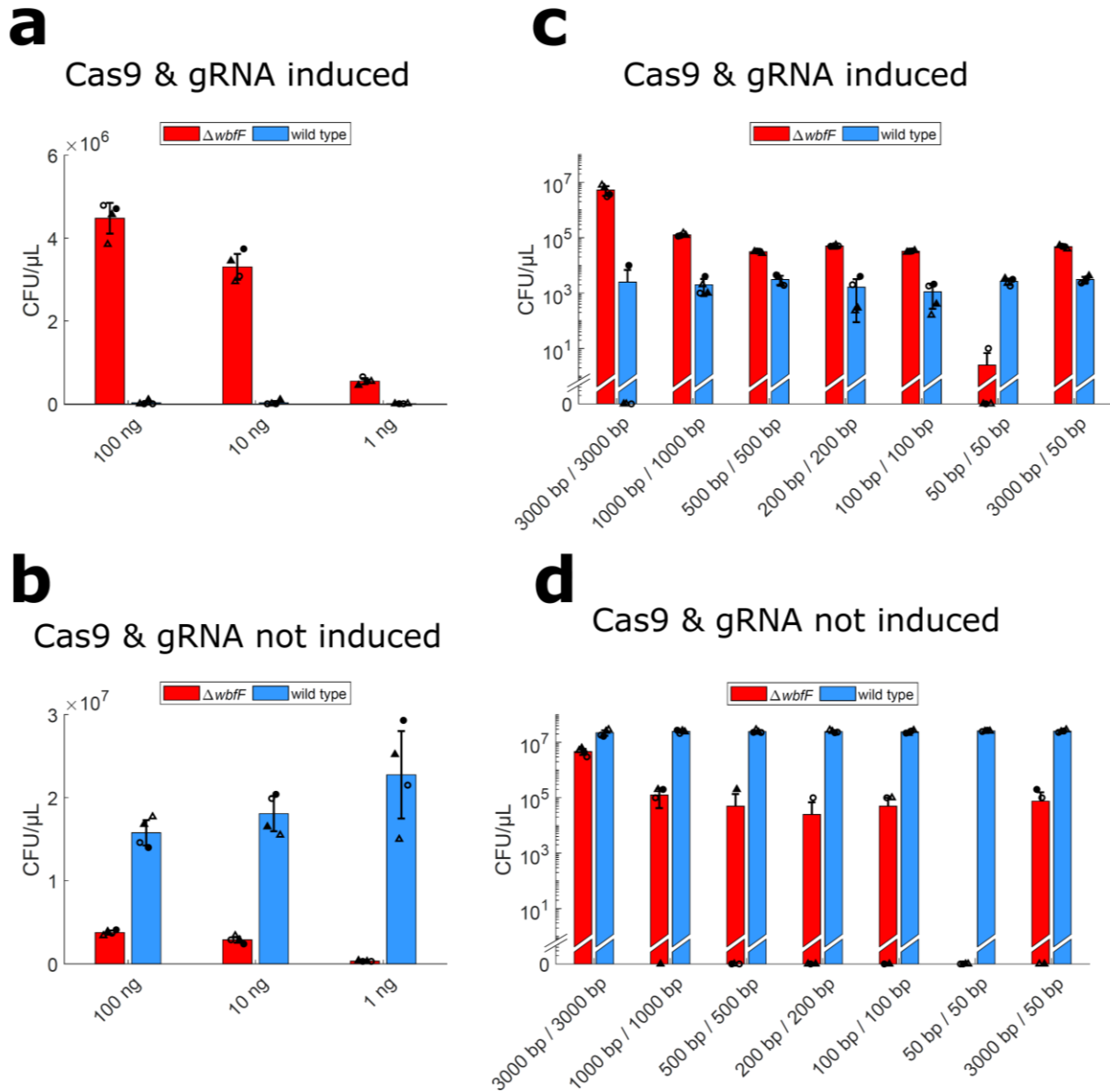
Supplementary Figure S7 - mScarlet-I/OD₆₀₀ signal of strains shown in Figure 4D

Supplementary Table S2 - Assembly of plasmids used in this study

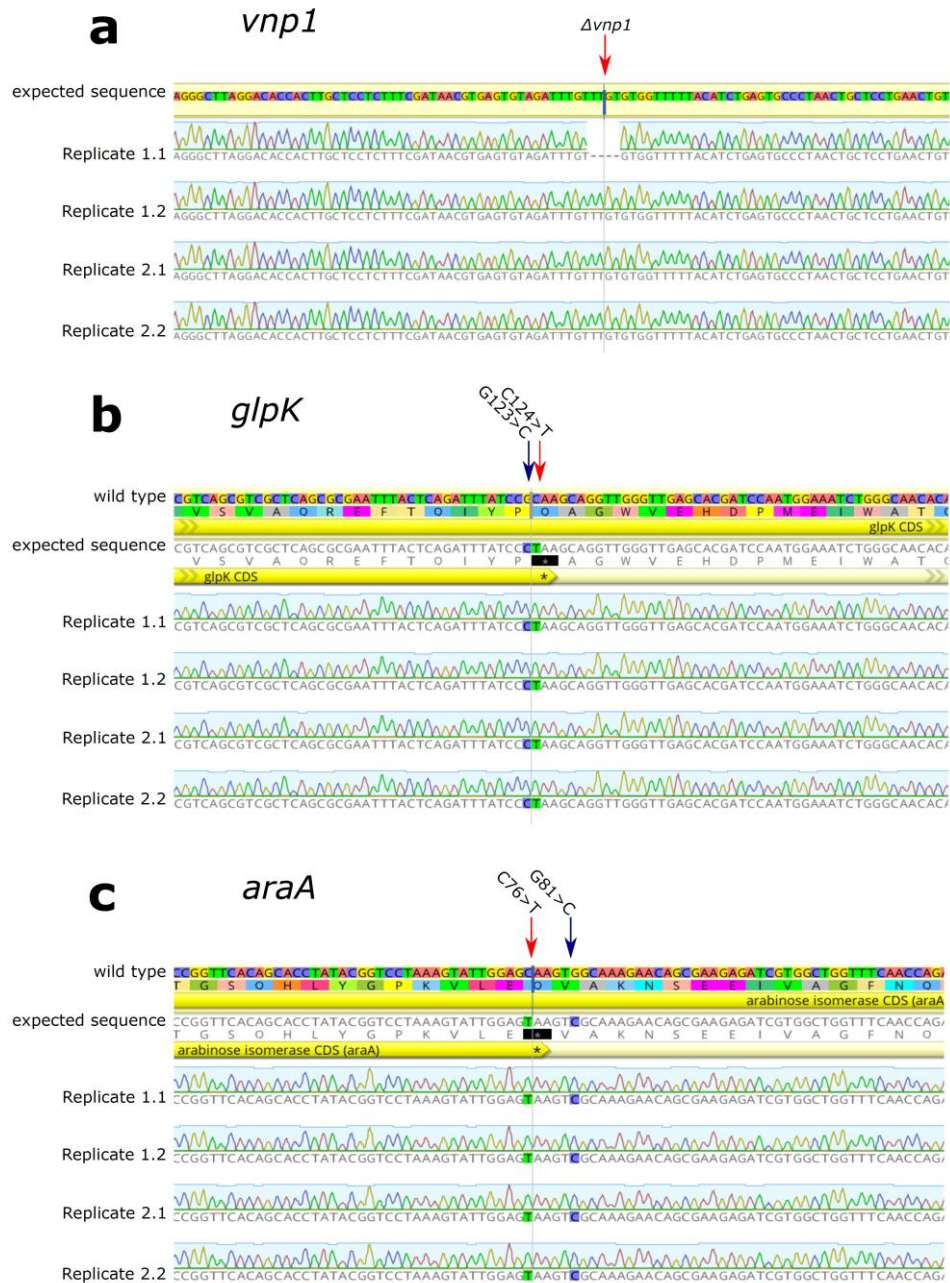
Supplementary References



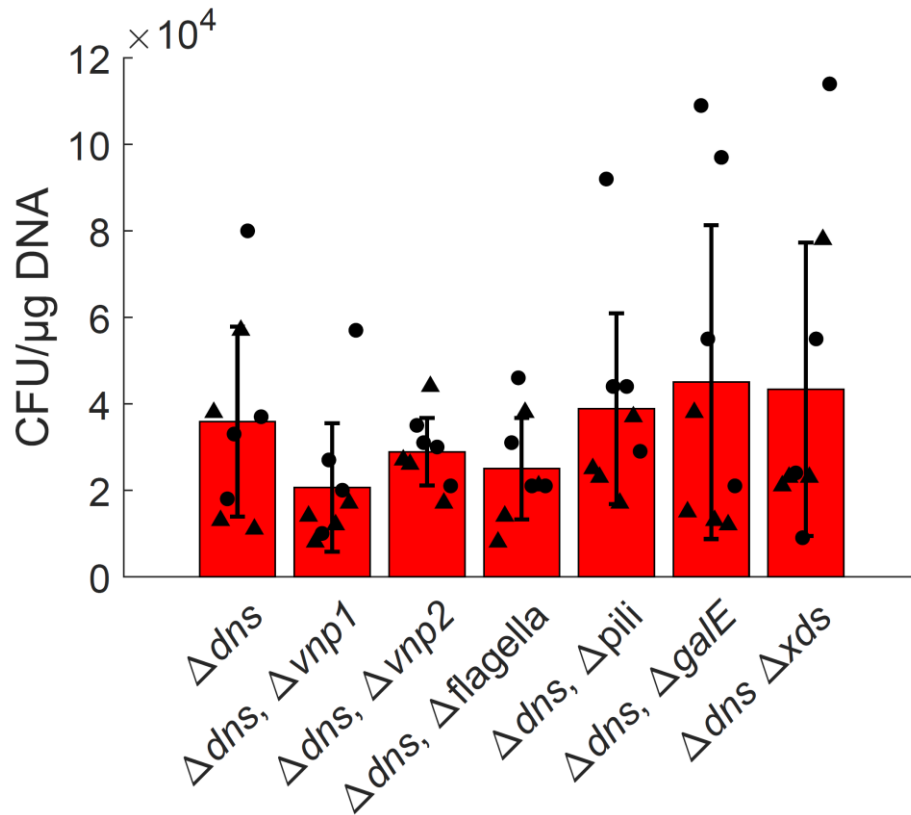
Supplementary Figure S1: Stoichiometry of Cas9 and *AcrIIA4* is essential for inducible cell killing. (a) Inducible cell killing in liquid culture, measured in a microplate reader. Constructs carry combinations of different RBS for *cas9* and *acrIIA4*, provided on top and left side and a *gRNA* expression cassette targeting *wbfF*. Strength of RBS, based on characterization experiments with fluorescent reporter genes¹, increases from left to right and top to bottom. $n = 4$ replicates, representing two independent biological replicates and two independent experiments. Curves show the mean of all replicates and error bars indicate standard deviation of the mean. Samples were induced with 200 ng/ μ L ATc (red) or remained uninduced (blue) at time point 0 (dashed lines). (b) Results of killing assay in the NT-CRISPR workflow. Killing efficiency is calculated as follows: $Killing\ efficiency\ [\%] = 1 - \frac{CFU/\mu L\ with\ counterselection}{CFU/\mu L\ without\ counterselection} * 100$. $n = 4$ replicates, representing two independent biological replicates (circle or triangle) and two independent experiments (filled or open symbols). Bars show the mean of all replicates and error bars indicate standard deviation of the mean. The dashed line indicates the highest possible value.



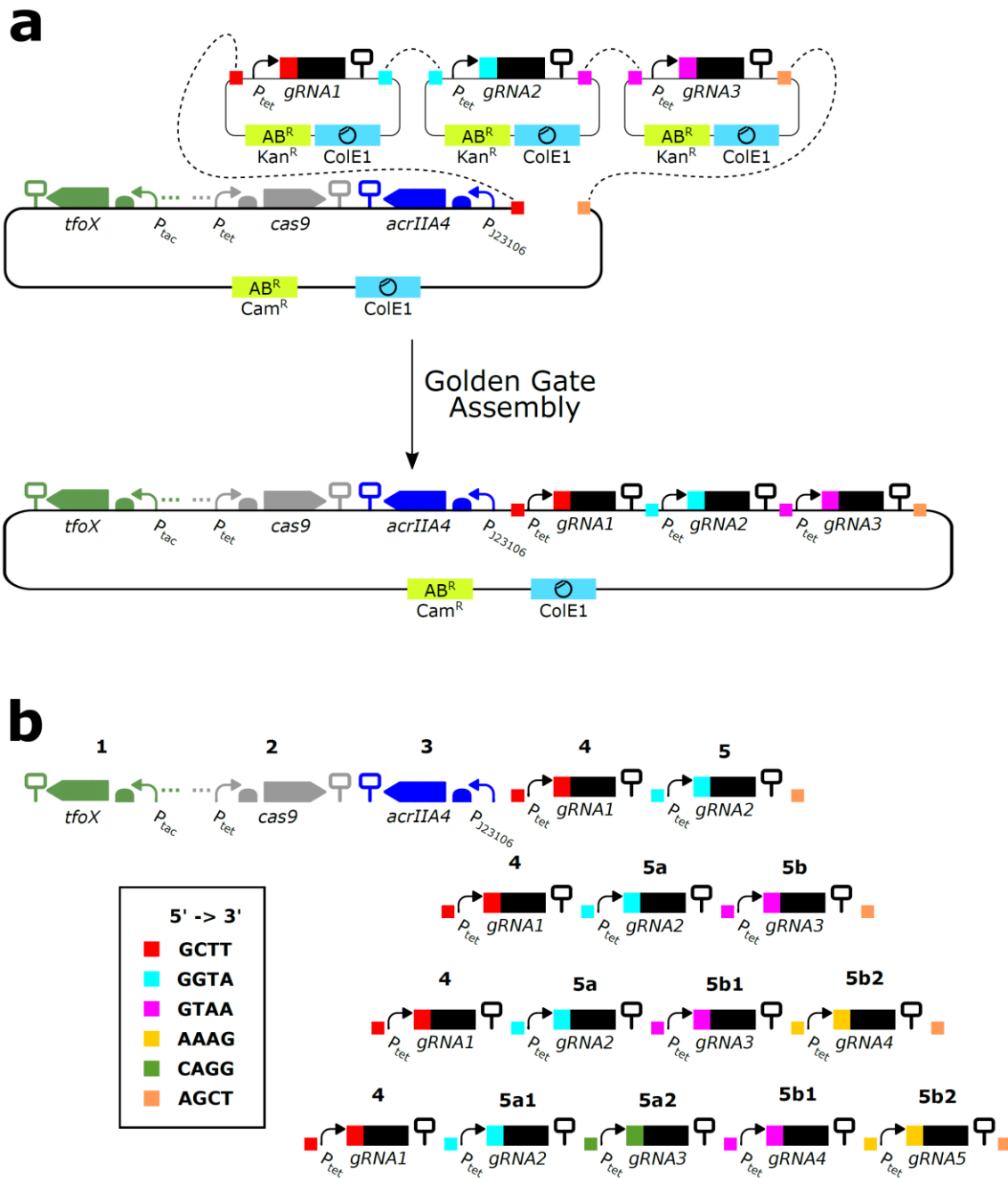
Supplementary Figure S2: Underlying CFU/ μL for Figure 2b and 2c. Red and blue bars show CFU/ μL for colonies with the transparent $\Delta wbfF$ morphology (red bars) or wild type morphology (blue bars). $n = 4$ replicates, representing two independent biological replicates (circle or triangle) and two independent experiments (filled or open symbols). Bars show the mean of all replicates and error bars indicate standard deviation of the mean. (a,b) CFU/ μL of experiment with different amounts of tDNA with 3000 bp homologous flanks upstream and downstream of the target sequence. (c,d) CFU/ μL of experiment with 100 ng of tDNA with different length of homologous flanks. (a,c) Results with CRISPR-based counterselection. (b,d) Results without CRISPR-based counterselection. $n = 4$ replicates, representing two independent biological replicates (circle or triangle) and two independent experiments (filled or open symbols). Bars show the mean of all replicates and error bars indicate standard deviation of the mean.



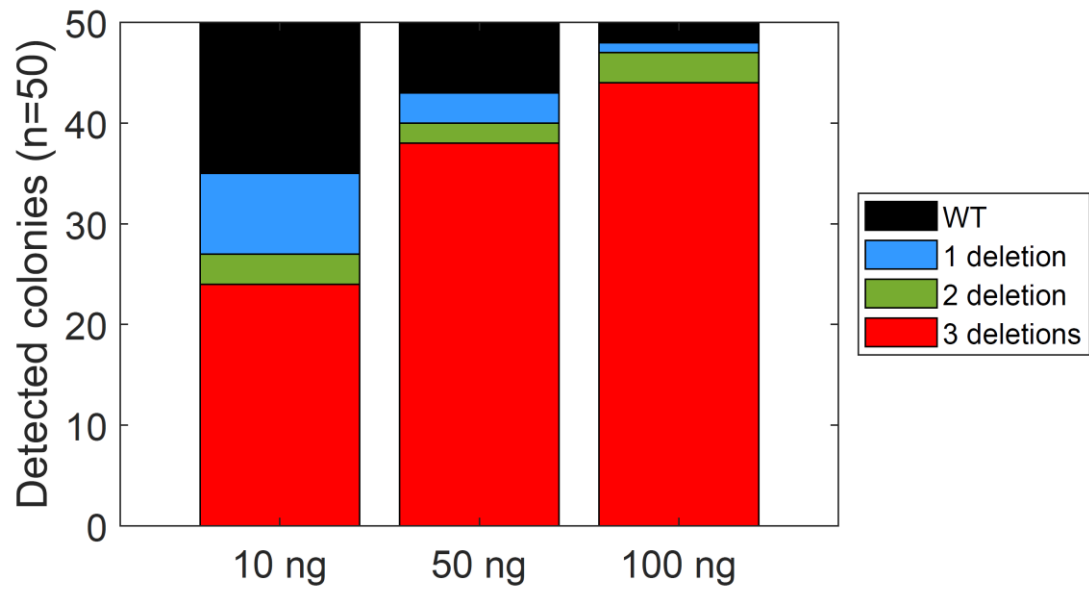
Supplementary Figure S3: Sequencing results of $\Delta vnp1$ and point mutations in *glpK* and *araA* genes. (a) The expected sequence for a $\Delta vnp1$ deletion is shown on top. The red arrow indicates the junction between upstream and downstream fragment surrounding the deleted sequence. $\Delta vnp1$ replicate 1.1 shows a deviation from the expected sequence with four missing bases. (b, c). Sequencing results of strains with desired point mutation, leading to a premature stop codon (red arrow) and an additional silent point mutation leading to a C-C mismatch (G \rightarrow C mutation). Wild type sequence and expected sequence with introduced mutations shown on top, followed by sequencing results of all four tested replicates. Sequence alignment was created with Geneious Prime 2021.2.1.



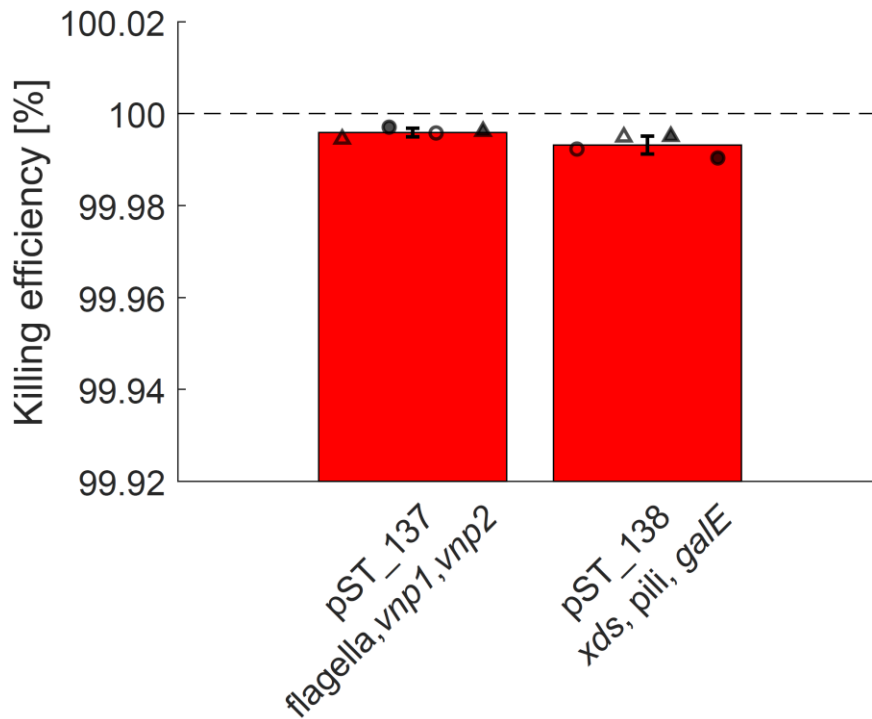
Supplementary Figure S4: Transformation efficiency of deletion strains. Parental strain Δdns and derivatives with additional deletions were tested for transformation efficiency. $n = 8$ replicates, representing four independent replicates (separate batches of competent cells from independent strains, resulting from NT-CRISPR editing) and two independent experiments (circle or triangle). Bars show the mean of all replicates and error bars indicate standard deviation of the mean. The plasmid pMC0_8_19¹, was used for this experiment.



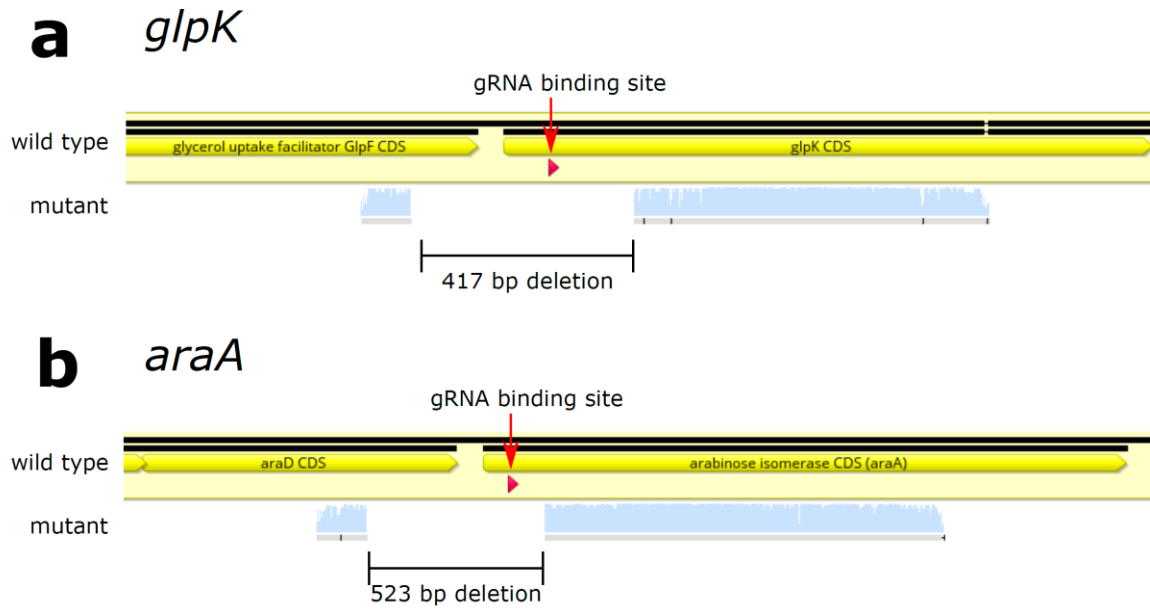
Supplementary Figure S5: Assembly of NT-CRISPR plasmid with multiple gRNAs. (a) Example of construction of NT-CRISPR plasmid with three gRNAs. First, individual gRNA expression cassettes are created in plasmids carrying a kanamycin resistance marker (Kan^R) and then subsequently integrated into a plasmid carrying all remaining components by Golden Gate Assembly with Esp31 as the type II restriction enzyme. Colored squares indicate matching fusion sites for Golden Gate Assembly. SBOL symbols for omitted detail (three points) represent the transcriptional unit for the regulatory proteins *Lacl* and *TetR* for P_{tac} and P_{tet} , respectively. (b) Detailed scheme for assembly of NT-CRISPR plasmid with two to five gRNAs. Bold numbers indicate the position of the respective transcriptional unit in the framework of the Marburg Collection¹. Position five was additionally split to accommodate further gRNAs. Novel fusion sites (5' \rightarrow 3' direction) are introduced based on predicted assembly efficiency² and are indicated in the inlay box.



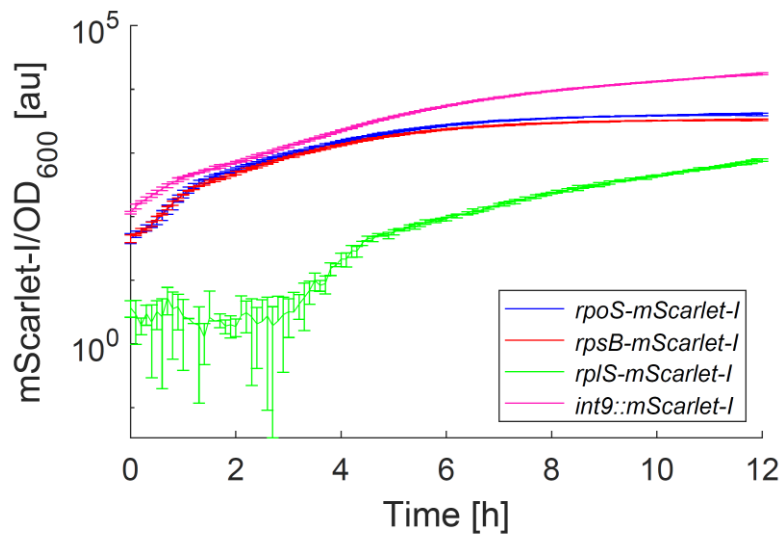
Supplementary Figure S6: Editing efficiency for deletion of the three targets *xds*, *galE* and the *pili* operon. Bars show number of colonies with none, one, two or three deletions when the indicated amount of tDNA was used for each target. The number of deletions was assessed by PCR (n = 50 colonies).



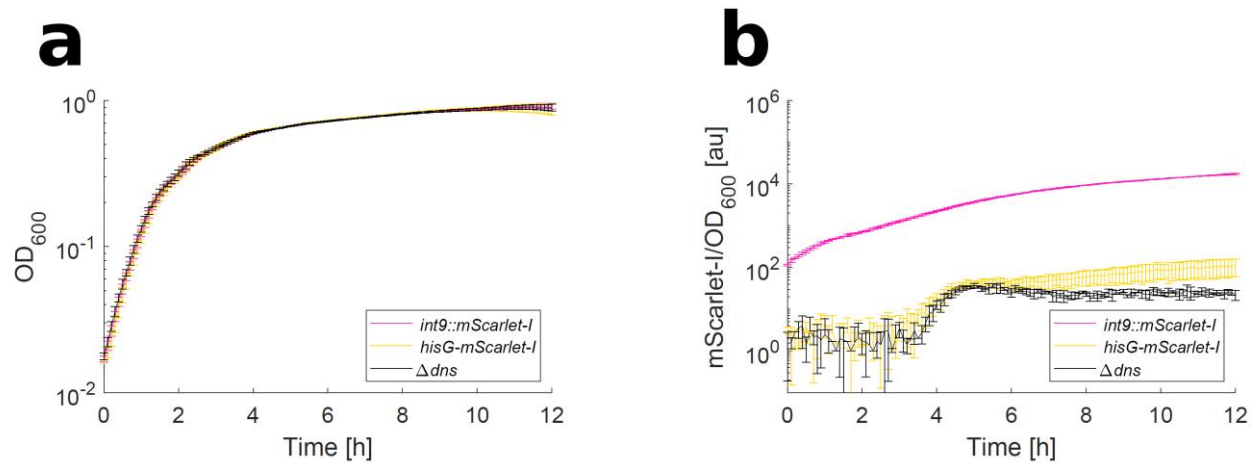
Supplementary Figure S7: Killing assay with strains carrying plasmids with three gRNAs. Killing efficiency is calculated as follows $Killing\ efficiency\ [\%] = 1 - \frac{CFU/\mu L\ with\ counterselection}{CFU/\mu L\ without\ counterselection} * 100$. $n = 4$ replicates, representing two independent biological replicates (circle or triangle) and two independent experiments (filled or open symbols). Bars show the mean of all replicates and error bars indicate standard deviation of the mean. Dashed line indicates the highest possible value.



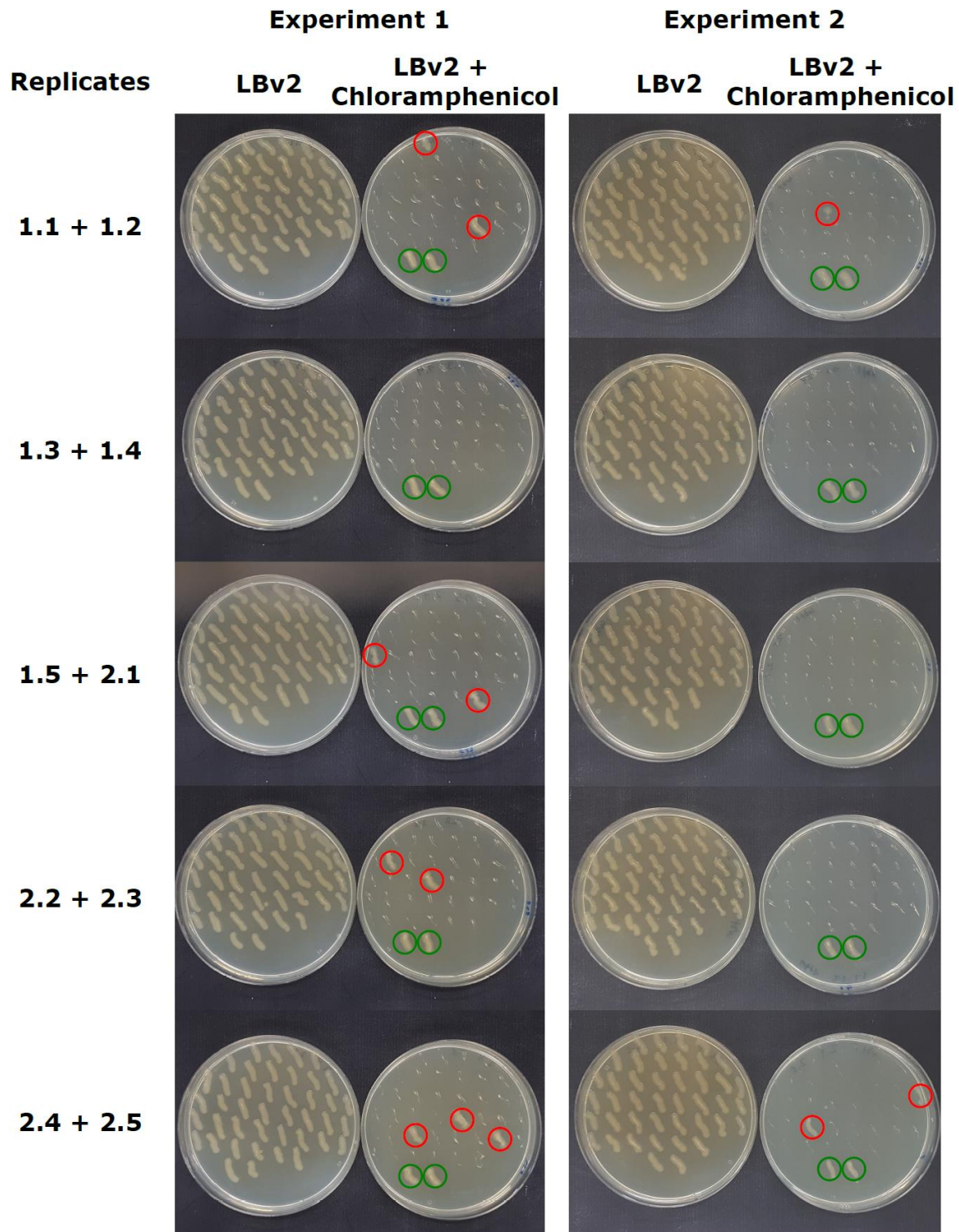
Supplementary Figure S8: Sequencing result of first attempt to introduce a point mutation into *glpK* (a) and *araA* (b) without an additional C-C mismatch mutation. Large regions are deleted in both mutants, including the gRNA binding site (red annotation). Sequence alignment was created with Geneious Prime 2021.2.1.



Supplementary Figure S9: mScarlet-I/OD₆₀₀ signal of strains shown in Figure 4d. Data represent the mean of four biological replicates. Error bars indicate standard deviation of the mean.



Supplementary Figure S10: Signal from *hisG-mScarlet-I* is too low for quantitative analysis. (a) Growth curves of strains with integrated constitutive *mScarlet-I* expression cassette, *hisG-mScarlet-I* and parental strain Δdns . $n = 8$ replicates, representing four independent biological replicates and two independent experiments. Curves show the mean of all replicates and error bars indicate standard deviation of the mean. (b) $mScarlet-I/OD_{600}$ of tested strains. *hisG-mScarlet-I* is almost indistinguishable from parental strain Δdns . $n = 8$ replicates, representing four independent biological replicates and two independent experiments. Curves show mean of all replicates and error bars indicate standard deviation of the mean.



Supplementary Figure S11: Streaked colonies to estimate plasmid curing efficiency. Patches growing on LBv2 with chloramphenicol are highlighted with red and green circles for supposedly plasmid cured colonies and colonies before plasmid curing as controls, respectively. For each replicate, 20 colonies were streaked and two replicates were streaked on the same plate.

Supplementary Table S2: Assembly of plasmids used in this study. Parts were assembled in the framework of the Marburg Collection ¹. Short nomenclature is provided in the table, e.g. 2_43 = pMCO_2_43_Ptac. Asterisks in plasmid names, according to the nomenclature of the Marburg Collection, were replaced with lower case x to allow saving of plasmid maps into files (e.g. 8*_06 → 8x_06). Parts and plasmids written in bold letters were assembled in this project and all remaining parts are available as genetic parts in the Marburg Collection. Part sequences for new parts are provided in Supplementary Table S1.

Plasmid	Parts and plasmid used for assembly	Description
pST_025	1x-6x Linker, 8x_06, 7x_01	Control plasmid
pST_032	pDS_120, 2_43 , 3_07, 4_45 , 5_08	Level 1, P _{tac} Tfox
pST_033	pDS_191, 2_42 , 3_04, 4_25 , 5a_07, 5b_02	Level 1, P _{tet} Cas9, RBS = B0031
pST_034	pDS_191, 2_42 , 3_02, 4_25 , 5a_07, 5b_02	Level 1, P _{tet} Cas9, RBS = B0029
pST_035	pDS_191, 2_42 , 3_06, 4_25 , 5a_07, 5b_02	Level 1, P _{tet} Cas9, RBS = B0033
pST_040	pST_032 , 8x_06, 7x_01, 1x-6x_03 Dropout	Level 2 Dropout plasmid, contains P _{tac} Tfox and Dropout for remaining positions
pST_084	pDS_187, 2_08, 3_04, 4_56 , 5_05	Level 1, J23106 AcrIIA4, RBS = B0031
pST_085	pDS_187, 2_08, 3_05, 4_56 , 5_05	Level 1, J23106 AcrIIA4, RBS = B0032
pST_086	pDS_187, 2_08, 3_07, 4_56 , 5_05	Level 1, J23106 AcrIIA4, RBS = B0034
pST_087	pDS_187, 2_08, 3_03, 4_56 , 5_05	Level 1, J23106 AcrIIA4, RBS = B0030
pST_107	pST_040 , gRNA Pos 4 (P _{tet}), TU5-6x_EL_04, pST_033 , pST_084	Level 2, NT-CRISPR, Cas9 RBS = B0031, AcrIIA4 RBS = B0031
pST_108	pST_040 , gRNA Pos 4 (P _{tet}), TU5-6x_EL_04, pST_033 , pST_085	Level 2, NT-CRISPR, Cas9 RBS = B0031, AcrIIA4 RBS = B0032
pST_109	pST_040 , gRNA Pos 4 (P _{tet}), TU5-6x_EL_04, pST_033 , pST_086	Level 2, NT-CRISPR, Cas9 RBS = B0031, AcrIIA4 RBS = B0034
pST_110	pST_040 , gRNA Pos 4 (P _{tet}), TU5-6x_EL_04, pST_033 , pST_087	Level 2, NT-CRISPR, Cas9 RBS = B0031, AcrIIA4 RBS = B0030
pST_111	pST_040 , gRNA Pos 4 (P _{tet}), TU5-6x_EL_04, pST_034 , pST_084	Level 2, NT-CRISPR, Cas9 RBS = B0029, AcrIIA4 RBS = B0031
pST_112	pST_040 , gRNA Pos 4 (P _{tet}), TU5-6x_EL_04, pST_034 , pST_085	Level 2, NT-CRISPR, Cas9 RBS = B0029, AcrIIA4 RBS = B0032
pST_113	pST_040 , gRNA Pos 4 (P _{tet}), TU5-6x_EL_04, pST_034 , pST_086	Level 2, NT-CRISPR, Cas9 RBS = B0029, AcrIIA4 RBS = B0034
pST_114	pST_040 , gRNA Pos 4 (P _{tet}), TU5-6x_EL_04, pST_034 , pST_087	Level 2, NT-CRISPR, Cas9 RBS = B0029, AcrIIA4 RBS = B0030
pST_115	pST_040 , gRNA Pos 4 (P _{tet}), TU5-6x_EL_04, pST_035 , pST_084	Level 2, NT-CRISPR, Cas9 RBS = B0033, AcrIIA4 RBS = B0031
pST_116	pST_040 , gRNA Pos 4 (P _{tet}), TU5-6x_EL_04, pST_035 , pST_085	Level 2, NT-CRISPR, Cas9 RBS = B0033, AcrIIA4 RBS = B0032
pST_117	pST_040 , gRNA Pos 4 (P _{tet}), TU5-6x_EL_04, pST_035 , pST_086	Level 2, NT-CRISPR, Cas9 RBS = B0033, AcrIIA4 RBS = B0034

pST_118	pST_040, gRNA Pos 4 (P_{tet}), TU5-6x_EL_04, pST_035, pST_087	Level 2, NT-CRISPR, Cas9 RBS = B0033, AcrIIA4 RBS = B0030
pST_119	pST_040, pST_035, pST_085, 1x-6x_09 Dropout	NT-CRISPR plasmid for multiple gRNAs, Cas9 RBS = B0033, AcrIIA4 RBS = B0032, Dropout for positions 4 and 5
pST_133	pDS_120, 2_13, 3_03, 4_12, 5_03	Level 1, strong constitutive mScarlet-I, used as template to construct tDNA for integration
pST_136	pDS_191, 2_42, 3_06, 4_60, 5a_07, 5b_02	Level 1, P_{tet} SpG Cas9, RBS = B0033
pST_137	pST_119, gRNA Pos4 (P_{tet} , flrB), gRNA Pos5a (P_{tet} , vnp1), gRNA Pos5b (P_{tet} , vnp2)	Level 2, NT-CRISPR plasmid with 3 gRNAs (flrB, vnp1, vnp2)
pST_138	gRNA Pos4 (P_{tet} , xds), gRNA Pos5a (P_{tet} , pilA), gRNA Pos5b (P_{tet} , galE)	Level 2, NT-CRISPR plasmid with 3 gRNAs (flrB, vnp1, vnp2)
pST_140	pST_040, gRNA Pos 4 (P_{tet}), TU5-6*_EL_04, pST_136, pST_085	Level 2, NT-CRISPR with SpG Cas9

Supplementary References

1. Stukenberg, D. *et al.* The Marburg Collection: A Golden Gate DNA Assembly Framework for Synthetic Biology Applications in *Vibrio natriegens*. *ACS Synth. Biol.* (2021) doi:10.1021/acssynbio.1c00126.
2. Pryor, J. M. *et al.* Enabling one-pot Golden Gate assemblies of unprecedented complexity using data-optimized assembly design. *PLoS One* **15**, e0238592 (2020).

Supplementary Table S1: New genetic parts generated in this study. Parts were assembled as described for the Marburg Collection. Asterisks in plasmid names, according to the nomenclature of the Marburg Collection, were replaced with lower case x to allow saving of plasmid maps into files (e.g. 8*_06 -> 8x_06). First and last four bases represent fusion sites for the subsequent assembly.

Part	Sequence
pMCO_2_42_Ptet*	<p>GGAGCTCAGATAAAATATTGCTCATGAGCCCGAAGTGGCGAGCCCGATCTCCCATCGTGATGTCGGCGATATAGGCCAGCAACCGCACCTGTGGCGCCGGTATGCCGGCCACGA TGCGTCCGGGTAGAGGATCGCTCATGTTGACAGCTTATCATCGATGCATAATGTCCTGTCAAATGGACGAAGCAGGGATTCTGCAAAACCCATGTACTCCCTCGAGCCGTCATTTCTG ATTCGTTACCAATTAGGATCCTTATCAGGACCCACTTTACATTTAAGTTGTTTTCTAATCCGATATGATCAATTCAGGCCGAATAAGAAAGGGTGGCTCGACCTTGGTGATCAAAATATT CGATAGCTTGTGTAATAATGGCGGCATACATCAGTAGTAGGTTTCCCTTCTCTTTAGCGACTGTATGCTCTTGATCTTCAATACGCAACCTAAAGTAAATGCCCCAGCGCTGAGT GCATATAATGCTTCTAGTGA AAAACCTGTTGGCATAAAAAGGCTAATGATTTTCGAGAGTTTCATACTGTTTTCTAGGCCGTGTACTAAATGTACTTTTGCCTCATCGGATGACT TAGTAAAGCACATCTAAAACCTTTAGCGTTATTACGTA AAAAATCTTCCAGCTTTCCCTTCTAAAGGGCAAAAAGTGAAGTATGGTGCCTATCTAACATCTCAATGGCTAAGGCGTCGAGCAAA GCCCGCTATTTTTACATGCCAATACAATAGGCTGCTCACACTAGCTTCCGGGCGATTTACGGGTTGTTAAACCTCGATTCCGACCTATAAGCACTTAAATGCGCTTAATCAC TTTACTTTATCTAATCTGGACATAATACCACCTGAATTGACTCTCTCCGGGCGTATATGCCATACCAGGAAAGGTTTTGCCGCTTCCGCTGTTTTACGAGGACGCACTGACCTCCCT ATCAGTGATAGAGATTGACATCCCTCATGATAGAGATACTGAGCACTACT</p>
pMCO_2_43_Ptac	<p>GGAGCTCAGATAAAATATTGCTCATGAGCCCGAAGTGGCGAGCCCGATCTCCCATCGTGATGTCGGCGATATAGGCCAGCAACCGCACCTGTGGCGCCGGTATGCCGGCCACGA TGCGTCCGGGTAGAGGATCGCTCATGTTGACAGCTTATCATCGATGCATAATGTCCTGTCAAATGGACGAAGCAGGGATTCTGCAAAACCCATGTACTCCCTCGAGCCGTCATTTCTG GATTCGTTACCAATTAGGATCCTTATCAGGACCCACTTTACATTTAAGTTGTTTTCTAATCCGATATGATCAATTCAGGCCGAATAAGAAAGGGTGGCTCGACCTTGGTGATCAAAATATT GTGGTTTTTCTTTTACCAGTGAAGACTGGCAACAGCTATTGCCCTTCCAGCTCCGCTGGCAGAGATTGCGCTTCCAGCGCTGGCAGAGATTGCGAGCAAGCGGTCCACGCTGTTGCCCGCAGCGGAAAAATCCTGTTTGTAGT GTGGTTAACCGCGGGATAAACAATGAGCTATCTTCGATGCTGATCCCACTACCGAGATATCCGCAACCGCGCACGCCGACTCGGTAATGGCGCATTGCGCCAGCCGCTACTG ATCGTTGGCAACCCAGCATCGCAGTGGGAACGATGCCCTCATTCAGATTTTGCATGTTTTGTA AAAACCGGACATGGCACTCCAGTCCGCTTCCGTTCCGCTAGCTGAAITTTGATTGCG AGTGAGATATTTGCCAGCCAGCAGCAGCAGCGCCGAGCAGAACTAATGGGCCCGCTAACCGCGCATTTGCTGGTGAAGAACGCAATGCTCCAGCCAGATGCTCCAGCCGCTGTCGCGTA CCGCTCTATGGGAGTAAATAACTGTTGATGGGTGTCTGTCAGAGCATCAAGAAATAACGCCGGAACATTAGTGCAGGCACTCCACAGCAATGGCATCTGCTCCAGCCGCTACT GTTAATGATCGCCCACTGACCGTTGCGCGAGAAAGATTGTGCAACC GCGCTTACAGGCTTCCAGCGCTTCTGTCCATCGACACCCACCGCTGACCCAGCTGATGCGGCGAG ATTTAATCGCCGCGCAATTTGCGAGCGCGCTGCGAGGGCAGACTGGAGTGGCAACGCCAATCGACAAAGCTGTTGCCCGCCAGTTGTTGCGCACCGGTTGGGAATGTAATTCAGC TCCACATCGCCGCTTCCACTTTTCCCGCTTTTCCGAGAAACGTGGCTGGCTGTTCACACGCGGAAACGGTCAATAAGAGACACCCGGCACTCTGCGACATCGTAAACGTTACT GGTTTCATATCCACCCCTGAATTGACTCTCTCCGGGCGTATCATGCCATACCAGGAAAGGTTTTGCCGCTTCCGCTGTTGACAATTAATCATCGCTGATAATGTGGAATTGTG AGCGCTCACAACTACT</p>
pMCO_4_25_CDSCas9	<p>AATGGATAAGAAATCAATAGGCTTAGATATCGGCACAAATAGCTCGGATGGCGGTGATCATGATGAATAAAGTTCCGCTCTAAAAGTTCAAGTTCTGGGAATACAGACC GCC ACAGTATCAAAAAAATCTTAGAGGGCTCTTTATTTGACAGTGGAGAGACAGCGGAAGCGACTCGTCTGAAACCGCACAGCTCTGAGAAAGTATACAGCTCGGAAGAATCGATTTGTTAT CTACAGGAGATTTTTCAAATGAGATGGCGAAAGTAGATGATGTTCTTTCATCGACTTGAAGAGTCTTTTTGGTGGAGAAGACAGAAAGCATCAATCTTTTGGAAATATA GTAGATGAAGTCTTATCAGAGAAATTCACACTACTCATCTCGCAAAAAAATTTGGTAGACTCTACTGATAAAGCGGATTTGCGCTTAATCTATTGGCCTTAGCCATATGATTAAGT TTCTGGTCTTTTTGATTGAGGGAGATTAATCTGATAAATGATGATGGCAAACTATTTACAGTTGGTACAAACCTACAATCAATTTTGAAGAAAAACCTATTAACGCAAGTGG AGTAGATGCTAAAGCGATTCTTTCGACGATTTGATTAATCAAGAGCTTACAGAAATCTTCTGCTCAGCTCCCGGTGAGAAGAAAAATGGCTTATTTGGGAATCTCATTGCTTTGCTATTG GGTTTGACCCCTAATTTTAAATCAATTTTGGTTGGCAGAAAGTGTCTAATACAGCTTTCAAAAAGATACTACTAGATGATGATTAATTTTGGCGCAAAATTTGACAAACGGCTCTATTCCGA TTTTTTTTGGCAGTAAAGATTTACAGATGCTATTTTACTTTTCAGATATCTAAGAGTAAACTGAAATAACTAAGGCTCCCTATCAGCTCAATGATTAACGCTACGATGAACATCATC AAGACTTACTTTTTAAAGCTTTAGTTCGACAACTTCCAGAAAAGTATAAAGAAATCTTTTTGATCAATCAAAAACCGGATATGAGGTTATATGATGGGGAGCTAGCCAAAGAA AATTTTATAAATTTTCAAACTAATTTTGA AAAAAGTACTACCAAAACATAGTTGCTTTGATGATGATTTTACGTTTATAACGAAATGCAAAAGTCAATATGTTACTGAGAAAGTGGCAAA TCAAACTACTTTGGTGGCTGATGCTATTTGAGAAGACAAGAACTTTTACCAATTTTAAAAGACAATCGTGAAGATTGAAAATCTTGACTTTGCTATTCCTATTATGTTGGT CATTTGGCGGTGGCAATAGTCTTTTGCATGGATGACTCGGAAGTCTGAAGAAACAATACCCCATGGAAATTTGAAAGATTGTCGATAAAGGTTGCTCAGCTCAATCATTTTGAACGCA TGACAAACTTTGATAAAATCTTCAAATGAAAAGTACTACCAAAACATAGTTGCTTTGATGATGATTTTACGTTTATAACGAAATGCAAAAGTCAATATGTTACTGAGAAAGTGGCAAA ACCAGCATTTCTTTCAGTGAACAGAAAGCAATGTTGATTACTCTTCAAAAACAAATCGAAAAGTAAACCGTTAAGCAATTAAGAAAGATTATCAAAAATAAGAAATGTTTGTATG GTTGAAATTTCCAGGAGTTGAAGATAGATTTAATGCTTCAATAGTACTACCATGATTTGTA AAAAATTTAAGATAAAGATTTTTGGATAATGAAGAAATGAAGATATCTTAGAGGATA TTGTTTTAACTGACTTTTGAAGATAGGGAGATGATTGAGGAAAGACTTAAAACATATGCTCACCTTTGATGATAAGGTGATGAACAGCTTAAACGTCGCCGTTATAGCTTTGTTGGG GACGTTTGTCTCGAAAAATGATTAATGTTATAGGGATAAAGCAATCTGGCAAAACATATAGATTTTTGAAATCAGATGTTTGGCAATCGCAATTTATGCACTGATCCATGATGATG TTTGACATTTAAGAAAGCAATCAAAAAGCACAAGTGTCTGGCAAGGCGATGTTTACATGAACATATTGCAAAATTTAGCTGGTAGCCCTGCTATTA AAAAAGGTTATTTACAGACTGTAAA AGTTGTTGATGAATTTGTTCAAAGTAAATGGGGCGCATAAGCCAGAAAATATCTGTTTGAATGGCAAGTGA AAAATCAGACAACCTCAAAAAGGGCCAGAAAATCGCGAGAGCGTATGAAA CGAATCGAAGAAAGTATCAAAAGTATAGGAAGTCAAGTCTTAAAGAGCATCTGTTGAAAATACTCAATGCAAAATGAAAAGCTCTACTCTATTATCTCAAAAATGGAAGAGACATGATG GTGGACCAAGAAATGATATTAATCGTTAAGTATTGATGTCGATCACATGTTCCAAAAGTTTCTTAAAGAGCATCAATAGACAATAGCTTAAACGCTTCTGATAAAAATCTGTG GTA AATCGGATAACGTTCCAAGTGAAGAAAGTATGTA AAAAAGTAAAGAACTTTGGAGCAACTTCTA AACCGCAAGTTAATCACTCAAGCTAAGTTTGATAATTTAACGAAAGCTGAACGT GGAGGTTTGAAGTGAATTTGATAAGCTGGTTTTATCAAAACGCAATTTGGTGAACCTCGCCAAATCACTAAGCATGGGCAAAAATTTGGATAGTGCATGAATACTAAATACGATGAAAAT GATAAACTATTTCAGAGGTTAAAGTATTACCTTAAATCTAAATGATTCTGACTCCGAAAAGATTCCAAATCTATAAAGTACGTGAGATTAACAATTAACATATGCTCCATGCTGATGCGTA TCTAAATGCCGCTGTTGAACTGCTTTGATTAAAGAAATCAAAAACCTGAATCGGAGTTGCTATGGTGATTATAAAGTTTATGATGTTGCTGAAAATGATTGCTAAGTCTGAGCAAGAAATA GGCAAGCAACCGCAAAATTTCTTTACTAATATCATGAATCTTCAAAAACGAAATACACTTGA AATGGAGAGATTGCAAAACCGCCCTCAATCGAAAATTAAGGGAACTGGA GAAATTTGCTGGGATAAAGGGCGAGATTTGCCACAGTGGCAAGATTTGCTCATGCCCAAGTCAATTTGCAAGAAAACAGAAAGTACAGACAGGCGGATTTCTCAAGGAGTCAATTTT ACCAAAAAGAAATCGGACAAGCTTATTGCTGTA AAAAAGACTGGATCAAAAATAATGGTGGTTTGTATGCTCAACCGTAGCTTATTCAGTCTAGTGGTGTAAAGTGGAAAAAG GGAAATCGAAGAGTAAATCCGTTAAAGAGTTACTAGGGATCACAATTTGGA AAAAGAGTTCTTTGAAA AAAATCCGATTGACTTTTGAAGCTAAAGGATATAAGGAGTTAAAAA GACTTAATCACTAACTAAATATAGTCTTTTTGAGTTAGAAAACGGTCTAAACGGATGCTGCTAGTGGCGGAGAAATTAACA AAAAGGAAATGAGCTGGCTCTGCCAAAGCAATATGT GAAATTTTATATTTAGCTAGTATTGAAAAGTTGAAGGGTAGTCCAGAAATAAACGAAACAAAACAAATTTGTTGGGAGCAGATAAGCAATTTTATGATGAGATTTATGAGCAAAATCAG TGAAATTTTCAAGCTGTTATTTAGCAGATGCCAATTTAGATAAAGTTCTTAGTGATATAACCAACTAGAGACAACCAATACGTGAACCAAGCAAAAATATTTACTTTATTTACGTTGA CGAATCTGGAGCTCCGCTGCTTTAAATATTTTGAACAACATGATCGTAAACAGTATCACTGCAAAAAGAAAGTTTATGATGCCACTTATCATCACTCACTGCTGCTTTATGAA ACACGATGATTGAGTCACTAGGAGGTGACGCT</p>
pMCO_4_56_CDS AcrIIA4	<p>AATGAACATTAACGACCTACAGAGAGATAAAGAACAAGATTAACCCGTCAAACTGTCAGAACTGATAGTAACCTCAATACCAGCTTATTTATCAGGGTAAACAATGATGGGAATGAAT ATGTGATATCTGAGAGCGAAAAACGAGTCTATGCTCGAGAAATTCATTTCCGCTTTTAAAGAACGGGTGGAATCAGGAATATGAGGATGAAGAAGAATTTACAATGACATGACAGATCAGC TTGAAAAGTGAACCTGAACTAAGCT</p>

pMC0x_gRNA_Pos5a_Ptet	<p>GGTCAAAATCACTGTAATGATCTTAATTCCTAATTTTTGTTGACACTCTATCATTGATAGAGTTATTTAGTCCAGAGACCAGAAAGTGAACCTGATTTTCATGCGTCATTTTGAAACATTTTGTAAT TCCTATTTAATAATGTGTGCGGCAATTCACATTTAATTTATGAATGTTTTCTTAACATCGCGCAACTCAAGAAACGGCAGGTTCCGATCTAGACTAGAGAAAGAGGAGAAATCTAGATG CGTAAAGGCGAAGAACCTTTCACTGCGGTAGTACCAATTTTAGTGGAGCTGGACGGAGATGTAATGGTCATAAGTTTTCACTGCGAGAGAAAGGGAAGGAGATGCAACTAACGGTAAGC TGACACTAAAGTTTATCTGTACCACGGGTAACCTGCGGTCCATGGCCGACACTGGTTACTACACTTACTTATGGTGACAATGCTTTGCTGTTATCTGACCATATGAAGCAGCACGATTT CTTCAAATCGGCCATGCCTGAAGGATACGTGCAAGAACGTACAATTAGCTTTAAAGATGACGGCACCTATAAAACGCGCCGAAAGTTAAATTCGAGGGTGACACATTTGGTTAATCGTATAG AACTTAAGGGCATTGACTTCAAAGAAGTGGCAACATCTTGGCCATAAACTGGAATATAATTTAACTCTCACAATGTCTACATTACGGCGGATAAACAAAAGAAATGGCATTAAAGCGAATT TCAAAATCCGCCACAATGTCGAAGACGGCTCGTTCAACTGGCGGACATTATCAGCAGAACACCCCAATCGGTGATGGCCGGTTCTGTTACCTGATAATCATTACCTTTCTACTCAAAGCG TTTTATCTAAAGATCTAACGAGAAGCGTGATCATATGGTTCTACTGGAATTTGTTACCGCAGCTGGTATCAGCAGCGCATGGATGAGCTGTATAAATAACAGGCATCAATAAAACGAAA GGCTCAGTCGAAAAGACTGGCCCTTCGTTTTATCTGTTGTTGTCGGTGAACGCTCTACTAGAGTCACACTGGCTCACCTTCGGGTGGCCCTTCTGCGTTTATAGGTCTCAGTTTCAGAGCT ATGCTGGAACAGCATAGCAAGTTGAAATAAGGCTAGTCCGTTATCAACTGAAAAGTGGCACCGAGTCGGTGCTTTTTCTCGGTACCAAAATCCAGAAAAGAGGCTCCCGAAAGGGGG GCCTTTTTCTGTTTGGTCCACCCTGCACGATAAACAAGTAAAGT</p>
pMC0x_gRNA_Pos5b_Ptet	<p>GTAACAAATCACTGTAATGATCTTAATTCCTAATTTTTGTTGACACTCTATCATTGATAGAGTTATTTAGTCCAGAGACCAGAAAGTGAACCTGATTTTCATGCGTCATTTTGAAACATTTTGTAAT TCCTATTTAATAATGTGTGCGGCAATTCACATTTAATTTATGAATGTTTTCTTAACATCGCGCAACTCAAGAAACGGCAGGTTCCGATCTAGACTAGAGAAAGAGGAGAAATCTAGATG CGTAAAGGCGAAGAACCTTTCACTGCGGTAGTACCAATTTTAGTGGAGCTGGACGGAGATGTAATGGTCATAAGTTTTCACTGCGAGAGAAAGGGAAGGAGATGCAACTAACGGTAAGC TGACACTAAAGTTTATCTGTACCACGGGTAACCTGCGGTCCATGGCCGACACTGGTTACTACACTTACTTATGGTGACAATGCTTTGCTGTTATCTGACCATATGAAGCAGCACGATTT CTTCAAATCGGCCATGCCTGAAGGATACGTGCAAGAACGTACAATTAGCTTTAAAGATGACGGCACCTATAAAACGCGCCGAAAGTTAAATTCGAGGGTGACACATTTGGTTAATCGTATAG AACTTAAGGGCATTGACTTCAAAGAAGTGGCAACATCTTGGCCATAAACTGGAATATAATTTAACTCTCACAATGTCTACATTACGGCGGATAAACAAAAGAAATGGCATTAAAGCGAATT TCAAAATCCGCCACAATGTCGAAGACGGCTCGTTCAACTGGCGGACATTATCAGCAGAACACCCCAATCGGTGATGGCCGGTTCTGTTACCTGATAATCATTACCTTTCTACTCAAAGCG TTTTATCTAAAGATCTAACGAGAAGCGTGATCATATGGTTCTACTGGAATTTGTTACCGCAGCTGGTATCAGCAGCGCATGGATGAGCTGTATAAATAACAGGCATCAATAAAACGAAA GGCTCAGTCGAAAAGACTGGCCCTTCGTTTTATCTGTTGTTGTCGGTGAACGCTCTACTAGAGTCACACTGGCTCACCTTCGGGTGGCCCTTCTGCGTTTATAGGTCTCAGTTTCAGAGCT ATGCTGGAACAGCATAGCAAGTTGAAATAAGGCTAGTCCGTTATCAACTGAAAAGTGGCACCGAGTCGGTGCTTTTTCTCGGTACCAAAATCCAGAAAAGAGGCTCCCGAAAGGGGG GCCTTTTTCTGTTTGGTCCACCCTGCACGATAAACAAGTAAAGT</p>
pMC0x_gRNA_Pos5a1_Ptet	<p>GGTCAAAATCACTGTAATGATCTTAATTCCTAATTTTTGTTGACACTCTATCATTGATAGAGTTATTTAGTCCAGAGACCAGAAAGTGAACCTGATTTTCATGCGTCATTTTGAAACATTTTGTAAT TCCTATTTAATAATGTGTGCGGCAATTCACATTTAATTTATGAATGTTTTCTTAACATCGCGCAACTCAAGAAACGGCAGGTTCCGATCTAGACTAGAGAAAGAGGAGAAATCTAGATG CGTAAAGGCGAAGAACCTTTCACTGCGGTAGTACCAATTTTAGTGGAGCTGGACGGAGATGTAATGGTCATAAGTTTTCACTGCGAGAGAAAGGGAAGGAGATGCAACTAACGGTAAGC TGACACTAAAGTTTATCTGTACCACGGGTAACCTGCGGTCCATGGCCGACACTGGTTACTACACTTACTTATGGTGACAATGCTTTGCTGTTATCTGACCATATGAAGCAGCACGATTT CTTCAAATCGGCCATGCCTGAAGGATACGTGCAAGAACGTACAATTAGCTTTAAAGATGACGGCACCTATAAAACGCGCCGAAAGTTAAATTCGAGGGTGACACATTTGGTTAATCGTATAG AACTTAAGGGCATTGACTTCAAAGAAGTGGCAACATCTTGGCCATAAACTGGAATATAATTTAACTCTCACAATGTCTACATTACGGCGGATAAACAAAAGAAATGGCATTAAAGCGAATT TCAAAATCCGCCACAATGTCGAAGACGGCTCGTTCAACTGGCGGACATTATCAGCAGAACACCCCAATCGGTGATGGCCGGTTCTGTTACCTGATAATCATTACCTTTCTACTCAAAGCG TTTTATCTAAAGATCTAACGAGAAGCGTGATCATATGGTTCTACTGGAATTTGTTACCGCAGCTGGTATCAGCAGCGCATGGATGAGCTGTATAAATAACAGGCATCAATAAAACGAAA GGCTCAGTCGAAAAGACTGGCCCTTCGTTTTATCTGTTGTTGTCGGTGAACGCTCTACTAGAGTCACACTGGCTCACCTTCGGGTGGCCCTTCTGCGTTTATAGGTCTCAGTTTCAGAGCT ATGCTGGAACAGCATAGCAAGTTGAAATAAGGCTAGTCCGTTATCAACTGAAAAGTGGCACCGAGTCGGTGCTTTTTCTCGGTACCAAAATCCAGAAAAGAGGCTCCCGAAAGGGGG GCCTTTTTCTGTTTGGTCCACCCTGCACGATAAACAAGTAAAGT</p>
pMC0x_gRNA_Pos5a2_Ptet	<p>CAGGCAAATCACTGTAATGATCTTAATTCCTAATTTTTGTTGACACTCTATCATTGATAGAGTTATTTAGTCCAGAGACCAGAAAGTGAACCTGATTTTCATGCGTCATTTTGAAACATTTTGTAAT ATCTATTTAATAATGTGTGCGGCAATTCACATTTAATTTATGAATGTTTTCTTAACATCGCGCAACTCAAGAAACGGCAGGTTCCGATCTAGACTAGAGAAAGAGGAGAAATCTAGATG CGTAAAGGCGAAGAACCTTTCACTGCGGTAGTACCAATTTTAGTGGAGCTGGACGGAGATGTAATGGTCATAAGTTTTCACTGCGAGAGAAAGGGAAGGAGATGCAACTAACGGTAAGC CTGACACTAAAGTTTATCTGTACCACGGGTAACCTGCGGTCCATGGCCGACACTGGTTACTACACTTACTTATGGTGACAATGCTTTGCTGTTATCTGACCATATGAAGCAGCACGATTT CTTCAAATCGGCCATGCCTGAAGGATACGTGCAAGAACGTACAATTAGCTTTAAAGATGACGGCACCTATAAAACGCGCCGAAAGTTAAATTCGAGGGTGACACATTTGGTTAATCGTATA GAACTTAAGGGCATTGACTTCAAAGAAGTGGCAACATCTTGGCCATAAACTGGAATATAATTTAACTCTCACAATGTCTACATTACGGCGGATAAACAAAAGAAATGGCATTAAAGCGAATT TTCAAAATCCGCCACAATGTCGAAGACGGCTCGTTCAACTGGCGGACATTATCAGCAGAACACCCCAATCGGTGATGGCCGGTTCTGTTACCTGATAATCATTACCTTTCTACTCAAAGCG GTTTTATCTAAAGATCTAACGAGAAGCGTGATCATATGGTTCTACTGGAATTTGTTACCGCAGCTGGTATCAGCAGCGCATGGATGAGCTGTATAAATAACAGGCATCAATAAAACGAAA AGGCTCAGTCGAAAAGACTGGCCCTTCGTTTTATCTGTTGTTGTCGGTGAACGCTCTACTAGAGTCACACTGGCTCACCTTCGGGTGGCCCTTCTGCGTTTATAGGTCTCAGTTTCAGAGCT TATGCTGGAACAGCATAGCAAGTTGAAATAAGGCTAGTCCGTTATCAACTGAAAAGTGGCACCGAGTCGGTGCTTTTTCTCGGTACCAAAATCCAGAAAAGAGGCTCCCGAAAGGGGG GGCCTTTTTCTGTTTGGTCCACCCTGCACGATAAACAAGTAAAGT</p>
pMC0x_gRNA_Pos5b1_Ptet	<p>GTAACAAATCACTGTAATGATCTTAATTCCTAATTTTTGTTGACACTCTATCATTGATAGAGTTATTTAGTCCAGAGACCAGAAAGTGAACCTGATTTTCATGCGTCATTTTGAAACATTTTGTAAT TCCTATTTAATAATGTGTGCGGCAATTCACATTTAATTTATGAATGTTTTCTTAACATCGCGCAACTCAAGAAACGGCAGGTTCCGATCTAGACTAGAGAAAGAGGAGAAATCTAGATG CGTAAAGGCGAAGAACCTTTCACTGCGGTAGTACCAATTTTAGTGGAGCTGGACGGAGATGTAATGGTCATAAGTTTTCACTGCGAGAGAAAGGGAAGGAGATGCAACTAACGGTAAGC TGACACTAAAGTTTATCTGTACCACGGGTAACCTGCGGTCCATGGCCGACACTGGTTACTACACTTACTTATGGTGACAATGCTTTGCTGTTATCTGACCATATGAAGCAGCACGATTT CTTCAAATCGGCCATGCCTGAAGGATACGTGCAAGAACGTACAATTAGCTTTAAAGATGACGGCACCTATAAAACGCGCCGAAAGTTAAATTCGAGGGTGACACATTTGGTTAATCGTATAG AACTTAAGGGCATTGACTTCAAAGAAGTGGCAACATCTTGGCCATAAACTGGAATATAATTTAACTCTCACAATGTCTACATTACGGCGGATAAACAAAAGAAATGGCATTAAAGCGAATT TCAAAATCCGCCACAATGTCGAAGACGGCTCGTTCAACTGGCGGACATTATCAGCAGAACACCCCAATCGGTGATGGCCGGTTCTGTTACCTGATAATCATTACCTTTCTACTCAAAGCG TTTTATCTAAAGATCTAACGAGAAGCGTGATCATATGGTTCTACTGGAATTTGTTACCGCAGCTGGTATCAGCAGCGCATGGATGAGCTGTATAAATAACAGGCATCAATAAAACGAAA GGCTCAGTCGAAAAGACTGGCCCTTCGTTTTATCTGTTGTTGTCGGTGAACGCTCTACTAGAGTCACACTGGCTCACCTTCGGGTGGCCCTTCTGCGTTTATAGGTCTCAGTTTCAGAGCT ATGCTGGAACAGCATAGCAAGTTGAAATAAGGCTAGTCCGTTATCAACTGAAAAGTGGCACCGAGTCGGTGCTTTTTCTCGGTACCAAAATCCAGAAAAGAGGCTCCCGAAAGGGGG GCCTTTTTCTGTTTGGTCCACCCTGCACGATAAACAAGTAAAGT</p>

pMC0x_gRNA_Pos5b2_Ptet	AAAGCAAATCACTGTAATGATCTTAATTCCTAATTTTTGTTGACACTCTATCATTGATAGAGTTATTTTAGTCCAGAGACCGAAAAGTAAACGTGATTCATGCGTCATTTTGAAACATTTGTAA ATCTTATTTAATAATGTGCGGCAATTCACATTTAATTTATGAATGTTTTCTTAACATCGCGCAACTCAAGAAACGGCAGGTTCCGGATCTTAGCTACTAGAGAAAGAGGAGAAATACTAGAT GCGTAAAGGCGAAGAACTTTTCACTGGCGTAGTACCAATTTTAGTGGAGCTGGACGGAGATGAAATGGTCATAAGTTTTCAAGTTCCAGTGAGGAGAAGGCGAAGGAGATGCAACTAACGGTAAG CTGACACTAAAGTTTATCTGTACCACGGGTAACCTGCCGGTCCCATGGCCGACACTGGTTACTACACTTACTTATGGGTGACAATGCTTTGCTCGTTATCCTGACCATATGAAGCAGCAGCATT TCTTCAAATCGGCCATGCCTGAAGGATACGTGCAAGAAGTACAATTAGCTTTAAAGATGACGGCACCTATAAAACGCGCGCGAAGTAAATTCGAGGGTGACACATTGGTTAATCGTATA GAACTTAAGGGCATTGACTTCAAAGAAGATGGCAACATCCTTGGCCATAAACTGGAATATAATTTTAACTCTCAATGTCTACATTACGGCGGATAACAAAAGAATGGCATTAAAGCGAAT TTCAAATCCGCCACAATGTCGAAGACGGTCCGGTTCACTGGCGGACCATTATCAGCAGAACACCCCAATCGGTGATGGCCCGGTTCTGTTACCTGATAATCATTACCTTTCTACTCAAAGC GTTTTATCTAAAGATCTAACGAGAAGCGTGATCATATGGTTCTACTGGAAATTTGTACCGCAGCTGGTATCACGCACGGCATGGATGAGCTGTATAAATAACCAGGCATCAAATAAACGAA AGGCTCAGTCGAAAGACTGGGCCTTTCTGTTTTATCTGTTTGTTCGGTGAACGCTCTCTACTAGAGTCACACTGGCTCACCTTCGGGTGGCCCTTCTGCGTTTATAGGTTCTCAGTTTCAGAGC TATGCTGGAACAGCATAGCAAGTTGAAATAAGGCTAGTCCGTTATCAACTTGAAAAAGTGGCACCAGTCCGGTCTTTTTTCTCGGTACCAAATTCAGAAAAGAGGCCTCCGAAAGGGG GGCCTTTTTTCGTTTTGGTCCACCTGCACGATAACTGAAGCT
------------------------	--

Supplementary Table S3: Oligonucleotides used to assemble gRNA sequences. All sequences written as 5' -> 3'. Oligonucleotides for *rhaA*, indicated with *, did not result in functional gRNAs.

Target	gRNA sequence	forward oligonucleotide		reverse oligonucleotide	
wbfF	TTAGCCAAGATCAGTCACGT	oDS_200_A_gRNA_wbf_1_fwd	GTCCTTAGCCAAGATCAGTCACGT	oDS_201_A_gRNA_wbf_1_rev	AAACACGTGACTGATCTTGCTAA
xds	ATATTCGGTAATCAAACCT	oDS_295_A_gRNA_xds_fwd	GTCCATATTCGGTAATCAAACCT	oDS_296_A_gRNA_xds_rev	AAACAAGTTTTGATTACGGAATAT
fliA (flagella)	AAGGATTAACGTTAGCTT	oDS_299_A_gRNA_fliA_fwd	GTCCAAGGATTAACGTTAGCTT	oDS_300_A_gRNA_fliA_rev	AAACAAGCTAACGTTTTAATCCTT
pilA (pili)	CTGATTTCTTTACGTAGTTT	oDS_309_A_gRNA_pilA_fwd	GTCCCTGATTTCTTTACGTAGTTT	oDS_310_A_gRNA_pilA_rev	AAACAAACTACGTAAGAAATCAG
galE	ATGTGTTACTACTACGTA	oDS_517_A_gRNA_galE_fwd	GTCCATGTGTTACTACTACGTA	oDS_518_A_gRNA_galE_rev	AAACTACGGTAGTAGTAACACAT
vnp1	ATGGAACAGACCTACCCAG	oDS_551_A_gRNA_vnp1_fwd	GTCCATGGAACAGACCTACCCAG	oDS_552_A_gRNA_vnp1_rev	AAACCTGGGTAGGTCTGTTCCAT
vnp2	TACTCACTGGAGCAGCAGCA	oDS_563_A_gRNA_vnp2_fwd	GTCCACTCACTGGAGCAGCAGCA	oDS_564_A_gRNA_vnp2_rev	AAACTGCTGCTGCCAGTGAGTA
rpoS (indirect)	AGTTCTGTGCACACGCCAAT	oDS_380_gRNA_rpoS_fwd	GTCCAGTTCTGTGCACACGCCAAT	oDS_381_gRNA_rpoS_rev	AAACATTGGCGTGTGCACAGAAT
hisG	TTGAAAAATGATGGAGTAA	oDS_435_A_gRNA_hisG_fwd	GTCCTTGAAAAATGATGGAGTAA	oDS_436_A_gRNA_hisG_rev	AAACTTACTCCATCATTTTTCAA
rplS (indirect)	CACCTGGTGCAAATTTAGGT	oDS_448_A_gRNA_rplS_ind_fwd	GTCCCACCTGGTGCAAATTTAGGT	oDS_449_A_gRNA_rplS_ind_rev	AAACACCTAAATTTGCACCAGGTG
rpsB	TCGTAGAAGCTGAATAATAG	oDS_459_A_gRNA_rpsB_fwd	GTCCTCGTAGAAGCTGAATAATAG	oDS_460_A_gRNA_rpsB_rev	AAACCTATTATTCAGCTTCTACGA
intergenic integration (int9)	AGTCGTTATGGCGTAAAG	oDS_473_A_gRNA_int9_fwd	GTCCAGTCGTTATGGCGTAAAG	oDS_474_A_gRNA_int9_rev	AAACCTTTCAGCCATAAGCGACT
malQ	TGGCGTTTAGAAACAGAGCA	oDS_399_A_gRNA_malQ_fwd	GTCCTGGCGTTTAGAAACAGAGCA	oDS_400_A_gRNA_malQ_rev	AAACTGCTGTTTTCTAAACGCCA
glpK	ACTCAGATTTATCCGCAAGC	oDS_596_A_gRNA_glpK_fwd	GTCCACTCAGATTTATCCGCAAGC	oDS_597_A_gRNA_glpK_rev	AAACGCTTGCGATAAATCTGAGT
rhaA (1)*	CAGGGTAGTTACCTGTTGCT	oDS_585_A_gRNA_rhaA_fwd	GTCCCAGGGTAGTTACCTGTTGCT	oDS_586_A_gRNA_rhaA_rev	AAACAGCAACAGGTAACCTACCTG
rhaA (2)*	AGTGGCGGTATCCAAGCAAC	oDS_635_A_gRNA_rhaA_2_fwd	GTCCAGTGGCGGTATCCAAGCAAC	oDS_636_A_gRNA_rhaA_2_rev	AAACGTTGCTTGATACCGCCACT
wbfF (PAM = NGA)	GTAAGAAACCATTCGCTT	oDS_617_A_gRNA_wbf_NGA_fwd	GTCCGTAAGAAACCATTCGCTT	oDS_618_A_gRNA_wbf_NGA_rev	AAACAAGCGGAATGGGTTTCTTAC
wbfF (PAM = NGC)	GATTGTAATCGTGACAGCG	oDS_619_A_gRNA_wbf_NGC_fwd	GTCCGATTGTAATCGTGACAGCG	oDS_620_A_gRNA_wbf_NGC_rev	AAACCGCTGTCAGGATTACCAATC
wbfF (PAM = NGT)	TGGATATCCAAGTACAGGG	oDS_621_A_gRNA_wbf_NGT_fwd	GTCCTGGATATCCAAGTACAGGG	oDS_622_A_gRNA_wbf_NGT_rev	AAACCCCTGATACTGGATATCCA
wbfF (PAM = NGC) (2)	ACGCGGGAATGGCTCAGAT	oDS_646_A_gRNA_wbf_NGC_2_fwd	GTCCACGCGGGAATGGCTCAGAT	oDS_647_A_gRNA_wbf_NGC_2_rev	AAACATCTGAAGCCATTCGCGCT
wbfF (PAM = NGA) (2)	ATACGTAACCTACTGACCG	oDS_648_A_gRNA_wbf_NGA_2_fwd	GTCCATACGTAACCTACTGACCG	oDS_649_A_gRNA_wbf_NGA_2_rev	AAACCGGTGAGTAAAGTTTACGTAT
rpoS (PAM = NGT)	TGTCGATTAGTCATCTTCA	oDS_623_A_gRNA_rpoS_NGT_fwd	GTCCTGTCGATTAGTCATCTTCA	oDS_624_A_gRNA_rpoS_NGT_rev	AAACTCGAAGTACTAATCGACA

Supplementary Table S4: Oligonucleotides used for the construction of tDNA template plasmids. All sequences written as 5' → 3'.

Plasmid	forward oligonucleotide		reverse oligonucleotide		PCR template
wbFf tDNA template	oDS_193_GA_dwbf_U_fwd	TAGCAACTGTTTTAGCGCTGAGC	oDS_194_GA_dwbf_U_rev	TATACATCAATTGCTTTTATCATCATACTATTCAATAAG	V. natriegens DNA
	oDS_195_GA_dwbf_D_fwd	TGATGATAAAAAGCAATTGATGTATAAAGCTCATTATTTCG	oDS_196_GA_dwbf_D_rev	GTGTCTCTGCGATAAGTATTGATC	V. natriegens DNA
	oDS_197_GA_dwbf_V_rev	ACGCTCAGCGCTAAAACAGTGTCTAGGCCGCGAATCCAGAAATC	oDS_198_GA_dwbf_V_fwd	GATCAATACTTACGACAGGAACACTAGTAGCGGCCGCTGCAGTC	pMC_V*_03
xds tDNA template	oDS_531_GA_xds_U_fwd	TGGTTACGTTTTTTCAGGAGC	oDS_532_GA_xds_U_rev	AAACACTATGTCCCATGTTTTATAGATTGAATGTTAATATCG	V. natriegens DNA
	oDS_533_GA_xds_D_fwd	TATAAAACATGGGACATAAGTGTTTATTGAAGTGAAGG	oDS_534_GA_xds_D_rev	TGCCGATTTTCCTCCCGATC	V. natriegens DNA
	oDS_536_GA_xds_V_fwd	GTGATGATCGGGACGAAAATCGGCATAGTAGCGGCCGCTGCAGTC	oDS_535_GA_xds_V_rev	CTTGGCTCTGAAAAACGTAACCGAGGCCGCGAATCCAGAAATC	pMC_V_01
flagella tDNA Template	oDS_355_GA_flagella_U_fwd	ACTTACAGAATGAGCGTAAATGG	oDS_356_GA_flagella_U_rev	AGTCAGTGTTTTAAATATGTGCTCCAATAAGATGAAGG	V. natriegens DNA
	oDS_357_GA_flagella_D_fwd	GGAGCACATATTTAAAACACTGACTTTATGATTCAGTGG	oDS_358_GA_flagella_D_rev	TGTCACCGCCACTTTGATGG	V. natriegens DNA
	oDS_360_GA_flagella_V_fwd	GATTACCATCAAAAGTCCGTTGACATAGTAGCGGCCGCTGCAGTC	oDS_359_GA_flagella_V_rev	TCCCATTTACGCTCATTCTGTAAGTGGCCGCGAATCCAGAAATC	pMC_V_01
pili tDNA template	oDS_497_GA_pili_U_fwd	CAGTTGCTCGAAAATCTCAACC	oDS_498_GA_pili_U_rev	GAAGGAAGAGAGATTTCACTTTGAACTAGCAGCCATTTAG	V. natriegens DNA
	oDS_499_GA_pili_D_fwd	TTCAAAGTGAATCTCTCTCTCTCATGAGATAG	oDS_500_GA_pili_D_rev	TGGTTGGATCTATAAAACAGCAAATC	V. natriegens DNA
	oDS_502_GA_pili_V_fwd	TTTGCTGTTTTATAGATCCAACATAGTAGCGGCCGCTGCAGTC	oDS_501_GA_pili_V_rev	TATGGTTGAGATTTTCGAGCAACTGGCCGCGAATCCAGAAATC	pMC_V_01
galE tDNA template	oDS_507_GA_galE_U_fwd	GCAAGCGCACGATTAACC	oDS_508_GA_galE_U_rev	CGGAGAAGTAAAAATTTTCATCCGGTGCAGTGCG	V. natriegens DNA
	oDS_509_GA_galE_D_fwd	ACCGGATGAAAATTTACTTCTCCGCTGTTGCTG	oDS_510_GA_galE_D_rev	ATTTTTTATGGAACTTGACTGGTTAG	V. natriegens DNA
	oDS_512_GA_galE_V_fwd	AACGAGTCAAGTCCAATAAAAAATTAGTAGCGGCCGCTGCAGTC	oDS_511_GA_galE_V_rev	GATTGGTTTTAATCGTGCCTTGCGCCGCGAATCCAGAAATC	pMC_V_01
vnp1 tDNA template	oDS_541_GA_vnp1_U_fwd	TGGGCACACAAATGGTACG	oDS_542_GA_vnp1_U_rev	AAAAACCACACAACAAATCTCACTCAGCTTATCG	V. natriegens DNA
	oDS_543_GA_vnp1_D_fwd	GTGTAGATGTTTTGTGTGGTTTTACATCTGAGTG	oDS_544_GA_vnp1_D_rev	ACCACAACACTCAATTTGGACG	V. natriegens DNA
	oDS_546_GA_vnp1_V_fwd	CGCGCTCAAATGAGTGTGGTTAGTAGCGGCCGCTGCAGTC	oDS_545_GA_vnp1_V_rev	AATAGCGTACCAATTTGTGCGCCGAGCCGCGAATCCAGAAATC	pMC_V_01
vnp2 tDNA template	oDS_553_GA_vnp2_U_fwd	CAAATCTTCGGACAGCAGAG	oDS_554_GA_vnp2_U_rev	TTCTAGTCAAAGGAAGAAAAAGTGGGCTGATTATC	V. natriegens DNA
	oDS_555_GA_vnp2_D_fwd	ACTTTTTCTCTTGTACTACGAAAATGGGGAAAC	oDS_556_GA_vnp2_D_rev	GCAGAGCAACACGCAAGCTC	V. natriegens DNA
	oDS_558_GA_vnp2_V_fwd	GACAAAGAGCTGCGTGTCTCTAGTAGCGGCCGCTGCAGTC	oDS_557_GA_vnp2_V_rev	TCTACTGTGCTCCGAAAGATTTGGGCCGCGAATCCAGAAATC	pMC_V_01
rpoS mScarlet-I tDNA template (indirect)	oDS_366_GA_rpoS_U_fwd	AAGCGCCATTTTGAGTCTGC	oDS_367_GA_rpoS_U_Mut_rev	TCACCACCAATAGCGGTGTCGACAG	V. natriegens DNA
	oDS_368_GA_rpoS_U_Mut_fwd	CTGTCGACACGCCTATTGGTGGTG	oDS_369_GA_rpoS_U_rev	TGATCACTGCTTACCTTTAGAAACGTCATCTTCGACGTTAAACAAG	V. natriegens DNA
	oDS_370_GA_rpoS_D_fwd	CGGTGGTATGGATGAACGTACAAAATAATGACATACATAAAGAGAAAAGGC	oDS_371_GA_rpoS_D_rev	ACTGATCGAGACGCTATCG	V. natriegens DNA
	oDS_373_GA_rpoS_V_fwd	TGCAACGATAGCGCTCTGCATCAGTTAGTAGCGGCCGCTGCAGTC	oDS_372_GA_rpoS_V_rev	TTGCCGACAGCTAAAATGGCGCTTGGCCGCGAATCCAGAAATC	pMC_V_01
	oDS_374_GA_mScarlet-I_fwd	GTTTCTAAAGGTGAAGCAGTGATC	oDS_375_GA_mScarlet-I_rev	TTGTACAGTTCATCCATACCAC	pMC0_4_12_CDSmScarlet-I (Vn)
rpoS mScarlet-I tDNA template (direct)	oDS_366_GA_rpoS_U_fwd	AAGCGCCATTTTGAGTCTGC	oDS_369_GA_rpoS_U_rev	TGATCACTGCTTACCTTTAGAAACGTCATCTTCGACGTTAAACAAG	V. natriegens DNA
	oDS_370_GA_rpoS_D_fwd	CGGTGGTATGGATGAACGTACAAAATAATGACATACATAAAGAGAAAAGGC	oDS_371_GA_rpoS_D_rev	ACTGATCGAGACGCTATCG	V. natriegens DNA
	oDS_373_GA_rpoS_V_fwd	TGCAACGATAGCGCTCTGCATCAGTTAGTAGCGGCCGCTGCAGTC	oDS_372_GA_rpoS_V_rev	TTGCCGACAGCTAAAATGGCGCTTGGCCGCGAATCCAGAAATC	pMC_V_01
tDNA template hisG-mScarlet-I	oDS_374_GA_mScarlet-I_fwd	GTTTCTAAAGGTGAAGCAGTGATC	oDS_375_GA_mScarlet-I_rev	TTGTACAGTTCATCCATACCAC	pMC0_4_12_CDSmScarlet-I (Vn)
	oDS_426_GA_hisG_U_fwd	TCACGCCATCTTACCATCAAAG	oDS_427_GA_hisG_U_rev	TGATCACTGCTTACCTTTAGAAACCTCCATCTTTTCAATTGGTATG	V. natriegens DNA
	oDS_428_GA_hisG_D_fwd	CGGTGGTATGGATGAACGTACAAAATAAGGGTCTAGGAAACAGTGTTTG	oDS_429_GA_hisG_D_rev	CCTGTCTCATCAAGATTACAG	V. natriegens DNA
tDNA template rplS-mScarlet-I (direct)	oDS_431_GA_hisG_V_fwd	TTGCCGTGAATCTTATGATGAGCAAGGTAGTAGCGGCCGCTGCAGTC	oDS_430_GA_hisG_V_rev	TACTTTGATGGTGAAGATGGCGTGAAGCCGCGAATCCAGAAATC	pMC_V_01
	oDS_374_GA_mScarlet-I_fwd	GTTTCTAAAGGTGAAGCAGTGATC	oDS_375_GA_mScarlet-I_rev	TTGTACAGTTCATCCATACCAC	pMC0_4_12_CDSmScarlet-I (Vn)
	oDS_437_GA_rplS_U_fwd	GATGATGGGTGAGATTAAGATC	oDS_440_GA_rplS_U_rev	TGATCACTGCTTACCTTTAGAAACCTTCTTAGCAAGTTTCTCTTGATAC	V. natriegens DNA
	oDS_441_GA_rplS_D_fwd	CGGTGGTATGGATGAACGTACAAAATAATGCTATAACTAGCCTTCTCATTAAC	oDS_442_GA_rplS_D_rev	TTATTGTTTTCTTGGTGTGGTGC	V. natriegens DNA
	oDS_444_GA_rplS_V_fwd	ACGACCACACCAAGAAAACAATAAGTAGCGGCCGCTGCAGTC	oDS_443_GA_rplS_V_rev	AAGATCTTTAATCTCACCCATCATCGGCCGCGAATCCAGAAATC	pMC_V_11
tDNA template rplS-mScarlet-I (indirect)	oDS_374_GA_mScarlet-I_fwd	GTTTCTAAAGGTGAAGCAGTGATC	oDS_375_GA_mScarlet-I_rev	TTGTACAGTTCATCCATACCAC	pMC0_4_12_CDSmScarlet-I (Vn)
	oDS_439_GA_rplS_U_Mut_fwd	ATCAGACTACCAAAATTTGCACCAGGTGAC	oDS_442_GA_rplS_D_rev	TTATTGTTTTCTTGGTGTGGTGC	tDNA template rplS-mScarlet-I (direct)
	oDS_444_GA_rplS_V_fwd	ACGACCACACCAAGAAAACAATAAGTAGCGGCCGCTGCAGTC	oDS_438_GA_rplS_U_Mut_rev	TGGTCAAATTTGGTAGGCTGATTTTCATTTG	tDNA template rplS-mScarlet-I (direct)
tDNA template rpsB-mScarlet-I	oDS_450_GA_rpsB_U_fwd	GATAAAACCTTTCATCATCTTTG	oDS_451_GA_rpsB_U_rev	TGATCACTGCTTACCTTTAGAAACCTTCTAGCTTCTACGAAACCCTC	V. natriegens DNA
	oDS_452_GA_rpsB_D_fwd	CGGTGGTATGGATGAACGTACAAAATAAGCGCTCTAGTCACAC	oDS_453_GA_rpsB_D_rev	ATACCAGTGTCTTCCGCTTGG	V. natriegens DNA
	oDS_455_GA_rpsB_V_fwd	AGCTAACCGCAGAAAACACTGGTATTAGTAGCGGCCGCTGCAGTC	oDS_454_GA_rpsB_V_rev	GAAATGATGATGAAGGAGTTTTATCGGCCGCGAATCCAGAAATC	pMC_V_11
	oDS_374_GA_mScarlet-I_fwd	GTTTCTAAAGGTGAAGCAGTGATC	oDS_375_GA_mScarlet-I_rev	TTGTACAGTTCATCCATACCAC	pMC0_4_12_CDSmScarlet-I (Vn)
	oDS_461_GA_int9_U_fwd	TTTGTTCGCCAGAGTATGGAG	oDS_462_GA_int9_U_rev	CGTCTTTTTCTGTTTTGGCTGTTTAAAGGGCAGCTTTTTCTTACTTTAAC	V. natriegens DNA

int9 mScarlet-I integration tDNA template	oDS_463_GA_int9_D_fwd	GCCTTTCTGCGTTTATACGCTTACTCACGCCATAAGCGACTAAGAAAC	oDS_464_GA_int9_D_rev	CTCCATGTTTATGTCTAACACGG	V. natriegens DNA
	oDS_466_GA_int9_V_fwd	TGCCGTGTAGACATAAACATGGAGTAGTAGCGGCCGTCGAGTC	oDS_465_GA_int9_V_rev	ACACTCCATACTCTGGCGAAACAAAGCCCGGAATCCAGAAATC	pMC_V_11
	oDS_467_GA_integration_insert_fwd	AACAGGACCAAAACGAAAAAGACG	oDS_468_GA_integration_insert_rev	AGTAAGCGTATAAACGCAGAAAGG	pST_133
malQ 298C>T tDNA Template	oDS_391_GA_malQ_U_fwd	CAAATATGGCACTAAGTTCAGC	oDS_392_GA_malQ_U_rev	TTAGAAACAGAGTAAGGAGAGGTACTTGAAGGC	V. natriegens DNA
	oDS_393_GA_malQ_D_fwd	GTACCTCTCTTACTCTGTTCTAAACGCCAGC	oDS_394_GA_malQ_D_rev	AAAGCTTTGTTGCGATTGAGATC	V. natriegens DNA
	oDS_396_GA_malQ_V_fwd	GTGATCTGAATCGCAACAAAGCTTTAGTAGCGGCCGTCGAGTC	oDS_395_malQ_V_rev	GGCTGAACACTTAGTGCCATATTTGGGCCGGAATCCAGAAATC	pMC_V_01
glpK C124>T tDNA template	oDS_587_GA_glpK_U_fwd	CCAAGAATGGCGTTTGCTGC	oDS_588_GA_glpK_U_rev	CCCAACCTGCTACGGATAAATCTGAGTAAATTC	V. natriegens DNA
	oDS_589_GA_glpK_D_fwd	CAGATTTATCCGTAAGCAGGTTGGGTTGAG	oDS_590_GA_glpK_D_rev	ATTCAAACCCGGTTTTTATCTCCG	V. natriegens DNA
	oDS_592_GA_glpK_V_fwd	CGGAGATAAAAACCGTTTTGAATTAGTAGCGGCCGTCGAGTC	oDS_591_GA_glpK_V_rev	CCGTGGCAGCAAACGCCATTCTGGGGCCGGAATCCAGAAATC	pMC_V_01
glpK G123>C, C124>T tDNA template	oDS_587_GA_glpK_U_fwd	CCAAGAATGGCGTTTGCTGC	oDS_644_GA_glpK C:C_U_rev	CCCAACCTGCTAGGGATAAATCTGAGTAAATTC	V. natriegens DNA
	oDS_645_GA_glpK C:C_U_fwd	CAGATTTATCCCTAAGCAGGTTGGGTTGAG	oDS_590_GA_glpK_D_rev	ATTCAAACCCGGTTTTTATCTCCG	V. natriegens DNA
	oDS_592_GA_glpK_V_fwd	CGGAGATAAAAACCGTTTTGAATTAGTAGCGGCCGTCGAGTC	oDS_591_GA_glpK_V_rev	CCGTGGCAGCAAACGCCATTCTGGGGCCGGAATCCAGAAATC	pMC_V_01
araA C76>T tDNA template	oDS_565_GA_araA_U_fwd	ATAGTTACGCCAGATAGGGCAG	oDS_566_GA_araA_U_rev	TCTTTGCCACTTACTCCAATACTTTAGGACC	V. natriegens DNA
	oDS_567_GA_araA_D_fwd	AAAGTATTGGAGTAAGTGGCAAAGAACAGC	oDS_568_GA_araA_D_rev	CTGGTGGAGATGTCAGTGTTTAC	V. natriegens DNA
	oDS_570_GA_araA_V_fwd	CGGTAACACTGACATCTCCACCACTAGTAGCGGCCGCTGAGTC	oDS_569_GA_araA_V_rev	TCGCTGCCCTATCTGGCGTAACTATGGCCGGAATCCAGAAATC	pMC_V_01
araA C76>T, G81>C tDNA template	oDS_565_GA_araA_U_fwd	ATAGTTACGCCAGATAGGGCAG	oDS_688_GA_araA C:C_U_rev_new	TCTTTGCGACTTACTCCAATACTTTAGGACCGTATAGG	V. natriegens DNA
	oDS_643_GA_araA C:C_U_fwd	AAAGTATTGGAGTAAGTGGCAAAGAACAGCGAAGAG	oDS_568_GA_araA_D_rev	CTGGTGGAGATGTCAGTGTTTAC	V. natriegens DNA
	oDS_570_GA_araA_V_fwd	CGGTAACACTGACATCTCCACCACTAGTAGCGGCCGCTGAGTC	oDS_569_GA_araA_V_rev	TCGCTGCCCTATCTGGCGTAACTATGGCCGGAATCCAGAAATC	pMC_V_01

Supplementary Table S5: Oligonucleotides to generate tDNA fragments from tDNA template plasmids. All sequences written as 5' → 3'.

tDNA	forward oligonucleotide		reverse oligonucleotide		PCR template
wbFF 3kb	oDS_193_GA_dwbF_U_fwd	TAGCAACTGTTTTAGCGCTGAGC	oDS_196_GA_dwbF_D_rev	GTGTTCTGCTGATAAGTATTGATC	wbFF tDNA template
wbFF 1kb	oDS_410_tDNA_wbF_1kb_U_fwd	GAACGATGTCGACAGCGATG	oDS_411_tDNA_wbF_1kb_D_rev	TCTAAATTTGTAATTTTTTCAATCATGATG	wbFF tDNA template
wbFF 500bp	oDS_412_tDNA_wbF_500bp_U_fwd	ACGAGCTTCATTGAGAAATATATACAC	oDS_413_tDNA_wbF_500bp_D_rev	ATGCAATGACCCAGTAATAAG	wbFF tDNA template
wbFF 200bp	oDS_414_tDNA_wbF_200bp_U_fwd	TTATCTAGGCGAGTTTTACGTCAG	oDS_415_tDNA_wbF_200bp_D_rev	TGTCATCGAAAGAACTCTTAATTTCCG	wbFF tDNA template
wbFF 100bp	oDS_416_tDNA_wbF_100bp_U_fwd	AAAAATCAGCAGAAACAACGACAC	oDS_417_tDNA_wbF_100bp_D_rev	GACCTAAAGAACGGGTGGATG	wbFF tDNA template
wbFF 50bp	oDS_418_PE_wbF_50bp_U_fwd	TGAAAATGCCTCTTTTTAAAACCTTAATGAATGAGTATGATGATAAAAGCAATTGATG	oDS_419_PE_wbF_50bp_U_rev	TTGTTTTTTGTTAACCAATTTACGAATAAATGACGCTTATACATCAATTGCTTTTTATC	Primer extension
wbFF 3kb/50bp	oDS_193_GA_dwbF_U_fwd	TAGCAACTGTTTTAGCGCTGAGC	oDS_616_tDNA_wbF_50bp_rev	TTGTTTTTTGTTAACCAATTTACGAATAAATG	wbFF tDNA template
xds	oDS_531_GA_xds_U_fwd	TCGGTTACGTTTTTCAGGAGC	oDS_534_GA_xds_D_rev	TGCCGATTTTCGTCGCCATC	xds tDNA template
flagella	oDS_355_GA_flagella_U_fwd	ACTTACAGAATGAGCGTAAATGG	oDS_358_GA_flagella_D_rev	TGTCACAGGCACCTTTGATGG	flagella tDNA Template
pili	oDS_497_GA_pili_U_fwd	CAGTTGCTGAAAACTCAACC	oDS_500_GA_pili_D_rev	TGGTTGGATCTATAAAAAAGCAAATC	pili tDNA template
galE	oDS_507_GA_galE_U_fwd	GCAAGGCGCAGCATTAAACC	oDS_510_GA_galE_D_rev	ATTTTTATTGGAACCTTGACTGGTTAG	galE tDNA template
vnp1	oDS_541_GA_vnp1_U_fwd	TCGGCACACAAATTTGGTACG	oDS_544_GA_vnp1_D_rev	ACCACAACACTCAATTTGGACG	vnp1 tDNA template
vnp2	oDS_553_GA_vnp2_U_fwd	CAAATCCTTCGGACAGCAGAG	oDS_556_GA_vnp2_D_rev	GCAGAGCAACACGCAGCTC	vnp2 tDNA template
rpoS-mScarlet-I (indirect)	oDS_366_GA_rpoS_U_fwd	AAGCGCCATTTGAGTCTGC	oDS_371_GA_rpoS_D_rev	ACTGATCGAGACGCCTATCG	rpoS mScarlet-I tDNA template (indirect)
rpoS-mScarlet-I (direct)	oDS_366_GA_rpoS_U_fwd	AAGCGCCATTTGAGTCTGC	oDS_371_GA_rpoS_D_rev	ACTGATCGAGACGCCTATCG	rpoS mScarlet-I tDNA template (direct)
hisG-mScarlet-I-I	oDS_426_GA_hisG_U_fwd	TCACGCCATCTCACCATCAAAG	oDS_429_GA_hisG_D_rev	CCTTGCTCATCAAGATTCAGC	tDNA template hisG-mScarlet-I
rplS-mScarlet-I (indirect)	oDS_437_GA_rplS_U_fwd	GATGATGGTGAGATTAAGATC	oDS_442_GA_rplS_D_rev	TTATTGTTTTCTTGGTGGTGGTCG	tDNA template rplS-mScarlet-I (indirect)
rplS-mScarlet-I (direct)	oDS_437_GA_rplS_U_fwd	GATGATGGTGAGATTAAGATC	oDS_442_GA_rplS_D_rev	TTATTGTTTTCTTGGTGGTGGTCG	tDNA template rplS-mScarlet-I (direct)
rpsB-Scarlet-I	oDS_450_GA_rpsB_U_fwd	GATAAACTCCTTCATCATCTTCG	oDS_453_GA_rpsB_D_rev	ATACCAGTGTTCCTGCCGTTAG	tDNA template rpsB-mScarlet-I
int9::mScarlet-I	oDS_461_GA_int9_U_fwd	TTTGTTCGCGAGATATGGAG	oDS_464_GA_int9_D_rev	CTCCATGTTTATGCTAACACGG	int9 mScarlet-I integration tDNA template
malQ 298C>T	oDS_391_GA_malQ_U_fwd	CAAATATGGCACTAAGTGTTCAGC	oDS_394_GA_malQ_D_rev	AAAGCTTTGTTGCGATTGATC	malQ tDNA Template
glpK C124>T	oDS_587_GA_glpK_U_fwd	CCAAGAATGGCGTTTGCTGC	oDS_590_GA_glpK_D_rev	ATTCAAAACCGGTTTTATCTCCG	glpK tDNA template
glpK G123>C C124>T,	oDS_587_GA_glpK_U_fwd	CCAAGAATGGCGTTTGCTGC	oDS_590_GA_glpK_D_rev	ATTCAAAACCGGTTTTATCTCCG	glpK C:C tDNA template
araA C76>T	oDS_565_GA_araA_U_fwd	ATAGTTACGCCAGATAGGGCAG	oDS_568_GA_araA_D_rev	CTGGTGGAGATGTCAGTGTTTAC	araA tDNA template
araA C76>T, G81>C	oDS_565_GA_araA_U_fwd	ATAGTTACGCCAGATAGGGCAG	oDS_568_GA_araA_D_rev	CTGGTGGAGATGTCAGTGTTTAC	araA C:C tDNA template

Supplementary Table S6: Oligonucleotides used for PCR screening of deletions and integrations. All sequences written as 5' - > 3'.

Mutation	forward oligonucleotide		reverse oligonucleotide	
Δ xds	oDS_537_S_xds_out_fwd	GTTTTCTTCCTACCTTTGAACG	oDS_538_S_xds_gap_rev	TAAACACTTATGTCCCATGTTTTATAG
Δ flagella	oDS_363_S_flagella_out_fwd	CTCGAAGCACGCCAAATTGC	oDS_361_S_flagella_gap_rev	ATCATAAAGTCAGTGTTTTAAATATGTGC
Δ pili	oDS_503_S_pili_out_fwd	ACGCTGTTTTCAAGATCTTTGG	oDS_504_S_pili_gap_rev	AGAAGGAAGAGAGATTTCACTTTG
Δ galE	oDS_513_S_galE_out_fwd	TTGGCTCCGGTAATCAAACG	oDS_514_S_galE_gap_rev	AGCGGAGAAGTAAAATTTTCATCC
Δ vnp1	oDS_547_S_vnp1_out_fwd	TCTGCTAGGTTTGCAACAAGC	oDS_548_S_vnp1_gap_rev	ATGTAAAAACCACACAAACAAATCTAC
Δ vnp2	oDS_559_S_vnp2_out_fwd	GATGGTTTAGGCTCCAATACC	oDS_560_S_vnp2_gap_rev	GTAGTCAAAGGAAGAAAAAAGTGG
rpoS-mScarlet-I (indirect)	oDS_377_S_rpoS_out_fwd	CTCGGTGTTCACTCTGTTGC	oDS_375_GA_mScarlet_rev	TTTGTACAGTTCATCCATACCAC
rpoS-mScarlet-I (direct)	oDS_377_S_rpoS_out_fwd	CTCGGTGTTCACTCTGTTGC	oDS_375_GA_mScarlet_rev	TTTGTACAGTTCATCCATACCAC
hisG-mScarlet-I	oDS_432_S_hisG_out_fwd	CACTTCTGAGTCATAGTGACG	oDS_375_GA_mScarlet_rev	TTTGTACAGTTCATCCATACCAC
rplS-mScarlet-I (indirect)	oDS_445_S_rplS_out_fwd	CGACGTTCTGATTGTCGATACC	oDS_375_GA_mScarlet_rev	TTTGTACAGTTCATCCATACCAC
rplS-mScarlet-I (direct)	oDS_445_S_rplS_out_fwd	CGACGTTCTGATTGTCGATACC	oDS_375_GA_mScarlet_rev	TTTGTACAGTTCATCCATACCAC
rpsB-Scarlet-I	oDS_456_S_rpsB_out_fwd	AGCCGCTCGCTGAAAATCG	oDS_375_GA_mScarlet_rev	TTTGTACAGTTCATCCATACCAC
int9::mScarlet-I	oDS_469_S_int9_out_fwd	GCATTGCAAAGCTGGCAACC	oDS_375_GA_mScarlet_rev	TTTGTACAGTTCATCCATACCAC

3.2. DNA replication is not a limiting factor for rapid growth of *Vibrio natriegens*

Lea Ramming*, Daniel Stukenberg*, María del Carmen Sánchez Olmos, Anke Becker, Daniel Schindler (* = shared first author)

bioRxiv, doi: <https://doi.org/10.1101/2023.05.26.541695>., in revision at *Communications Biology*

In this publication we report the fusion of both chromosomes of *V. natriegens* to create the single chromosome strain synSC1.0. We designed a configuration, in which Chr2 is integrated in the Ter region of Chr1 to preserve important chromosome features, e.g. Ori to Ter orientation of highly expressed genes or the polarity of KOPS. With this design, the *dif* sequence on Chr1, as well as the Ori2 was lost in the creation of synSC1.0.

To fuse both chromosomes, we integrated two 3 kbp sequences, identical to the sequences flanking the Ter of Chr1, next to the Ori region of Chr2. This was done in two steps using the NT-CRISPR method (Stukenberg et al., 2022, **Chapter 3.1**). Initially we planned to target the Ori of Chr2 with CRISPR-Cas9 after integration of those two 3 kbp sequences. The rationale behind this strategy was to either force fusion by inducing a DNA double strand break or to select for cells in which the chromosome fusion already occurred spontaneously. However, while verifying the integration of the second flanking region by colony PCR, we were surprised to find one clone with a band pattern matching with the pattern expected for a fused chromosome configuration. Fusion of both chromosomes was later confirmed by Sanger sequencing of the fusion site, whole genome sequencing using the Nanopore and Illumina sequencing technologies, as well as by pulse field gel electrophoresis.

We proceeded by investigating possible phenotypic differences of synSC1.0 compared to the parental strain. The doubling time of synSC1.0 was slightly elevated (7 %). However, this difference was not statistically significant. Cell length and width of synSC1.0 was slightly, but significantly, larger compared to the parental strain.

As a next step, we performed marker frequency analysis based on short read sequencing data from exponentially growing, as well as from stationary cultures. We found an Ori/Ter ratio of approximately four and two for Chr1 and Chr2 of the parental strain, respectively. In case of synSC1.0, the Ori/Ter ratio for the single chromosome was approximately six.

From all results described in this publication, we concluded that the bipartite chromosome configuration of the wild type *V. natriegens* strain is not a requirement for its rapid growth.

Personal contribution

I envisioned the project together with Daniel Schindler. I built the synSC1.0 strain and verification of chromosome fusion by colony PCR and Sanger sequencing of the fusion site. Furthermore, I prepared the DNA for the whole genome sequencing with the Illumina technology, which was used for the marker frequency analysis. Writing of the manuscript was mostly done by Daniel Schindler, with contributions from all other authors, including myself.

DNA replication is not a limiting factor for rapid growth of *Vibrio natriegens*

Authors: Lea Ramming^{1,#}, Daniel Stukenberg^{2,#}, María del Carmen Sánchez Olmos¹,
Anke Becker^{2,3}, Daniel Schindler^{1,3,*}

Affiliations

¹ Max Planck Institute for Terrestrial Microbiology, Marburg, Germany

² Department of Biology, Philipps-Universität Marburg, Marburg, Germany

³ Center for Synthetic Microbiology (SYNMIKRO), Philipps-Universität Marburg, Marburg, Germany

contributed equally; alphabetical order

* correspondence to: daniel.schindler@mpi-marburg.mpg.de

Abstract

DNA replication prior to cell division is essential for the proliferation of all cells. Bacterial chromosomes are replicated bidirectionally from a single origin of replication, with replication proceeding at about 1000 bp per second. For the best-studied model organism, *Escherichia coli*, this translates into a replication time of about 40 min for its 4.6 Mb chromosome. Nevertheless, *E. coli* can propagate by overlapping replication cycles with a maximum short doubling time of 20 min. The fastest growing bacterium known today, *Vibrio natriegens*, is able to replicate with a generation time of less than 10 min. It has a bipartite genome with chromosome sizes of 3.2 and 1.9 Mb. Is simultaneous replication from two origins a prerequisite for its rapid growth? We fused the two chromosomes of *V. natriegens* to create a strain carrying a 5.2 Mb chromosome with a single origin of replication. Compared to the wild-type, this strain showed little deviation in growth rate. This suggests that the split genome is not a prerequisite for rapid growth, and that DNA replication is not an important growth rate-limiting factor.

Keywords: DNA replication, bacterial growth rate, *Vibrio natriegens*, chromosome fusion, bipartite genome

Introduction

Every cell must replicate its genome prior to cell division. Canonical initiation of DNA replication in bacteria is primed at a single origin of replication (*ori*) from which the chromosome (*chr*) is replicated bidirectionally once per cell cycle (Reyes-Lamothe et al., 2012). The processive rate of DNA polymerase is approximately 1000 bp per second (Baker and Bell, 1998). Since DNA must be replicated prior to completing the cell cycle, replication rate can determine generation time. To overcome this bottleneck, some bacteria have evolved a system of overlapping replication cycles to increase growth rates (Cooper and Helmstetter, 1968). Notably, initiation of DNA replication still takes place only once per cell cycle but daughter cells are already born with replicating chromosomes (Skarstad et al., 1986; Fossum et al., 2007). By maintaining high *ori:ter* ratios, *Escherichia coli*, achieves doubling times of 20 min (Cooper and Helmstetter, 1968). The genome of *E. coli* is organized in a single chromosome with a size of 4.6 Mb. In contrast, the human pathogen *V. cholerae* has a bipartite genome with chromosome sizes of 3.0 Mb and 1.1 Mb, respectively (Heidelberg et al., 2000). *V. cholerae* was reported to achieve doubling times faster than *E. coli*, and the bipartite genome may be a reason for its faster growth (Couturier and Rocha, 2006). In an earlier study researchers were able to engineer the *V. cholerae* genome into a single chromosome strain and a strain with equal sized chromosomes (Val et al., 2012). Interestingly, both strains exhibit an increased doubling time in defined rich media of 26 and 34.8%, respectively. Growth rate alteration in single-chromosome strain may be explained by the extended replication time necessary to duplicate the fused chromosome from a single *ori*.

In recent years, *Vibrio natriegens* has received increased attention because of its rapid growth with reported doubling times <10 min, despite already being known for > 60 years (Payne, 1958; Eagon, 1962; Hoff et al., 2020). *Vibrio natriegens* has a bipartite genome with chromosome sizes of 3.2 Mb and 1.9 Mb, respectively. Researchers have identified a set of 587 *V. natriegens* genes required for rapid growth in rich media, identified by CRISPRi screening (Lee et al., 2019). Among those genes are ribosomal proteins, metabolic genes, and genes of the DNA polymerase. As expected, the reduction of essential proteins such as the DNA polymerase results in reduced growth rate. However, this result does not determine whether DNA replication is a rate limiting factor for *V. natriegens*' rapid growth.

To investigate the role of DNA replication on maximum cellular growth rate, we reconfigured the chromosomal architecture to require all replication to fire from a single origin. We created and characterized the *V. natriegens* strain synSC1.0 (synthetic single chromosome v.1.0), a strain derivative of

ATCC14048 with its two chromosomes fused into a singular chromosome. We prove by replication pattern analysis that the replication of the fused chromosome is initiated from a single origin of replication. We were expecting increased doubling times in synSC1.0 based on the existing reports of work with *V. cholerae* MCV1. However, our results indicate that the consequences of extended DNA replicon length in synSC1.0 are negligible for its rapid growth. The strain synSC1.0 will allow novel approaches to study chromosome biology in this rapidly growing bacterium. *V. natriegens* may be a suitable alternative to *V. cholerae*, the currently most well-studied model organism for bipartite microbial genomes, allowing to study chromosome biology without the risk of infections. Besides its application in basic research synSC1.0 may be an interesting chassis for synthetic biology and applied research, e.g. for hosting an additional synthetic chromosome.

Results

Construction and validation of a single chromosome V. natriegens strain

Assuming a replication speed of 1000 bp/s, the replication time for the *E. coli* genome is approx. 40 minutes, which is in line with the literature (Baker and Bell, 1998). Transferring this replication speed to the bipartite genome of *V. natriegens* would result in a replication time of 27 minutes for the larger chr1 (3.2 Mb), while in a strain with fused chromosomes (5.2 Mb) the replication time would be approx. 43 minutes, an increase of around 60%. To test if DNA replication is the rate limiting factor of *V. natriegens* rapid growth, we fused the two chromosomes by replacing the deletion-induced filamentation (*dif*) site (Kuempel et al., 1991) of chr1 with the whole chr2 except for the *ori2* region. The fused chromosome possesses *ori1* for initiation of DNA replication and *dif2* for chromosome dimer resolution (*cf.* Figure 1A). The *ori2* region contains the genes for the partitioning system ParAB₂ and the chr2 replication initiator protein RctB. The strain construction was performed utilizing our earlier published NT-CRISPR procedure (Figure 1A). In two subsequent editing steps, we integrated homologous sequences of chr1 flanking the *dif1* site upstream and downstream of the *ori2* region in chr2. Initially we planned to enforce chromosome fusion through a gRNA directing Cas9 to the *ori2* region. Surprisingly, we did not observe any inducible cell killing and, upon further inspection, we found that the chromosomes were already fused while integrating the second homologous flank. The obtained strain was termed *V. natriegens* synSC1.0 and was verified after initial Sanger sequencing of the fusion sites by pulsed-field-gel-electrophoresis (PFGE) and long-read whole-genome sequencing (Figure 1B). The PFGE shows two bands of 1.9 and 3.2 Mb for the parental strain, which are absent in synSC1.0, showing only a single band with increased size of approx. 5.2 Mb. Long-read *de novo* assembly resulted in two circular contigs for the parental strain and a single

circular contig for synSC1.0 with sizes of 3.2, 1.9 and 5.2 Mb, respectively. Analysis of the chromosome fusion region in synSC1.0 revealed the absence of *dif1* and *ori2* as well as the expected chromosome fusion regions, despite a small deletion of 38 nucleotides corresponding to the ARNold (Naville et al., 2011) predicted terminator of the deleted *rctB* gene, and was considered to be negligible (Figure 1C).

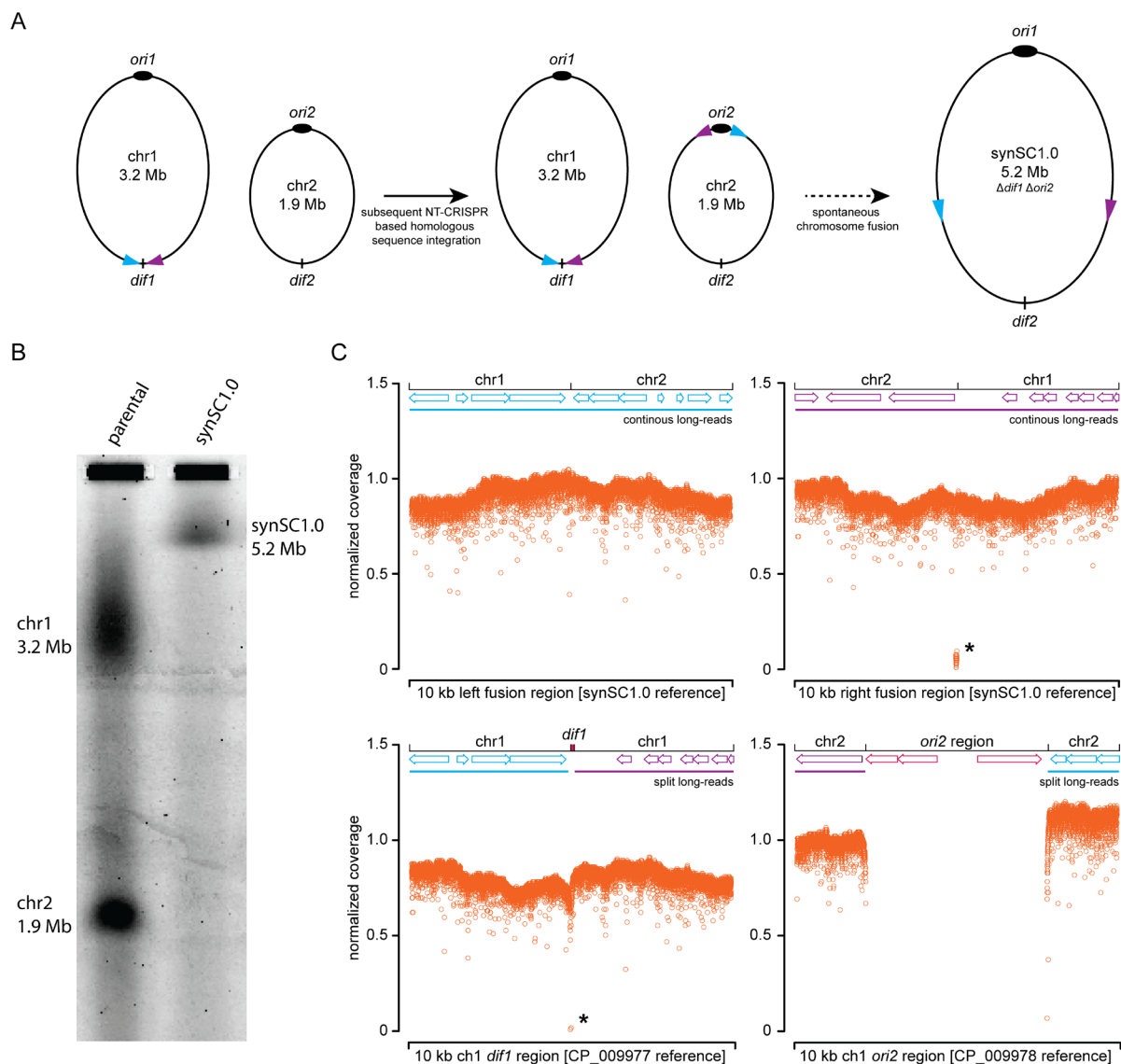


Figure 1 | Construction and validation of the *V. natriegens* strain synSC1.0. (A) Scheme of the developed strategy for chromosome fusion and large-scale genome engineering of *V. natriegens*. NT-CRISPR is utilized to subsequently integrate homologous flanking sequences into the second chromosome in the initial step. The picked homologous sequences and their orientation are indicated by blue and purple arrows. We planned to select for the fused chromosome with deleted *dif1* and *ori2* with double strand breaks from CRISPR/Cas9. To our surprise, the chromosome fusion already occurred in the initial step while integrating the second homologous region. Sizes are not to scale and differences in chromosomes sizes are due to truncation. (B) PFGE shows two bands for the parental strain with sizes of approx. 3.2 and 1.9 Mb representing chromosome 1 and 2, respectively. For synSC1.0, only a single band with an

increased size of approx. 5.2 Mb is visible. The sizes were estimated by using *S. cerevisiae* and *S. pombe* samples as reference (data not shown). (C) Long-read sequencing of synSC1.0 confirms fusion of the two chromosomes and deletion of *dif1* and the *ori2* region. The two top panels show the confirmation of the left and right fusion sites visualized by the normalized coverage for a 10 kb window using the designed synSC1.0 reference. The right panel indicates the small deletion of 38 nucleotides indicated by an asterisk. The two bottom panels show the data plotted against the CP_009977 and CP_009978 references respectively to validate the deletion of *dif1* (left panel, indicated by an asterisk) and the *ori2* region (right panel). X-axis resembles a 10 kb window. Zero values are not plotted. The top of each graph contains a scheme open reading frame annotations of the genetic content in this region, while the lines indicate long-reads either spanning the whole region (continuous color, top panel) or continue at different coordinates (split color, lower panel) based on the indicated fusion sites and reference sequence. Blue and purple indicate the left and right fusion region, respectively, and deleted regions are annotated in red.

Fusing the two chromosomes of V. natriegens results only in minor growth differences

To answer the most pressing question if the bipartite genome organization and the resulting time for DNA replication is the speed-limiting factor of *V. natriegens* rapid growth we performed comparative growth rate determination. We compared the growth of the parental strain with synSC1.0 and used *E. coli* MG1655 wild type cells as an outgroup in LBv2 media (Weinstock et al., 2016)(Figure 2A). The minimal doubling time was determined to be 12 min 11 s (+/- 34.5 s) for the parental strain and 13 min 2 s (+/- 27.1 s) for synSC1.0 under our experimental conditions. The difference in growth is 7%, which is only a fraction of the expected 60% if replication would be the speed-limiting factor for *V. natriegens* rapid growth. This difference is lower compared to the observed generation time increase for the engineered *V. cholerae* MCH1, where an increase of 26% was observed (Val et al., 2012). A detailed analysis of the growth curves indicates no drastic alteration regarding lag-phase and total biomass under the tested growth conditions (Figure 2B). In defined M9 media supplemented with 20.5 g/L NaCl and 0.4% glucose the doubling time is 22 min 46 s and 23 min 39 s for the parental and synSC1.0 strain, respectively (Figure S1). To our surprise, synSC1.0 grown under these conditions exhibited a reduced lag-phase compared to the parental strain (data not shown). Taking the increased time for DNA replication into account, we wondered if the parental strain would have an advantage under conditions causing replication stress. To test this, we assessed growth in the presence of ciprofloxacin or nalidixic acid, both gyrase inhibitors, initially in a minimum inhibitory concentration assay (MIC) (Figure 2C) and subsequently in growth assays with fine adjusted concentrations (data not shown), but could not observe growth differences between the two strains. Further, we checked if synSC1.0 possesses an increased mutation rate in fluctuation assays but could not observe significant differences in the presence of ethyl methanesulfonate (EMS) or methyl methanesulfonate (MMS), respectively. Suggesting DNA repair mechanisms are not impaired under the tested conditions (data not shown). To check whether an altered cell phenotype (e.g. elongated cell morphology) affected our optical density measurements, we performed light microscopy (Figure 2D-

E). No drastic differences were observed, which is consistent with the previously described chromosome fusion of *V. cholerae* MCV1 (Val et al., 2012) but not with the drastic phenotypic alteration for a natural single chromosome isolate of *V. cholerae* observed earlier (Bruhn et al., 2018). Nevertheless, we observed individual aberrant cells in the synSC1.0 with a higher frequency compared to the parental strain (Figure 2E, Figure S2). The result may indicate an issue with chromosome segregation or chromosome dimer resolution at *dif2*. An increased number of chromosome dimers with increasing chromosome size was described previously in the study characterizing *V. cholerae* MCV1 and would match the *dif* associated filamentation phenotype (Kuempel et al., 1991; Val et al., 2012). However, taking our results together, the drastic genome rearrangement does not cause major phenotypic alterations under the tested conditions.

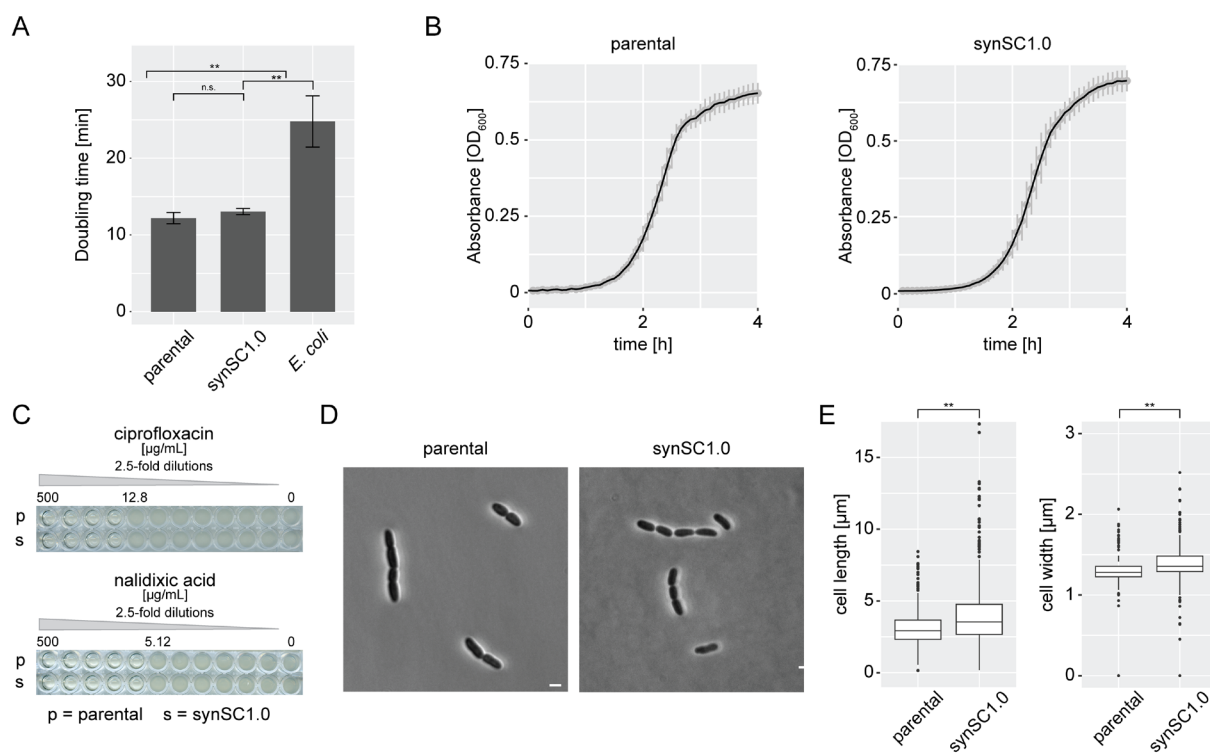


Figure 2 | Comparative growth analysis of wild type *V. natriegens* and synSC1.0. (A) Doubling times are determined to be 12 min 11 s (+/- 34.5 s) and 13 min 2 s (+/- 27.1 s) for the parental and synSC1.0 strain, respectively. The difference in growth rate is 7%. *E. coli* was used as a control under the same conditions and doubling time was determined to be 24 min 47 s (+/- 40.1 s). Student's t-test was applied to determine the significance; *: $p < 0.01$, **: $p < 0.001$, n.s. not significant. Experiments were performed in technical triplicates with biological quadruplicates. (B) Comparison of the parental and synSC1.0 growth curve do not reveal obvious differences. The growth curves show mean of biological quadruplicates, each consisting of three technical replicates. Standard deviation is indicated by grey bars. (C) MIC determination for ciprofloxacin and nalidixic acid for parental and synSC1.0. Both substances generate DNA replication stress by inhibiting gyrase function. No differences can be observed under the tested conditions. MIC tests were performed in quadruplicates and representative examples are shown, with the highest concentration allowing growth

indicated. (D) Comparison of parental strain (left panel) and synSC1.0 (right panel) cells by microscopy. There were no drastic morphological differences for the average cells. A representative image in DIC is shown for both strains. Scale bar indicates 2 μm . (E) Comparative evaluation of cell length and cell diameter for the parental and synSC1.0 strain. Values were obtained using bacstalk from four biological replicates (Hartmann et al., 2020); $n = 663$ ($n_1 = 32$, $n_2 = 130$, $n_3 = 213$, $n_4 = 288$) and $n = 517$ ($n_1 = 38$, $n_2 = 103$, $n_3 = 247$, $n_4 = 129$) for the parental and synSC1.0, respectively. The synSC1 strain shows on average a slight increased cell sizes. Student's t-test was applied to determine the significance; *: $p < 0.01$, **: $p < 0.001$, n.s. not significant.

Replication pattern analysis indicates no differences

To prove that the *ori2* was eliminated and no cryptic *ori* is responsible for the observed growth rate we performed replication pattern analysis of synSC1.0 in comparison to the parental strain (Figure 3, Figure S3). Genomic DNA of replicating cells in early stationary phase was extracted and submitted to whole genome sequencing. Replication pattern analysis of the parental strain shows the expected pattern for chr1 and chr2 with the highest marker frequency in the regions of *ori1* and *ori2* (Figure 3A). The pattern of the data is consistent with the termination synchrony of the two chromosomes observed in *Vibrionaceae* (Kemter et al., 2018). A single peak in our replication pattern analysis of synSC1.0 verifies that the 5.2 Mb chromosome is replicated from *ori1* and no cryptic *ori* was formed (Figure 3B). Notably the stationary phase culture of synSC1.0 was not fully stationary in contrast to the parental strain and a small fraction was still replicating (Figure S3B). The *ori:ter* ratio was calculated based on the median reads per bin of the exponentially growing samples obtained by Repliscope for the *ori* and *ter* regions (*ori*: median of highest 100 bins, *ter*: median of lowest 200 bins). The *ori:ter* ratio for the parental strain was determined to be 4.15 and 2.32 for chr1 (*ori* median: 1662.5; *ter* median: 359.5) and chr2 (*ori* median: 827.5; *ter* median: 356.5), respectively. The synSC1.0 strain has an *ori:ter* ratio of 6.65 (*ori* median: 4539.5; *ter* median: 683). The higher *ori:ter* ratio for synSC1.0 is expected based on the extended chromosome size resulting in a higher ratio during exponential growth; notably it is close to the addition of the ratios for chr1 and chr2 (6.47 vs 6.65). Our attempts to determine the number of replication forks using established rifampicin/cephalexin replication run-out experiments based on flow cytometry did not work (data not shown) which is consistent with reports for *V. cholerae* (Srivastava and Chatteraj, 2007; Stokke et al., 2011). The long- and short-read sequencing data of stationary phase samples were combined to perform a hybrid assembly to construct reference sequences for the parental and synSC1.0 strains with annotations based on the reference sequences of Lee *et al.* 2019. The resulting GenBank files are deposited within the BioProject PRJNA948340.

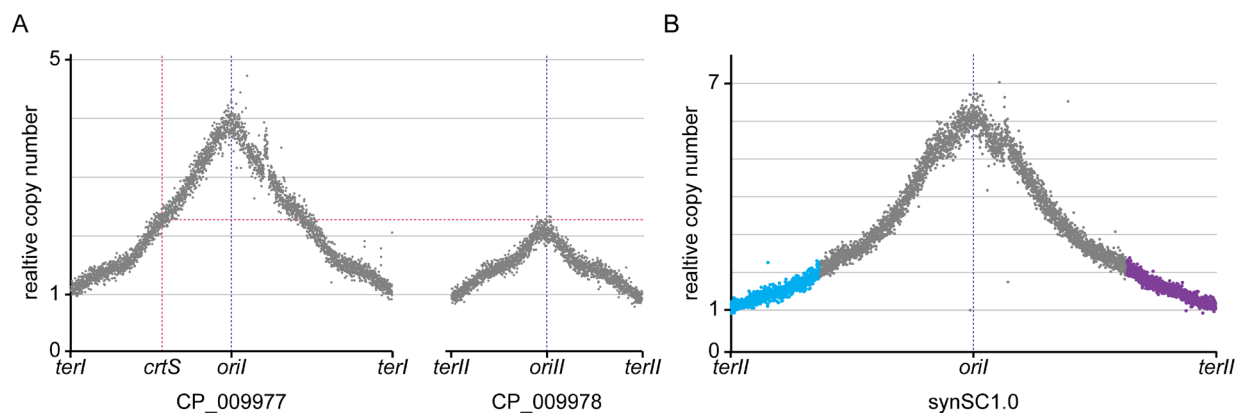


Figure 3 | Comparative replication pattern analysis of wild type *V. natriegens* and synSC1.0. (A) and (B) show relative read numbers for 1000 bp bins for the parental strain and synSC1.0, respectively. The blue dotted lines correspond to the corresponding *ori* locations. (A) Replication pattern analysis of the wild type *V. natriegens* strain shows a single peak for each chromosome at the coordinates of the *oril* and *orill*. The relative copy number of *orill* matches, as expected, to the relative copy number of location of the *crtS* site on chr1 indicated by red dotted lines. (B) Replication pattern analysis of synSC1.0 shows a single peak with its maximum at the *oril* coordinates. These results confirm the fusion of the two chromosomes, the removal of *orill*, and the absence of alternative or cryptic *oris*. Blue and purple indicate the chr2 halves according to the fusion site color code (cf. Fig. 1A).

Discussion

V. natriegens is the fastest growing bacterium known today and possesses a bipartite genome (Eagon, 1962; Hoff et al., 2020). We fused the two chromosomes into a single chromosome replicated from a single *ori* and were expecting a strongly reduced growth rate for *V. natriegens*. However, the growth rate only slightly deviated from that of the parental strain. This is in contrast to what was observed in *V. cholerae*, where a bigger difference was measured (Val et al., 2012). We conclude that the growth rate of the wild type *V. natriegens* is not limited by DNA replication even with a 60% increased replicon size in our study.

It seems that our engineering approach does not disrupt the described replication-associated gene dosage relevant for the fast growth in *V. natriegens*, which is in contrast to what was described to be relevant for *V. cholerae* growth rate (Couturier and Rocha, 2006). This is in line with the findings of Lee *et al.* 2019 that the content of chr2 is less relevant for *V. natriegens* rapid growth. The gene dose of chr2 encoded genes under rapid growth conditions is reduced in synSC1.0 (cf. Figure 3). This may result in reduced expression causing lower protein abundances. The genes encoded on chr2 could be required for niche adaptation but seem to be dispensable for growth under rich or laboratory conditions. It is tempting to speculate that the reorganized chromosome configuration of synSC1.0 lowers expression of these dispensable genes thereby liberating resources for growth related processes like ribosomes and enzymes of central

metabolism, which in itself could increase growth rate. The very minor decrease in growth rate of synSC1.0 compared to the parental strain could therefore be a combination of a beneficial effect of lowering expression of non-essential genes of chr2 and the potentially detrimental effect of an increased replicon size.

The synSC1.0 strain characterized herein is a valuable resource to study chromosome biology in fast growing bacteria. synSC1.0 allows for systematic genome engineering approaches by using the *ori2* region to build synthetic, single copy chromosomes and utilize the constructs as expression platforms or to relocate and isolate genes for distinct biological functions for their in depth characterization (Messerschmidt et al., 2015; Schindler et al., 2018; Schindler, 2020). Recently, developed genetic engineering tools such as the NT-CRISPR procedure and a reusable modular cloning part collection make this organism highly accessible (Stukenberg et al., 2021; Stukenberg et al., 2022). Further, genome-scale modeling was established giving insights into *V. natriegens* metabolism and making this organism more predictable (Coppens et al., 2023). An additional advantage over the well-established *V. cholerae* model is the lack of pathogenicity allowing to conduct work in a biosafety level 1 environment, making synSC1.0 and its parental strain relevant to biotechnological and synthetic biology applications (Weinstock et al., 2016; Hoffart et al., 2017; Hoff et al., 2020; Thoma and Blombach, 2021). The halophilic nature of *V. natriegens* allows the use of sea water for its cultivation, making it a relevant emerging host in regard to a sustainable bioeconomy (Meng et al., 2022).

Material and Methods

Strains and growth conditions

V. natriegens was routinely grown in LB supplemented with v2 salts (204 mM NaCl, 4.2 mM KCl, and 23.14 mM MgCl₂) (Weinstock et al., 2016) or in M9 media supplemented with 20.5 g/L NaCl and the indicated carbon source. Chloramphenicol was added to a final concentration of 4 µg/mL for liquid and 2 µg/mL for solid medium if applicable. Standard *E. coli* laboratory strains were used for cloning, propagation and archiving of plasmid DNA, all strains used and constructed in this study are provided in table 1. Cultures were incubated at 37 °C and at 200 rpm in case of liquid cultures if not stated otherwise. Growth comparison of *E. coli* and *V. natriegens* was performed with v2 salt containing or NaCl supplemented media for all strains.

Table 1 | Strains used and generated in this study.

Name	Relevant features	Parental strain	Reference
<i>E. coli</i> K12 MG1655	K-12 F ⁻ λ ⁻		(Blattner et al., 1997)
<i>E. coli</i> NEB Turbo	K-12 <i>glnV44 thi-1 Δ(lac-proAB) galE15 galK16 R(zgb-210::Tn10)Tet^S endA1 fhuA2 Δ(mcrB-hsdSM)5(r_K⁻m_K⁻) F'[traD36 proAB⁺ lacI^q lacZΔM15]</i>		New England Biolabs (#C2984H)
<i>V. natriegens</i> Δ <i>dns</i>	Δ <i>dns</i>	<i>V. natriegens</i> ATCC14048	(Stukenberg et al., 2021)
<i>V. natriegens</i> , DST026	Δ <i>dns</i> with 3' homology flank integrated between PN96_16275 and PN96_16280	<i>V. natriegens</i> Δ <i>dns</i>	this study
<i>V. natriegens</i> synSC1.0	Δ <i>dns</i> Δ <i>dif1</i> Δ <i>ori2</i>	<i>V. natriegens</i> , DST026	this study

Plasmids and oligonucleotides used in this study

Oligonucleotides were ordered and synthesized by Integrated DNA Technologies in 25 or 100 nM scale as standard desalted oligonucleotides (Tab. S1). All of the plasmids used in this study are listed in table 2 and the plasmid files of the created plasmids are provided as GenBank files with the supporting data.

Table 2 | Plasmids used and generated in this study.

Name	Relevant features	Parental plasmid	Reference
pST_116 + 892/893	NT-CRISPR plasmid with gRNA for integration of 3' homology flank. Created by oligo annealing of oDS_892 and oDS_893.	pST_116_LVL2 cam	(Stukenberg et al., 2022)
pST_116 + 1420/1421	NT-CRISPR plasmid with gRNA for integration of 5' homology flank. Created by oligo annealing of oDS_1420 and oDS_1421.	pST_116_LVL2 cam	(Stukenberg et al., 2022)

Genetic engineering of *V. natriegens*

tDNAs for integration of homology flanks through NT-CRISPR were generated by overlap extension PCR (Higuchi et al., 1988). Sequences of tDNAs are provided in the supporting data as GenBank files. The construction of NT-CRISPR plasmids with gRNAs targeting the integration sites were constructed as described previously through annealing of oligonucleotides (Stukenberg et al., 2022). Annealing reactions were set up by mixing 1.5 μL of each oligonucleotide (100 μM) with 5 μL T4-DNA ligase buffer (Thermo Scientific) in a total reaction volume of 50 μL. Reactions are incubated in a heat block at 95 °C for 15 min, before switching off the heat block for slowly cooling down the samples to room temperature (~1 h). Cloning reaction with the NT-CRISPR plasmids was set up with ~200 ng of the respective plasmid, 3 μL annealed oligonucleotides, 0.5 μL of T4-DNA Ligase (5 Weiss U/μL, Thermo Scientific) and BsaI (10 U/μL) and 1 μL T4-DNA ligase buffer in a total reaction volume of 10 μL. Reactions were run in a thermocycler with 30 cycles of 37 °C (2 min) and 16 °C (5 min), followed by a final digestion step at 37 °C for 30 min and an enzyme denaturation step at 80 °C for 10 min.

The integration of the homologous flanks were performed as described for the NT-CRISPR method (Stukenberg et al., 2022). tDNAs consisted of 3 kb homologous flanks and 3 kb insert sequence. The insert sequence is identical to the sequence upstream and downstream of *dif1* and enable fusion of chromosomes. At first, we integrated the 3' homology flank and subsequently the 5' homology flank. Successful integration of the 3' homology flank was confirmed by cPCR with oligonucleotides oDS_920 and oDS_921. Integration of 5' homology flanks and the spontaneous fusion of both chromosomes was confirmed with the primer pairs oDS_914/oDS_915 and oDS_916/oDS_917. Generation of a PCR fragment for both primer pairs indicates successful integration of 5' homology flank without chromosome fusion, while the absence of a band for oDS_916/oDS_917 indicates chromosome fusion. Chromosome fusion was subsequently verified through Sanger sequencing (Microsynth Seqlab). Two PCR fragments spanning the junctions were generated with the primer pairs oDS_1462/oDS_1464 and with oDS_1460 and oDS_1461, each amplicon was sequenced with two reactions with primers oDS_1463/oDS_1477 and oDS_1455/oDS_1459, respectively.

Pulsed-field-gel-electrophoresis

Plug preparation for yeast standards was performed according to described methods by Hage and Houseley (Hage and Houseley, 2013). Bacterial plug preparation was performed similar, with the following alterations: Cultures were grown overnight at 30 °C with 200 rpm. An equivalent of 1 mL OD₆₀₀ = 5 was harvested and used for plug preparation. The concentration of low melting agarose (SeaKem LE, Lonza) for plug preparation was reduced to 0.8% and lysozyme (1 mg/mL) was used instead of lyticase. PFGE was undertaken by running samples on a 0.8% agarose gel using Pulsed Field Certified Agarose (Bio-Rad) in 1X TAE buffer at 14 °C on a Bio-Rad clamped homogeneous electric field apparatus (CHEF-DR III, Bio-Rad). 3 V/cm were used with 96 h switch time of 600 s at 120°. The resulting gel was stained with 1X SYBR Safe (ThermoFisher Scientific) and imaged using Typhoon RGB laser scanning system. The known karyotypes of *S. cerevisiae* and *S. pombe* served as size standards.

Nanopore sequencing and data analysis

V. natriegens strains were cultured in 10 mL LBv2 overnight. DNA was extracted using the Monarch Genomic DNA Purification Kit (NEB) according to the manufacturer guidelines. Each sample was split in 4 purifications which were pooled subsequently again. 2 µg gDNA, corresponding to a 5-fold increase to the recommended input DNA was used as input for the library preparation using the SQK-LSK109 kit; the reason for the increase was the use of approx. 50 kb high molecular weight DNA compared to the 10 kb

sized input DNA according to the protocol. The remaining procedure was performed according to the manufacturer guidelines. Each sample was sequenced on a single Flongle flow cell (FLO-FLG001 (R9.4.1)). Basecalling of raw sequencing data was performed utilizing guppy (version 6.4.6+ae70e8f; Oxford Nanopore Technologies). Basecalled raw data are deposited in BioProject PRJNA948340 individual accession IDs are provided in table S2. Initial *de novo* assembly was performed with canu (version 2.2)(Koren et al., 2017) resulting in two and one circular chromosomes for the parental and synSC1.0 strains respectively. Dot blots of *de novo* assemblies in comparison to the corresponding references based on *V. natriegens* ATCC 14048 reference sequences (CP009977 and CP009978) and the *in silico* designed single chromosome reference (deposited under BioProject PRJNA948340, *cf.* table S2) were performed using mummer (version: 3.5)(Delcher et al., 1999). Analysis of dot blots indicated duplicated segments which were later identified as assembly artifacts (data not shown) and were the reason to generate reference sequences by combining long and short-read sequencing data of this study (*cf.* section *hybrid assembly and reference construction*).

Plate reader based growth assays

Plate reader based growth assays were adjusted to *Vibrio natriegens* based on our previously published procedure (Köbel et al., 2022; Brück et al., 2023). Briefly, *Vibrio natriegens* precultures were inoculated from a single colony and grown for 6 hours in LBv2 at 37 °C with 200 rpm. Cultures were arranged in microtiter plates and subsequently inoculated into clear, flat bottom microtiter plates (#655185, Greiner Bio-One GmbH) using a Rotor HDA+ screening robot (Singer Instruments) containing the indicated media and supplements. Plates were sealed using a PlateLoc plate sealer (Agilent) with optical clear seal. Growth was monitored in ClarioStar Plus plate readers (BMG) equipped with specific plate holders for extensive kinetics under shaking conditions. Different settings were extensively tested (data not shown) prior the following settings were identified to be the best conditions for *V. natriegens* with our setup and used throughout the study: 2 min linear shaking prior OD₆₀₀ measurement, 800 rpm orbital shaking during idle time at 37 °C, cycle time was set to 5 min and kinetic was monitored for up to 24 hours. Raw data was exported and analyzed in R with the growthcurver package (v0.3.1)(Sprouffske and Wagner, 2016). All experiments were performed in biological quadruplicates each with technical triplicates. *E. coli* K-12 MG1655 served as an external control.

Minimum inhibitory concentration (MIC) assay

MIC tests were performed as kinetic in ClarioStar Plus plate readers (BMG) with the settings described above for plate reader based growth assays. The only alteration was the preparation of the microtiter plate where the broth dilution method was used to determine the MIC as described previously (Köbel et al., 2022). The rationale behind this procedure was to be able to analyze growth in detail in contrast to only perform an endpoint measurement. In addition, microtiter plates were scanned at the end of the assay using an Epson Perfection V700 Photo scanner. All experiments were performed in biological quadruplicates.

Rifampicin fluctuation assay to determine mutation frequency

Bacterial cultures were grown overnight from a single colony. 3 mL of LBv2 media without substance or test conditions (EMS [1:1,000](Sigma-Aldrich, #M0880) or MMS [1:10,000](Sigma-Aldrich, #129925)) were inoculated 1:1,000 and grown for 6 h at 37 °C with 200 rpm, respectively. 100 µL of respective dilutions were plated onto LBv2 media (10^{-6} to 10^{-8}) with and without 50 µg/mL rifampicin (10^0 to 10^{-1}). The mutation frequency was determined based on CFUs, documented using a photo system (PhenoBooth, Singer Instruments). All experiments were performed in biological quadruplicates.

Microscopic imaging and analysis

V. natriegens precultures were grown overnight from a single colony, inoculated 1:100 in LBv2 media and grown at 37 °C with 200 rpm for 1.5 h. 1.5 µL of exponential phase cultures were immobilized on 2% low gelling agarose (Sigma) pads containing LBv2 media and analyzed using an Axioplan 2 phase contrast microscope (Zeiss) and a Plan Neofluar 100X objective (Zeiss). Extraction of cell length and width was performed using bacstalk (Hartmann et al., 2020).

Replication pattern analysis

Cultures for extraction of genomic DNA for replication pattern analysis were started from an overnight culture in 5 mL LBv2, (16 h, 37 °C, 200 rpm) to an OD_{600} of 0.001 in 100 mL in 1 L baffled shake flasks. Samples for exponential phase were taken after 2.5 h ($OD_{600} \approx 0.5$). Samples for stationary phase were taken after 9.75 h ($OD_{600} \approx 14$). A culture volume equivalent to 1 mL of $OD_{600} = 2$ was harvested by centrifugation for 1 min at 20,000 x g at 4 °C. Supernatant was discarded and pellet was stored at -80 °C. DNA was extracted using the Monarch Genomic DNA Purification Kit (NEB) according to the manufacturer guidelines. Library generation and short-read sequencing was performed by an external service provider

with a PCR-free 150 paired-end sequencing workflow (Novogene). Replication pattern analysis was performed with Repliscope (v1.1.1)(Müller et al., 2014). All short-read sequencing raw data are deposited in BioProject PRJNA948340 and individual accession IDs are provided in table S2.

Hybrid assembly and reference construction

Flye (version 2.9.1-b1780) was used for *de novo* assembly of long-reads (Kolmogorov et al., 2019). Resulting assemblies were corrected against the corresponding references using RagTag (version 2.1.0)(Alonge et al., 2019), respectively; *V. natriegens* ATCC 14048 (CP009977 and CP009978)(Lee et al., 2019); *V. natriegens* synSC1.0 (SAMN35394727). Polypolish (version 0.5.0) was used with standard settings to obtain polished reference genomes for both strains using short-reads from stationary phase samples (Tab. S2)(Wick and Holt, 2022). Validation and quality assessment of the assemblies was performed using Quast (version 5.2.0)(Gurevich et al., 2013). The origin of replication of each reference were set to nucleotide +1, resulting references are deposited within the BioProject PRJNA948340 (Tab. S2).

Supporting information

- Supporting information (Figures S1-S3 and tables S1-S2)
- Supporting data (GenBank files of plasmids and tDNAs)

Data availability

The data underlying this study are available in the published article and its online supplementary material. Sequencing raw reads and constructed reference sequences are deposited under BioProject PRJNA948340. All material created within this study is available from the corresponding author upon request.

Acknowledgments

We thank the Becker and Schindler research groups and the MaxGENESYS biofoundry team for fruitful and inspiring discussions. We thank Tania Köbel for technical support throughout the study, Adán Andrés Ramírez-Rojas for performing the Nanopore sequencing and Timon Alexander Lindeboom for help with the pulsed-field-gel-electrophoresis. We are thankful to Christoph Klaus Spahn for support with microscopic imaging and Scott Scholz for carefully reading the manuscript.

Funding

This work was supported by the Max Planck Society within the framework of the MaxGENESYS project (DSc), the International Max Planck Research School for Environmental, Cellular and Molecular Microbiology (DSt) and the International Max Planck Research School for Principles of Microbial Life: From molecules to cells, from cells to interactions (MCSO), the European Union (NextGenerationEU) via the European Regional Development Fund (ERDF) by the state Hesse within the project “*biotechnological production of reactive peptides from waste streams as lead structures for drug development*” (DSc) and a grant (01DN23012) by the German federal ministry of education and research (BMBF) (DSc), as well as by the state Hesse by LOEWE cluster MOSLA (AB).

Contributions

DSc and DSt conceived, planned and designed the study with input of AB. LR, DSt and DSc performed experiments and analyzed the data with support of MCSO. DSc and DSt wrote the manuscript with input of all authors. All authors approved the final manuscript.

Competing interests

The authors declare that the research was conducted in the absence of any commercial or financial relationships that could be construed as a potential conflict of interest.

References

- Alonge, M., Soyk, S., Ramakrishnan, S., Wang, X., Goodwin, S., Sedlazeck, F.J., et al. (2019). RaGOO: Fast and accurate reference-guided scaffolding of draft genomes. *Genome Biol* 20(1), 224. doi: 10.1186/s13059-019-1829-6.
- Baker, T.A., and Bell, S.P. (1998). Polymerases and the replisome: machines within machines. *Cell* 92(3), 295-305. doi: 10.1016/s0092-8674(00)80923-x.
- Blattner, F.R., Plunkett, G., 3rd, Bloch, C.A., Perna, N.T., Burland, V., Riley, M., et al. (1997). The complete genome sequence of *Escherichia coli* K-12. *Science* 277(5331), 1453-1462. doi: 10.1126/science.277.5331.1453.
- Brück, M., Berghoff, B.A., and Schindler, D. (2023). *In silico* design, *in vitro* construction and *in vivo* application of synthetic small regulatory RNAs in bacteria. *arXiv*. doi: 10.48550/arXiv.2304.14932.
- Bruhn, M., Schindler, D., Kemter, F.S., Wiley, M.R., Chase, K., Koroleva, G.I., et al. (2018). Functionality of two origins of replication in *Vibrio cholerae* strains with a single chromosome. *Front Microbiol* 9, 2932. doi: 10.3389/fmicb.2018.02932.
- Cooper, S., and Helmstetter, C.E. (1968). Chromosome replication and the division cycle of *Escherichia coli* B/r. *J Mol Biol* 31(3), 519-540. doi: 10.1016/0022-2836(68)90425-7.
- Coppens, L., Tschirhart, T., Leary, D.H., Colston, S.M., Compton, J.R., Hervey, W.J.t., et al. (2023). *Vibrio natriegens* genome-scale modeling reveals insights into halophilic adaptations and resource allocation. *Mol Syst Biol* 19(4), e10523. doi: 10.15252/msb.202110523.

- Couturier, E., and Rocha, E.P. (2006). Replication-associated gene dosage effects shape the genomes of fast-growing bacteria but only for transcription and translation genes. *Mol Microbiol* 59(5), 1506-1518. doi: 10.1111/j.1365-2958.2006.05046.x.
- Delcher, A.L., Kasif, S., Fleischmann, R.D., Peterson, J., White, O., and Salzberg, S.L. (1999). Alignment of whole genomes. *Nucleic Acids Res* 27(11), 2369-2376. doi: 10.1093/nar/27.11.2369.
- Eagon, R.G. (1962). *Pseudomonas natriegens*, a marine bacterium with a generation time of less than 10 minutes. *J Bacteriol* 83(4), 736-737. doi: 10.1128/jb.83.4.736-737.1962.
- Fossum, S., Crooke, E., and Skarstad, K. (2007). Organization of sister origins and replisomes during multifork DNA replication in *Escherichia coli*. *EMBO J* 26(21), 4514-4522. doi: 10.1038/sj.emboj.7601871.
- Gurevich, A., Saveliev, V., Vyahhi, N., and Tesler, G. (2013). QUAST: Quality assessment tool for genome assemblies. *Bioinformatics* 29(8), 1072-1075. doi: 10.1093/bioinformatics/btt086.
- Hage, A.E., and Houseley, J. (2013). Resolution of budding yeast chromosomes using pulsed-field gel electrophoresis. *Methods Mol Biol* 1054, 195-207. doi: 10.1007/978-1-62703-565-1_13.
- Hartmann, R., van Teeseling, M.C.F., Thanbichler, M., and Drescher, K. (2020). BacStalk: A comprehensive and interactive image analysis software tool for bacterial cell biology. *Mol Microbiol* 114(1), 140-150. doi: 10.1111/mmi.14501.
- Heidelberg, J.F., Eisen, J.A., Nelson, W.C., Clayton, R.A., Gwinn, M.L., Dodson, R.J., et al. (2000). DNA sequence of both chromosomes of the cholera pathogen *Vibrio cholerae*. *Nature* 406(6795), 477-483. doi: 10.1038/35020000.
- Higuchi, R., Krummel, B., and Saiki, R.K. (1988). A general method of *in vitro* preparation and specific mutagenesis of DNA fragments: Study of protein and DNA interactions. *Nucleic Acids Res* 16(15), 7351-7367. doi: 10.1093/nar/16.15.7351.
- Hoff, J., Daniel, B., Stukenberg, D., Thuronyi, B.W., Waldminghaus, T., and Fritz, G. (2020). *Vibrio natriegens*: An ultrafast-growing marine bacterium as emerging synthetic biology chassis. *Environ Microbiol* 22(10), 4394-4408. doi: 10.1111/1462-2920.15128.
- Hoffart, E., Grenz, S., Lange, J., Nitschel, R., Muller, F., Schwentner, A., et al. (2017). High substrate uptake rates empower *Vibrio natriegens* as production host for industrial biotechnology. *Appl Environ Microbiol* 83(22). doi: 10.1128/AEM.01614-17.
- Kemter, F.S., Messerschmidt, S.J., Schallopp, N., Sobetzko, P., Lang, E., Bunk, B., et al. (2018). Synchronous termination of replication of the two chromosomes is an evolutionary selected feature in *Vibrionaceae*. *PLoS Genet* 14(3), e1007251. doi: 10.1371/journal.pgen.1007251.
- Köbel, T.S., Melo Palhares, R., Fromm, C., Szymanski, W., Angelidou, G., Glatter, T., et al. (2022). An easy-to-use plasmid toolset for efficient generation and benchmarking of synthetic small RNAs in bacteria. *ACS Synth Biol* 11(9), 2989-3003. doi: 10.1021/acssynbio.2c00164.
- Kolmogorov, M., Yuan, J., Lin, Y., and Pevzner, P.A. (2019). Assembly of long, error-prone reads using repeat graphs. *Nat Biotechnol* 37(5), 540-546. doi: 10.1038/s41587-019-0072-8.
- Koren, S., Walenz, B.P., Berlin, K., Miller, J.R., Bergman, N.H., and Phillippy, A.M. (2017). Canu: Scalable and accurate long-read assembly via adaptive k-mer weighting and repeat separation. *Genome Res* 27(5), 722-736. doi: 10.1101/gr.215087.116.
- Kuempel, P.L., Henson, J.M., Dircks, L., Tecklenburg, M., and Lim, D.F. (1991). *dif*, a *recA*-independent recombination site in the terminus region of the chromosome of *Escherichia coli*. *New Biol* 3(8), 799-811.
- Lee, H.H., Ostrov, N., Wong, B.G., Gold, M.A., Khalil, A.S., and Church, G.M. (2019). Functional genomics of the rapidly replicating bacterium *Vibrio natriegens* by CRISPRi. *Nat Microbiol* 4(7), 1105-1113. doi: 10.1038/s41564-019-0423-8.

- Meng, W., Zhang, Y., Ma, L., Lu, C., Xu, P., Ma, C., et al. (2022). Non-sterilized fermentation of 2,3-butanediol with seawater by metabolic engineered fast-growing *Vibrio natriegens*. *Front Bioeng Biotechnol* 10, 955097. doi: 10.3389/fbioe.2022.955097.
- Messerschmidt, S.J., Kemter, F.S., Schindler, D., and Waldminghaus, T. (2015). Synthetic secondary chromosomes in *Escherichia coli* based on the replication origin of chromosome II in *Vibrio cholerae*. *Biotechnol J* 10(2), 302-314. doi: 10.1002/biot.201400031.
- Müller, C.A., Hawkins, M., Retkute, R., Malla, S., Wilson, R., Blythe, M.J., et al. (2014). The dynamics of genome replication using deep sequencing. *Nucleic Acids Res* 42(1), e3. doi: 10.1093/nar/gkt878.
- Naville, M., Ghuillot-Gaudeffroy, A., Marchais, A., and Gautheret, D. (2011). ARNold: A web tool for the prediction of Rho-independent transcription terminators. *RNA Biol* 8(1), 11-13. doi: 10.4161/rna.8.1.13346.
- Payne, W.J. (1958). Studies on bacterial utilization of uronic acids. III. Induction of oxidative enzymes in a marine isolate. *J Bacteriol* 76(3), 301-307. doi: 10.1128/jb.76.3.301-307.1958.
- Reyes-Lamothe, R., Nicolas, E., and Sherratt, D.J. (2012). Chromosome replication and segregation in bacteria. *Annu Rev Genet* 46, 121-143. doi: 10.1146/annurev-genet-110711-155421.
- Schindler, D. (2020). Genetic engineering and synthetic genomics in yeast to understand life and boost biotechnology. *Bioengineering (Basel)* 7(4). doi: 10.3390/bioengineering7040137.
- Schindler, D., Dai, J., and Cai, Y. (2018). Synthetic genomics: A new venture to dissect genome fundamentals and engineer new functions. *Curr Opin Chem Biol* 46, 56-62. doi: 10.1016/j.cbpa.2018.04.002.
- Skarstad, K., Boye, E., and Steen, H.B. (1986). Timing of initiation of chromosome replication in individual *Escherichia coli* cells. *EMBO J* 5(7), 1711-1717. doi: 10.1002/j.1460-2075.1986.tb04415.x.
- Sprouffske, K., and Wagner, A. (2016). Growthcurver: An R package for obtaining interpretable metrics from microbial growth curves. *BMC Bioinformatics* 17, 172. doi: 10.1186/s12859-016-1016-7.
- Srivastava, P., and Chatteraj, D.K. (2007). Selective chromosome amplification in *Vibrio cholerae*. *Mol Microbiol* 66(4), 1016-1028. doi: 10.1111/j.1365-2958.2007.05973.x.
- Stokke, C., Waldminghaus, T., and Skarstad, K. (2011). Replication patterns and organization of replication forks in *Vibrio cholerae*. *Microbiology (Reading)* 157(Pt 3), 695-708. doi: 10.1099/mic.0.045112-0.
- Stukenberg, D., Hensel, T., Hoff, J., Daniel, B., Inckemann, R., Tedeschi, J.N., et al. (2021). The Marburg Collection: A Golden Gate DNA assembly framework for synthetic biology applications in *Vibrio natriegens*. *ACS Synth Biol* 10(8), 1904-1919. doi: 10.1021/acssynbio.1c00126.
- Stukenberg, D., Hoff, J., Faber, A., and Becker, A. (2022). NT-CRISPR, combining natural transformation and CRISPR-Cas9 counterselection for markerless and scarless genome editing in *Vibrio natriegens*. *Commun Biol* 5(1), 265. doi: 10.1038/s42003-022-03150-0.
- Thoma, F., and Blombach, B. (2021). Metabolic engineering of *Vibrio natriegens*. *Essays Biochem* 65(2), 381-392. doi: 10.1042/EBC20200135.
- Val, M.E., Skovgaard, O., Ducos-Galand, M., Bland, M.J., and Mazel, D. (2012). Genome engineering in *Vibrio cholerae*: A feasible approach to address biological issues. *PLoS Genet* 8(1), e1002472. doi: 10.1371/journal.pgen.1002472.
- Weinstock, M.T., Heseck, E.D., Wilson, C.M., and Gibson, D.G. (2016). *Vibrio natriegens* as a fast-growing host for molecular biology. *Nat Methods* 13(10), 849-851. doi: 10.1038/nmeth.3970.
- Wick, R.R., and Holt, K.E. (2022). Polypolish: Short-read polishing of long-read bacterial genome assemblies. *PLoS Comput Biol* 18(1), e1009802. doi: 10.1371/journal.pcbi.1009802.

Supporting Information

DNA replication is not a limiting factor for the rapid growth of *Vibrio natriegens*

Authors: Lea Ramming^{1,#}, Daniel Stukenberg^{2,#}, María del Carmen Sánchez Olmos¹,
Anke Becker^{2,3}, Daniel Schindler^{1,3,*}

Affiliations

¹ Max Planck Institute for Terrestrial Microbiology, Marburg, Germany

² Department of Biology, Philipps-Universität Marburg, Marburg, Germany

³ Center for Synthetic Microbiology, Philipps-Universität Marburg, Marburg, Germany

contributed equally; alphabetical order

* correspondence to: daniel.schindler@mpi-marburg.mpg.de

This file contains:

Figure S1-S3

Table S1-S2

Supporting References

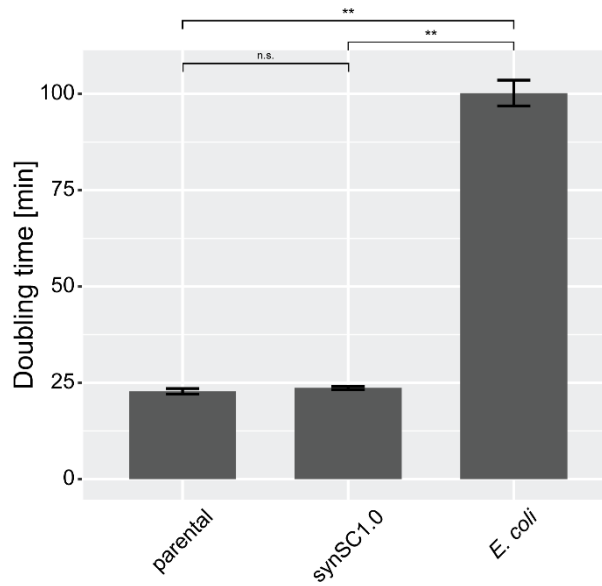


Figure S1 | Comparative growth assay for *V. natriegens* and synSC1.0 in M9 media supplemented with 20.5 g/L NaCl and 0.4% glucose. Doubling times are determined to be 22 min 46 s (+/- 43.8 s) and 23 min 39 s (+/- 24.6 s) for the parental and synSC1.0 strain, respectively. The difference in growth rate is 4.1%. *E. coli* was used as a control under the same conditions and doubling time was determined to be 1 h 40 min 12 s (+/- 3 min 20.8 s). However, the conditions presumably cause high salt stress for *E. coli*. Student's t-test was applied to determine the significance; *: $p < 0.01$, **: $p < 0.001$, n.s. not significant. Experiments were performed biological quadruplicates each with technical triplicates.

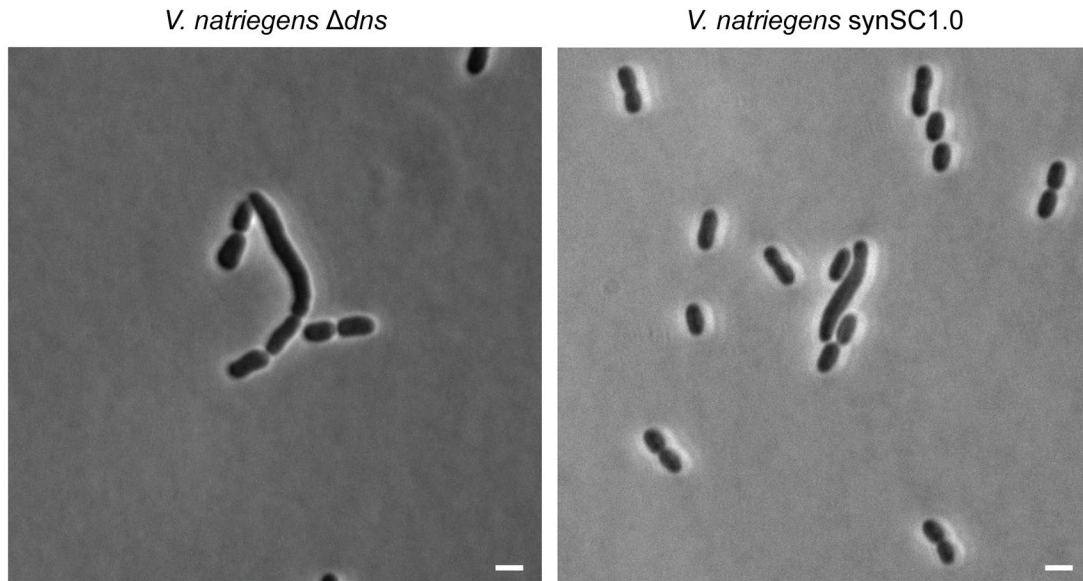


Figure S2 | Elongated cell phenotype observed for *Vibrio natriegens* under rapid growth conditions. Elongated cells were sporadic observed in both the parental and synSC1.0 strain. Representative image for the parental (left panel) and synSC1.0 (right panel) are shown. The observed phenotype was more frequent for synSC1.0 (*cf.* Figure 2F). It may be the result of reduced chromosome dimer resolution fidelity previously observed in *V. cholerae* (Val et al., 2012). More severe phenotypes affecting the whole cell population were described earlier for a natural isolate with fused chromosomes of *V. cholerae* but are not observed for synSC1.0 (Bruhn et al., 2018). Scale bar 2 μ m.

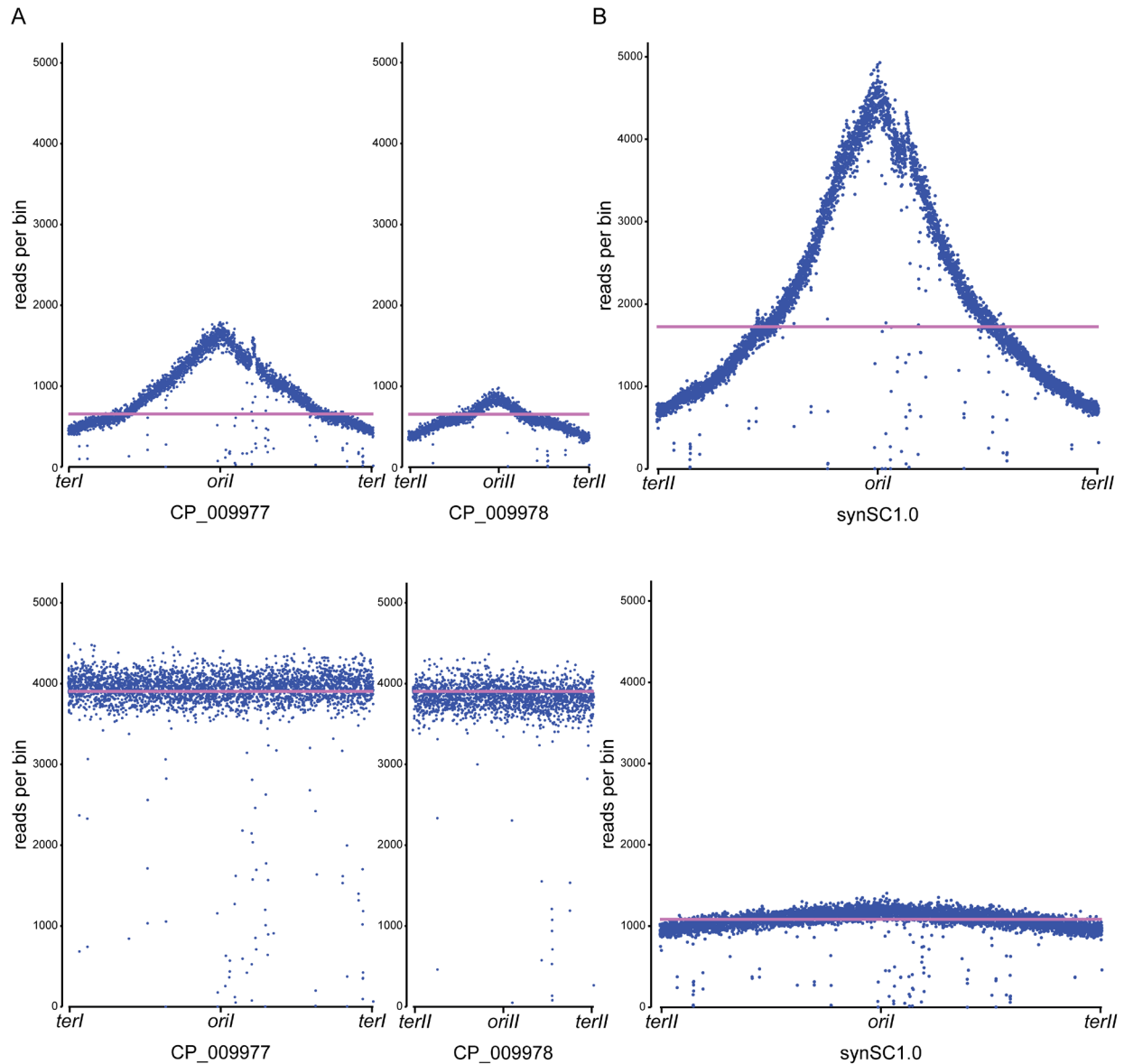


Figure S3 | Coverage plots of samples for replication pattern analysis based on bin read count for each sample. (A) Overall read abundances per bin (1000 bp) for *V. natriegens* parental strain in exponential growth phase (top panel) and early stationary phase (bottom panel) sequencing samples. Exponential and stationary phase samples show the expected read distribution. The magenta line indicates the sample wide median read per bin distribution. (B) Overall read abundances per bin (1000 bp) for *V. natriegens* synSC1.0 in exponential growth phase (top panel) and early stationary phase (bottom panel) sequencing samples. The stationary phase sample for synSC1.0 contained still cells undergoing DNA replication. The magenta line indicates the sample wide median read per bin distribution. All plots were generated utilizing Repliscope (Müller et al., 2014).

Table S1 | Oligonucleotides used in this study.

ID	Sequence (5'→3')	Purpose
oDS_892	GTCCCTATCTATTAATCATCAGAA	Forward oligo for construction of gRNA. Integration of 3' homology flank. Targeting intergenic region between PN96_16275 and PN96_16280.
oDS_893	AAACTTCTGATGATTAATAGATAG	Reverse oligo for construction of gRNA. Integration of 3' homology flank. Targeting intergenic region between PN96_16275 and PN96_16280.
oDS_1420	GTCCGATCGGCAAGCAAAAACAAC	Forward oligo for construction of gRNA. Integration of 5' homology flank. Targeting intergenic region between PN96_16260 and PN96_16265.
oDS_1421	AAACGTTGTTTTTGCTTGCCGATC	Reverse oligo for construction of gRNA. Integration of 5' homology flank. Targeting intergenic region between PN96_16260 and PN96_16265.
oDS_904	GTTACAGCGTCACACATTTACATTG	Construction of tDNA for integration of 3' homology flank. Forward primer of upstream fragment.
oDS_905	TTTTGAGTCAACTTTAAATCGCCATTCATCAAGAGC	Construction of tDNA for integration of 3' homology flank. Reverse primer of upstream fragment.
oDS_906	GCGTTATGCTTTGAATAGACTTCGCGAGTTTCTG	Construction of tDNA for integration of 3' homology flank. Forward primer of downstream fragment.
oDS_907	GAAAGTTGACAAAAACATTAACCATTGAAG	Construction of tDNA for integration of 3' homology flank. Reverse primer of downstream fragment.
oDS_924	ATGGCGATTTAAAGTTGACTCAAAAGAACCAGCATACG	Construction of tDNA for integration of 3' homology flank. Forward primer of insert fragment.
oDS_925	GCGAAGTCTATTCAAAGCATAACGCTACGCCAAATCTTTACTC	Construction of tDNA for integration of 3' homology flank. Reverse primer of insert fragment.
oDS_896	TGACTTCATCACCAACATTGACAG	Construction of tDNA for integration of 5' homology flank. Forward primer of upstream fragment.
oDS_1427	CTTTTAACCCTTTGTTGTTTTTGCTTGCCGATCAG	Construction of tDNA for integration of 5' homology flank. Reverse primer of upstream fragment.
oDS_1430	TATAGTAGACTGTGGCATAAAAAAACCGCCGAAG	Construction of tDNA for integration of 5' homology flank. Forward primer of downstream fragment.
oDS_899	ACCATGGATTTTATCGCCTCCTTG	Construction of tDNA for integration of 3' homology flank. Reverse primer of downstream fragment.
oDS_1428	AGCAAAAACAACAAAGGGTTAAAAGATTAACAGTGCTG	Construction of tDNA for integration of 3' homology flank. Forward primer of upstream fragment.
oDS_1429	TTTTTTTATGCCACAGTCTACTATAACCCGTATGG	Construction of tDNA for integration of 3' homology flank. Reverse primer of insert fragment.
oDS_920	CTTTCGCCCTCTAATAGAGC	Primer for cPCR. Confirming integration of 3' homology flank. Binds in 3' homology flank.

ID	Sequence (5' -> 3')	Purpose
oDS_921	GGTATCCAGCAAAGTCTGTC	Primer for cPCR. Confirming integration of 3' homology flank. Binds in chr2 sequence downstream of integration site.
oDS_914	GGGATCCCTTTAGTAGCAGG	Primer for cPCR. Confirming integration of 5' homology flank. Binds in chr2 sequence upstream of integration site.
oDS_915	CCAGAGCGAAGCATGAATCC	Primer for cPCR. Confirming integration of 5' homology flank. Binds in 5' homology flank.
oDS_916	GGATTCATGCTTCGCTCTGG	Primer for cPCR. Confirming integration of 5' homology flank.
oDS_917	CATGACATTTGTACAGGTTATCC	Primer for cPCR. Confirming integration of 5' homology flank. Binds in <i>orill</i> region on chr2.
oDS_1462	ACCCGGAAAGATGATCAAGG	Forward primer to generate PCR fragment for Sanger sequencing to confirm chromosome fusion.
oDS_1464	AATCAGGTGAATTTATTAATGTAAAGGAC	Forward primer to generate PCR fragment for Sanger sequencing to confirm chromosome fusion.
oDS_1463	CCAAGCAAAGTTATTAAGCTCAGC	Sequencing primer to confirm chromosome fusion.
oDS_1477	CATTATGTTTAAATGAAAGCCTCAAACC	Sequencing primer to confirm chromosome fusion.
oDS_1460	GGGTGCCTTGCGATATAGC	Forward primer to generate PCR fragment for Sanger sequencing to confirm chromosome fusion.
oDS_1461	ATTCACCGACACAAAACCAACG	Reverse primer to generate PCR fragment for Sanger sequencing to confirm chromosome fusion.
oDS_1455	GAACGAAGTGATAAGTTCGTTTTGC	Sequencing primer to confirm chromosome fusion.
oDS_1459	AAGTAGGGTACTTGGAACTTTTCC	Sequencing primer to confirm chromosome fusion.

Table S2 | Sequencing data deposited under BioProject PRJNA948340.

IDs	Type of data	Platform	Strain	Additional information
SAMN35035422	Raw reads	Illumina (150 PE)	<i>V. natriegens</i> Δ <i>dns</i>	exponential growing sample
SAMN35035423	Raw reads	Illumina (150 PE)	<i>V. natriegens</i> Δ <i>dns</i>	stationary phase sample
SAMN35035424	Raw reads	Illumina (150 PE)	<i>V. natriegens</i> synSC1.0	exponential growing sample
SAMN35035425	Raw reads	Illumina (150 PE)	<i>V. natriegens</i> synSC1.0	stationary phase sample
SAMN35035426	Raw reads	Nanopore (MinION)	<i>V. natriegens</i> Δ <i>dns</i>	stationary phase sample
SAMN35035427	Raw reads	Nanopore (MinION)	<i>V. natriegens</i> synSC1.0	stationary phase sample
SAMN35394727	Reference	NA	Designed <i>V. natriegens</i> synSC1.0	designed based on CP009977 and CP009978 (Lee et al., 2019)
SAMN35394728	Reference	NA	<i>V. natriegens</i> synSC1.0	sequencing validated reference
SAMN35394729	Reference	NA	<i>V. natriegens</i> Δ <i>dns</i>	sequencing validated reference

Supporting References

- Bruhn, M., Schindler, D., Kemter, F.S., Wiley, M.R., Chase, K., Koroleva, G.I., et al. (2018). Functionality of two origins of replication in *Vibrio cholerae* strains with a single chromosome. *Front Microbiol* 9, 2932. doi: 10.3389/fmicb.2018.02932.
- Lee, H.H., Ostrov, N., Wong, B.G., Gold, M.A., Khalil, A.S., and Church, G.M. (2019). Functional genomics of the rapidly replicating bacterium *Vibrio natriegens* by CRISPRi. *Nat Microbiol* 4(7), 1105-1113. doi: 10.1038/s41564-019-0423-8.
- Müller, C.A., Hawkins, M., Retkute, R., Malla, S., Wilson, R., Blythe, M.J., et al. (2014). The dynamics of genome replication using deep sequencing. *Nucleic Acids Res* 42(1), e3. doi: 10.1093/nar/gkt878.
- Val, M.E., Skovgaard, O., Ducos-Galand, M., Bland, M.J., and Mazel, D. (2012). Genome engineering in *Vibrio cholerae*: A feasible approach to address biological issues. *PLoS Genet* 8(1), e1002472. doi: 10.1371/journal.pgen.1002472.

3.3. graded-CRISPRi, a novel tool for tuning the strengths of CRISPRi-mediated knockdowns in *Vibrio natriegens* using gRNA libraries

Daniel Stukenberg, Anna Faber, Anke Becker

bioRxiv, doi: <https://doi.org/10.1101/2024.01.29.577714>, submitted to *ACS Synthetic Biology*

In this publication, we developed a novel CRISPRi tool for *V. natriegens*. Therefore, we created a plasmid carrying the sequences coding for the catalytically inactive Cas9 (dCas9) and gRNA under control of two different inducible promoters. This system was first characterized in a strain with a constitutively expressed *mScarlet-I* fluorescent reporter gene. We tested different concentrations of the two inducers anhydrotetracycline (ATc) and dihydroxybenzoic acid (DHBA) for the promoters driving expression of *dcas9* and *gRNA*, respectively. As expected, addition of both inducers is necessary to achieve a strong repression of ~ 40 -fold in minimal medium and ~ 8 -fold in rich medium. We further analyzed single-cell behavior of mScarlet-I production with flow cytometry of samples treated with different inducer levels. In all cases, a unimodal distribution was obtained but with a high cell-to-cell variability for intermediate induction levels.

After these initial benchmarking experiments, we wanted to develop this tool further to allow the generation of strain libraries, in which each variant has a different knockdown strength of the target gene. This was achieved through the construction of gRNA libraries with mismatches to the target sequence. Additionally, we used truncated gRNAs to further weaken binding of the dCas9-gRNA complex to the DNA target sequence. We could show that such a plasmid library leads to a wide range of signals when reporter genes were targeted.

To allow quantification of knockdown strengths in future experiments with native genes, we established the HiBiT tag system for *V. natriegens*. This system relies on the complementation of a core luciferase enzyme with the HiBiT tag. Only complementation leads to a functional enzyme which is capable of producing bioluminescence (Schwinn et al., 2018). When the HiBiT tag is fused to a protein of interest, the resulting bioluminescence correlates linearly with the abundance of the tagged protein. We demonstrated the applicability of this system for *V. natriegens* by using two reporters (mScarlet-I and firefly luciferase) tagged at the carboxy-terminus (C-terminus) with the HiBiT tag. We obtained a very high correlation between the signal of the reporter proteins and the luminescence obtained in the HiBiT assay, thereby

demonstrating the use of the HiBiT tag system for the quantification of protein abundances in *V. natriegens*.

Next, we wanted to expand this approach to multiple targets. Therefore, we created a strain with four different reporter genes integrated into distinct loci on both chromosomes. We created plasmid libraries with four gRNAs and introduced them into the strain with four reporter genes. When analyzing the signals from all reporter proteins, we obtained a huge variety between members of the library. Some variants led to a moderate repression of all four reporter genes, while other variants led to a strong repression of one or two and no or only little repression of the other reporter genes.

As a last goal of this project, we wanted to demonstrate that we can target native genes with graded-CRISPRi. This was done for four genes, from which we expected different outcomes. Two genes, *eno* and *metA*, were previously described as being important for growth in minimal medium (Lee et al., 2019). When targeting these genes with graded-CRISPRi, we obtained a wide range of growth defects. We measured abundance of the target proteins through the HiBiT tag system and found that none of the samples with a control-like growth rate had a significantly reduced luminescence. This suggests that even a minor reduction of the abundance of these enzymes leads to a significant growth defect. Two other genes, *metE* and *argA*, were targeted because they were not found to be important for growth in minimal medium in *V. natriegens* (Lee et al., 2019), while they are important under similar conditions in *E. coli* (Wang et al., 2018). When targeting these genes with graded-CRISPRi, no effect on growth by any of the gRNA variants was visible. When analyzing protein abundance through the HiBiT tag system, we obtained a wide range of values with some samples having a 10 – 20-fold reduced abundance. As a control, we created clean deletions of *metE* and *argA* and showed that the resulting strains did not grow differently in minimal medium compared to the parental strain.

Personal contribution

I designed the graded-CRISPRi tool based on discussions with Reza Rohani and inspired by pioneering experiments executed by Anna Faber. I created all strains and plasmids used in the experiments described in this publication. The inducible promoters used for this CRISPRi tool were first constructed and characterized by Anna Faber. I performed all experiments described

in this publication and I wrote the first draft of the manuscript which was later improved based on feedback from all other authors.

1 **graded-CRISPRi, a novel tool for tuning the strengths of CRISPRi-mediated** 2 **knockdowns in *Vibrio natriegens* using gRNA libraries**

3 Daniel Stukenberg^{1,2}, Anna Faber^{1,2,#}, Anke Becker^{1,2,*}

4 ¹ Center for Synthetic Microbiology, Philipps-Universität Marburg, Marburg, Germany

5 ² Department of Biology, Philipps-Universität Marburg, Marburg, Germany

6 *For correspondence: anke.becker@synmikro.uni-marburg.de

7 # Current address: School of Molecular Sciences, The University of Western Australia, Crawley,
8 Australia

9 Keywords: CRISPR interference, gene repression, gradual downregulation of gene expression,
10 gRNA variants, *Vibrio natriegens*

11 **Abstract**

12 In recent years, the fast-growing bacterium *Vibrio natriegens* has gained increasing attention as it has the
13 potential to become a next-generation chassis for Synthetic Biology. A wide range of genetic parts and
14 genome engineering methods have already been developed. However, there is still a need for a well-
15 characterized tool to effectively and gradually reduce the expression level of native genes. To bridge this
16 gap, we created graded-CRISPRi, a system utilizing gRNA variants that lead to varying levels of repression
17 strength. By incorporating multiple gRNA sequences into our design, we successfully extended this concept
18 to simultaneously repress four distinct reporter genes. Furthermore, we demonstrated the capability of
19 using graded-CRISPRi to target native genes, thereby examining the effect of various knockdown levels on
20 growth.

21 **Introduction**

22 *Vibrio natriegens* is the fastest growing organism known to date with a reported doubling time of less than
23 10 minutes under optimal conditions (Eagon, 1961; Hoffart *et al.*, 2017). In addition to its rapid growth,
24 *V. natriegens*' broad substrate spectrum (Hoffart *et al.*, 2017) and its active metabolism (Long *et al.*, 2017;
25 Coppens *et al.*, 2023) are considered beneficial properties for biotechnological applications (Hoff *et al.*,
26 2020; Thoma and Blombach, 2021). Furthermore, several pioneering studies have demonstrated the
27 applicability of employing *V. natriegens* for the production of chemical compounds (Dalia *et al.*, 2017;
28 Wang *et al.*, 2020; Thoma *et al.*, 2022). To fully establish *V. natriegens* as a novel, fast-growing model
29 organism, a set of reliable and efficient genetic tools is indispensable. Over the last years, we and others
30 have made significant progress in developing *V. natriegens* into a next-generation SynBio chassis by
31 characterizing standardized genetic parts (Tschirhart *et al.*, 2019; Stukenberg *et al.*, 2021; Tietze *et al.*,
32 2022) and developing genome engineering tools (Weinstock *et al.*, 2016; Dalia *et al.*, 2017; Stukenberg *et al.*,
33 2022). These tools allow the construction of heterologous pathways or genetic circuits, as well as the
34 introduction of permanent genetic modification into the genome of *V. natriegens*.

35 However, a set of tools for the precise regulation of native gene expression in *V. natriegens* is not yet
36 available. In particular, a system enabling graded repression of gene expression, as opposed to a binary

37 on/off switch, would support or even enable a broad spectrum of basic and applied scientific research in
38 this chassis. Among various possibilities, such an approach could lead to interesting insights into the
39 metabolism of *V. natriegens*. For example, recent studies in *Escherichia coli* showed that the abundance
40 of many proteins can be reduced with little to no effect on growth, even though the respective genes are
41 essential under the specific conditions (O'Brien, Utrilla and Palsson, 2016; Sander *et al.*, 2019; Hawkins *et*
42 *al.*, 2020). From an application-oriented perspective, it has been demonstrated that repression of
43 competing pathways, resulting in redirection of metabolic fluxes, can enhance the efficiency of a
44 heterologous pathway. (Kim *et al.*, 2017; Tian *et al.*, 2019).

45 To enable similar approaches in *V. natriegens*, we developed a CRISPRi-based tool for the targeted
46 repression of endogenous genes. CRISPRi uses a catalytically inactive Cas9 (dCas9), which is guided to a
47 DNA sequence by a programmable gRNA to block transcription (Qi *et al.*, 2013). CRISPRi was used before
48 in *V. natriegens* to perform a genome-wide screen identifying essential genes and those necessary for
49 rapid growth under specific conditions (Lee *et al.*, 2019). In the referenced study, the CRISPRi tool lacked
50 tight control, and the authors took advantage of the system's inherent leaky expression to generate
51 growth-defective phenotypes (Lee *et al.*, 2019). However, the leakiness of this system complicates the
52 study of essential genes as it creates a strong selection pressure for adaptational mutations or inactivation
53 of the CRISPRi system itself. In our study, we therefore envisioned a CRISPRi-based tool that can generate
54 libraries of strains with different knockdown strengths. This approach is especially beneficial in scenarios
55 where the level of repression required to achieve a desired phenotype is lacking.

56 Here, we report the development and characterization of graded-CRISPRi as a novel tool for *V. natriegens*.
57 By using two different inducible promoters, we achieved tight regulation of the CRISPRi system that did
58 not show a measurable effect in the absence of inducers. Next, we achieved graded repression strengths
59 by varying the binding strength of the dCas9-gRNA complex to the DNA target sequence. This was achieved
60 by using gRNA libraries with spacers of different lengths and with various mismatches to the target
61 sequence. We further demonstrated the simultaneous targeting of multiple reporter genes with several
62 gRNAs, leading to a set of strains with different expression levels of each reporter gene. Lastly, we used
63 graded-CRISPRi for the down-regulation of metabolic genes in *V. natriegens* and investigated the
64 phenotype resulting from different knockdown strengths.

65 **Results and discussion**

66 **Establishing a tightly controlled CRISPRi tool for *V. natriegens***

67 As a first step in the development of graded-CRISPRi, we focused on the tight regulation of CRISPRi in
68 *V. natriegens*. It was shown previously that the activity of CRISPRi-based tools is dependent on sufficient
69 expression of both *dcas9* and *gRNA* (Fontana *et al.*, 2018). Thus, we concluded that employing two
70 orthogonal inducible promoters to control the expression of both genes should achieve the most stringent
71 control of the system. This is because simultaneous leaky expression of *dcas9* and *gRNA* in the same cell
72 would be necessary to produce a functional dCas9-gRNA complex. A further rationale for utilizing two
73 separate inducible promoters for *dcas9* and *gRNA* expression was the ability to independently regulate
74 the expression strength of both CRISPRi components. This strategy was vital to mitigate toxicity and reduce
75 metabolic burden. For the two inducible promoters, we chose modified versions of the P_{tet} and P_{3b5b}
76 inducible promoters with their corresponding inducers anhydroteracycline (ATc) and dihydroxybenzoic
77 acid (DHBA) (Meyer *et al.*, 2019). To benchmark the new inducible CRISPRi system in *V. natriegens*, we

78 targeted a chromosomally integrated and strongly constitutively expressed *mScarlet-I* reporter gene (Fig.
79 1a).

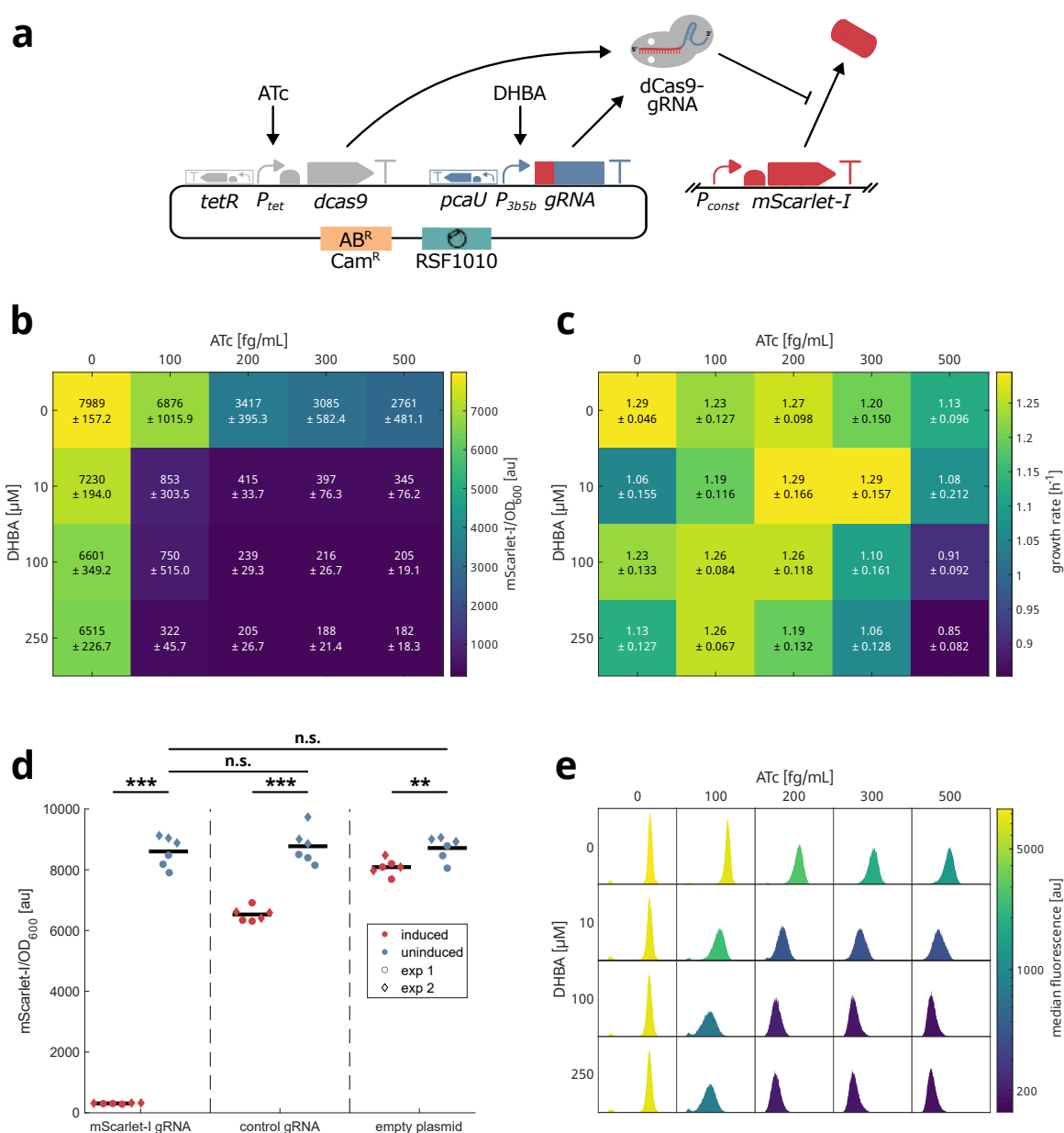
80 Firstly, we measured the mScarlet-I signal from *V. natriegens* cultures in minimal medium (M9 + Glucose
81 = M9G) and rich medium (LBv2) with different inducer concentrations. In M9G, we achieved an
82 approximately 40-fold reduction of the mScarlet-I signal at the highest tested concentrations of ATc and
83 DHBA. As expected, this strong effect was only visible when both inducers were added (Fig. 1b). However,
84 induction of *dcas9* with ATc alone also resulted in a three-fold repression, while induction of *gRNA* with
85 DHBA alone led to a smaller but still noticeable decrease in reporter signal (1.25-fold) (Fig. 1b). When
86 comparing growth rates resulting from cells treated with different inducer concentrations, it became
87 apparent that especially the addition of ATc resulted in a noticeable decrease of up to 1.2-fold, at the
88 highest tested concentration (Fig. 1c). This is most likely the consequence of a metabolic burden, which
89 we described before for high expression of reporter genes (Stukenberg *et al.*, 2021). Alternatively,
90 unspecific toxicity of dCas9 (Cho *et al.*, 2018) could be an explanation for the decrease in growth rate. We
91 finally decided to use 200 fg/mL for ATc and 100 μ M DHBA for further experiments in M9G, as we
92 considered these concentrations as a good middle ground between strong gene repression and an
93 acceptable effect on growth.

94 We also determined optimal inducer concentrations for application of this CRISPRi system in LBv2. Similar
95 to the results from experiments in M9G, only addition of both inducers led to the strongest mScarlet-I
96 repression. Interestingly, we only achieved an approximately 8-fold reduction of the mScarlet-I signal in
97 LBv2, compared to a 40-fold reduction in M9G. Additionally, a higher concentration of ATc was required
98 to achieve this repression (Fig. S1). Unexpectedly, we observed a slightly increased growth rate at low
99 inducer concentration in LBv2, possibly because the reduced expression of *mScarlet-I* overcompensated
100 the burden arising from expression of *dcas9* (Fig. S2). For further experiments in LBv2, we decided to use
101 1000 fg/mL for ATc and 100 μ M DHBA. Overall, differences in growth rate in LBv2 were smaller than in
102 M9G (Fig. S2, Fig. 1c).

103 To evaluate the leakiness of the inducible CRISPRi system, we compared the mScarlet-I signals across three
104 strains, each carrying a different plasmid. The first strain was equipped with a CRISPRi system targeting
105 mScarlet-I, the second with a CRISPRi system featuring a non-binding gRNA, and the third carried an empty
106 plasmid devoid of any CRISPRi system. Neither in M9G (Fig. 1d) nor in LBv2 (Fig. S3), a significant difference
107 was detected between the strains confirming a tight regulation of the graded-CRISPRi system. However,
108 we observed that induction of the CRISPRi system with the non-binding control gRNA in M9G resulted in
109 an unexpected drop of reporter signal (1.3-fold) (Fig. 1d). To investigate whether this was caused by
110 expression of *dcas9*, *gRNA* or both, we measured mScarlet-I signal at different concentrations of both
111 inducers in cells carrying a CRISPRi system encoding the non-binding control gRNA construct. We found
112 that the combination of both inducers led to the strongest reduction of mScarlet-I signal (Fig. S4). Although
113 determining the exact mechanism behind this effect is beyond the scope of this work, we assume that a
114 regulatory response of the cells reduces transcription from the constitutive promoter of *mScarlet-I*. It was
115 shown before in *E. coli* that production of heterologous proteins in *E. coli* can trigger the σ^{32} -mediated heat
116 shock response, which reduces expression from σ^{70} -dependent constitutive promoters through sigma
117 factor competition (Ceroni *et al.*, 2018). Sequestration of RNA polymerases for the transcription of *dcas9*
118 and *gRNA* is likely to also result in a reduction of free RNA polymerases.

119 One desired feature of the graded-CRISPRi tool is the generation of libraries of variants leading to different
120 knockdown strengths. We saw that different inducer concentrations lead to different reporter signals and

121 therefore to different knockdown strengths. However, previous studies have shown that controlling
 122 CRISPRi repression strength through limiting either dCas9 or gRNA availability results in high population
 123 heterogeneity (Vigouroux *et al.*, 2018). To determine if this is also the case with our system in
 124 *V. natriegens*, we measured the mScarlet-I signal at the single cell level in a flow cytometer. At all
 125 concentrations, we observe a unimodal distribution (Fig. 1e). However, consistent with literature on *E. coli*
 126 (Vigouroux *et al.*, 2018), the histogram at moderate inducer concentrations is lower but wider compared
 127 to higher concentrations, indicating a high population heterogeneity both in M9G (Fig. 1e) and LBv2 (Fig.
 128 S5). Consequently, we did not consider adjusting CRISPRi strength through titration of dCas9 and gRNA
 129 expression to be a suitable strategy to obtain graded knockdown levels in *V. natriegens*.



130

131

132 **Figure 1: Initial characterization of CRISPRi in *V. natriegens***

133 **(a)** System for the characterization of the CRISPRi tool in *V. natriegens*. All components of the CRISPRi
134 system were located on a single plasmid (pST_300). Expression of *dcas9* is controlled by a P_{tet} promoter,
135 which can be activated through addition of ATc. Expression of the gRNA is controlled through a P_{3b5b}
136 promoter and is activated by DHBA. The gRNA is composed of a target specific spacer sequence (red) and
137 a gRNA scaffold sequence (blue). This system is tested in a strain carrying a chromosomally integrated
138 mScarlet-I expression cassette (DST018). Expression of mScarlet-I is controlled through a strong
139 constitutive promoter (P_{J23111}). **(b, c)** Testing combinations of DHBA and ATc for their impact on knockdown
140 strengths **(b)** and growth rate **(c)**. Colors in the heatmap indicates growth rate of the cultures. Embedded
141 text reports the mean growth rate, as well as the standard deviation from the mean. This data is based on
142 two independent experiments with three biological replicates. Experiments were performed in M9G. **(d)**
143 Testing inducibility of the CRISPRi system and comparison with control constructs. Induced samples (200
144 fg/mL ATc, 100 μM DHBA) and uninduced samples are shown in red and blue, respectively. Data points
145 from the first independent experiment are shown as circles and data from the second experiment are
146 displayed as diamonds. Control gRNA refers to a gRNA targeting *dns*, which is deleted in this strain. The
147 experiment was performed in M9G with CRISPRi plasmid pST_300 in DST018. Significances were calculated
148 with a two-sample t-test. n.s.: p > 0.05, *: p > 0.01, **: p > 0.001, ***: p < 0.001. **(e)** Analyzing mScarlet-I
149 signal resulting from different combinations of DHBA and ATc at the single cell level. Fluorescence was
150 measured with a flow cytometer. Displayed is a representative histogram from six measurements (three
151 biological replicates, and two independent experiments). The color of the histograms represents the
152 median fluorescence. Samples were drawn from cultures grown in M9G with CRISPRi plasmid pST_300 in
153 strain DST018.

154 **Achieving a graded-CRISPRi repression through gRNA libraries**

155 As a promising alternative to tuning inducer concentrations, we considered using gRNAs with mismatches
156 to the target sequence to adjust CRISPRi knockdown efficiency, similar to previous work (Hawkins *et al.*,
157 2020). As a proof of concept, we exemplarily tested the targeting of mScarlet-I using a gRNA sequence
158 with two defined mismatches at position five and ten from the PAM proximal nucleotide (C5T, A10G). As
159 a result, we obtained an approximately seven- and two-fold reduction of the mScarlet-I signal in M9G and
160 LBv2, respectively (Fig. 2a, Fig. S6). Hence, we found a weaker repression of the mScarlet-I signal in both
161 minimal and rich media in comparison to a CRISPRi system with a perfectly matching gRNA.

162 One desired capability of the graded-CRISPRi tool is to generate mild knockdowns to reveal interesting
163 phenotypes at a reduced abundance of essential proteins. We assume that even the reduced repression
164 strength, which we obtained with the exemplarily tested C5T, A10G mismatches, would still be too strong
165 and prevent growth when targeting essential genes. To generate gRNA variants with even weaker DNA
166 binding strengths, we tested truncated gRNA sequences in combination with the above-described
167 mismatches. Truncated gRNAs have been used before to reduce off-target effects of CRISPR-Cas9 systems
168 for genome editing. The reduction in off-target effects results from weakening the DNA binding strength
169 of the Cas9-gRNA complex through gRNA truncation (Fu *et al.*, 2014). When using the *mScarlet-I* targeting
170 gRNAs with the spacer sequence truncated to 14 nucleotides featuring C5T and A10G mismatches, the
171 knockdown effect was reduced to just 1.3- and 1.1-fold in M9G and LBv2, respectively (Fig. 2a, Fig. S6).
172 Intermediate knockdown effects were obtained for gRNA variants with shorter truncation or no
173 mismatches (Fig. 2a). These results encouraged us to design libraries of gRNAs with spacers of different
174 lengths (20, 16, and 14 nucleotides) in combination with random mismatches at position five and ten from

175 the PAM-proximal nucleotide. Additionally, we included a second distinct gRNA sequence which targeted
176 a different section of the *mScarlet-I* sequence to expand the range of possible knockdown effects even
177 further.

178 In theory, 96 distinct gRNA ($2 \times 2^4 \times 3 = 96$) can be obtained by combining two different gRNA sequences
179 with two randomized nucleotides and three different lengths. We designed and constructed such a library
180 targeting *mScarlet-I*. We then introduced this plasmid library into *V. natriegens* and identified the gRNA
181 spacer sequence of 48 randomly picked colonies by Sanger sequencing, eventually obtaining 33 unique
182 gRNA variants (Table S1). To check if this is within the expected range, we calculated a probability
183 distribution for the number of unique variants when 48 variants are randomly selected from a library of
184 96 possible and equally probable variants. In this distribution, finding 38 unique variants is the most
185 probable outcome, which is slightly higher than the 33 unique variants that we found here (Fig. S7).
186 Nevertheless, we concluded that we generated a sufficiently large sequence diversity to proceed with an
187 experimental characterization of these gRNA variants. Consequently, we next assessed the repression
188 strength of these gRNA variants by analyzing their targeting of *mScarlet-I* at the single-cell level. For this,
189 we employed flow cytometry to resolve differences between individual cells within the population. As
190 expected, we observed very high to very low mScarlet-I signals, indicating weak and strong repression,
191 respectively (Fig. 2b).

192 Next, we examined whether modifying repression strength through limiting inducer concentrations or by
193 using a CRISPRi system with one of the gRNA library variants leads to a more homogenous population.
194 Therefore, we compared samples yielding a similar median fluorescence signal originating from either
195 strategy. In accordance with literature (Vigouroux *et al.*, 2018), our flow cytometry data revealed that
196 strains with a gRNA library variant exhibited a slightly narrower and therefore more uniform fluorescence
197 distribution compared to those with a fully binding gRNA but with reduced inducer concentrations. This
198 finding confirms that the goal of attenuated repression of gene expression can be achieved better with
199 lower cell-to-cell variability by using mismatch gRNA libraries, as opposed to attenuation by lower *gRNA*
200 or *dcas9* induction (Fig. S8).

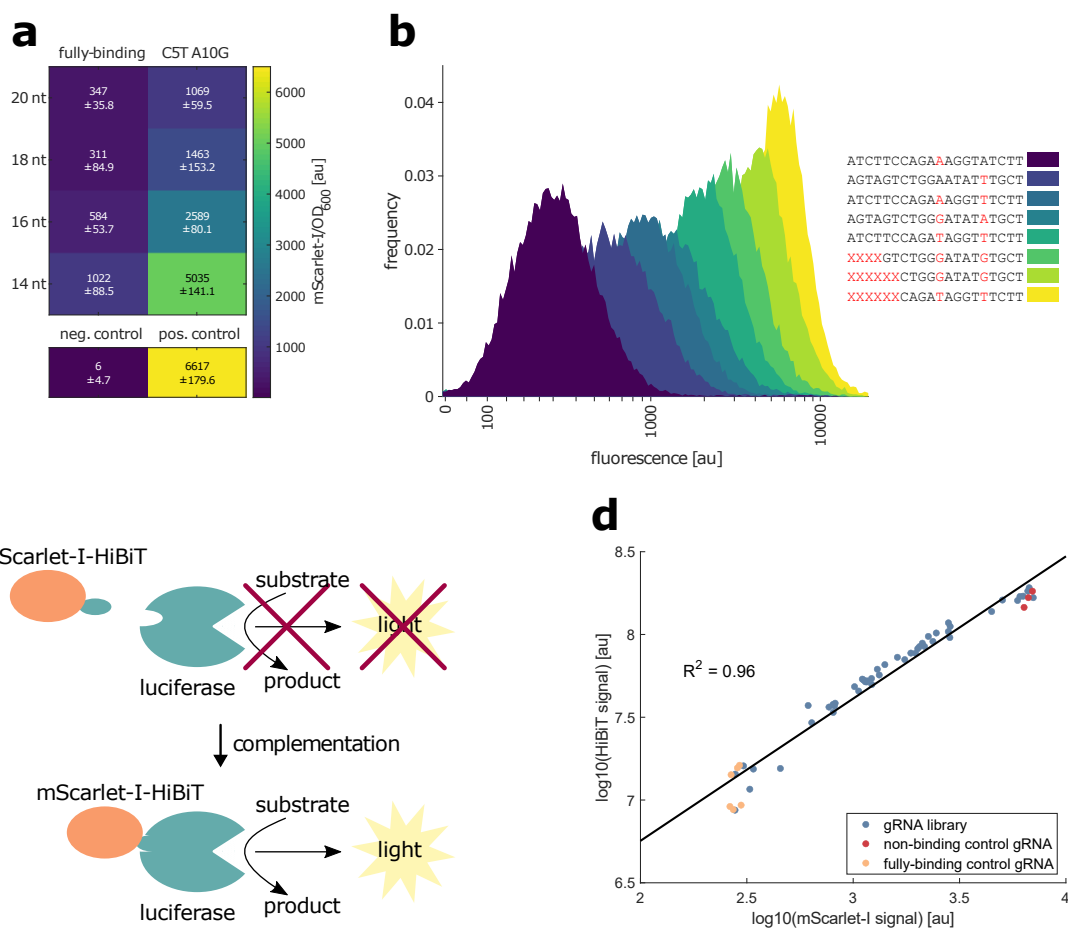
201 **Tracking the reduced protein abundance using the HiBiT tag system**

202 So far, the characterization of the graded-CRISPRi tool relied on the simple quantification of mScarlet-I as
203 a fluorescent protein. To apply graded-CRISPRi for the repression of other genes, a convenient strategy is
204 desired to quantify the resulting change in protein abundance. While adding a fluorescent reporter as a
205 tag to the target protein seems to be the most obvious approach, it comes with several drawbacks. Firstly,
206 the fused fluorescent protein would be expressed in a 1:1 stoichiometry with the tagged protein. For this
207 strategy, the inevitable translation of an additional ~ 250 amino acids for each fluorescent tag could result
208 in a substantial metabolic burden which might significantly impact the strain's phenotype. These concerns
209 would particularly apply when examining highly abundant proteins and therefore reduce the applicability
210 of this strategy. Secondly, attaching fluorescent tags to proteins for tracking expression levels carries the
211 risk of adversely affecting the functionality of the tagged proteins. Lastly, the limited sensitivity of
212 fluorescent proteins might set limits to the detection of protein abundance, especially for less abundant
213 protein targets.

214 To mitigate these limitations, we tested the HiBiT peptide tag system, which was developed and
215 commercialized by Promega (Schwinn *et al.*, 2018). The HiBiT tag is an eleven amino acids long peptide,
216 which complements a luciferase enzyme to generate bioluminescence (Schwinn *et al.*, 2018) (Fig. 2c). The
217 emitted signal is supposed to follow a linear correlation with the abundance of the HiBiT peptide and

218 therefore with the tagged protein of interest. Due to the ~20-fold shorter size of the HiBiT tag compared
 219 to a fluorescent protein, we expect a neglectable metabolic burden caused by the additional synthesis of
 220 the tag. Furthermore, we anticipate a reduced risk of impairing the target protein's functionality due to
 221 the smaller size of the HiBiT tag compared to that of a fluorescent protein. These benefits motivated us to
 222 use this reporter system for protein quantification in our study. However, it is important to acknowledge
 223 that a limitation of the HiBiT tag system remains in its reliance on an endpoint enzyme reaction for signal
 224 measurement. Therefore, this approach does not allow for tracking of the change in protein abundance
 225 over time, unless samples are taken at several timepoints during the experiment.

226 To assess the HiBiT system's effectiveness in quantifying protein abundance, we engineered a C-terminal
 227 fusion of mScarlet-I with the HiBiT tag. Consequently, we anticipated a linear correlation between
 228 fluorescence and luminescence signals, derived from the 1:1 stoichiometry between the fluorescent
 229 reporter mScarlet-I and the attached HiBiT tag. Subsequently, we employed the strain library with gRNA
 230 variants targeting mScarlet-I to create a spectrum of protein abundance levels in the different
 231 *V. natriegens* strains. As a result, we obtained a strong linear correlation between both reporter signals
 232 with $R^2 = 0.96$ (Fig. 2d). In a comparable experiment using the firefly luciferase (Fluc) in place of mScarlet-
 233 I with the HiBiT tag, we achieved an even stronger correlation, with an R^2 value of 0.99 (Fig. S9).



235 **Figure 2: Testing mismatched and truncated gRNAs for CRISPRi in *V. natriegens***

236 **(a)** Analyzing repression strengths of gRNAs with mismatches and different spacer lengths. C5T and A10G
237 indicate mismatches to the target sequence and are counted from the PAM proximal nucleotide of the
238 spacer sequence. neg. control: strain without integrated mScarlet-I cassette (DST016). pos. control: strain
239 integrated mScarlet-I cassette (DST018) with a CRISPRi plasmid with a non-binding control gRNA. Colors in
240 the heatmap indicate the mScarlet-I fluorescence signal. Embedded text represents the mean mScarlet-I
241 signal, as well as the standard deviation from the mean. This data is based on two independent
242 experiments with three biological replicates. Experiments were performed in M9G with the CRISPRi
243 plasmid pST_300. **(b)** Analyzing fluorescence from gRNA variants by flow cytometry. Histograms from
244 selected variants are displayed and their gRNA spacer sequence is provided in the legend. Coloring does
245 not reflect fluorescence and only serves to distinguish samples. Red letters in the legend indicate
246 mismatches in the gRNA variants. Red “X” letters indicate truncations. **(c)** Scheme of the HiBiT tag system.
247 The HiBiT tag is attached to the C-terminal end of a protein of interest (here mScarlet-I). This HiBiT tag
248 complements an otherwise unfunctional luciferase core enzyme, leading to the generation of light. **(d)**
249 Correlation between mScarlet-I and HiBiT signal. The experiment is based on a gRNA library targeting
250 mScarlet-I (see Fig. 2b) in a strain with a chromosomally integrated mScarlet-I-HiBiT expression cassette
251 (DST018). Each data point represents a single measurement from a variant of the gRNA library (blue), the
252 non-binding control gRNA (red) or the fully-binding gRNA (yellow). R^2 is derived from a linear regression of
253 the log₁₀ fluorescence and luminescence values. Experiments performed in M9G with induction of the
254 CRISPRi system (200 fg/mL ATC, 100 μM DHBA).

255 **Targeting multiple reporters simultaneously**

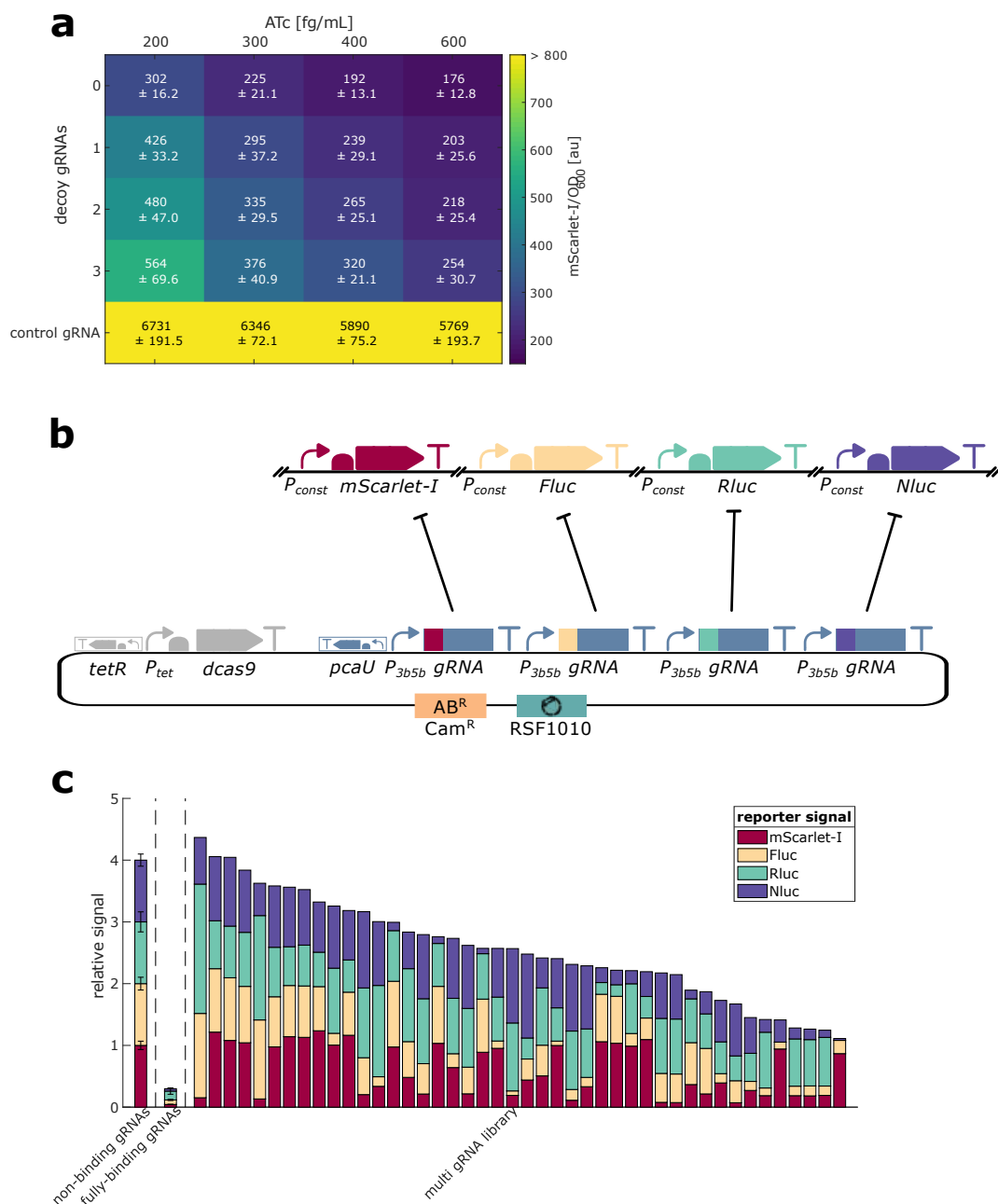
256 Furthermore, we wondered if we could expand graded-CRISPRi to target multiple genes simultaneously.
257 Since CRISPR-Cas9-based systems are inherently modular, repression of multiple targets can be
258 accomplished by integrating several gRNA expression cassettes into the plasmid that carries the *dcas9*
259 sequence. Our previous experiments have shown that a strong repression of the target gene through the
260 CRISPRi system depends on the sufficient expression of both gRNA and *dcas9* (Fig. 1b, Fig. S1). Therefore,
261 we reasoned that we would require stronger *dcas9* induction, as introducing additional gRNA cassettes
262 leads to a higher total gRNA abundance. To test this, we created a set of plasmids encoding one *mScarlet-I*
263 targeting gRNA and up to three additional non-binding decoy gRNAs. Subsequently, we evaluated the
264 repression strength of the mScarlet-I reporter across strains carrying plasmids encoding zero to three
265 decoy gRNAs. As expected, addition of decoy gRNAs reduced the knockdown strength at our usual ATc
266 inducer concentration of 200 fg/mL in M9G. This indicates that dCas9 is not sufficiently abundant to
267 efficiently repress the expression of the target when more than one gRNA cassette is present. This effect
268 was not observed at higher ATc concentrations when more dCas9 is produced.

269 Specifically, a concentration of 600 fg/mL of ATc is necessary with three decoy gRNA cassettes to achieve
270 the same level of *mScarlet-I* repression as with constructs without additional gRNA cassettes. (Fig. 3a).
271 Unfortunately, this increased *dcas9* expression also leads to a noticeable reduction in growth rate (Fig.
272 S10). Therefore, it's important to always consider the trade-off between strong repression and an
273 undesired impact on growth, carefully balancing the implications of either a weaker repression or a more
274 pronounced growth defect.

275 We could already show that generating libraries of gRNA sequences with mismatches to the target leads
276 to variable repression strengths. This motivated us to test if we can also apply this approach to multiple
277 targets. To distinguish the repression of multiple targets, we created a *V. natriegens* strain with four

278 different reporter cassettes integrated into distinct regions of the genome. We used mScarlet-I, firefly
279 luciferase (Fluc), renilla luciferase (Rluc), and nano luciferase (Nluc). After creating a *V. natriegens* strain
280 with all four reporters, as well as strains with each reporter alone, we performed an initial experiment to
281 check for crosstalk between the reporters. We observed no crosstalk, with the exception of Nluc, which
282 generated a moderate luminescence signal with Coelenterazine, the substrate of Rluc (Fig. S11). For the
283 goal of this experiment, we consider this moderate crosstalk acceptable but note that the measured value
284 for Rluc might be slightly overestimated due to the reaction of Nluc with the Rluc substrate.

285 To evaluate graded-CRISPRi against multiple targets, we created a plasmid library, with each variant
286 encoding a different combination of different gRNAs targeting the four reporters (Fig. 3b). Upon testing
287 this library in the strain containing four reporters, we observed a wide range of outcomes, which varied
288 depending on the gRNA variants utilized in the CRISPRi system. Certain combinations of gRNA variants led
289 to strong repression of one or two reporters, while other gRNA applications resulted in moderate
290 repression across all four reporter genes (Fig. 3c). There was no correlation between the four reporter
291 signals, indicating that this approach led to independent repression of all four reporter genes (Fig. S12).
292 Therefore, graded-CRISPRi with multiple gRNAs holds potential for future applications in tuning the
293 expression levels of several endogenous target genes, such as in metabolic engineering projects. This could
294 be used to fine-tune through gene expression control levels of enzymes in pathways either feeding into or
295 competing with an introduced heterologous pathway. Then, variants with the desired phenotype could be
296 screened for, followed by investigating which changes have led to this result.



297

298 **Figure 3: Expanding graded-CRISPRi to multiple targets**

299 **(a)** Testing the effect of additional gRNAs on repression strength at different ATc concentrations. CRISPRi
300 plasmids encoding a gRNA targeting mScarlet-I and up to three decoy gRNAs (targeting *dns* = non-binding
301 gRNA) were tested at different ATc concentrations and the same DHBA concentration (100 μ M). Colors in
302 the heatmap indicate mScarlet-I fluorescence signal. Embedded text represents the mean mScarlet-I
303 signal, as well as the standard deviation from the mean. This data is based on two independent
304 experiments with three biological replicates. Experiments were performed in M9G in strain DST018. **(b)**
305 Scheme for the simultaneous targeting of four reporter genes. The reporter genes are integrated at distinct
306 sites in chromosome 1 (mScarlet-I, Fluc, Rluc) and chromosome 2 (Nluc) and are expressed from
307 constitutive promoters. The CRISPRi plasmid encodes four gRNA expression cassettes, each targeting one

308 reporter gene. (c) Targeting four reporter genes with gRNA libraries. The controls carry either a CRISPRi
309 plasmid encoding four non-binding gRNAs or one fully-binding gRNA for each reporter. The stacked bars
310 show the relative signal compared to the control with four non-binding gRNAs. Error bars displayed for the
311 controls indicate the standard deviation from the mean of three biological replicates. Stacked bars of the
312 library clones were sorted according to the sum of all relative reporter signals. Experiments were
313 performed in M9G with induction of the CRISPRi system (600 fg/mL ATC, 100 μ M DHBA).

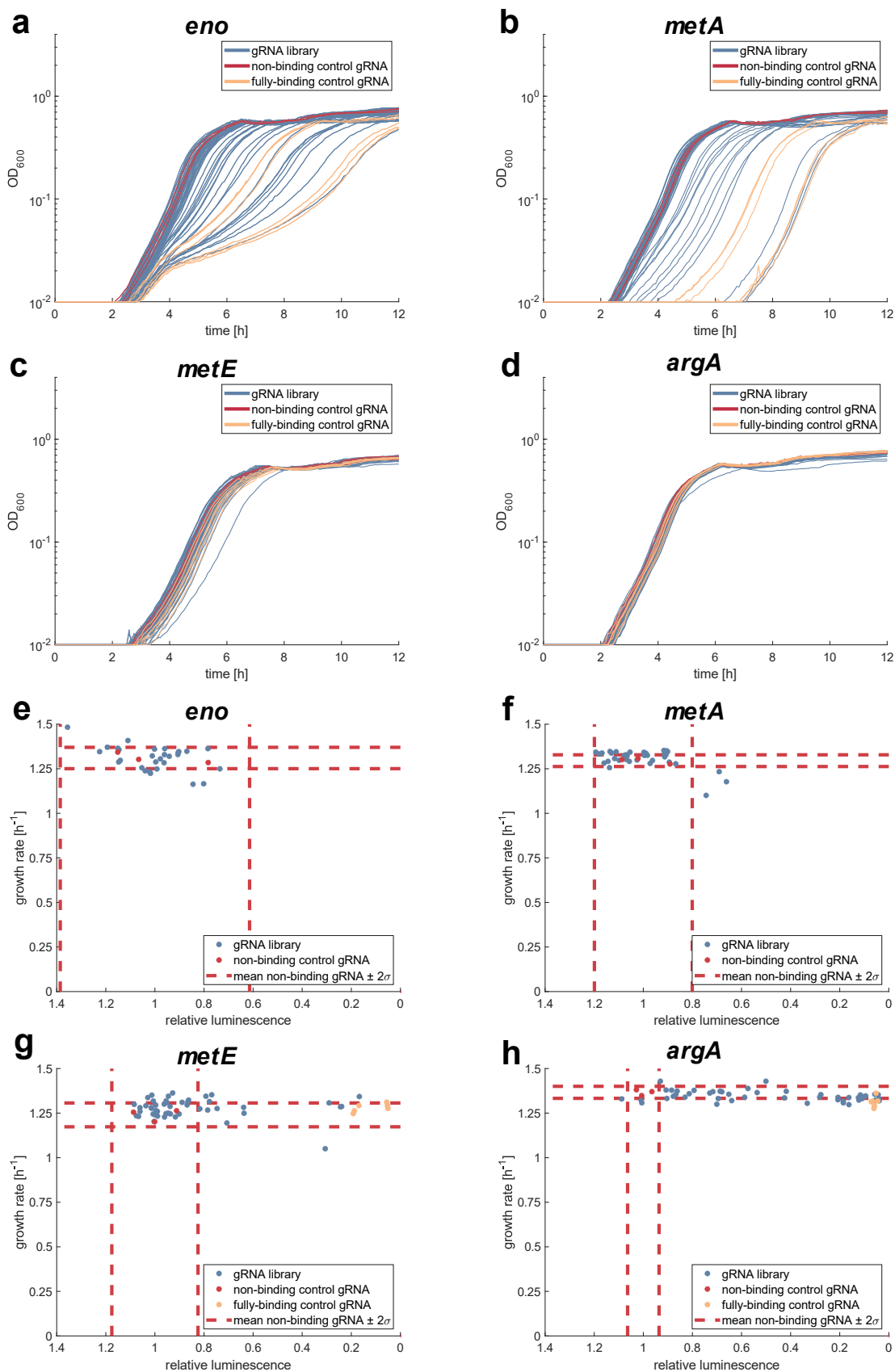
314 Targeting native genes

315 So far, we exclusively targeted chromosomally integrated reporter genes. While this allowed for the
316 characterization of the graded-CRISPRi tool, targeting native genes is clearly the more relevant application
317 for future research. As a proof of concept, we selected four endogenous metabolic genes of *V. natriegens*
318 – *eno*, *metA*, *metE*, and *argA*. According to a CRISPRi screen conducted by Lee et al. (2019), repressing *eno*
319 and *metA* led to reduced fitness in minimal media, which aligns with their roles in glycolysis and amino
320 acid biosynthesis, respectively. In contrast, targeting *metE* and *argA* appeared to have no significant effect
321 (Lee et al., 2019). This outcome was unexpected, especially since a similar CRISPRi screen in *E. coli* (Wang
322 et al., 2018) highlighted the importance of *metE* and *argA* for growth in minimal medium. Given this
323 context, we chose to target *eno*, *metA*, *metE*, and *argA* in *V. natriegens* using our graded-CRISPRi tool. Our
324 aim was to explore the effects of varying repression strengths on these genes. Hence, we created
325 translational fusions of *eno*, *metA*, *metE*, and *argA* with the HiBiT tag to enable quantification of the
326 knockdown strengths. Firstly, we could show that the integration of the HiBiT tag did not affect growth of
327 the resulting strains (Fig. S13). Secondly, we created gRNA libraries targeting each of these endogenous
328 genes. For *eno* and *metA*, this resulted in a diverse array of growth phenotypes (Fig. 4a, Fig. 4b). In contrast,
329 all samples targeting *metE* and *argA* exhibited growth patterns similar to strains with the non-binding
330 control gRNA. (Fig. 4c, Fig. 4d). These results are in accordance with the data from a previously published
331 CRISPRi screen in *V. natriegens* (Lee et al., 2019).

332 Moreover, it was shown before in *E. coli* that some important enzymes are overabundant and that their
333 abundance can be significantly reduced without an effect on growth (Sander et al., 2019). We therefore
334 wanted to test if we can find variants in the *eno* and *metA* libraries with reduced abundance of the
335 respective protein but without an effect on growth. For example, if we observe a strain with a two-fold
336 reduced enzyme abundance but with a control-like growth rate, this will tell us that the respective enzyme
337 has a higher abundance than necessary to sustain fast growth.

338 To quantify the abundance of the chosen enzymes, we repeated the cultivation of the samples without a
339 growth defect and harvested the cultures in the exponential phase. We then proceeded with the
340 quantification of the HiBiT tag to investigate the abundance of the tagged enzymes. Fig. 4e – Fig. 4h
341 illustrate the relationship between growth rate and luminescence signal. For *metA* and *eno*, almost all
342 included samples are within two standard deviations of the values for the non-binding control gRNA (Fig.
343 4e, Fig. 4f). None of the strains with a control-like growth rate had a significantly reduced luminescence
344 signal. The absence of strains with a control-like growth behavior but with reduced luminescence suggests
345 that even a moderate reduction of the respective enzymes affects growth. The picture is different for *metE*
346 and *argA* (Fig. 4g, Fig. 4h). We found variants with 10 to 20-fold reduced luminescence signals but without
347 an effect on growth rate. This confirms that our CRISPRi tool can lead to a strong repression of native
348 genes. Also, this result is in accordance with the results from the CRISPRi screen (Lee et al., 2019), which
349 showed no effect of a CRISPRi mediated knockdown of *metA* and *argA* on growth in minimal medium.
350 However, even with a 10 to 20-fold reduction in abundance, it cannot be excluded that the enzyme level

351 is still sufficient to support growth. We therefore created deletion strains of *argA* and *metE* and tested
352 their ability to grow in M9G. Those strains did not show a major grow defect compared to the parental
353 strain, confirming that these genes are not necessary for growth of *V. natriegens* in M9G (Fig. S14).
354 Literature provides some insights into these observations. Several marine bacteria possess an *argH(A)*
355 gene encoding a bifunctional enzyme capable of catalysing both the initial and final steps of arginine
356 biosynthesis (Xu *et al.*, 2000, 2006). This could compensate for the loss of *argA* in our gene deletion
357 experiment and explain consistent growth rates. The larger size of ArgH in *V. natriegens* compared to
358 *E. coli* (624 vs. 456 amino acids) suggests that *V. natriegens*' ArgH might also function as a bifunctional
359 ArgH(A) enzyme, functionally replacing ArgA. Regarding *metE*, the presence of a second ORF (PN96_19000)
360 with the same annotation might indicate a gene duplicate, which we speculate could compensate for *metE*
361 loss.



363 **Figure 4: Targeting native genes with graded-CRISPRi**

364 **(a - d)** Growth curves resulting from targeting of native genes by graded-CRISPRi. Each line represents one
365 variant of the gRNA library (blue), the non-binding control gRNA (red) or the fully-binding gRNA (yellow).
366 Strains carry a C-terminal HiBiT tag fusion of the target protein **(e - h)** Scatter plot between growth rate
367 and luminescence from the HiBiT tag. Relative luminescence was calculated relative to the mean of the
368 values obtained from the non-binding control strains. Each data point represents a single measurement
369 from a variant of the gRNA library (blue), the non-binding control gRNA (red) or the fully-binding gRNA
370 (yellow). Dotted red lines indicate the mean values from three replicates of the non-binding control gRNA
371 plus and minus two standard deviations. Only samples with a growth behavior similar to the non-binding
372 control strains were analyzed. Experiments were performed in M9G with induction of the CRISPRi system
373 (200 fg/mL ATC, 100 μ M DHBA). The CRISPRi plasmid pST_300 was used as well as the strains DST025 (eno-
374 HiBiT), DST024 (metA-HiBiT), DST031 (metE-HiBiT), DST023 (argA-HiBiT).

375 **Conclusion**

376 We developed and characterized a tightly controllable CRISPRi system for *V. natriegens*. By using libraries
377 of gRNA sequences leading to a weaker binding of the dCas9-gRNA complex to the target DNA sequence,
378 we obtained graded repression. We could show that graded-CRISPRi can be used to target native genes,
379 which resulted in diverse growth behaviors. In future studies, this approach could be expanded to target
380 other essential or non-essential genes to study the phenotypes resulting from different knockdown
381 strengths. To allow quantification of the resulting protein abundance, we established the HiBiT tag system
382 for use in *V. natriegens*. Beyond being used in combination with graded-CRISPRi, the HiBiT tag system
383 might be an interesting alternative for the quantification of the abundance of single proteins in different
384 strains or different conditions. We demonstrated the applicability of graded-CRISPRi for the simultaneous
385 repression of four reporter genes. This could be used in studies where only a specific combination of
386 expression levels from multiple genes leads to a favorable outcome.

387 **Methods**

388 **Bacterial strains and culture conditions**

389 All strains created in this work are based on a *V. natriegens* strain ATCC14048 with a deletion of the *dns*
390 gene (Stukenberg *et al.*, 2021). This gene codes for a DNA endonuclease, which prevents efficient
391 transformation with plasmid DNA using the heat-shock transformation protocol. *V. natriegens* was
392 routinely grown in LBv2 (Weinstock *et al.*, 2016). Whenever selection was required, chloramphenicol was
393 added to the medium with a final concentration of 4 μ g/mL or 2 μ g/mL for liquid and solid medium,
394 respectively. Glycerol stocks were prepared for long term storage at -80°C by growing cultures for 6 – 8 h
395 at 37 °C and mixing 700 μ L of the grown cultures with 700 μ L of 50% glycerol. Experiments were performed
396 either in buffered M9 minimal medium ([recipe in Tables S2 – S5](#)) with glucose as the sole carbon source
397 (M9G) or in LBv2 (Weinstock *et al.*, 2016).

398 **Preparation of chemically competent *V. natriegens* cells and heat-shock transformation**

399 Preparation of chemically competent cells and heat-shock transformation were performed as described
400 before (Stukenberg *et al.*, 2021). A preculture of the respective *V. natriegens* strain was inoculated from a
401 glycerol stock and grown overnight at 30 °C and 200 rpm. On the next day, 125 mL of preheated LBv2
402 medium (37 °C) were inoculated with the overnight culture to a final OD₆₀₀ of 0.01 in a 1 L baffled shake

403 flask. This culture was grown at 200 rpm (37 °C) until an OD₆₀₀ between 0.5 and 0.7 was reached. The
404 culture was then transferred to pre-chilled 50 mL falcon tubes and incubated on ice for 10 min, followed
405 by centrifugation for 10 min at 3000 × g at 4 °C. The supernatant was discarded, and the pellets were
406 resuspended in 40 mL cold TB buffer per 125 mL bacterial culture (TB buffer: 10 mM Pipes, 15 mM CaCl₂,
407 250 mM KCl, pH adjusted to 6.7 with KOH, then add 55 mM MnCl₂, filter sterilized). The cells were again
408 incubated on ice for 10 min and further centrifuged for 10 min at 3000 × g at 4 °C. The supernatant was
409 removed, and pellets were resuspended in 5 mL cold TB buffer per 125 mL starting culture and
410 consolidated in a single falcon tube, before adding 350 μL dimethyl sulfoxide. After another 10 min
411 incubation on ice, 50 μL aliquots were prepared in 1.5 mL tubes and snap frozen in liquid nitrogen. Aliquots
412 were stored at -80 °C until further use.

413 Chemically competent *V. natriegens* cells were transformed through the addition of plasmid DNA to an
414 aliquot of 50 μL competent cells and incubated on ice for 30 min. After 30 min, cells were heat shocked in
415 a water bath at 42 °C for 45 s then immediately incubated on ice for 15 min before recovery. The cells were
416 recovered in 1 mL 37 °C warm LBv2 medium, followed by shaking at 37 °C for 1 h at 700 rpm. After
417 recovery, the cells were pelleted by centrifugation at 3000 × g for 3 min, the supernatant was decanted,
418 and the pellet was resuspended in the remaining ~ 100 μL residual medium. The whole volume was plated
419 on 37 °C warm LBv2 plates containing the appropriate antibiotic and incubated overnight at 37 °C.

420 **Genome engineering of *V. natriegens***

421 Genome engineering of *V. natriegens* was performed with the NT-CRISPR method (Stukenberg *et al.*,
422 2022). Integration of the HiBiT tag sequence was facilitated with a gRNA that overlaps the integration site
423 so that integration of the HiBiT tag sequence disrupts the gRNA binding site and therefore prevents
424 CRISPR-Cas9 mediated cell killing. The plasmid pST_116 was used when a NGG PAM site was available at
425 the integration site. The variant pST_140, carrying the almost PAM less spG Cas9 variant (Walton *et al.*,
426 2020), was used with gRNAs relying on alternative NGN PAM sequences. The NT-CRISPR plasmids pST_116
427 and pST_140 were adapted for different target genes by replacing the *sfGFP* dropout with annealed
428 oligonucleotides in a Golden Gate Assembly reaction. The annealing reactions were set up by mixing 1.5 μL
429 of each oligonucleotide (100 μM) with 5 μL T4-DNA ligase buffer (Thermo Scientific) in a total reaction
430 volume of 50 μL. Reactions are incubated in a heat block at 95 °C for 15 min, before the heat block was
431 switched off to allow the samples to slowly cool down to room temperature (~1 h). Cloning reactions with
432 the NT-CRISPR plasmids were set up with ~200 ng of the respective plasmid, 3 μL annealed
433 oligonucleotides, 0.5 μL of T4-DNA Ligase (5 Weiss U/μL, Thermo Scientific) and BsaI (10 U/μL, Thermo
434 Scientific) and 1 μL T4-DNA ligase buffer (Thermo Scientific) in a total reaction volume of 10 μL. Reactions
435 were run in a thermocycler with 30 cycles of 37 °C (2 min) and 16 °C (5 min), followed by a final digestion
436 step at 37 °C for 30 min and an enzyme denaturation step at 80 °C for 10 min. Oligonucleotides used for
437 the construction of gRNAs are provided in Table S12. NT-CRISPR plasmids were first assembled in *E. coli*
438 NEB Turbo, the plasmid DNA was then isolated and used for the transformation of *V. natriegens* Δ*dns*.

439 tDNAs with homologous regions of 3 kb per arm were prepared by first constructing a tDNA template
440 plasmid and then generating the tDNA in a PCR. The tDNA template plasmids were generated in a three
441 fragment Gibson Assembly from two fragments comprising ~ 3kb of sequence upstream and downstream
442 of the integration site, amplified from genomic DNA of *V. natriegens*, as well as a backbone fragment,
443 which was amplified from the part entry vector of the Marburg Collection pMC_V_01 (Stukenberg *et al.*,
444 2021) or a low copy variant pMC_V_11, carrying a p15A origin of replication. The tDNA was generated in
445 a subsequent PCR reaction (Q5 High-Fidelity DNA Polymerase, NEB) and purified using the E.Z.N.A Cycle

446 Pure Kit (Omega Bio-Tek), according to manufacturer's instructions. The tDNAs for the integration of the
447 luciferase expression cassettes could not be generated with this approach, presumably due to toxicity of
448 the homologous flanks of the integration sites or the constitutive expression of the luciferases on a multi-
449 copy plasmid in *E. coli*. Instead, these tDNAs were created by fusion PCR. Therefore, the upstream and
450 downstream fragments were prepared as described above. The insert fragments, carrying the luciferase
451 expression cassette, was amplified from a level 1 plasmid which was assembled using the Marburg
452 Collection (Stukenberg *et al.*, 2021). Level 1 plasmids constructed in this study are listed in [Table S6](#) and
453 their plasmids maps are provided in [Supplementary Data S1](#). For the fusion PCR to generate the final tDNA
454 fragment, we used 50 ng of each fragment in a 25 μ L PCR reaction with the outermost primers. Sequences
455 of all primers and the templates used for the construction of tDNAs are provided in [Table S13](#).

456 The NT-CRISPR protocol was performed as described before (Stukenberg *et al.*, 2022). Precultures were
457 grown overnight (16 – 17 h) at 30 °C and 200 rpm in 5 mL LBv2 with 4 μ g/mL chloramphenicol and 100 μ M
458 IPTG (Roth, CAS: 367-93-1) to induce *tfoX* expression. The natural transformation was started by adding
459 3.5 μ L of the precultures ($OD_{600} \sim 9 - 11$) to 350 μ L sea salt medium (28 g/L (Sigma, S9883)) with 100 μ M
460 IPTG and 100 ng of tDNA in a 1.5 mL reaction tube. Samples were briefly vortexed and then incubated
461 statically at 30 °C for 5 h. In a subsequent step, 1 mL LBv2 without antibiotics was added to the cells. For
462 CRISPR-Cas9 induction, 200 ng/mL ATc (Alfa Aesar, 13803-65-1) was added to the LBv2 medium. Tubes
463 were mixed by inversion and incubated at 300 rpm and 30 °C for 1 h. Finally, 100 μ L of appropriate
464 dilutions were plated on LBv2 agar plates with 2 μ g/mL chloramphenicol and 200 ng/mL ATc.

465 After overnight incubation at 37 °C, colonies were screened for the desired modification by colony PCR. A
466 colony was resuspended in 20 μ L of H₂O, incubated for 10 – 15 min at 95 °C for cell lysis and cell debris
467 was pelleted by centrifugation for 3 min at maximum speed. The PCR reaction was set up with 1 μ L of the
468 supernatant in a 12.5 μ L reaction with Taq polymerase (NEB), according to manufacturer's instruction.

469 Positive colonies were further verified by Sanger sequencing. Sequencing was performed by Microsynth
470 Seqlab using PCR fragments and a primer close to the modified site.

471 In parallel to colony PCR screening, cells were cured from the NT-CRISPR plasmid by inoculating 5 mL of
472 antibiotic free LBv2. After 6 – 7 h of growth at 37 °C and 200 rpm, 100 μ L of a 10^{-7} dilution were plated on
473 antibiotic free LBv2 agar plate. After overnight incubation at 37 °C, colonies were patched on LBv2 with
474 and without 2 μ g/mL chloramphenicol to check for plasmid loss. Colonies growing on the antibiotic free
475 agar plates but not on agar plates containing chloramphenicol were considered to consist of plasmid-cured
476 cells. Glycerol stocks of plasmid-cured strains were prepared as described above.

477 An overview of strains created using NT-CRISPR is shown in [Table S7](#).

478 **Construction of CRISPRi plasmids**

479 The plasmid pST_300 was used for all CRISPRi experiments with a single gRNA. pST_300 carries *dcas9*
480 under control of the ATc inducible P_{tet} and a *gRNA* expression cassette under control of the DHBA inducible
481 P_{3b5b}. Both promoters were optimized by directed evolution for *E. coli* (Meyer *et al.*, 2019). The P_{3b5b}
482 promoter was further modified to start transcription at the first nucleotide of the *gRNA* sequence in the
483 final plasmid configuration. The promoter sequences including information of the -35 box, -10 box, and +1
484 position were taken from Meyer *et al.* (2019).

485 The *gRNA* expression cassette carries a dropout part, which contains a *sfGFP* marker and a *sacB* expression
486 cassette, to allow for visual identification of correctly assembled plasmids through loss of *sfGFP* and for

487 the inhibition of cells transformed with religated pST_300 plasmid in the preparation of CRISPRi plasmids
488 with mismatched gRNA libraries (see below). Plasmid assembly was done within the framework of the
489 Marburg Collection (Stukenberg *et al.*, 2021). pST_300 is a level 2 plasmid which was built from level 0*
490 parts and the level 1 plasmid pST_236 using Esp3I. pST_236 was built with level 0 parts using BsaI. Golden
491 Gate Assembly reactions were performed in a volume of 10 μ L with 0.5 μ L of either Esp3I (10,000 U/mL,
492 NEB) or BsaI (10,000 U/mL Thermo Scientific), 0.5 μ L T4-DNA ligase (5 Weiss U/ μ L, Thermo Scientific), 1 μ L
493 T4-DNA ligase buffer (Thermo Scientific) and approximately 25 fmol of each precursor plasmid. Reactions
494 were run in a thermocycler with 30 cycles of 37 $^{\circ}$ C (5 min) and 16 $^{\circ}$ C (10 min), followed by a final digestion
495 step at 37 $^{\circ}$ C for 60 min and an enzyme denaturation step at 80 $^{\circ}$ C for 10 min. Information about the
496 generated level 1 and level 2 plasmids and the corresponding plasmid maps are provided in [Table S6](#) and
497 [Supplementary Data S1](#).

498 We designed two gRNA sequences for each target gene, binding the first third of the coding sequence. The
499 choice of gRNA sequences was done with the help of a web based tool ([https://crispr-
500 browser.pasteur.cloud/guide-rna-design](https://crispr-browser.pasteur.cloud/guide-rna-design)) (Calvo-Villamañán *et al.*, 2020). Two oligonucleotides were used
501 for each gRNA and integrated into the CRISPRi plasmid pST_300 exactly as described above for the NT-
502 CRISPR plasmids. Sequences of the used gRNA spacers are provided in [Table S14](#).

503 **Construction of CRISPRi plasmids with mismatched gRNA libraries**

504 For each fully-binding gRNA, we purchased three ssDNA oligonucleotide (20, 16 and 14 nucleotides),
505 containing “N” nucleotides at positions five and ten from the PAM proximal nucleotide inside the gRNA
506 spacer sequence. The spacer sequence of the gRNA was flanked by inward facing BsaI recognition sites,
507 which are necessary to generate the fusion sites for the subsequent integration in pST_300. Additionally,
508 the ssDNA oligo was flanked by primer adaptor sequences (Organick *et al.*, 2018). To generate dsDNA,
509 which is necessary for the subsequent cloning step, a 10 pM dilution of the ssDNA oligonucleotide ([Table
510 S15](#)) was used in a Q5 PCR reaction with the primers oDS_1184 and oDS_1185, binding to the primer
511 adaptor sequences. These primers each carry a 20-nucleotide overhang with a random sequence, to
512 extend the final PCR fragment to \sim 120 bp. Due to this extended size, the PCR fragment could be purified
513 using the E.Z.N.A Cycle Pure Kit (Omega Bio-Tek), according to manufacturer’s instructions. The purified
514 PCR fragments from all six oligonucleotides per target (two different gRNA sequences and three lengths)
515 were mixed in equal amounts. This mixture was then used in threefold molar excess to 200 ng of the
516 CRISPRi plasmid pST_300 in a 10 μ L Golden Gate Assembly reaction. In this case, 0.5 μ L BsaI-HFv2 (NEB,
517 20,000 U/mL) and 0.5 μ L T4 DNA Ligase (NEB, 400,000 U/mL) were used with 1 μ L T4 DNA Ligase Reaction
518 Buffer (NEB, 10x). We found that using these enzymes resulted in higher efficiency and fidelity for the
519 cloning of mismatched gRNA libraries. Reactions were run in a thermocycler with 30 cycles of 37 $^{\circ}$ C (5 min)
520 and 16 $^{\circ}$ C (10 min), followed by a final digestion step at 37 $^{\circ}$ C for 60 min and an enzyme denaturation step
521 at 80 $^{\circ}$ C for 10 min.

522 These cloning reactions were introduced into *E. coli* NEB Turbo through electroporation. Competent cells
523 were prepared according to a glycerol/mannitol density step centrifugation protocol (Warren, 2011). A
524 volume of 5 mL precultures of NEB Turbo cells was grown overnight in SOB medium (20 g/L tryptone, 5
525 g/L yeast extract, 0.58 g/L NaCl, 0.186 g/L KCl) at 30 $^{\circ}$ C and 200 rpm for 16-17 h and then used to inoculate
526 200 mL SOB in a 1 L baffled shake flask to a starting OD₆₀₀ of 0.01. The culture was incubated and the OD₆₀₀
527 carefully monitored. At an OD₆₀₀ of approximately 0.5, the culture was distributed into four 50 mL falcon
528 tubes and incubated for 5 min on ice. Cells were then harvested by centrifugation for 15 min at 2000 g and
529 4 $^{\circ}$ C in a swing rotor in a Sigma 4K15 centrifuge. All following steps were performed on ice. After

530 centrifugation, the supernatant was first decanted and then remaining volume removed by aspiration.
531 Each of the four pellets was gently resuspended in 10 mL of cold H₂O. Two cell suspensions of each sample
532 were consolidated in a clean 50 mL falcon tubes. The cold glycerol/mannitol solution (20 % glycerol (w/V),
533 1.5 % mannitol (g/L)) was used to create a bottom layer below the cell suspension. Approximately 12 mL
534 of the glycerol/mannitol solution were aspirated in a 10 mL glass pipette. The glass pipette was used to
535 pierce through the cell suspension and the glycerol/mannitol solution was slowly (~ 20 s per tube)
536 dispensed, resulting in an upward displacement of the cell suspension. The cells were forced through the
537 dense glycerol/mannitol solution by another centrifugation step (2000 g, 15 min, 4 °C, acceleration and
538 deceleration set to 2) and thereby cleaned from any remaining salts which would interfere with the
539 electroporation. After this centrifugation step, the supernatant was carefully removed by aspiration,
540 starting with the upper water phase, followed by the lower glycerol/mannitol phase. Each cell pellet was
541 then resuspended in 200 µL of cold glycerol mannitol solution and cells from both falcon tubes were
542 combined. Aliquots with 40 µL of cells were prepared in cold 1.5 mL reaction tubes and 4 µL of the Golden
543 Gate Assembly reaction was added to the cells. The cell suspension was then transferred to a pre-chilled
544 electroporation cuvette and after approximately 5 – 10 min electroporated in the eporator electroporator
545 (Eppendorf) set to 1850 V. Immediately after electroporation, 1 mL of pre-warmed (37°C) SOC medium
546 (Table S8) was added to the electroporation cuvette, mixed with the electroporated cells, and then
547 transferred to a 1.5 mL reaction tube. Cells were recovered for 1 h at 37 °C and 700 rpm. After recovery
548 100 µL of the cell suspension was spread on LB agar plates (without NaCl) containing 25 µg/mL
549 chloramphenicol and 10 % sucrose for SacB-mediated counterselection. These plates were incubated for
550 20 - 24 h at 30 °C to allow colonies to form. These colonies were scraped off with 2 mL of 1 % NaCl (w/v)
551 and the resulting cell suspension was used for plasmid isolation with the E.Z.N.A. Plasmid DNA Mini Kit
552 (Omega Bio-Tek).

553 Plasmid DNA resulting from this procedure was used to transform the relevant *V. natriegens* strains. After
554 transformation, we used 48 colonies per target gene to generate glycerol stocks as described above which
555 were then used for the respective experiments.

556 **Construction of CRISPRi plasmids with multiple gRNA sequences**

557 Assembly of CRISPRi plasmids with multiple gRNA sequences was performed in two steps. In a first step,
558 gRNA sequences were integrated into gRNA position vectors (Table S9). In the second step, the gRNA
559 sequences from these position vectors were assembled with the CRISPRi dropout plasmid pST_301 (Fig.
560 S15). pST_301 resembles pST_300 (used for CRISPRi with a single target) but carries an *mScarlet-I* and *sacB*
561 expression cassette as a dropout for positions 2 – 5, according to the nomenclature of the Marburg
562 Collection (Stukenberg *et al.*, 2021).

563 Integration of the gRNA sequences into the position vectors was done in the same way as described before
564 for pST_300 with the difference that kanamycin was used for selection instead of chloramphenicol. These
565 gRNA position vectors carry a *sfGFP* and *sacB* expression cassette as a dropout to allow visual identification
566 through loss of sfGFP production and by the inability to grow on LB sucrose due to SacB-mediated
567 counterselection. Assembly of the final CRISPRi plasmid was done by combining the libraries of the gRNA
568 position vectors with the pST_301 plasmid in a Golde Gate reaction as described above but with Esp3I
569 (NEB, 10,000 U/mL) instead of BsaI. The cloning reaction was electroporated into *E. coli* NEB Turbo as
570 described above and plated on LB sucrose agar plates with chloramphenicol to select for colonies
571 harboring the correctly assembled plasmid. Plasmid DNA resulting from this procedure was used to

572 transform the *V. natriegens* strain DST050 (four reporter genes integrated into the chromosome) to
573 generate the strains for subsequent experiments.

574 **Measurement of growth rates and mScarlet-I fluorescence in a microplate reader**

575 The Tecan infinite f200pro microplate reader infinite F200PRO was used for all experiments performed in
576 96-well plate. Plate reader protocols are provided in [Table S10](#) and [S11](#) for experiments without and with
577 fluorescence measurements, respectively.

578 All experiments started from a precultures that were inoculated by first resuspending material from
579 glycerol stocks in 50 μ L of LBv2 (with added antibiotics if applicable) and then by adding 5 μ L of this
580 suspension to 95 μ L of LBv2 (with added antibiotics if applicable). LBv2 was also used for precultures in
581 cases where the main experiment was performed in minimal medium. The precultures was diluted 1:2000
582 to inoculate the 96-well plate for the experiment. The 1:2000 dilution was obtained with an intermediate
583 dilution step (1:50) and a second dilution step (1:40). Experiments in LBv2 were performed in a total
584 volume of 100 μ L, while experiments in M9G were performed in a total volume of 150 μ L to adjust to the
585 longer experimental time and consequently for the increased evaporation over the time course of the
586 experiment. For each well, the intermediate dilution step was performed with the exact same medium,
587 including the exact concentrations of antibiotics and inducers as in the final experiment. For experiments
588 using CRISPRi, precultures were induced with the same concentration of ATc and DHBA as in the main
589 culture to induce *cas9* and *gRNA* expression and to deplete the target protein before the start of the main
590 culture. Unless indicated otherwise, we used 200 ng/mL ATc and 100 μ M DHBA as inducer concentrations
591 for experiments in M9G and 1 μ g/mL ATc and 100 μ M DHBA for experiments in LBv2.

592 The growth rate for each culture in the 96-well plate was calculated from an exponential fit on all data
593 points between OD₆₀₀ values of 0.01 and 0.1, which represents the exponential growth phase.

594 **Measurement of mScarlet-I expression using flow cytometry**

595 Single cell measurements of mScarlet-I signal and the effect of CRISPRi repression were performed with
596 the BD Fortessa flow cytometer. Precultures and cultures for the measurements were grown in 96-well
597 plates in the Tecan infinite f200pro microplate reader as described above. At an OD₆₀₀ of approximately
598 0.1, when cells are in late exponential phase, the microplate reader measurement was aborted and
599 cultures were diluted with PBS pH 7.4 to yield approximately 10,000 events/ μ L in the flow cytometry
600 measurement. Samples were measured with the following settings: Sample flow rate = 2.0 μ L/s, Sample
601 Volume = 30 μ L, Mixing Volume = 100 μ L, Mixing Speed = 180 μ L/s, Number of Mixes = 2, Wash Volume =
602 800 μ L, Enable BLR = yes, BLR Period = 100. No events were excluded through gating of the raw data.

603 **HiBiT Assay**

604 Abundance of the protein of interest, carrying a C-terminal fusion of the HiBiT tag, was performed with
605 the Nano-Glo[®] HiBiT Lytic Detection System (Promega). Precultures and cultures for the measurements
606 were grown in 96-well plates in the Tecan infinite f200pro microplate reader as described above. At an
607 OD₆₀₀ of approximately 0.1, when cells are in late exponential phase, the microplate reader measurement
608 was aborted. Cells were transferred into a 96-well PCR plate and frozen at -80°C for at least 24 h. We found
609 that a single freeze thaw cycle aids in cell lysis with the lysis buffer provided with the kit. Cultures were
610 thawed immediately before the experiment at room temperature. HiBiT Assay reaction mix was freshly
611 prepared for each experiment according to manufacturer's instructions. All components, including thawed
612 samples, were allowed to reach room temperature. The luminescence measurement was performed in a

613 Tecan infinite f200pro microplate reader in black 384-well plates. For each well, 15 μ L of reaction mix was
614 combined with 15 μ L of samples. To reduce spillover of luminescence, only every other row and column
615 was used. However, as the luminescence vanishes completely after multiple days, the skipped wells could
616 be used in later experiments. A 10 min shaking step in orbital mode with an amplitude of 3.5 mm and a
617 frequency of 88 rpm was performed in the Tecan infinite f200pro microplate reader, before luminescence
618 of the whole 384-well plate was performed every three minutes with an integration time of 200 ms and a
619 settling time of 10 ms for 3 h. To correct for differences in culture density, all luminescence values were
620 normalized by the last OD₆₀₀ data point before the measurement was aborted. All luminescence values
621 over the time course of 3 h were summed up to yield the final data point for the respective samples.

622 **Fluc and Nluc Assay**

623 Signal of the Fluc reporter was quantified with the ONE-Glo Luciferase Assay System (Promega) and Nluc
624 reporter was quantified with Nano-Glo Luciferase Assay System (Promega). The substrate was prepared
625 according to manufacturer's instructions. Samples were prepared as described for the HiBiT assay. The
626 measurements were started by adding 15 μ L of thawed samples to 15 μ L of substrate in a black 384-well
627 plate. Measurement and data analysis was done as described for the HiBiT assay.

628 **Rluc Assay**

629 Signal of the Fluc reporter was quantified with the Renilla Luciferase Assay System (Promega). The
630 substrate was prepared according to manufacturer's instructions. Samples were prepared as described for
631 the HiBiT assay. After thawing, the samples were diluted with 2 x Luciferase Assay Lysis Buffer (diluted
632 from 5 x with H₂O) and incubated for at least 10 min at room temperature. Due to the shorter signal half-
633 life time compared to the other luciferase systems, the assay was performed differently than for the other
634 luciferases. 15 μ L of the samples (after dilution with lysis buffer) were transferred to wells of a black 384-
635 well plate. 15 μ L of the substrate was added to the cells with 10 s delay between wells. A single
636 luminescence measurement was done also with a 10 s delay between wells, to ensure the same time delay
637 from addition of substrate to measurement for each well. Six samples per run were processed to minimize
638 loss of signal before the measurements.

639 **Calculation of probability distribution**

640 A probability distribution was generated to predict the expectable number of unique variants from gRNA
641 libraries. Therefore, a custom MATLAB script was created with the following steps. First, a random number
642 between 1 and 96 was generated, each representing one of the 96 theoretically possible variants from the
643 gRNA library. This was repeated 48 times, representing the 48 sequenced variants. Next, the number of
644 unique variants was determined. Finally, this was repeated 10,000 times to generate the histogram for the
645 probability of obtaining a specific number of unique variants.

646 **Supporting Information**

647 Figure S1: Effect of inducer concentrations on repression strength in LBv2.

648 Figure S2: Effect of inducer concentrations on growth rate in LBv2.

649 Figure S3: Inducibility of CRISPRi system and comparison with control constructs in LBv2.

650 Figure S4: Effect of inducer concentrations on mScarlet-I signal with non-binding control gRNA.

- 651 Figure S5: Analyzing the mScarlet-I signal resulting from different combinations of DHBA and ATc at the
652 single cell level in LBv2.
- 653 Figure S6: Repression strengths with gRNAs featuring mismatches and different spacer lengths in LBv2.
- 654 Figure S7: Probability distribution for number of unique variants.
- 655 Figure S8: Comparing single-cell distribution from mismatched and truncated gRNAs with limiting inducer
656 concentrations.
- 657 Figure S9: Correlation between Fluc and HiBiT signal.
- 658 Figure S10: Testing the effect of additional gRNAs on growth rate at different ATc concentrations.
- 659 Figure S11: Crosstalk between reporter signals.
- 660 Figure S12: Correlation between reporter signals from a multi gRNA library experiment (Fig. 3c).
- 661 Figure S13: Growth curves of HiBiT fusion strains.
- 662 Figure S14: Growth curves of *argA* and *metE* deletion strains.
- 663 Table S1: Sequencing results of mScarlet-I gRNA library variants.
- 664 Table S2: Recipe for buffered M9 minimal medium with 0.4 % (w/w) glucose (M9G).
- 665 Table S3: Recipe 5X M9 salts solution.
- 666 Table S4: Composition of 100X trace elements solution.
- 667 Table S5: Preparation of 100x trace elements solution.
- 668 Table S6: Level 1 and level 2 plasmids assembled in this study.
- 669 Table S7: *V. natriegens* strains with chromosomal modification
- 670 Table S8: Recipe for SOC medium
- 671 Table S9: gRNA position vectors for assembly of multi gRNA CRISPRi plasmids.
- 672 Table S10: Protocol for microplate reader measurements without fluorescence measurement
- 673 Table S11: Protocol for microplate reader measurements with fluorescence measurement
- 674 Table S12: Oligonucleotides used to assemble gRNA sequences for NT-CRISPR
- 675 Table S13: Oligonucleotides used for the construction of tDNA template plasmids and tDNAs
- 676 Table S14: Oligonucleotides used to assemble gRNA sequences for CRISPRi
- 677 Table S15: ssDNA templates for the generation of gRNA libraries
- 678 Data S1: Plasmid maps

679 **Author Information**

680 **Corresponding author**

681 **Anke Becker** - *Center for Synthetic Microbiology, Philipps-Universität Marburg, Marburg,*
682 *Germany and Department of Biology, Philipps-Universität Marburg, Marburg, Germany*
683 Email: anke.becker@synmikro.uni-marburg.de

684 **Authors**

685 **Daniel Stukenberg** - *Center for Synthetic Microbiology, Philipps-Universität Marburg, Marburg,*
686 *Germany and Department of Biology, Philipps-Universität Marburg, Marburg, Germany*

687 **Anna Faber** - *Center for Synthetic Microbiology, Philipps-Universität Marburg, Marburg,*
688 *Germany and Department of Biology, Philipps-Universität Marburg, Marburg, Germany*
689 *Current address: School of Molecular Sciences, The University of Western Australia, Crawley,*
690 *Australia*

691 **Author contributions**

692 D.S., A.F., and A.B. conceived this project. A.F. performed proof-of-concept experiments and D.S.
693 performed all experiments described in this publication. D.S. constructed all strains and plasmids used in
694 this study. D.S. analyzed the data and created all figures. D.S., A.F., and A.B. wrote the manuscript. A.B.
695 supervised the study.

696 **Acknowledgements**

697 This work was funded by the State of Hesse (Germany) through the LOEWE cluster Diffusible signals. D.S.
698 received funding through the International Max Planck Research School for Environmental, Cellular, and
699 Molecular Microbiology (IMPRS-Mic). We thank Prof. Christopher A. Voigt for the Marionette Sensor
700 Collection, which was supplied through Addgene (Addgene Kit #1000000137) and Silvia González Sierra
701 for her assistance with flow cytometry measurements. Furthermore, we thank Reza Rohani and Lucas
702 Coppens for sharing their insights into the metabolism of *V. natriegens*.

References

Calvo-Villamañán, A. *et al.* (2020) 'On-target activity predictions enable improved CRISPR–dCas9 screens in bacteria', *Nucleic acids research*, 48(11), pp. e64–e64. Available at: <https://doi.org/10.1093/nar/gkaa294>.

Ceroni, F. *et al.* (2018) 'Burden-driven feedback control of gene expression', *Nature Methods*, 15(5), pp. 387–393. Available at: <https://doi.org/10.1038/nmeth.4635>.

Cho, S. *et al.* (2018) 'High-Level dCas9 Expression Induces Abnormal Cell Morphology in *Escherichia coli*', *ACS Synthetic Biology*, 7(4), pp. 1085–1094. Available at: <https://doi.org/10.1021/acssynbio.7b00462>.

Coppens, L. *et al.* (2023) '*Vibrio natriegens* genome-scale modeling reveals insights into halophilic adaptations and resource allocation', *Molecular Systems Biology*, 19(4), p. e10523. Available at: <https://doi.org/10.15252/msb.202110523>.

Dalia, T.N. *et al.* (2017) 'Multiplex Genome Editing by Natural Transformation (MuGENT) for Synthetic Biology in *Vibrio natriegens*', *ACS Synthetic Biology*, 6(9), pp. 1650–1655. Available at: <https://doi.org/10.1021/acssynbio.7b00116>.

Eagon, R.G. (1961) 'Generation Time of Less Than 10 Minutes', pp. 1961–1962.

Fontana, J. *et al.* (2018) 'Regulated Expression of sgRNAs Tunes CRISPRi in *E. coli*', *Biotechnology Journal*, 13(9), p. 1800069. Available at: <https://doi.org/10.1002/biot.201800069>.

Fu, Y. *et al.* (2014) 'Improving CRISPR-Cas nuclease specificity using truncated guide RNAs', *Nature biotechnology*, 32(3), pp. 279–284. Available at: <https://doi.org/10.1038/nbt.2808>.

Hawkins, J.S. *et al.* (2020) 'Mismatch-CRISPRi Reveals the Co-varying Expression-Fitness Relationships of Essential Genes in *Escherichia coli* and *Bacillus subtilis*', *Cell Systems*, 11(5), pp. 523-535.e9. Available at: <https://doi.org/10.1016/j.cels.2020.09.009>.

Hoff, J. *et al.* (2020) '*Vibrio natriegens*: an ultrafast-growing marine bacterium as emerging synthetic biology chassis', *Environmental microbiology*, 22(10), pp. 4394–4408. Available at: <https://doi.org/10.1111/1462-2920.15128>.

Hoffart, E. *et al.* (2017) 'High substrate uptake rates empower *Vibrio natriegens* as production host for industrial biotechnology', *Applied and environmental microbiology*, 83(22), pp. 1–10. Available at: <https://doi.org/10.1128/AEM.01614-17>.

Kim, S.K. *et al.* (2017) 'CRISPR interference-guided multiplex repression of endogenous competing pathway genes for redirecting metabolic flux in *Escherichia coli*', *Microbial Cell Factories*, 16(1), p. 188. Available at: <https://doi.org/10.1186/s12934-017-0802-x>.

Lee, H.H. *et al.* (2019) 'Functional genomics of the rapidly replicating bacterium *Vibrio natriegens* by CRISPRi', *Nature Microbiology*, 4(7), pp. 1105–1113. Available at: <https://doi.org/10.1038/s41564-019-0423-8>.

Long, C.P. *et al.* (2017) 'Metabolism of the fast-growing bacterium *Vibrio natriegens* elucidated by (13)C metabolic flux analysis', *Metabolic engineering*, 44, pp. 191–197. Available at: <https://doi.org/10.1016/j.ymben.2017.10.008>.

Meyer, A.J. *et al.* (2019) '*Escherichia coli* "Marionette" strains with 12 highly optimized small-molecule sensors', *Nature Chemical Biology*, 15(2), pp. 196–204. Available at: <https://doi.org/10.1038/s41589-018-0168-3>.

O'Brien, E.J., Utrilla, J. and Palsson, B.O. (2016) 'Quantification and Classification of *E. coli* Proteome Utilization and Unused Protein Costs across Environments', *PLoS Computational Biology*, 12(6), p. e1004998. Available at: <https://doi.org/10.1371/journal.pcbi.1004998>.

Organick, L. *et al.* (2018) 'Random access in large-scale DNA data storage', *Nature biotechnology*, 36(3), pp. 242–248. Available at: <https://doi.org/10.1038/nbt.4079>.

Qi, L.S. *et al.* (2013) 'Repurposing CRISPR as an RNA-Guided Platform for Sequence-Specific Control of Gene Expression', *Cell*, 152(5), pp. 1173–1183. Available at: <https://doi.org/10.1016/j.cell.2013.02.022>.

Sander, T. *et al.* (2019) 'Allosteric Feedback Inhibition Enables Robust Amino Acid Biosynthesis in *E. coli* by Enforcing Enzyme Overabundance', *Cell Systems*, 8(1), pp. 66–75.e8. Available at: <https://doi.org/10.1016/j.cels.2018.12.005>.

Schwinn, M.K. *et al.* (2018) 'CRISPR-Mediated Tagging of Endogenous Proteins with a Luminescent Peptide', *ACS Chemical Biology*, 13(2), pp. 467–474. Available at: <https://doi.org/10.1021/acscchembio.7b00549>.

Stukenberg, D. *et al.* (2021) 'The Marburg Collection: A Golden Gate DNA Assembly Framework for Synthetic Biology Applications in *Vibrio natriegens*', *ACS Synthetic Biology*, 10(8), pp. 1904–1919. Available at: <https://doi.org/10.1021/acssynbio.1c00126>.

Stukenberg, D. *et al.* (2022) 'NT-CRISPR, combining natural transformation and CRISPR-Cas9 counterselection for markerless and scarless genome editing in *Vibrio natriegens*', *Communications Biology*, 5(1), p. 265. Available at: <https://doi.org/10.1038/s42003-022-03150-0>.

Thoma, F. *et al.* (2022) 'Metabolic engineering of *Vibrio natriegens* for anaerobic succinate production', *Microbial Biotechnology*, 15(6), pp. 1671–1684. Available at: <https://doi.org/10.1111/1751-7915.13983>.

Thoma, F. and Blombach, B. (2021) 'Metabolic engineering of *Vibrio natriegens*', *Essays in Biochemistry*. Edited by D. Mattanovich and P. Ivan Nikel, 65(2), pp. 381–392. Available at: <https://doi.org/10.1042/EBC20200135>.

Tian, T. *et al.* (2019) 'Redirecting Metabolic Flux via Combinatorial Multiplex CRISPRi-Mediated Repression for Isopentenol Production in *Escherichia coli*', *ACS Synthetic Biology*, 8(2), pp. 391–402. Available at: <https://doi.org/10.1021/acssynbio.8b00429>.

Tietze, L. *et al.* (2022) 'Identification and Cross-Characterisation of Artificial Promoters and 5' Untranslated Regions in *Vibrio natriegens*', *Frontiers in Bioengineering and Biotechnology*, 10. Available at: <https://www.frontiersin.org/articles/10.3389/fbioe.2022.826142> (Accessed: 13 September 2023).

Tschirhart, T. *et al.* (2019) 'Synthetic Biology Tools for the Fast-Growing Marine Bacterium *Vibrio natriegens*', *ACS Synthetic Biology*, 8(9), pp. 2069–2079. Available at: <https://doi.org/10.1021/acssynbio.9b00176>.

Vigouroux, A. *et al.* (2018) 'Tuning dCas9's ability to block transcription enables robust, noiseless knockdown of bacterial genes', *Molecular systems biology*, 14(3), pp. e7899–e7899. Available at: <https://doi.org/10.15252/msb.20177899>.

Walton, R.T. *et al.* (2020) 'Unconstrained genome targeting with near-PAMless engineered CRISPR-Cas9 variants', *Science*, 368(6488), p. 290 LP – 296. Available at: <https://doi.org/10.1126/science.aba8853>.

Wang, T. *et al.* (2018) 'Pooled CRISPR interference screening enables genome-scale functional genomics study in bacteria with superior performance', *Nature Communications*, 9(1), p. 2475. Available at: <https://doi.org/10.1038/s41467-018-04899-x>.

Wang, Z. *et al.* (2020) 'Melanin produced by the fast-growing marine bacterium *Vibrio natriegens* through heterologous biosynthesis: Characterization and application', *Applied and environmental microbiology*, 86(5), pp. e02749-19. Available at: <https://doi.org/10.1128/AEM.02749-19>.

Warren, D.J. (2011) 'Preparation of highly efficient electrocompetent *Escherichia coli* using glycerol/mannitol density step centrifugation', *Analytical Biochemistry*, 413(2), pp. 206–207. Available at: <https://doi.org/10.1016/j.ab.2011.02.036>.

Weinstock, M.T. *et al.* (2016) '*Vibrio natriegens* as a fast-growing host for molecular biology', *Nature Methods*, 13(10), pp. 849–851. Available at: <https://doi.org/10.1038/nmeth.3970>.

Xu, L. *et al.* (2006) 'Average Gene Length Is Highly Conserved in Prokaryotes and Eukaryotes and Diverges Only Between the Two Kingdoms', *Molecular Biology and Evolution*, 23(6), pp. 1107–1108. Available at: <https://doi.org/10.1093/molbev/msk019>.

Xu, Y. *et al.* (2000) 'Evolution of Arginine Biosynthesis in the Bacterial Domain: Novel Gene-Enzyme Relationships from Psychrophilic *Moritella* Strains (*Vibrionaceae*) and Evolutionary Significance of N- α -Acetyl Ornithinase', *Journal of Bacteriology*, 182(6), pp. 1609–1615. Available at: <https://doi.org/10.1128/jb.182.6.1609-1615.2000>.

Supplementary Material to

graded-CRISPRi, a novel tool for tuning the strengths of CRISPRi-mediated knockdowns in *Vibrio natriegens* using gRNA libraries

Daniel Stukenberg^{1,2}, Anna Faber^{1,2,#}, Anke Becker^{1,2,*}

¹Center for Synthetic Microbiology, Philipps-Universität Marburg, Marburg, Germany

²Department of Biology, Philipps-Universität Marburg, Marburg, Germany

Current address: School of Molecular Sciences, The University of Western Australia, Crawley, Australia

*For correspondence: anke.becker@synmikro.uni-marburg.de

Contents:

Figure S1: Effect of inducer concentrations on repression strength in LBv2

Figure S2: Effect of inducer concentrations on growth rate in LBv2

Figure S3: Inducibility of CRISPRi system and comparison with control constructs in LBv2

Figure S4: Effect of inducer concentrations on mScarlet-I signal with non-binding control gRNA

Figure S5: Analyzing the mScarlet-I signal resulting from different combinations of DHBA and ATc at the single cell level in LBv2

Figure S6: Repression strengths with gRNAs featuring mismatches and different spacer lengths in LBv2

Figure S7: Probability distribution for number of unique variants

Figure S8: Comparing single-cell distribution from mismatched and truncated gRNAs with limiting inducer concentrations

Figure S9: Correlation between Fluc and HiBiT signal

Figure S10: Testing the effect of additional gRNAs on growth rate at different ATc concentrations

Figure S11: Crosstalk between reporter signals

Figure S12: Correlation between reporter signals from a multi gRNA library experiment (Fig. 3c)

Figure S13: Growth curves of HiBiT fusion strains

Figure S14: Growth curves of *argA* and *metE* deletion strains

Table S1: Sequencing results of mScarlet-I gRNA library variants

Table S2: Recipe for buffered M9 minimal medium with 0.4 % (w/w) glucose (M9G)

Table S3: Recipe 5X M9 salts solution

Table S4: Composition of 100X trace elements solution

Table S5: Preparation of 100x trace elements solution

Table S6: Level 1 and level 2 plasmids assembled in this study

Table S7: *V. natriegens* strains with chromosomal modification

Table S8: Recipe for SOC medium

Table S9: gRNA position vectors for assembly of multi gRNA CRISPRi plasmids

Table S10: Protocol for microplate reader measurements without fluorescence measurement

Table S11: Protocol for microplate reader measurements with fluorescence measurement

Supplementary Figures

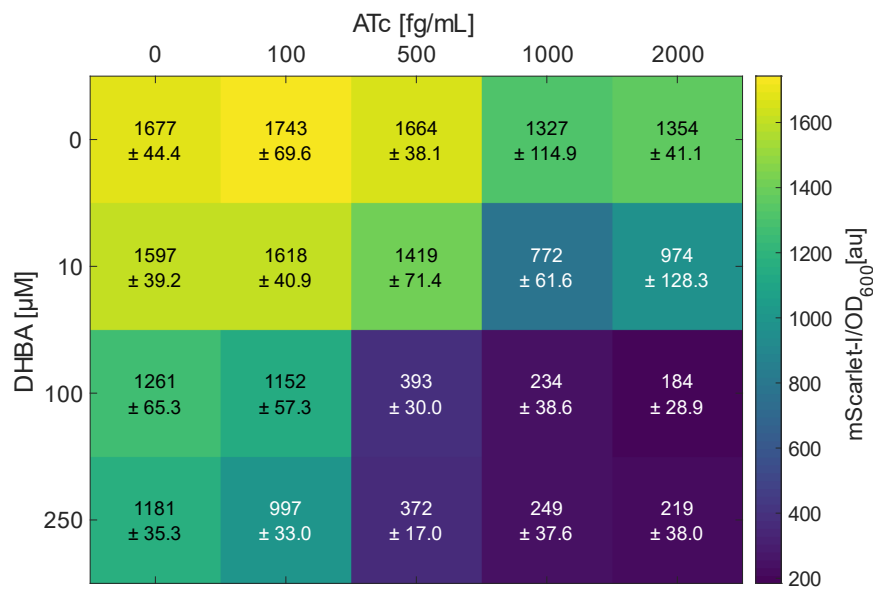


Figure S1: Effect of inducer concentrations on repression strength in LBv2. Colors in the heatmap indicate mScarlet-I fluorescence signal. Embedded text reports the mean mScarlet-I signal, as well as the standard deviation from the mean. This data is based on two independent experiments with three biological replicates. Experiments were performed in LBv2 with CRISPRi plasmid pST_300 and strain DST018.

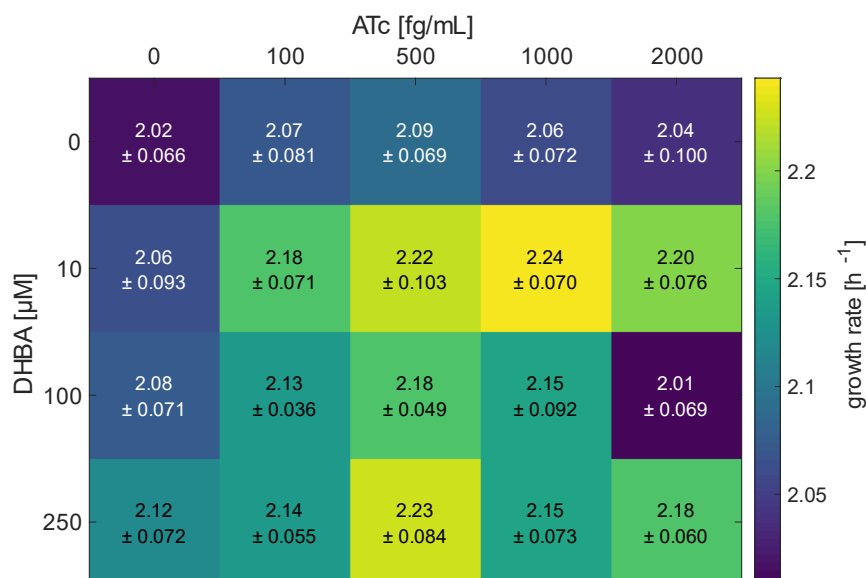


Figure S2: Effect of inducer concentrations on growth rate in LBv2. Colors in the heatmap indicate the growth rate of the cultures of strain DST018 harboring the CRISPRi plasmid pST_300 in LBv2. Embedded text reports the mean growth rate, as well as the standard deviation from the mean. This data is based on two independent experiments with three biological replicates.

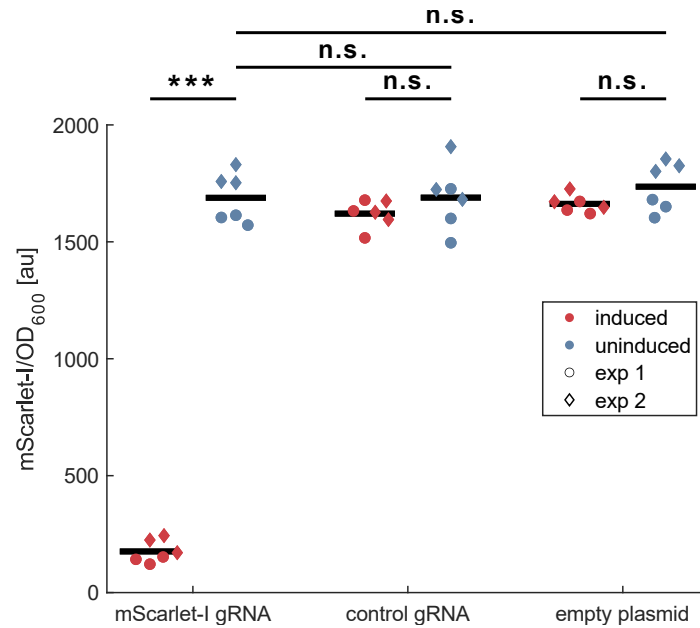


Figure S3: Inducibility of CRISPRi system and comparison with control constructs in LBv2. Induced samples (1000 fg/mL ATc, 100 μ M DHBA) and uninduced samples are shown in red and blue, respectively. Data points from the first independent experiment are shown as circles and data from the second experiment are displayed as diamonds. Control gRNA refers to a gRNA targeting *dns*, which is deleted in this strain. The experiment was performed in LBv2 with the CRISPRi plasmid pST_300 in strain DST018. Significances were calculated with a two-sample t-test. n.s.: $p > 0.05$, *: $p > 0.01$, **: $p > 0.001$, ***: $p < 0.001$.

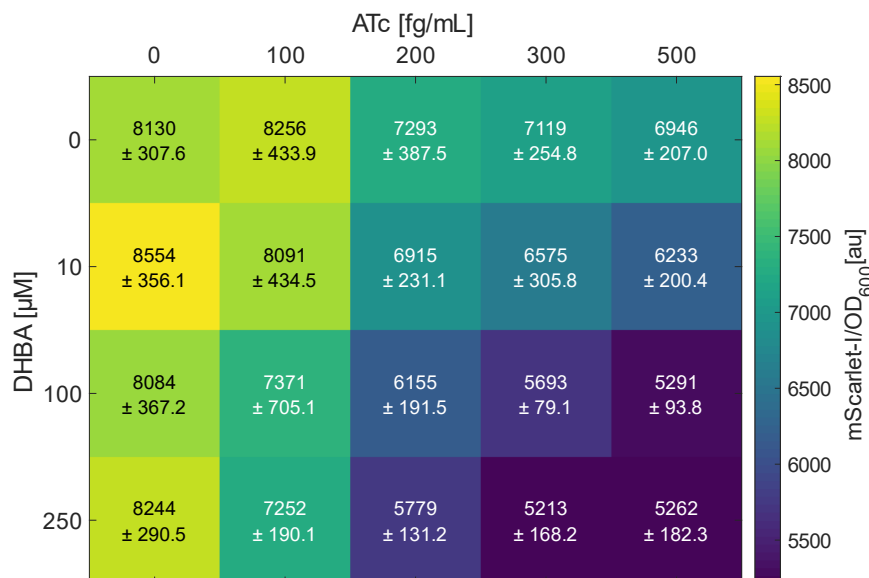


Figure S4: Effect of inducer concentrations on mScarlet-I signal with non-binding control gRNA. Colors in the heatmap indicate mScarlet-I fluorescence signal. Embedded text represents the mean mScarlet-I signal, as well as the standard deviation from the mean. This data is based on two independent experiments with three biological replicates. Experiments were performed in M9G with the CRISPRi plasmid pST_300 and strain DST018. A gRNA targeting *dns* (deleted in this strain) was used.

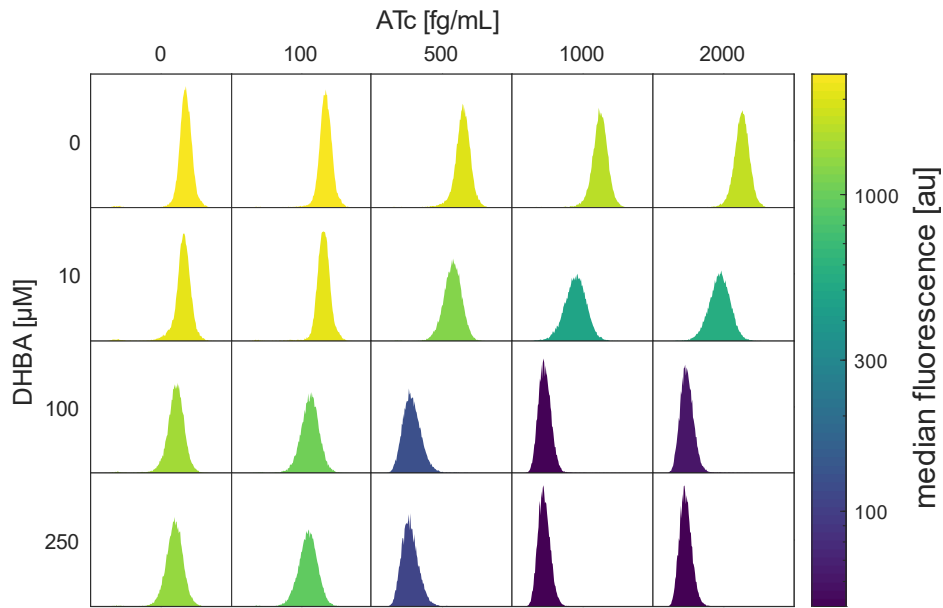


Figure S5: Analyzing the mScarlet-I signal resulting from different combinations of DHBA and ATc at the single cell level in LBv2. Fluorescence was measured with a flow cytometer. Displayed is a representative histogram from six measurements (three biological replicates, and two independent experiments). The color of the histograms represents the median fluorescence. Samples were drawn from cultures grown in LBv2 with the CRISPRi plasmid pST_300 in the strain DST018.

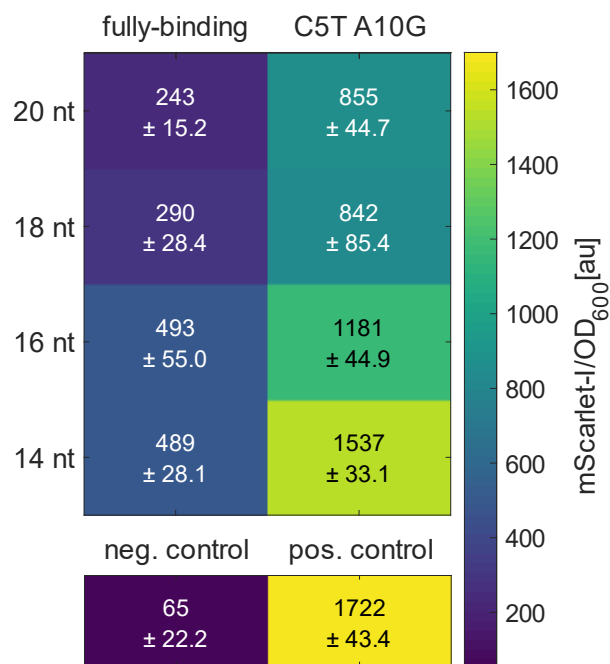


Figure S6: Repression strengths with gRNAs featuring mismatches and different spacer lengths in LBv2. C5T and A10G indicate mismatches to the target sequence and are counted from the PAM proximal nucleotide of the spacer sequence. - strain: strain without integrated mScarlet-I cassette (DST016). + strain: strain integrated mScarlet-I cassette (DST018) with a CRISPRi plasmid with a non-binding control gRNA. Colors in the heatmap indicate mScarlet-I fluorescence signal. Embedded text represents the mean mScarlet-I signal, as well as the standard deviation from the mean. This data is based on two independent experiments with three biological replicates. Experiments were performed in LBv2 with the CRISPRi plasmid pST_300.

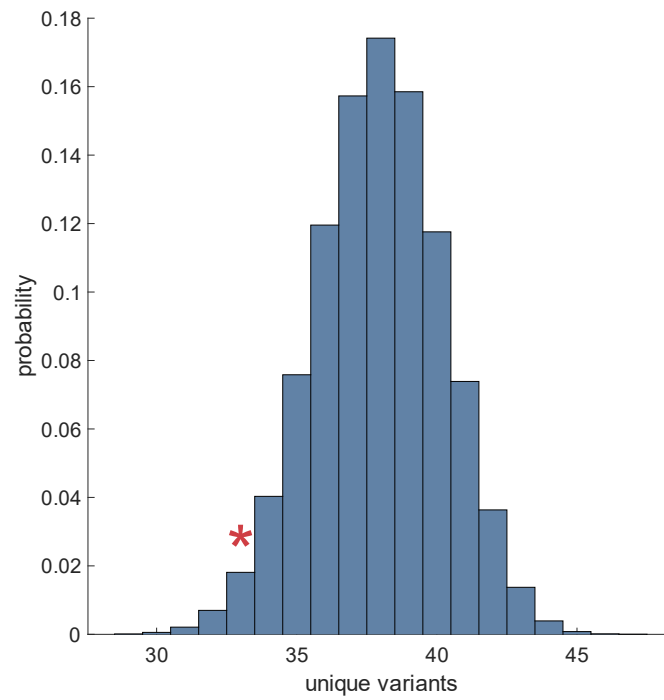


Figure S7: Probability distribution for number of unique variants. Histogram depicting the probability distribution of obtaining a specific number of unique variants when 48 clones are tested from 96 theoretically possible unique variants. The red asterisk indicates the number of unique variants obtained when testing 48 colonies from the gRNA library targeting mScarlet-I.

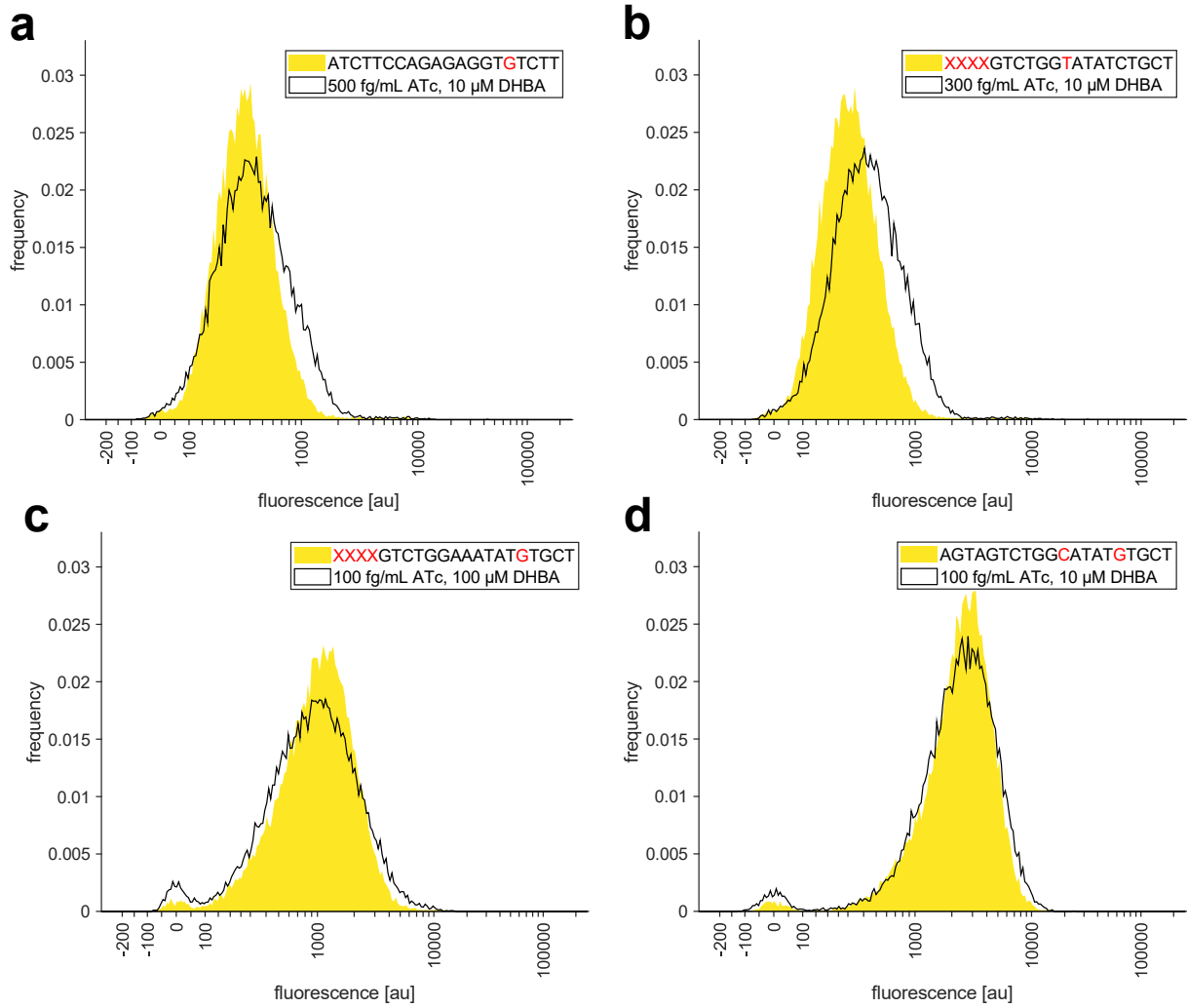


Figure S8: Comparing single-cell distribution from mismatched and truncated gRNAs with limiting inducer concentrations. Filled yellow histograms represent result from fully induced CRISPRi system (200 fg/mL ATc, 100 μ M DHBA) with mismatched and truncated gRNAs. Red letters in the legend indicate mismatches in the gRNA variants. Red “X” letters indicate truncations. Black line represents the outline of a histogram from samples with fully-binding gRNA against mScarlet-I but with limiting inducer concentrations (specified in the legend). Experiments were performed in M9G with the CRISPRi plasmid pST_300 and strain DST018.

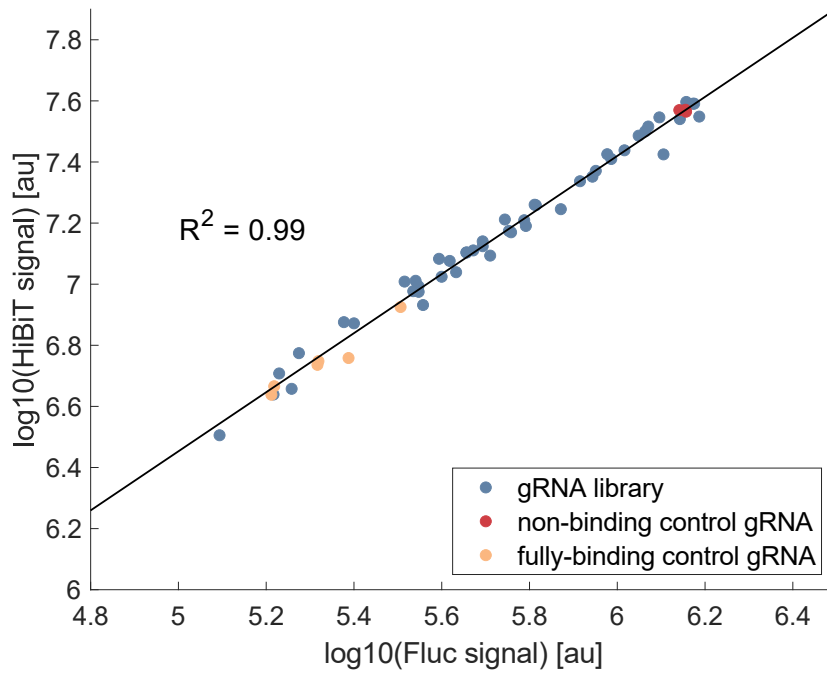


Figure S9: Correlation between Fluc and HiBiT signal. The experiment is based on a gRNA library targeting Fluc in a strain with a chromosomally integrated Fluc-HiBiT expression cassette (DST046). Each data point represents a single measurement from a variant of the gRNA library (blue), the non-binding control gRNA (red) or the fully-binding gRNA (yellow). R^2 is derived from a linear regression of the \log_{10} of the luminescence values from Fluc and HiBiT. Experiments performed in M9G with induction of the CRISPRi system (200 fg/mL ATc, 100 μ M DHBA).

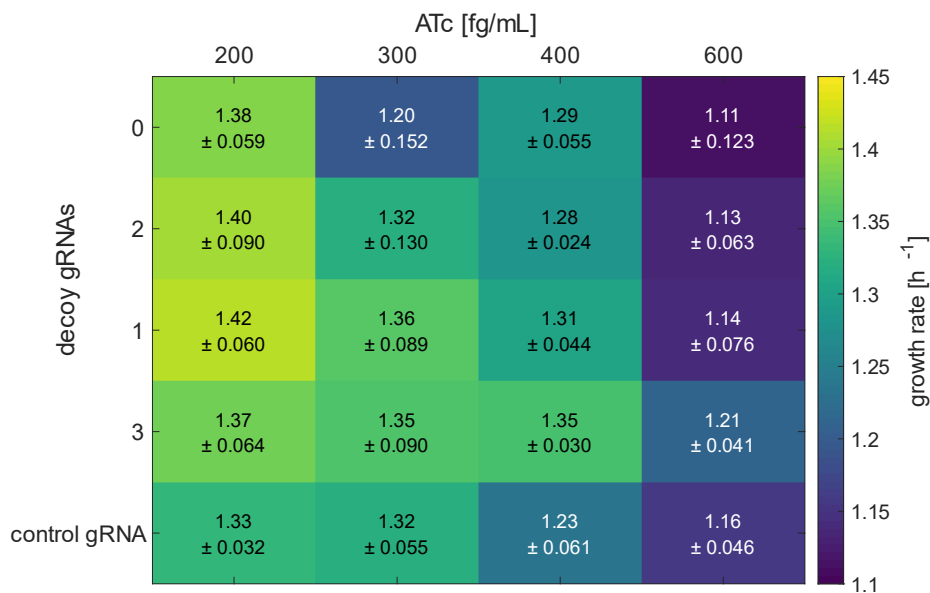


Figure S10: Testing the effect of additional gRNAs on growth rate at different ATc concentrations. CRISPRi plasmids encoding a gRNA targeting mScarlet-I and up to three decoy gRNAs (targeting *dns* = non-binding gRNA) were tested at different ATc concentrations and the same DHBA concentration (100 μ M). Colors in the heatmap indicate the growth rate of the cultures. Embedded text represents the mean growth rate, as well as the standard deviation from the mean. This data is based on two independent experiments with three biological replicates. Experiments were performed in M9G in strain DST018.

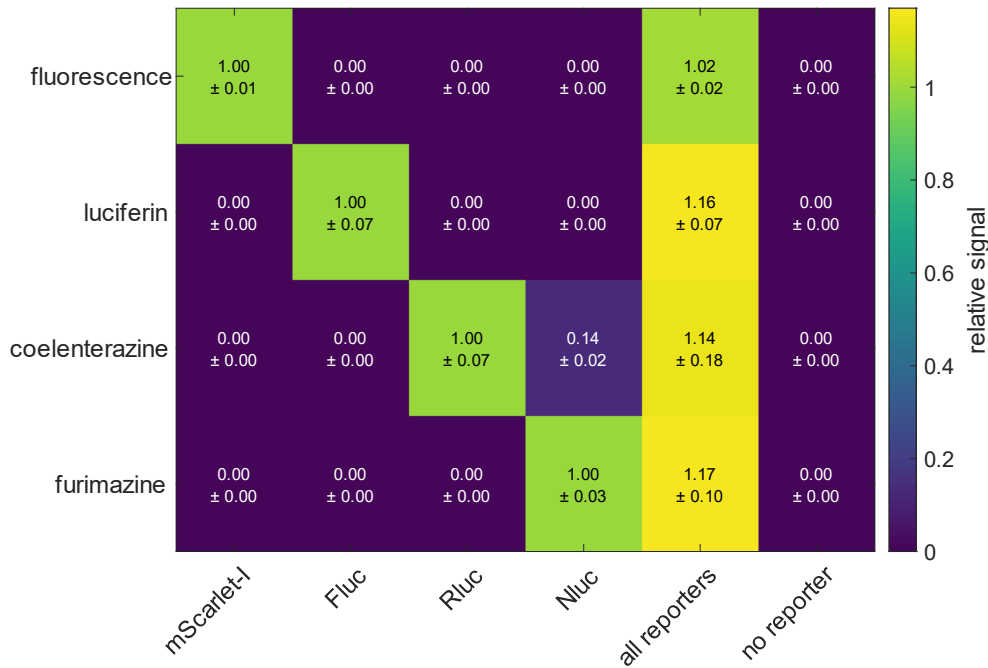


Figure S11: Crosstalk between reporter signals. Strains encoding one of the reporter proteins mScarlet-I, Fluc, Rluc, Nluc, a strain with all four reporter genes and a strain without any reporter gene were tested. The heatmap shows the mean signal from three biological replicates, relative to the respective single reporter strain, from either fluorescence or the respective luciferase substrates (see methods chapter). Embedded text reports the mean relative signal, as well as the standard deviation from the mean. This data is derived from three biological replicates and the samples were obtained from cultures grown in M9G.

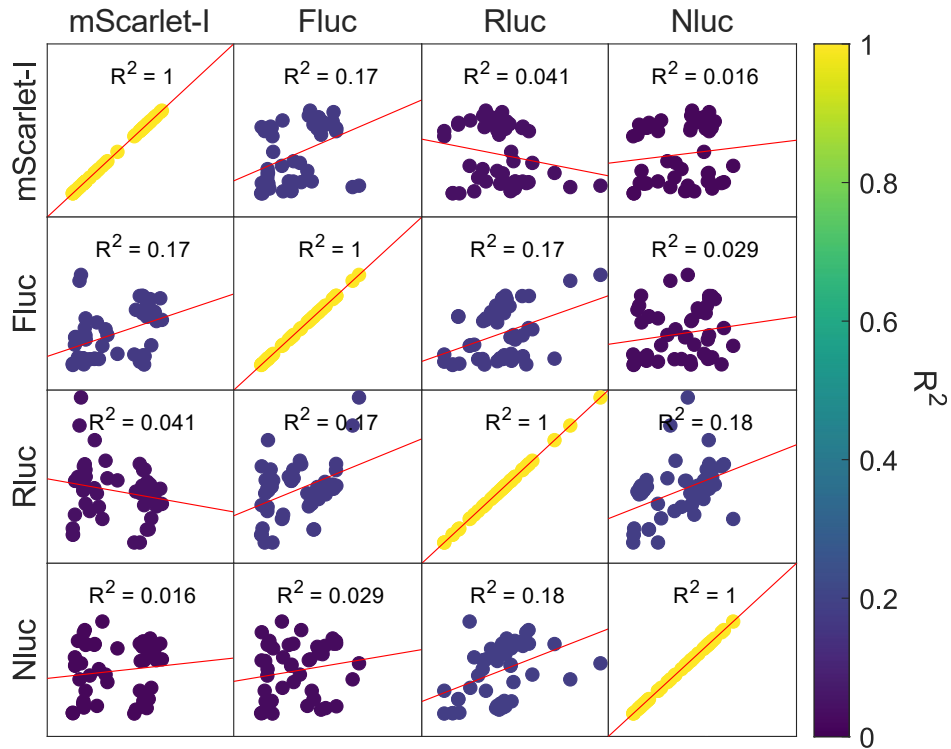


Figure S12: Correlation between reporter signals from a multi gRNA library experiment (Fig. 3c). Relative signals from the respective reporter genes are shown as a scatter plot. Dots are colored according to the R^2 value obtained from a linear regression between the relative signals of both reporters.

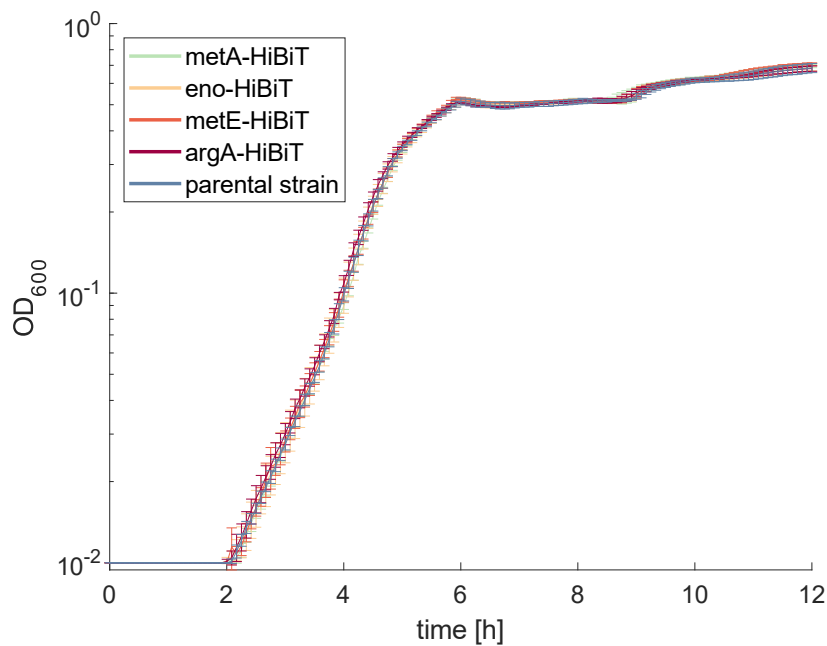


Figure S13: Growth curves of HiBiT fusion strains. Growth of strains with fusion of HiBiT sequence to native genes in comparison to the parental strain (DST016). The lines reflect the mean from three biological replicates and error bars indicate standard deviation from the mean. The experiment was performed in M9G.

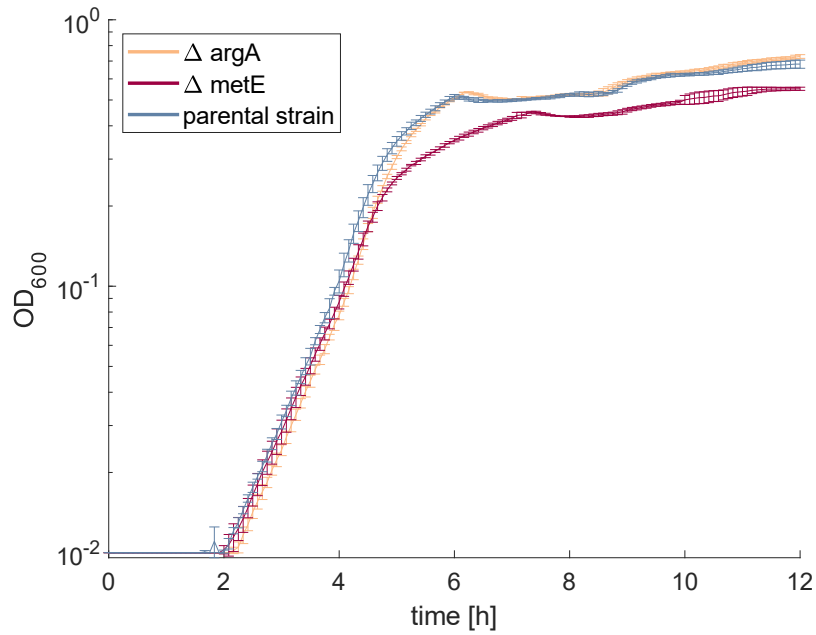


Figure S14: Growth curves of *argA* and *metE* deletion strains. Growth of strains deletion of *argA* and *metE* in comparison to the parental strain (DST016). The lines reflect the mean from three biological replicates and error bars indicate the standard deviation from the mean. The experiment was performed in M9G.

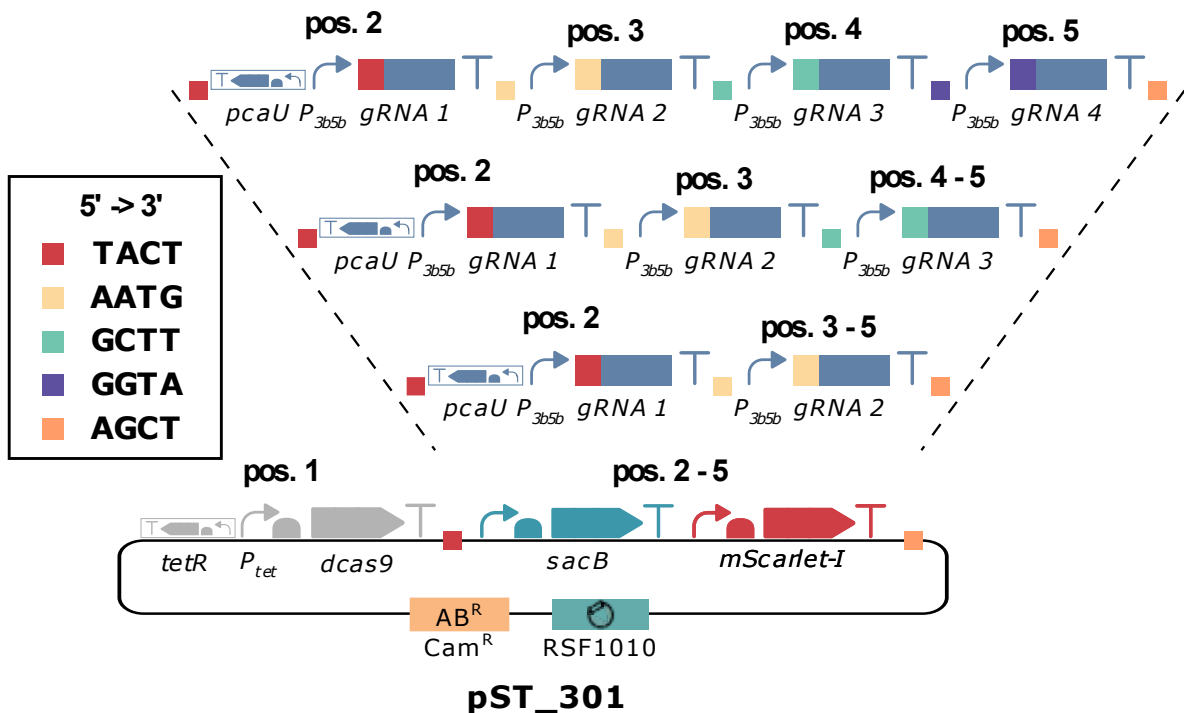


Figure S15: Assembly scheme for CRISPRi plasmids with multiple gRNAs. pST_301 carries a *sacB*-*mScarlet-I* dropout part, which is replaced with the respective gRNA expression cassettes. Different gRNA position vectors are used, depending on the number of desired gRNAs in the final construct.

Supplementary Tables

Table S1: Sequencing results of mScarlet-I gRNA library variants.

Clone	gRNA	length	mismatch
1	1	14	A10C
2	1	16	C5G
3	1	20	C5G, A10C
4	2	20	A5G
5	1	16	C5A, A10G
6	1	14	C5G, A10T
7	1	16	C5A, A10G
8	1	20	C5A, A10G
9	1	20	A10C
10	2	20	A5T, G10T
11	2	20	none
12	2	20	A5G, G10T
13	1	16	A5G, A10G
14	1	20	C5G, A10C
15	2	20	A5T, G10A
16	1	14	C5T, A10G
17	2	16	A5C, G10T
18	1	20	none
19	2	20	A5T, G10C
20	1	14	A10C
21	1	16	C5G, A10C
22	1	16	C5T, A10G
23	2	20	A5T, G10T
24	1	16	A10C
25	1	16	A10T
26	2	20	G10A
27	1	20	C5T
28	1	14	A10G
29	2	20	A5T, G10A
30	2	14	A5T, G10T
31	2	14	A5T
32	1	16	A10C
33	2	16	A5C
34	2	20	A5G, G10A
35	1	16	A10C
36	2	16	A5T
37	2	14	A5T
39	2	20	A5T, G10A
40	1	14	C5G, A10G
41	1	16	C5T, A10G
43	1	20	C5A, A10G
44	1	20	none
45	2	20	A5G, G10A

46	1	20	A10T
47	1	14	A10G
48	1	20	none
49	2	16	A5C, G10C
50	2	14	A5G, G10T

Table S2: Recipe for buffered M9 minimal medium with 0.4 % (w/w) glucose (M9G).

Component	Volume
NaCl solution (20% w/w)	5 mL
5X M9 salts solution	10 mL
Glucose solution (20% w/w)	1 mL
100X trace elements solution	500 μ L
H ₂ O	Add up to 50 mL
MgSO ₄ (1 M)	50 μ L
CaCl ₂ (1M)	15 μ L
K ₂ HPO ₄ (1 M)	2.5 mL
KH ₂ PO ₄ (1 M)	2.5 mL

Table S3: Recipe 5X M9 salts solution.

Component	Concentration
KH ₂ PO ₄	15 g/L
Na ₂ HPO ₄ + 7 H ₂ O	64 g/L
NaCl	2.5 g/L
NH ₄ Cl	5 g/L

Table S4: Composition of 100X trace elements solution.

Component	Concentration
EDTA	5 g /L
FeCl ₃ + 6H ₂ O	830 mg/L
ZnCl ₂	84 mg/L
CuCl ₂ + 2H ₂ O	13 mg/L
CoCl ₂ + 2H ₂ O	10 mg/L
H ₃ BO ₃	10 mg/L
MnCl ₂ + 4H ₂ O	1.6 mg/L

Table S5: Preparation of 100x trace elements solution. Dissolve 5 g EDTA in 800 mL water and adjust the pH to 7.5 with NaOH. Stock solutions for all other components were prepared, filter sterilized and added in the amounts described below. Add water to 1 L and filter sterilize.

Component	Stock concentration	Quantity for 1 L
FeCl ₃ + 6H ₂ O		830 mg
ZnCl ₂		84 mg
CuCl ₂ + 2H ₂ O	1.7 g / 100 mL	765 μ L
CoCl ₂ + 2H ₂ O	4.76 g / 100 mL	210 μ L
H ₃ BO ₃	0.62 g / 100 mL	1.6 mL
MnCl ₂ + 4H ₂ O	19.8 g / 100 mL	8.1 μ L

Table S6: Level 1 and level 2 plasmids assembled in this study. Assembly was done within the framework of the Marburg Collection (Stukenberg *et al.*, 2021). Plasmid maps are provided in Supplementary Data 1.

Plasmid name	Description
pST_236	Level 1 plasmid with dCas9 transcription unit for construction of pST_300 and pST_301, Promoter: P _{tet} , RBS: B0029, CDS: dCas9, degradation tag: M0050, terminator: B0015
pST_237	Level 1 plasmid, mScarlet-I-HiBiT transcription unit, used as PCR template for preparation of tDNA
pST_240	Empty plasmid as control
pST_300	CRISPRi plasmid for single gRNAs
pST_301	CRISPRi plasmid for multiple gRNAs
pST_302	Level 1 plasmid, Fluc-HiBiT transcription unit, used as PCR template for preparation of tDNA
pST_303	Level 1 plasmid, Rluc-HiBiT transcription unit, used as PCR template for preparation of tDNA
pST_310	Level 1 plasmid, Nluc-HiBiT transcription unit, used as PCR template for preparation of tDNA

Table S7: *V. natriegens* strains with chromosomal modification

Strain	Genotype	Parental strain
DST016	Δ dns	<i>V. natriegens</i> ATCC14048
DST018	Δ dns, int9::mScarlet-I-HiBiT	DST016
DST023	Δ dns, argA-HiBiT	DST016
DST024	Δ dns, metA-HiBiT	DST016
DST025	Δ dns, eno-HiBiT	DST016
DST046	Δ dns, int12::Fluc-HiBiT	DST016
DST047	Δ dns, int14::Rluc-HiBiT	DST016
DST048	Δ dns, int9::mScarlet-HiBiT, int12::Fluc-HiBiT	DST018
DST049	Δ dns, int9::mScarlet-HiBiT, int12::Fluc-HiBiT, int14::Rluc-HiBiT	DST048
DST050	Δ dns, int9::mScarlet-HiBiT, int12::Fluc-HiBiT, int14::Rluc-HiBiT, int18::Nluc-HiBiT	DST049
DST051	Δ dns, int18::Nluc-HiBiT	DST016
DST052	Δ dns, Δ argA	DST016
DST053	Δ dns, Δ metE	DST016

Table S8: Recipe for SOC medium

Component	Concentration
Tryptone	20 g/L
Yeast extract	5 g/L
NaCl	0.58 g/L
H ₂ O	Ad ~ 900 mL
Autoclave	
MgSO ₄ (1 M)	10 mL
MgCl ₂ (1 M)	10 mL
Glucose (2 M)	10 mL
H ₂ O	Ad 1 L

Table S9: gRNA position vectors for assembly of multi gRNA CRISPRi plasmids. Position of these gRNA cassettes according to the nomenclature of the Marburg Collection (Stukenberg *et al.*, 2021). Scheme for the assembly of multi gRNA CRISPRi plasmids is shown in Figure S15. Plasmid maps are provided in Supplementary Data 1.

Plasmid name	Description
pMCO*_gRNA_Pos2_P _{3b5b} _pcaU (sacB-sfGFP)	Position 2, carries expression cassette for repressor <i>pcaU</i> , dropout <i>sacB-sfGFP</i> which is replaced by gRNA spacer
pMCO*_gRNA_Pos3_P _{3b5b} (sacB-sfGFP)	Position 3, dropout <i>sacB-sfGFP</i> which is replaced by gRNA spacer
pMCO*_gRNA_Pos4_P _{3b5b} (sacB-sfGFP)	Position 4, dropout <i>sacB-sfGFP</i> which is replaced by gRNA -spacer
pMCO*_gRNA_Pos5_P _{3b5b} (sacB-sfGFP)	Position 5, dropout <i>sacB-sfGFP</i> which is replaced by gRNA spacer
pMCO*_gRNA_Pos3-5_P _{3b5b} (sacB-sfGFP)	Position 3-5, dropout <i>sacB-sfGFP</i> which is replaced by gRNA spacer
pMCO*_gRNA_Pos4-5_P _{3b5b} (sacB-sfGFP)	Position 4-5, dropout <i>sacB-sfGFP</i> which is replaced by gRNA spacer

Table S10: Protocol for microplate reader measurements without fluorescence measurement

Temperature	37°C
Kinetic duration	5 min
Shaking (orbital) duration	120 s
Shaking (orbital) amplitude	2 mm
Shaking (linear) duration	120 s
Shaking (linear) amplitude	2 mm
Absorbance measurement	
Measurement wavelength	595 nm
Bandwidth	10 nm
Number of flashes	5
Settle time	10 ms

Table S11: Protocol for microplate reader measurements with fluorescence measurement

Temperature	37°C
Kinetic duration	5 min
Shaking (orbital) duration	100 s
Shaking (orbital) amplitude	2 mm
Shaking (linear) duration	100 s
Shaking (linear) amplitude	2 mm
Absorbance measurement	
Measurement wavelength	595 nm
Bandwidth	10 nm
Number of flashes	5
Settle time	10 ms
Fluorescence measurement	
Excitation wavelength	560 nm
Emission wavelength	610 nm
Excitation bandwidth	20 nm
Emission bandwidth	20 nm
Gain	50
Number of flashes	5
Integration time	20 μ s
Lag time	0 μ s
Settle time	10 ms
Mirror (automatic)	50% mirror

Supplementary Table S12: Oligonucleotides used to assemble gRNA sequences for NT-CRISPR. All sequences written as 5' -> 3'.

Modification	forward oligonucleotide		reverse oligonucleotide		NT-CRISPR plasmid
int9::mScarlet-I-HiBiT	oDS_473	GTCCAGTCGCTTATGGCGTGAAAG	oDS_474	AAACCTTTCACGCCATAAGCGACT	pST_116
int12::Fluc-HiBiT	oDS_484	GTCCTGCGTAAGCGAAGTTCGCTT	oDS_640	AAACAAGCGAACTTCGCTTACGCA	pST_116
int14::Rluc-HiBiT	oDS_1796	GTCCGTAGGGTTAATTATAATGAT	oDS_1797	AAACATCATTATAATTAACCCTAC	pST_116
int18::Nluc-HiBiT	oDS_1800	GTCCATAACATTTGATTATATAAA	oDS_1801	AAACTTTATAAATCGAAATGTTAT	pST_116
argA-HiBiT	oDS_978	GTCCTCTTAGCTTTAGATTTATAA	oDS_979	AAACTTATAAATCTAAAGCTAAGA	pST_140
metE-HiBiT	oDS_998	GTCCACTGAGCTAGCATAAACAGC	oDS_999	AAACGCTGTTTATGCTAGCTCAGT	pST_140
eno-HiBiT	oDS_1196	GTCCGGCCAAGCTTAATTCTTAAT	oDS_1197	AAACATTAAGAATTAAGCTTGGCC	pST_140
metA-HiBiT	oDS_994	GTCCTAAAGATGACTAATCCAATG	oDS_995	AAACCATTGGATTAGTCATCTTTA	pST_140
Δ argA	oDS_1146	GTCCTCACCATCATCGAAAAAGAT	oDS_1147	AAACATCTTTTTCGATGATGGTGA	pST_116
Δ metE	oDS_1154	GTCCTGAAATCATTGATTCAGTTG	oDS_1155	AAACCAACTGAATCAATGATTTCA	pST_116

Supplementary Table S13: Oligonucleotides used for the construction of tDNA template plasmids and tDNAs. All sequences written as 5' -> 3'. tDNAs for integration of Fluc, Rluc and Nluc (indicated with *) were created directly by fusion PCR

tDNA	forward oligonucleotide	reverse oligonucleotide	PCR template
tDNA int9::mScarlet-HiBit	oDS_461 TTTGTTTCGCCAGAGTATGGAG	oDS_462 CGTCTTTTTCGTTTTGGTCTGTAAAGGGGCACGTTTTCTATTCTTTAAC	V. natriegens DNA
	oDS_463 GCCTTTCTGCGTTTATACGCTTACTACGCCATAAGCGACTAAGAAAC	oDS_464 CTCCATGTTTATGTCTAACACGG	V. natriegens DNA
	oDS_466 TGCCGTGTAGACATAAACATGGAGTAGTACGGCCGCTGCACTC	oDS_465 ACACTCCATACTCTGGCGAAACAAAGGCCGCAATTCAGAAATC	pST_237
	oDS_467 AACAGGACCAAAACGAAAAAGACG	oDS_468 AGTAAGCGTATAAACGCAGAAAGG	pMC_V_11
tDNA int12::Fluc-HiBit*	oDS_475 TCACGCTAACTTTGTTTTGTTGATG	oDS_476 CGTCTTTTTCGTTTTGGTCTGTCTTTGGTTAGCAAACCTCTATGATT	V. natriegens DNA
	oDS_477 GCCTTTCTGCGTTTATACGCTTACTCGAACTTCGCTTACGCACTATT	oDS_478 AATTTAAGTTGTTTGGCTTACTGATCAG	V. natriegens DNA
	oDS_467 AACAGGACCAAAACGAAAAAGACG	oDS_468 AGTAAGCGTATAAACGCAGAAAGG	pST_302
tDNA int14::Rluc-HiBit*	oDS_1810 GATGAAGTTGGTGAAGAGATATC	oDS_1811 CGTCTTTTTCGTTTTGGTCTGTAAATTAACCTACCAAGTACTATGG	V. natriegens DNA
	oDS_1812 GCCTTTCTGCGTTTATACGCTTACTATAATGATAGGTTAACGTATAATAGG	oDS_1813 GTGCTTATAATATCGATGGAAAGG	V. natriegens DNA
	oDS_467 AACAGGACCAAAACGAAAAAGACG	oDS_468 AGTAAGCGTATAAACGCAGAAAGG	pST_303
tDNA int18::Nluc-HiBit*	oDS_1820 CGTCTTTTTCGTTTTGGTCTGTTCGAAATGTTATCAGAACTAGTTTTGG	oDS_1821 GCCTTTCTGCGTTTATACGCTTACTTTATAAACGGTATGTTGTTGTGTTTTTC	V. natriegens DNA
	oDS_1822 GGCAAAGACATCACAATACTGG	oDS_1823 CAAACAGAGAGACGATTAATCACTGTGGCCGCAATTCAGAAATC	V. natriegens DNA
	oDS_467 AACAGGACCAAAACGAAAAAGACG	oDS_468 AGTAAGCGTATAAACGCAGAAAGG	pST_310
tDNA template argA-HiBit	oDS_1200 TGACGAGCAAGACGAAGAGG	oDS_1201 GTTTCTGGTTGGCGTTTATTTAAGAAAATTTCTTAAAGATTAAGAAAGACCGAGTGCATAC	V. natriegens DNA
	oDS_1202 TCTTAAATAAACGCCAACCCAGAACACCAGAGCCTAAATCTAAAGCTAAGATTTTTGATTTGC	oDS_1203 CCATTGGTAACAGTGAATGC	V. natriegens DNA
	oDS_1204 CAAATCCTCTTCGCTTCTGCTCGTCACTCATCGCTCTAGAAGCG	oDS_1205 GCGGGCATTCCACTGTACCAATGGCACTCATCGCGACTAGTAGC	pMC_V_01
tDNA template metA-HiBit	oDS_1236 ATCACGGAGTTTCATTTCCATTTTC	oDS_1237 GTTCTGTTGGCGTTTATTTAAGAAAATTTCTTAAATCAATGCGTTAACTTTGTGAAC	V. natriegens DNA
	oDS_1238 TCTTAAATAAACGCCAACCCAGAACACCAGAGCCGTCATCTTAGTGAAAGCAGACTC	oDS_1239 GATTCATAACTCATCGCAGG	V. natriegens DNA
	oDS_1240 CGAAATGAAATGAAACTCCGTGATCACTCATCGCTCTAGAAGCG	oDS_1241 AATCCCTGCGATGAGTTAGTGAATCCACTCATCGCGACTAGTAGC	pMC_V_01
tDNA template metE-HiBit	oDS_1245 ACGCGGCTGAATATCCGAAG	oDS_1246 TCTTAAATAAACGCCAACCCAGAACACCAGAGCCTGCTAGCTCAGTACGTAGCTTTTTTC	V. natriegens DNA
	oDS_1247 GTTCTGTTGGCGTTTATTTAAGAAAATTTCTTAAACAGCAGTTAAGAAAAGCAGG	oDS_1248 GAACATGGAAGCAGTGCAAAA	V. natriegens DNA
	oDS_1249 TATTACTCGGATATTCAGCCGCTCACTCATCGCTCTAGAAGCG	oDS_1250 CGTCTTTGCACTGCTTCCATGTTCCACTCATCGCGACTAGTAGC	pMC_V_01
tDNA template eno-HiBit	oDS_1254 GTTACTGGCGGGTTGTATC	oDS_1255 TCTTAAATAAACGCCAACCCAGAACACCAGAGCCAGCTTGGCCTTTAACTCTTTAAG	V. natriegens DNA
	oDS_1256 GTTCTGTTGGCGTTTATTTAAGAAAATTTCTTAAATCTTAAATGAATAAAGTTAGCTAAATAGC	oDS_1257 ACTAACTCACGAACAATGGATGATG	V. natriegens DNA
	oDS_1258 GAGAGGATACAAACCCGCGAGTAACCACTCATCGCTCTAGAAGCG	oDS_1259 CTACATCCATTGTTCTGTGAGTTAGTCACTCATCGCGACTAGTAGC	pMC_V_01
tDNA template ΔargA	oDS_1200 TGACGAGCAAGACGAAGAGG	oDS_1890 GGAATGGCTGAAGATTAAGAAAGACCGAGTGCATAC	V. natriegens DNA
	oDS_1891 GTCTTTTTAATCTTACAGCCATTCTTGTGTTTATTTATGC	oDS_1892 AACTTGGCGGTAGCGATCTTC	V. natriegens DNA
	oDS_1893 CTGGGAAGATCGCTACCGCAAGTTAGTAGCGGCCGCTGCACTC	oDS_1204 CAAATCCTCTTCGCTTCTGCTCGTCACTCATCGCTCTAGAAGCG	pMC_V_11
tDNA template ΔmetE	oDS_1894 TGATCTCGGTTATCGAAGATCTG	oDS_1895 TTTAACTGCTGTTCCCTAGTCTTATTATTAGTTTATTTTGG	V. natriegens DNA
	oDS_1896 AAGGACTAGGGAAACAGCAGTTAAGAAAAGCAGG	oDS_1248 GAACATGGAAGCAGTGCAAAA	V. natriegens DNA
	oDS_1250 CGTCTTTGCACTGCTTCCATGTTCCACTCATCGCGACTAGTAGC	oDS_1897 TCCAGATCTCGATAACCGAGATCAGGCCGCAATTCAGAAATC	pMC_V_11

Supplementary Table S14: Oligonucleotides used to assemble gRNA sequences for CRISPRi. All sequences written as 5' -> 3'.

CRISPRi gRNA	forward oligonucleotide		reverse oligonucleotide	
mScarlet-I gRNA 1	oDS_231	GTCCAGTAGTCTGGAATATCTGCT	oDS_232	AAACAGCAGATATTCCAGACTACT
mScarlet-I gRNA 2	oDS_1422	GTCCATCTTCCAGAGAGGTATCTT	oDS_1423	AAACAAGATACCTCTCTGGAAGAT
mScarlet-I gRNA 1 18 nt	oDS_1510	GTCCTAGTCTGGAATATCTGCT	oDS_1511	AAACAGCAGATATTCCAGACTA
mScarlet-I gRNA 1 16 nt	oDS_1512	GTCCGTCTGGAATATCTGCT	oDS_1513	AAACAGCAGATATTCCAGAC
mScarlet-I gRNA 1 14 nt	oDS_1514	GTCCCTGGAATATCTGCT	oDS_1515	AAACAGCAGATATTCCAG
mScarlet-I gRNA 1 C5T A10G 20 nt	oDS_1516	GTCCAGTAGTCTGGGATATTTGCT	oDS_1517	AAACAGCAAATATCCCAGACTACT
mScarlet-I gRNA 1 C5T A10G 18 nt	oDS_1518	GTCCTAGTCTGGGATATTTGCT	oDS_1519	AAACAGCAAATATCCCAGACTA
mScarlet-I gRNA 1 C5T A10G 16 nt	oDS_1520	GTCCGTCTGGGATATTTGCT	oDS_1521	AAACAGCAAATATCCCAGAC
mScarlet-I gRNA 1 C5T A10G 14 nt	oDS_1522	GTCCCTGGGATATTTGCT	oDS_1523	AAACAGCAAATATCCCAG
metA gRNA 1	oDS_1068	GTCCCGGTAGGCGTATTTTTACTC	oDS_1069	AAACGAGTAAAAATACGCCTACCG
metA gRNA 2	oDS_1070	GTCCAATTCGACATTGACTTGCAA	oDS_1071	AAACTTGCAAGTCAATGTGCAATT
eno gRNA 1	oDS_1124	GTCCCCGTTGATGATGTTTCATCAT	oDS_1125	AAACATGATGAACATCATCAACGG
eno gRNA 2	oDS_1126	GTCCAGAGGCATTGAGAATTGACC	oDS_1127	AAACGGTCAATTCTCAATGCCTCT
metE gRNA 1	oDS_1076	GTCCATCATACCAGGCAAAGTCGC	oDS_1077	AAACGCGACTTTGCCTGGTATGAT
metE gRNA 2	oDS_1078	GTCCGTATCGTCTTTGCTAAATTC	oDS_1079	AAACGAATTTAGCAAAGACGATAC
argA gRNA 1	oDS_1036	GTCCAAGCTTCTTCATCAGTAATT	oDS_1037	AAACAATTACTGATGAAGAAGCTT
argA gRNA 2	oDS_1038	GTCCCAGCCATAGGTGTATTGTTC	oDS_1039	AAACGAACAATACACCTATGGCTG
Fluc gRNA 1	oDS_1772	GTCCATAAATAACGCGCCCAACAC	oDS_1773	AAACGTGTTGGGCGCGTTATTTAT
Fluc gRNA 2	oDS_1774	GTCCAAATCGTATTCATTAACCC	oDS_1775	AAACGGTTTTAATGAATACGATTT
Rluc gRNA 1	oDS_1778	GTCCGGTATAATACACCGCGCTAC	oDS_1779	AAACGTAGCGCGGTGTATTATACC
Rluc gRNA 2	oDS_1782	GTCCATCATCCGTTTCCTTTGTTC	oDS_1783	AAACGAACAAAGGAAACGGATGAT
Nluc gRNA 1	oDS_1804	GTCCCACCACCTTGTCTAAAAC	oDS_1805	AAACAGTTTTAGAACAAAGGTGGTG
Nluc gRNA 3	oDS_1808	GTCCCTTAATACGATACGTTGAAT	oDS_1809	AAACATTCAACGTATCGTATTAAG

Supplementary Table S15: ssDNA templates for the generation of gRNA libraries. All sequences written as 5' -> 3'.

Target	ssDNA template		Description
mScarlet-I	oDS_949	AAGGCAAGTTGTTACCAGCAGGTCTCTGTCCAGTAGTCTGGNATATNTGCTGTTTAGAGACCTTGGTTTGATTACGGTCGCA	gRNA 1, 5N 10N, 20 nt
	oDS_1524	AAGGCAAGTTGTTACCAGCAGGTCTCTGTCCGTCTGGNATATNTGCTGTTTAGAGACCTTGGTTTGATTACGGTCGCA	gRNA 1, 5N 10N, 16 nt
	oDS_1525	AAGGCAAGTTGTTACCAGCAGGTCTCTGTCCCTGGNATATNTGCTGTTTAGAGACCTTGGTTTGATTACGGTCGCA	gRNA 1, 5N 10N, 14 nt
	oDS_1424	AAGGCAAGTTGTTACCAGCAGGTCTCTGTCCATCTCCAGANAGGTNTCTTGTGTTAGAGACCTTGGTTTGATTACGGTCGCA	gRNA 2, 5N 10N, 20 nt
	oDS_1526	AAGGCAAGTTGTTACCAGCAGGTCTCTGTCCCTCCAGANAGGTNTCTTGTGTTAGAGACCTTGGTTTGATTACGGTCGCA	gRNA 2, 5N 10N, 16 nt
	oDS_1527	AAGGCAAGTTGTTACCAGCAGGTCTCTGTCCAGANAGGTNTCTTGTGTTAGAGACCTTGGTTTGATTACGGTCGCA	gRNA 2, 5N 10N, 14 nt
metA	oDS_1470	AAGGCAAGTTGTTACCAGCAGGTCTCTGTCCCGTAGGCGTNTTTNACTCGTTTAGAGACCTTGGTTTGATTACGGTCGCA	gRNA 1, 5N 10N, 20 nt
	oDS_1533	AAGGCAAGTTGTTACCAGCAGGTCTCTGTCCAGGCGTNTTTNACTCGTTTAGAGACCTTGGTTTGATTACGGTCGCA	gRNA 1, 5N 10N, 16 nt
	oDS_1534	AAGGCAAGTTGTTACCAGCAGGTCTCTGTCCGCGTNTTTNACTCGTTTAGAGACCTTGGTTTGATTACGGTCGCA	gRNA 1, 5N 10N, 14 nt
	oDS_1535	AAGGCAAGTTGTTACCAGCAGGTCTCTGTCCAATTCGACATNGACTNGCAAGTTTAGAGACCTTGGTTTGATTACGGTCGCA	gRNA 2, 5N 10N, 20 nt
	oDS_1536	AAGGCAAGTTGTTACCAGCAGGTCTCTGTCCGACATNGACTNGCAAGTTTAGAGACCTTGGTTTGATTACGGTCGCA	gRNA 2, 5N 10N, 16 nt
	oDS_1537	AAGGCAAGTTGTTACCAGCAGGTCTCTGTCCACATNGACTNGCAAGTTTAGAGACCTTGGTTTGATTACGGTCGCA	gRNA 2, 5N 10N, 14 nt
eno	oDS_1472	AAGGCAAGTTGTTACCAGCAGGTCTCTGTCCCCGTGATGANGTTCNTCATGTTTAGAGACCTTGGTTTGATTACGGTCGCA	gRNA 1, 5N 10N, 20 nt
	oDS_1543	AAGGCAAGTTGTTACCAGCAGGTCTCTGTCCGTGATGANGTTCNTCATGTTTAGAGACCTTGGTTTGATTACGGTCGCA	gRNA 1, 5N 10N, 16 nt
	oDS_1544	AAGGCAAGTTGTTACCAGCAGGTCTCTGTCCATGANGTTCNTCATGTTTAGAGACCTTGGTTTGATTACGGTCGCA	gRNA 1, 5N 10N, 14 nt
	oDS_1545	AAGGCAAGTTGTTACCAGCAGGTCTCTGTCCAGAGGCATTNGAATNGACCGTTTAGAGACCTTGGTTTGATTACGGTCGCA	gRNA 2, 5N 10N, 20 nt
	oDS_1546	AAGGCAAGTTGTTACCAGCAGGTCTCTGTCCGATTNGAATNGACCGTTTAGAGACCTTGGTTTGATTACGGTCGCA	gRNA 2, 5N 10N, 16 nt
	oDS_1547	AAGGCAAGTTGTTACCAGCAGGTCTCTGTCCATTNGAATNGACCGTTTAGAGACCTTGGTTTGATTACGGTCGCA	gRNA 2, 5N 10N, 14 nt
rpsB	oDS_1837	AAGGCAAGTTGTTACCAGCAGGTCTCTGTCCAACGGTTGTTNACGTNGTACGTTTAGAGACCTTGGTTTGATTACGGTCGCA	gRNA 1, 5N 10N, 20 nt
	oDS_1838	AAGGCAAGTTGTTACCAGCAGGTCTCTGTCCGTTGTTNACGTNGTACGTTTAGAGACCTTGGTTTGATTACGGTCGCA	gRNA 1, 5N 10N, 16 nt
	oDS_1839	AAGGCAAGTTGTTACCAGCAGGTCTCTGTCCGTTNACGTNGTACGTTTAGAGACCTTGGTTTGATTACGGTCGCA	gRNA 1, 5N 10N, 14 nt
	oDS_1840	AAGGCAAGTTGTTACCAGCAGGTCTCTGTCCGCTAGAGCGTNGTTGNACATGTTTAGAGACCTTGGTTTGATTACGGTCGCA	gRNA 2, 5N 10N, 20 nt
	oDS_1841	AAGGCAAGTTGTTACCAGCAGGTCTCTGTCCGCTNGTTGNACATGTTTAGAGACCTTGGTTTGATTACGGTCGCA	gRNA 2, 5N 10N, 16 nt
	oDS_1842	AAGGCAAGTTGTTACCAGCAGGTCTCTGTCCGAGCGTNGTTGNACATGTTTAGAGACCTTGGTTTGATTACGGTCGCA	gRNA 2, 5N 10N, 14 nt
rRNA	oDS_1843	AAGGCAAGTTGTTACCAGCAGGTCTCTGTCCCAACTAGCTNATCCNACCTGTTTAGAGACCTTGGTTTGATTACGGTCGCA	gRNA 1, 5N 10N, 20 nt
	oDS_1844	AAGGCAAGTTGTTACCAGCAGGTCTCTGTCCCTAGCTNATCCNACCTGTTTAGAGACCTTGGTTTGATTACGGTCGCA	gRNA 1, 5N 10N, 16 nt
	oDS_1845	AAGGCAAGTTGTTACCAGCAGGTCTCTGTCCAGCTNATCCNACCTGTTTAGAGACCTTGGTTTGATTACGGTCGCA	gRNA 1, 5N 10N, 14 nt
	oDS_1846	AAGGCAAGTTGTTACCAGCAGGTCTCTGTCCCTCCGATTANCGCGNCTGCGTTTAGAGACCTTGGTTTGATTACGGTCGCA	gRNA 2, 5N 10N, 20 nt
	oDS_1847	AAGGCAAGTTGTTACCAGCAGGTCTCTGTCCGATTANCGCGNCTGCGTTTAGAGACCTTGGTTTGATTACGGTCGCA	gRNA 2, 5N 10N, 16 nt
	oDS_1848	AAGGCAAGTTGTTACCAGCAGGTCTCTGTCCATTANCGCGNCTGCGTTTAGAGACCTTGGTTTGATTACGGTCGCA	gRNA 2, 5N 10N, 14 nt
	oDS_1857	AAGGCAAGTTGTTACCAGCAGGTCTCTGTCCAAGCTTCTTCNTCAGNAATTGTTTAGAGACCTTGGTTTGATTACGGTCGCA	gRNA 1, 5N 10N, 20 nt

argA	oDS_1858	AAGGCAAGTTGTTACCAGCAGGTCTCTGTCCCTTCTTCNTCAGNAATTGTTTAGAGACCTTGGTTTGATTACGGTCGCA	gRNA 1, 5N 10N, 16 nt
	oDS_1859	AAGGCAAGTTGTTACCAGCAGGTCTCTGTCCCTTCTTCNTCAGNAATTGTTTAGAGACCTTGGTTTGATTACGGTCGCA	gRNA 1, 5N 10N, 14 nt
	oDS_1860	AAGGCAAGTTGTTACCAGCAGGTCTCTGTCCAGCCATAGNGTATNGTTCGTTTAGAGACCTTGGTTTGATTACGGTCGCA	gRNA 2, 5N 10N, 20 nt
	oDS_1861	AAGGCAAGTTGTTACCAGCAGGTCTCTGTCCATAGNGTATNGTTCGTTTAGAGACCTTGGTTTGATTACGGTCGCA	gRNA 2, 5N 10N, 16 nt
	oDS_1862	AAGGCAAGTTGTTACCAGCAGGTCTCTGTCCATAGNGTATNGTTCGTTTAGAGACCTTGGTTTGATTACGGTCGCA	gRNA 2, 5N 10N, 14 nt
metE	oDS_1863	AAGGCAAGTTGTTACCAGCAGGTCTCTGTCCATCATACCAGNCAAANTCGCGTTTAGAGACCTTGGTTTGATTACGGTCGCA	gRNA 1, 5N 10N, 20 nt
	oDS_1864	AAGGCAAGTTGTTACCAGCAGGTCTCTGTCCATCATACCAGNCAAANTCGCGTTTAGAGACCTTGGTTTGATTACGGTCGCA	gRNA 1, 5N 10N, 16 nt
	oDS_1865	AAGGCAAGTTGTTACCAGCAGGTCTCTGTCCAGNCAAANTCGCGTTTAGAGACCTTGGTTTGATTACGGTCGCA	gRNA 1, 5N 10N, 14 nt
	oDS_1866	AAGGCAAGTTGTTACCAGCAGGTCTCTGTCCGATCGTCTTNGCTANATTCGTTTAGAGACCTTGGTTTGATTACGGTCGCA	gRNA 2, 5N 10N, 20 nt
	oDS_1867	AAGGCAAGTTGTTACCAGCAGGTCTCTGTCCGCTTNGCTANATTCGTTTAGAGACCTTGGTTTGATTACGGTCGCA	gRNA 2, 5N 10N, 16 nt
oDS_1868	AAGGCAAGTTGTTACCAGCAGGTCTCTGTCCCTTNGCTANATTCGTTTAGAGACCTTGGTTTGATTACGGTCGCA	gRNA 2, 5N 10N, 14 nt	
Fluc	oDS_1869	AAGGCAAGTTGTTACCAGCAGGTCTCTGTCCATAAATAACNGGCCNACACGTTTAGAGACCTTGGTTTGATTACGGTCGCA	gRNA 1, 5N 10N, 20 nt
	oDS_1870	AAGGCAAGTTGTTACCAGCAGGTCTCTGTCCATAACNGGCCNACACGTTTAGAGACCTTGGTTTGATTACGGTCGCA	gRNA 1, 5N 10N, 16 nt
	oDS_1871	AAGGCAAGTTGTTACCAGCAGGTCTCTGTCCAACNGGCCNACACGTTTAGAGACCTTGGTTTGATTACGGTCGCA	gRNA 1, 5N 10N, 14 nt
	oDS_1872	AAGGCAAGTTGTTACCAGCAGGTCTCTGTCCAAATCGTATTNATTANAACCGTTTAGAGACCTTGGTTTGATTACGGTCGCA	gRNA 2, 5N 10N, 20 nt
	oDS_1873	AAGGCAAGTTGTTACCAGCAGGTCTCTGTCCGATTNATTANAACCGTTTAGAGACCTTGGTTTGATTACGGTCGCA	gRNA 2, 5N 10N, 16 nt
oDS_1874	AAGGCAAGTTGTTACCAGCAGGTCTCTGTCCATTNATTANAACCGTTTAGAGACCTTGGTTTGATTACGGTCGCA	gRNA 2, 5N 10N, 14 nt	
Rluc	oDS_1875	AAGGCAAGTTGTTACCAGCAGGTCTCTGTCCGGTATAATACNCCGCNCTACGTTTAGAGACCTTGGTTTGATTACGGTCGCA	gRNA 1, 5N 10N, 20 nt
	oDS_1876	AAGGCAAGTTGTTACCAGCAGGTCTCTGTCCATAATACNCCGCNCTACGTTTAGAGACCTTGGTTTGATTACGGTCGCA	gRNA 1, 5N 10N, 16 nt
	oDS_1877	AAGGCAAGTTGTTACCAGCAGGTCTCTGTCCATACNCCGCNCTACGTTTAGAGACCTTGGTTTGATTACGGTCGCA	gRNA 1, 5N 10N, 14 nt
	oDS_1878	AAGGCAAGTTGTTACCAGCAGGTCTCTGTCCATCATCCGTTNCTTNGTTCGTTTAGAGACCTTGGTTTGATTACGGTCGCA	gRNA 2, 5N 10N, 20 nt
	oDS_1879	AAGGCAAGTTGTTACCAGCAGGTCTCTGTCCATCATCCGTTNCTTNGTTCGTTTAGAGACCTTGGTTTGATTACGGTCGCA	gRNA 2, 5N 10N, 16 nt
oDS_1880	AAGGCAAGTTGTTACCAGCAGGTCTCTGTCCGTTNCTTNGTTCGTTTAGAGACCTTGGTTTGATTACGGTCGCA	gRNA 2, 5N 10N, 14 nt	
Nluc	oDS_1881	AAGGCAAGTTGTTACCAGCAGGTCTCTGTCCACCACCTTGNTCTANAACCTGTTTAGAGACCTTGGTTTGATTACGGTCGCA	gRNA 1, 5N 10N, 20 nt
	oDS_1882	AAGGCAAGTTGTTACCAGCAGGTCTCTGTCCACCTTGNTCTANAACCTGTTTAGAGACCTTGGTTTGATTACGGTCGCA	gRNA 1, 5N 10N, 16 nt
	oDS_1883	AAGGCAAGTTGTTACCAGCAGGTCTCTGTCCCTTGNTCTANAACCTGTTTAGAGACCTTGGTTTGATTACGGTCGCA	gRNA 1, 5N 10N, 14 nt
	oDS_1887	AAGGCAAGTTGTTACCAGCAGGTCTCTGTCCCTAATACGANACGTNGAATGTTTAGAGACCTTGGTTTGATTACGGTCGCA	gRNA 3, 5N 10N, 20 nt
	oDS_1888	AAGGCAAGTTGTTACCAGCAGGTCTCTGTCCATACGANACGTNGAATGTTTAGAGACCTTGGTTTGATTACGGTCGCA	gRNA 3, 5N 10N, 16 nt
oDS_1889	AAGGCAAGTTGTTACCAGCAGGTCTCTGTCCACGANACGTNGAATGTTTAGAGACCTTGGTTTGATTACGGTCGCA	gRNA 3, 5N 10N, 14 nt	

4. Discussion

4.1. Does *V. natriegens* have the right properties for a new SynBio chassis?

The most obvious strength of *V. natriegens* is its rapid growth with a reported doubling time of under ten minutes under optimal conditions (Eagon, 1961; Hoffart et al., 2017). While this growth speed was only observed in rich medium, *V. natriegens* also showed remarkably high growth rates in minimal media with a range of different carbon sources (Hoffart et al., 2017). The rapid growth of *V. natriegens* is clearly advantageous in all cases where long incubation times, in which the operator simply waits for the bacterial cultures to grow, represent major bottlenecks in a process or workflow. One such example is the assembly of recombinant DNA, which to date is mostly performed using *E. coli*. It was shown before, that the use of *V. natriegens* can accelerate this process (Weinstock et al., 2016). Another example is the production of recombinant proteins, which also involves several incubation steps (Weinstock et al., 2016). While these proof-of-concept experiments clearly support the promises of accelerating standard laboratory procedures by using *V. natriegens*, own experience and anecdotal evidence from members of the *V. natriegens* community suggest that the currently used strains are not sufficiently robust for routine use and require further optimization.

One further challenge for the widespread adoption of *V. natriegens* as the go-to SynBio chassis is its high susceptibility towards metabolic burden. We frequently observed that the production of heterologous proteins, e.g. mScarlet-I or dCas9 (Stukenberg et al., 2021; Stukenberg et al., 2024; **Chapter 3.3**), causes substantial growth defects. This property will likely become a major obstacle for future projects requiring either high production of a single protein or the expression of several genes, e.g. for sophisticated genetic circuits or ambitious metabolic engineering projects. Nevertheless, several successful metabolic engineering projects (Dalia et al., 2017; Thoma et al., 2022; Thoma and Blombach, 2021; Zhang et al., 2021) suggest the general feasibility of using *V. natriegens* for interesting biotechnological applications.

The properties of *V. natriegens* discussed above were mostly observed for wild type isolates or strains with only a low number of genetic modifications. We should therefore consider which of these challenges can be addressed through strain engineering. Can we, for example, design and build a *V. natriegens* strain, which can be used for the assembly of recombinant

DNA as efficiently and robustly as *E. coli*? Can we overcome the susceptibility towards metabolic burden, thereby enabling future ambitious projects requiring high production of heterologous proteins? And can we do all that while maintaining the most interesting property of *V. natriegens*, the rapid growth in a wide range of media?

4.2. Do we already have the tools for ambitious SynBio projects with *V. natriegens*?

As discussed above, *V. natriegens* holds enormous promises as a fast-growing SynBio chassis, while also coming with several major challenges. To fully exploit the interesting properties of *V. natriegens* for diverse applications, we need a set of efficient and well-characterized tools.

Major progress has already been made in the development and characterization of genetic parts, e.g. constitutive and inducible promoters, terminators, 5' untranslated regions (5' UTRs), plasmid replication origins, and antibiotic resistance markers (Stukenberg et al., 2021; Tietze et al., 2022; Tschirhart et al., 2019; Wu et al., 2020). My work, prior to this thesis, led to the development of the Marburg Collection, a Golden Gate Cloning-based plasmid toolbox with almost 200 genetic parts (Stukenberg et al., 2021). This toolbox served as a platform for all projects in this thesis and was constantly expanded with additional part. For example, optimized inducible promoters, initially developed by Meyer *et al.* (Meyer et al., 2019), were added as new parts to the Marburg Collection and thoroughly characterized (Faber, 2020). This work was crucial for the development of the CRISPR-Cas9-based tools described in this thesis, as it allowed the tight regulation of (*d*)*cas9* and *gRNA* expression (Stukenberg et al., 2022; **Chapter 3.1**, Stukenberg et al., 2022; **Chapter 3.3**). While adding new features to the Marburg Collection is always a worthy task, I consider the set of currently available genetic parts for *V. natriegens* to be quite extensive and sufficient for most applications.

In contrast to the large number of available genetic parts, tools for genome engineering were rather scarce. While the first methods for genome engineering were already published several years ago, they all suffered from different drawbacks. In 2016, Weinstock *et al.* demonstrated that they could perform deletions of sequences of the *V. natriegens* genome as well as the integration of foreign DNA into the chromosome (Weinstock et al., 2016). They conjugated a suicide plasmid from *E. coli* into *V. natriegens*, which carried homologous regions to the target region. Through homologous recombination, the desired modification was achieved. An

4. Discussion

antibiotic resistance marker was integrated into the genome in the process, which was then recycled through Cre/*loxP*-mediated recombination (Weinstock et al., 2016). This method is very labor intensive, and the recycling of the antibiotic resistance marker leaves scars of the *loxP* sequence at the modified locus.

Lee *et al.* attempted to develop a recombineering-based method for *V. natriegens* (Lee et al., 2017). This approach is similar to the λ Red system (Ellis et al., 2001), which is commonly used in genome engineering tools for *E. coli* (Ellis et al., 2001; Reisch and Prather, 2015). Recombineering is based on the electroporation of short ssDNA oligonucleotides, which anneal to the ssDNA in the replication fork of the chromosome with the help of ssDNA binding proteins, thereby introducing modifications to the hosts genome (Mosberg et al., 2010). Unfortunately, the attempts to establish *V. natriegens* were not fully successful, as the editing efficiency was too low for routine usage (Lee et al., 2017).

Dalia *et al.* developed Multiplex Genome Editing by Natural Transformation (MuGENT) by taking advantage of one exciting ability of *V. natriegens*, which is to take up linear tDNA from the environment and integrate it into its genome through a process called natural transformation (Dalia et al., 2017). Natural transformation was used for the deletion of a specific sequence with a tDNA carrying an antibiotic resistance cassette, flanked by sequences homologous to the region upstream and downstream of the desired modification. Successfully edited cells can be selected for the presence of the antibiotic resistance cassette (Dalia et al., 2017). Even though not described in that publication, the antibiotic resistance cassette could then be recycled through a recombinase system like Cre/*loxP*, resulting in a scar at the edited site. Dalia *et al.* used the high efficiency of natural transformation to perform additional unselected edits in parallel to the integration of the antibiotic resistance cassette, thereby achieving multiplexing of several different modifications (Dalia et al., 2017). However, the authors only showed small deletions (~ 500 bp) as unselected edits. Even though not discussed by the authors, the efficiency of unselected edits would likely be too low for larger deletions, which would prevent the complete removal of an average-sized prokaryotic gene of ~ 1000 bp (Xu et al., 2006).

After considering the strengths and limitations of the available genome engineering methods for *V. natriegens*, we decided that none of the already available tools would be sufficient for

ambitious strain engineering projects and consequently we decided to develop NT-CRISPR to fill this gap.

4.3. Advantages and limitations of NT-CRISPR compared to other genome engineering methods for *V. natriegens*

After we decided to develop a new genome engineering method, we envisioned a tool with the following capabilities: First, we wanted to achieve a high editing efficiency to reduce the necessary effort to identify correctly edited clones. Second, in contrast to most of the tools described above, we favored a scarless system, which has several important advantages. After multiple rounds of editing, defined scars, e.g. after Cre//loxP-mediated marker recycling, would be scattered across the chromosome and might result in genomic instability due to unintended recombination events. Also, a scarless genome editing tool would allow small modifications on the genome like point mutations or small insertions, where an introduced scar might influence the function of the surrounding sequence.

As described above, the MuGENT method, which uses natural transformation for the replacement of a target gene with an antibiotic resistance marker, showed a very high editing efficiency (Dalia et al., 2017). Therefore, we decided to also use natural transformation for our novel genome engineering tool. No changes were necessary to the natural transformation protocol to reproduce the high editing efficiency of up to 10 – 20 % even without selection (Dalia et al., 2017a; Stukenberg et al., 2022, **Chapter 3.1**). As an alternative to selecting for the integration of an antibiotic resistance marker, we used CRISPR-Cas9-based counterselection. This counterselection happens in a temporally distinct second step after the editing natural transformation has happened (Stukenberg et al., 2022, **Chapter 3.1**). This leads to a drastic enrichment of correctly modified cells, as non-modified cells are efficiently killed. It is plausible that the formation of escapees from the CRISPR-Cas9-based counterselection is slightly higher than the emergence of spontaneous resistant cells, which would be the most likely escape mechanism for the selection through antibiotic resistance in MuGENT. However, we measured very high killing efficiencies in the NT-CRISPR protocol of up to 99.999%, meaning that non-edited cells are almost completely eliminated. The main advantage of a CRISPR-Cas9-based counterselection over selection through an antibiotic resistance marker is that no additional sequences (antibiotic resistance marker or recombinase scars) are inserted at the target site, thereby allowing any modification to be performed with single-base precision.

The biggest advantage of NT-CRISPR over MuGENT is the ability to perform multiple modifications with selection for each of those edits. While MuGENT also allows multiple simultaneous deletions, there is no selection pressure for the unselected edits beyond the general natural competence of a cell, which can be screened for through the introduction of the antibiotic resistance cassette (Dalia et al., 2017). In NT-CRISPR, up to three gRNAs can be directed against three distinct sequences in the chromosome, thereby separately selecting for each modification. This allowed us to simultaneously delete three large gene clusters with a combined size of 106 kbp (Stukenberg et al., 2022, **Chapter 3.1**). It is implausible that such a challenging genome editing process would be possible with MuGENT without efficient selection for each deletion. However, the MuGENT method enables one use case, which is impossible with NT-CRISPR. MuGENT allows multiplexing, which can be used to generate a library of mutant strains with a random combination of several different edits (Dalia et al., 2017). Dalia *et al.* used this strategy to increase the PHB production of *V. natriegens* by targeting nine genes with a putative role in PHB biosynthesis (Dalia et al., 2017).

In summary, the capabilities of NT-CRISPR are clearly superior to MuGENT for most applications, especially for the generation of multiple simultaneous edits. However, if multiplexing is desired for a project, then MuGENT should be preferred over NT-CRISPR.

4.4. Future directions for improvement of NT-CRISPR

The high efficiency and simple applicability of NT-CRISPR has enabled a range of own projects (Ramming et al., 2023, **Chapter 3.2**; Stukenberg et al., 2024, **Chapter 3.3**), and is also being used intensively by the *V. natriegens* community (personal communication). While it is unlikely that the natural transformation and counterselection steps of the NT-CRISPR process can be significantly improved further, I see a large potential for the streamlining of the workflow. The whole NT-CRISPR workflow, as described in Stukenberg *et al.* (2022, **Chapter 3.1**), takes five days, starting with the transformation of the parental strain with the NT-CRISPR plasmid and ending with the preparation of a glycerol stock for long-term storage of a plasmid-cured, successfully edited strain (Stukenberg et al., 2022, **Chapter 3.1**). Only one day is necessary for the actual natural transformation, including CRISPR-Cas9-mediated counterselection, while all other days are incubation steps for the introduction of the NT-CRISPR plasmid into the parental strain before the editing step and curing of the same plasmid thereafter. Especially when multiple sequential rounds of NT-CRISPR are needed to construct a strain with dozens of

4. Discussion

modifications, these incubation steps represent a time-consuming bottleneck. Together with Jakob Wenning, I devised a strategy to intertwine incubation steps for curing the NT-CRISPR plasmid from the previous cycle with the transformation of the NT-CRISPR for the subsequent cycle (Wenning, 2023). In that strategy, the culture, which is grown without selection pressure to cure the NT-CRISPR plasmid, is directly used for the preparation of competent cells for the introduction of the next NT-CRISPR plasmid. Instead of plating the transformed cells to obtain single colonies, the transformation mixture is directly used to inoculate the preculture for the next natural transformation step. There are two requirements to facilitate this improved workflow. First, the natural transformation step of the NT-CRISPR protocol has to be performed with a modified preculture. In the published protocol, the preculture is grown from a glycerol stock containing cells that were previously transformed with the NT-CRISPR plasmid (Stukenberg et al., 2022, **Chapter 3.1**). Instead, we wanted to inoculate the preculture directly from cells after the recovery step of the plasmid transformation protocol. This improvement shortens the NT-CRISPR workflow by one day because no culture for a glycerol stock needs to be grown after transformation with the NT-CRISPR plasmid. Jakob Wenning could successfully implement this modification to the NT-CRISPR workflow (Wenning, 2023).

The second requirement is an extremely efficient plasmid curing step. This is necessary because each round of editing requires an NT-CRISPR plasmid specifically designed for the intended genomic modifications. Therefore, we need to ensure that the NT-CRISPR plasmid from the previous cycle is removed entirely from the edited cells before the NT-CRISPR plasmid for the next cycle is introduced. Otherwise, cells still carrying the previous NT-CRISPR plasmid could not be distinguished from cells with the newly introduced plasmid. It is therefore crucial to establish a protocol for the guaranteed removal of a plasmid. Unfortunately, none of the strategies tested so far was sufficiently efficient (Wenning, 2023).

One yet unexplored route for more efficient plasmid curing would be the production of a toxin, e.g. CcdB, controlled through an inducible promoter, as was described for *V. natriegens* before (Weinstock et al., 2016). When the production of the toxin is induced at the end of the plasmid curing step, it should efficiently select against all cells still carrying the NT-CRISPR plasmid.

With the improvements discussed above, one NT-CRISPR cycle would only take two instead of five days. Assuming three deletions are being performed per cycle, we could achieve up to

nine deletions per week. This would enable ambitious strain engineering projects which require dozens of genomic modifications.

4.5. Developing a CRISPRi-based tool leading to different knockdown strengths

We developed NT-CRISPR as an efficient genome engineering tool, which enables us to perform deletions, integrations, and point mutations (Stukenberg et al., 2022, **Chapter 3.1**). This method leads to the modification of the cell's genome sequence, thereby permanently changing its properties. For many applications, this is the desired outcome. However, in some cases, the target gene is essential for growth, or its permanent deletion might result in instability of the strain or the formation of suppressor mutants. In these cases, a transient knockdown might have advantages over a permanent knockout. One strategy to achieve a transient knockdown is the use of CRISPRi. CRISPRi differs from most other CRISPR-Cas9-based methods in the fact that a catalytically inactive Cas9 (dCas9) is used. This protein can be directed by a guide RNA (gRNA) to a target sequence where it binds but is unable to introduce a DNA DSB (Qi et al., 2013). This can be used to block transcription by inhibiting either translation initiation, when the dCas9-gRNA binds to the promoter region, or translation elongation when the DNA of the coding sequence of the gene is bound. We established a CRISPRi-based tool for *V. natriegens* to be able to investigate the response of the cells to the repression of essential genes (Stukenberg et al., 2024, **Chapter 3.3**). CRISPRi was used in *V. natriegens* before in a library-based approach to study the essentiality of all genes (Lee et al., 2019). While the resulting data is a highly appreciated resource, the used CRISPRi tool has one undesirable characteristic. Lee *et al.* used an arabinose promoter for the expression of *cas9* and a strong constitutive promoter for the expression of the gRNA (Lee et al., 2019). The authors describe that their system was not inducible, meaning that strong repression was observed even in the absence the inducer arabinose (Lee et al., 2019). This leakiness diminishes one major advantage of CRISPRi-mediated knockdowns over the permanent deletion of the target genes. Consequently, cells with a CRISPRi system targeting essential genes are under strong selection pressure immediately after transformation with the CRISPRi plasmid. This might result in mutations disabling the CRISPRi system or other types of compensatory mutations in the host's genome in incubation steps before the start of the actual experiment. Due to this major limitation of the only published CRISPRi tool for

V. natriegens, we decided to develop an improved tool. One priority was to achieve tight control over *dCas9* and *gRNA* expression to have a truly inducible system. We achieved that by using two different inducible promoters, P_{tet} and P_{3b5b} for the production of *dCas9* and *gRNA*, respectively (Stukenberg et al., 2024, **Chapter 3.3**). When testing the designed construct against a chromosomally integrated *mScarlet-I* expression cassette, we observed an approximately 40-fold reduction of fluorescence signal when both promoters were induced. In the absence of inducer, no significant difference was observed between the *mScarlet-I* targeting *gRNA* and a non-binding control *gRNA* (Stukenberg et al., 2024, **Chapter 3.3**). This result shows that we have succeeded in developing a tightly controllable CRISPRi tool for *V. natriegens*.

Several recent studies have shown that gene essentiality can be a quantitative rather than a qualitative trait. This means that a gene product, even though required for growth under a specific condition, can be overabundant. Consequently, a strain with a moderate knockdown of a target gene might not show any obvious growth impairment, even though a complete deletion of that gene would prevent growth in the given condition (Donati et al., 2021; Hawkins et al., 2020; Sander et al., 2019).

We thought that the study of protein-abundance-dependent phenotypes in *V. natriegens* could be an interesting future research direction. Therefore, we wanted to add an approach to this tool, which would lead to graded knockdowns. In the past, this was achieved through two conceptually different approaches. First, a graded CRISPRi strength can be achieved by limiting the number of active *dCas9*-*gRNA* complexes, usually by using different inducer concentrations for either *dCas9*, *gRNA* or both (Fontana et al., 2018; Lee et al., 2016; Li et al., 2016). As expected, high production of both *dCas9* and *gRNA* leads to a strong repression, while a weaker repression is observed when one or both of the components is limiting (Fontana et al., 2018; Lee et al., 2016; Li et al., 2016). The second distinct approach to achieve a graded knockdown is to use *gRNAs* leading to a weaker binding of the *dCas9*-*gRNA* complex to the DNA target sequence which can be achieved through the introduction of mismatches between the *gRNA* and DNA target sequence (Feng et al., 2021; Hawkins et al., 2020). The work of Vigouroux *et al.* discusses the strengths and weaknesses of these two approaches to adjust the strength of CRISPRi-mediated repression (Vigouroux et al., 2018). By analyzing single-cell data using flow cytometry, they showed that titrating *dCas9* and *gRNA* production

4. Discussion

through different inducer levels results in very high cell-to-cell variability. In contrast, a more homogenous population was obtained when the binding strength of the dCas9-gRNA complex to the target DNA is reduced (Vigouroux et al., 2018). They also provide a potential mechanism to explain this behavior. They suggest that at low inducer concentrations, the expression of dCas9 and gRNA is noisy and therefore differs between isogenic cells in the population (Vigouroux et al., 2018). They also show that spontaneous unbinding of the dCas9-gRNA complex from the target DNA sequence is rare but that the dCas9-gRNA complex is ejected by the replication fork during DNA replication (Vigouroux et al., 2018). After the target DNA sequence is replicated, there might be a short time window allowing transcription of the otherwise inhibited gene before the target is bound again by dCas9-gRNA. The length of this time window should correlate with the abundance of dCas9-gRNA complexes in the cell. However, this process is highly stochastic when only a small number of active dCas9-gRNA complexes, while almost immediate re-binding can be assumed at higher concentrations of dCas9-gRNA. Hence several transcriptional bursts might be possible in some cells, while the target gene is blocked immediately after replication in other cells. Consequently, this leads to the observed high cell-to-cell variability (Vigouroux et al., 2018).

When using different binding strengths of the dCas9-gRNA complex to the DNA target sequence, the authors suggest a “kick-out model” to explain the more homogenous distribution of the reporter signal in the population. During transcription elongation, the RNA polymerase collides with the dCas9-gRNA complex bound to the target DNA sequence. Vigouroux *et al.* argue that the binding strength of dCas9-gRNA to the DNA sequence determines with which probability either the RNA polymerase or the dCas9-gRNA complex is ejected from the DNA. While the former scenario would prevent expression of the target gene due to aborted transcription, the latter case would result in successful transcription and consequently expression of the target gene (Vigouroux et al., 2018). Hawkins *et al.* showed that using libraries with different mismatches, and thereby different binding strengths to the target sequence, results in a range of knockdown strengths (Hawkins et al., 2020).

With these considerations in mind, we decided to follow the strategy of using mismatched gRNAs to achieve graded CRISPRi strengths. We achieved this by constructing libraries with “N” nucleotides in positions five and ten from the PAM proximal site. To further diversify repression strengths, we used truncated gRNAs with 16 and 14 instead of 20 nucleotides. This

truncation is expected to further reduce the binding strength of the dCas9-gRNA complex to the target sequence. Truncated gRNAs have been used before to reduce off-target effects of catalytically active Cas9 enzymes (Fu et al., 2014), but to the best of my knowledge, not to modulate the efficiency of CRISPRi approaches. We analyzed the distribution of a fluorescent reporter of single cells from samples with either a fully binding gRNA with different inducer concentrations or samples with different mismatches in the gRNA sequences. Our results show a narrower distribution for samples with mismatched gRNAs and are therefore in accordance with previous studies (Hawkins et al., 2020; Vigouroux et al., 2018).

Lastly, we explored the possibility of simultaneously targeting multiple genes with CRISPRi. This could open interesting future applications where the exact stoichiometry of multiple genes in a regulatory network or metabolic pathway needs to be identified to achieve the desired phenotype. CRISPRi systems with multiple gRNAs have been successfully tested before (Kim et al., 2017; Vigouroux et al., 2018). In accordance with previous studies (Vigouroux et al., 2018), we found that additional gRNAs reduce the repression strength of a single target gene when abundance of dCas9 is not sufficient. However, we also showed that increased expression of *dcas9* overcomes this bottleneck (Stukenberg et al., 2024, **Chapter 3.3**). We explored the capabilities of this system by assembling mismatched gRNA libraries for four different chromosomally integrated reporter genes. As a result, we obtained a collection of strains with different expression levels of all four reporter genes.

One drawback of most CRISPRi approaches is that the quantification of repression strengths is not trivial as soon as endogenous genes are targeted instead of reporter genes. Hawkins *et al.* predicted the knockdown strength of their mismatched gRNA libraries and compared it with measured reporter signals (Hawkins et al., 2020). They obtained a decent correlation between predicted and measured values ($R^2 = 0.56$). However, we decided that directly measuring the abundance of the target protein is advantageous as it directly allows the association between an observed phenotype and the measured protein abundance of the target gene. We tested if the HiBiT tag system, which was developed and commercialized by Promega (Schwinn et al., 2018), is suitable for tracking the reduced abundance of the target protein after CRISPRi knockdown in *V. natriegens*. The HiBiT assay is based on a split luciferase system, where the larger component of the NanoLuc enzyme needs to be complemented with the HiBiT peptide, to generate luminescence. This HiBiT peptide can be fused to the N- or C-terminus of a protein

of interest. The abundance of the fused peptide can then be quantified in a simple luminescence reaction (Schwinn et al., 2018). We succeeded in establishing a workflow for the quantification of protein abundances with the HiBiT tag system in *V. natriegens* (Stukenberg et al., 2024, **Chapter 3.3**). In combination with the generation of graded knockdown strengths using gRNA libraries, the HiBiT tag system now allows us to investigate relationships between phenotypes and the abundance of a specific gene product.

4.6. Metabolic burden in experiments with CRISPRi

During the characterization of this CRISPRi tool, we observed that sufficient production of dCas9 for a strong knockdown of the target gene leads to a significant reduction of growth. This was also the case when a reporter gene is targeted, or a non-binding gRNA is used, suggesting a target-independent effect (Stukenberg et al., 2024, **Chapter 3.3**). Several studies have shown that dCas9 leads to toxicity, possibly due to unspecific binding to chromosomal DNA and thereby to disruption of gene expression across the chromosome (Cho et al., 2018; Rock et al., 2017; Zhang and Voigt, 2018). While it is certainly possible that toxicity through unspecific binding contributes to the observed growth defects, there is at least one additional probable reason. The effect of the production of “unnecessary proteins” has been studied extensively (reviewed in Borkowski et al., 2016). In brief, the production of these proteins requires cellular resources, which are then missing for the production of proteins required for rapid growth (Scott et al., 2010). One strategy to mitigate this effect could be the use of alternative CRISPR systems with a smaller DNA-binding Cas protein. The dCas9 used in this project originates from *Streptococcus pyogenes* and has a size of ~ 1400 amino acids (aa). The Cas9 of *Campylobacter jejuni* (984 aa) (Kim et al., 2017), Un1Cas12f1 from an uncultured archaeon (529 aa) (Okano et al., 2021) and CasΦ (700 – 800 aa) from a huge phage of the Biggiephage clade (Pausch et al., 2020) could be used as smaller alternative Cas proteins. However, these variants are far less established, and it is not clear whether they would be similarly suitable for CRISPRi as the dCas9 of *S. pyogenes* used in this project. Furthermore, they have different, and in most cases longer, PAM requirements (Xin et al., 2022), which might result in additional challenges for their use as a tool.

4.7. Potential mechanistic causes for the high susceptibility of *V. natriegens* towards metabolic burden

The finding that the growth of *V. natriegens* is slowed down drastically when forced to produce heterologous proteins is a recurring observation throughout own projects (Stukenberg et al., 2021; Stukenberg et al., 2024, **Chapter 3.3**). While the use of smaller Cas proteins might be a solution for the development of a CRISPRi system with a reduced metabolic burden, the high susceptibility of *V. natriegens* towards the overproduction of heterologous proteins questions the value of this organism as a SynBio chassis in general. Ambitious metabolic engineering projects, which require high production of multiple enzymes would lead to a severe growth defect canceling the main advantage of *V. natriegens*, its rapid growth. Furthermore, the cells are under strong selection pressure to relieve the metabolic burden by acquisition of mutations in the designed pathways.

To develop *V. natriegens* into a competitive SynBio chassis, it is crucial to understand the origin of this phenomenon and, based on this understanding, develop mitigation strategies. To the best of my knowledge, the response of *V. natriegens* to the production of heterologous proteins has not been investigated yet. However, several side observations of previous projects, together with extensive literature from other bacteria provide sufficient clues for informed speculation.

The simplest concept of the response of bacteria towards the production of heterologous proteins can be deduced from the proteome allocation model (Scott et al., 2010). In this concept, the proteome of a cell is finite and can be coarse-grained into three sectors, representing major cellular functions. The R-sector contains ribosomal protein as well as additional proteins required for translation, e.g. elongation and initiation factors, the P-sector contains metabolic enzymes, and the Q-sector comprises all other proteins crucial for cell growth and division (Scott et al., 2010). Production of “unnecessary proteins” is covered by an additional U-sector. In this concept, the proteome is finite. Therefore, increase of the U-sector leads to a reduction of the R- and P-sector, while the Q-sector is considered to be unaffected (Scott et al., 2010). In accordance with this model, Scott *et al.* found a linear decrease in the growth rate with increasing production of heterologous proteins (Scott et al., 2010). When the “unnecessary protein” comprises 15% of the whole proteome, the growth rate is decreased approximately two-fold (Scott et al., 2010).

4. Discussion

In addition to the coarse-grained proteome allocation model, the effect of heterologous protein production on gene expression and other cell properties, e.g., cell shape has been studied extensively (Basan et al., 2015; Bienick et al., 2014; Ceroni et al., 2018; Nikolados et al., 2019; Shachrai et al., 2010). An important study investigating the regulatory response of *E. coli* towards production of heterologous proteins was executed by Ceroni *et al.* (Ceroni et al., 2018). They characterized the transcriptomic changes of *E. coli* at different time points after inducing the production of heterologous proteins (Ceroni et al., 2018). They found that many genes associated with the heat-shock response, and known to be regulated by the corresponding sigma factor RpoH, are strongly upregulated (Ceroni et al., 2018). They concluded that *E. coli* senses heterologous protein production similarly to a heat shock and responds accordingly by increasing the production of chaperones (Ceroni et al., 2018). The regulon of RpoH comprises several hundred genes including some coding for proteins involved in the protection of its DNA and RNA at high temperature, as well as additional transcription factors to trigger additional regulatory pathways (Roncarati and Scarlato, 2017). It is unlikely that all genes of the RpoH regulon are necessary to cope with heterologous protein production and therefore, the generic RpoH-mediated response, beyond the production of chaperones and proteases, could be regarded as a “collateral expression burden”. This would lead to additional “unnecessary proteins” adding to the burden from the desired heterologous protein and thereby amplifying the impact on growth. While the activation of RpoH as a response to heterologous protein production is probably the best-understood consequence, there is at least one more possible pathway which might lead to “collateral gene expression burden”.

RpoS is known as the sigma factor mediating transition into and survival in the stationary phase by directly or indirectly regulating more than 1000 genes in *E. coli* (Schellhorn, 2020). RpoS abundance is kept low during the exponential phase through its degradation by the ClpXP protease machinery (Schweder et al., 1996). It was proposed that saturation of the ClpXP protease machinery by a high concentration of misfolded heterologous proteins prevents the degradation of RpoS in the exponential phase, thereby leading to increased expression of the RpoS regulon (Cookson et al., 2011). Even a minor activation of the more than 1000 genes in the RpoS regulon could contribute to the hypothesized “collateral expression burden”.

During the characterization of the parts of the Marburg Collection, we made one observation, which could support the idea of an RpoS-mediated “collateral expression burden”. We tested

different degradation tags, which direct the tagged proteins to the ClpXP machinery (Farrell et al., 2005). As expected, we observed a lower signal of the tagged mScarlet-I reporter protein, compared to a non-tagged control construct. However, this reduction was only visible at low expression of the reporter and there was no difference at high mScarlet-I expression, suggesting that the ClpXP machinery was saturated by the high abundance of tagged reporter protein (Stukenberg et al., 2021). At high expression, the tagged mScarlet-I led to a stronger reduction in growth rate compared to the non-tagged version (Stukenberg et al., 2021). While this single observation is clearly not sufficient to prove the model of “collateral gene expression burden” it hints at a regulatory component beyond the effect which could be derived from a simple proteome allocation model. In our design of the graded-CRISPRi tool, the dCas9 was also equipped with a strong degradation tag (Stukenberg et al., 2024, **Chapter 3.3**) to reduce its abundance prior to induction to achieve tighter control over CRISPRi activity. Nevertheless, it is unclear whether the observed metabolic burden caused by dCas9 production would be lower without tagging dCas9 with a degradation tag.

The above-discussed responses of cells to heterologous proteins are mostly based on literature about *E. coli*. If the responses of *V. natriegens* and *E. coli* are qualitatively similar, how would that explain the observed high susceptibility of *V. natriegens* toward protein production burden? Several studies have shown that an increased abundance of alternative sigma factors can reduce growth due to the redistribution of resources away from growth-related and towards stress-related processes and that fast-growing cells have low activity of the stress sigma factor regulons (Mauri and Klumpp, 2014; Patange et al., 2018). It is plausible that the fast growth of *V. natriegens* requires a strong focus of all available resources towards growth-related processes, which would require a low basal activity of stress-related functions. Consequently, a minor upregulation of the regulons of stress sigma factors might result in a comparably higher fold-change of the respective genes as they come from a lower basal level.

4.8. Possible strategies to solve the metabolic burden susceptibility

As discussed in the previous chapter, the exact reason for the high susceptibility of *V. natriegens* towards heterologous protein expression is not clear. Therefore, investigating the underlying regulatory mechanisms should precede any attempts to mitigate the negative effects of protein production. However, we can conceive strategies under the assumption that

the above-discussed hypothesis of “collateral expression burden”, resulting from the activation of stress sigma factors, can be confirmed.

The concept is based on the notion that the regulatory response towards the production of “unnecessary proteins” leads to increased expression of genes coding for chaperones and proteases, which might be an adequate coping strategy of the cell. Additionally, this response also increases the expression of other genes in the stress sigma factor regulons of RpoH and RpoS, which leads to the production of many proteins which are not needed to cope with stress resulting from the “unnecessary proteins”. However, this would divert resources away from growth-related processes. In that case, efforts should focus on increasing the adequate while reducing the inadequate response. This could be achieved through increased abundance of the relevant chaperones and proteases, e.g., by integrating a second copy on the chromosome. A higher abundance of proteases and chaperones should result in a weaker activation of the stress sigma factor regulons because the abundance and activity of both RpoS and RpoH are directly linked to the load of the capacity utilization of proteases and chaperones (Cookson et al., 2011; Schweder et al., 1996; Yura et al., 2007). While the additional abundance of chaperones and proteases requires resources in the first place, the reduced activation of RpoS and RpoH regulons might save sufficient resources to make this design beneficial.

An alternative approach to mitigate metabolic burden might be a genome reduction or proteome streamlining strategy. Many studies in a range of different bacteria have shown that deletion of genes coding for proteins with a high cost (high abundance and large size) which are unnecessary under the specific growth condition can liberate resources for the production of heterologous proteins (Aguilar Suárez et al., 2019; Bienick et al., 2014; Lee et al., 2009).

With NT-CRISPR as a very efficient genome engineering tool, especially after implementing the discussed optimizations to the workflow (**Chapter 4.4**), deletion of a few dozen genes is certainly feasible. Information about the necessity of a specific gene can be obtained from the CRISPRi screen (Lee et al., 2019), while information about the abundance of the encoded proteins can be extracted from published proteome data sets (Coppens et al., 2023).

4.9. synSC1.0 as a platform strain for future projects

We created synSC1.0 as the first *V. natriegens* strain with a single chromosome by fusing both chromosomes of the parental strain (Ramming et al., 2023, **Chapter 3.2**). synSC1.0 shows only

4. Discussion

minor phenotypic differences compared to the parental strain with only a slightly increased doubling time (7%) and slightly longer and wider cells (Ramming et al., 2023, **Chapter 3.2**). In addition to gaining interesting insights regarding chromosome replication of *V. natriegens*, the creation of synSC1.0 might solve one other previously unaddressed challenge. There are several Ori parts available and characterized to facilitate replication of plasmids (Stukenberg et al., 2021; Tschirhart et al., 2019). However, the well-functioning Oris all result in medium to high copy numbers of the respective plasmids (Tschirhart et al., 2019). p15A, the origin leading to the lowest measured copy number so far (Tschirhart et al., 2019), showed a very heterogeneous cell-to-cell distribution in single-cell experiments (Stukenberg et al., 2021). Therefore, a stably replicating Ori leading to a single or low copy number is still missing in the toolbox for *V. natriegens*.

It was shown before that the origin of Chr2 of *V. cholerae* can be used to construct synthetic secondary chromosomes in *E. coli* with a copy number similar to the host's chromosome (Messerschmidt et al., 2015). Construction of such a synthetic secondary chromosome in the wild type *V. natriegens* strain is not possible, as the replication and segregation machineries of Chr2 of different *Vibrionaceae* are too similar and therefore incompatible (Messerschmidt et al., 2016). As a result, it is most likely impossible to introduce a synthetic chromosome based on the Ori of Chr2 of any *Vibrionaceae* in a *V. natriegens* strain with the bipartite genome configuration of the wild type strain. However, in the monopartite synSC1.0 strain, the sequence of Ori2, including the neighboring genes encoding for the replication initiator protein RctB and the partitioning proteins ParA and ParB were intentionally deleted during the chromosome fusion (Ramming et al., 2023, **Chapter 3.2**). This should now allow the introduction of a new synthetic chromosome, based on the Ori2 from *V. natriegens* or any other member of the *Vibrionaceae*. A sophisticated regulatory network for the timing of replication (de Lemos Martins et al., 2018; Kemter et al., 2018) and chromosome segregation (Fogel and Waldor, 2005; Srivastava et al., 2006) of Chr2 evolved in *Vibrionaceae* (**Chapter 1.3**). Therefore, a synthetic chromosome based on the Ori of Chr2 from *V. natriegens* or from another member of the *Vibrionaceae* should seamlessly integrate into the cell cycle as it would be controlled by its native replication and segregation machinery. Replication of such a synthetic secondary chromosome in synSC1.0 is expected to be initiated right after replication of the *crtS* sequence on the fused chromosome, similar to the replication of the native Chr2 in *Vibrionaceae* (Val et al., 2016). Consequently, the copy number of the synthetic chromosome

would be similar to the copy number of the *crtS* sequence on the fused chromosome. Depending on the growth conditions, this would result in a copy number of one or two in slow-growing conditions and a slightly higher copy number in growth conditions leading to multifork replication as this would also result in an increased copy number of the *crtS* sequence.

In Summary, using the Ori of Chr2 in synSC1.0 would allow the construction of an actively segregated synthetic chromosome with a tightly regulated low copy number and the potential to carry large exogenous DNA sequences.

4.10. Which tools are still missing to fully establish *V. natriegens* as a next-generation SynBio chassis?

So far, our genome engineering efforts have been focused on defined modifications. For this purpose, NT-CRISPR is a powerful tool, which is however limited to applications where sufficient *a priori* knowledge is available to decide on the necessary modifications.

Other strain engineering approaches are based on the generation of strain libraries with thousands of variants, followed by high throughput screening for candidates with the desired properties. For example, the multiplex automated genome engineering (MAGE) method is based on lambda-red mediated recombineering and can be used to generate a seemingly unlimited number of mutations in *E. coli* (Wang et al., 2009). As a more recent example, a large number of heat-sensitive mutants was extracted from a library of more than 15000 mutants, each with a point mutation leading to a single amino acid substitution (Schramm et al., 2023).

Projects like these are not possible with the methods currently available in *V. natriegens*. NT-CRISPR is not suitable for multiplexed approaches, as the introduced tDNA has to match the gRNA on the NT-CRISPR plasmid in the naturally competent cell (Stukenberg et al., 2022, **Chapter 3.1**). The MuGENT method can in principle be used for multiplexed editing (Dalia et al., 2017). Unfortunately, due to the long size of the tDNA fragments required for efficient editing, the generation of thousands of different tDNA sequences for such an approach is not economically feasible.

Recently, a novel method based on retrons was developed for the highly efficient generation of strain libraries (Schubert et al., 2021). In this approach, the sequence of the retron is first transcribed from a plasmid, and the resulting RNA is reverse-transcribed to generate ssDNA *in vivo*. The resulting ssDNA then introduces changes into the DNA sequence of the host cell with

the help of a single-strand annealing protein, e.g. the beta protein of phage lambda, similar to the steps in the classical lambda-red-based recombineering method (Schubert et al., 2021). Establishing such a tool for *V. natriegens* would allow large screening-based strain engineering projects where the exact mutations leading to the desired phenotype are impossible to predict.

A second methodological gap is the simple integration of large sequences into the chromosome. To the best of my knowledge, the largest integration with NT-CRISPR into the chromosome of *V. natriegens* was approximately 7 kbp (Hoff, 2023). This integration comprised the sequence for the T7 RNA polymerase and its regulatory features (Hoff, 2023). While this could be done successfully, the efficiency was very low, suggesting that this integration approached the upper size limit of NT-CRISPR (Hoff, 2023). To enable larger integrations for future project, we can potentially take inspiration from previously published tools for *E. coli*.

One established method for integration of whole plasmids into *E. coli* relies on site specific recombination with the help of phage-derived integrases into phage attachment sites (Vecchione and Fritz, 2019). In case of *E. coli*, the phage attachment sites naturally present in the chromosome can be used with their cognate integrases (Vecchione and Fritz, 2019). As these phage attachment sites are absent in *V. natriegens*, they could either be chromosomally integrated to allow the use of the integrases derived from *E. coli* (Vecchione and Fritz, 2019), or one could try to identify pairs of cognate phage integrases and attachment sites from the few phages known to infect *V. natriegens* (Harris et al., 2020; Li et al., 2022; Pfeifer et al., 2019).

5. Conclusion

Within the scope of this thesis, a range of new tools and methods were developed to expand the toolbox for *V. natriegens*. With NT-CRISPR, we developed the most efficient genome engineering tool for *V. natriegens* so far, which allows the generation of deletions, integration, and point mutations in a scarless and markerless manner. We demonstrated that up to three deletions can be performed simultaneously (Stukenberg et al., 2022, **Chapter 3.1**). With minor modifications to the workflow, NT-CRISPR could be improved for sequential rounds of editing, which will enable even more ambitious strain engineering projects in the future (**Chapter 4.4**).

We additionally developed a tightly regulated CRISPRi tool, which allowed us to investigate phenotypes resulting from different knockdown strengths when either targeting essential or non-essential genes. Tight regulation was achieved by using two different inducible promoters for the expression of dCas9 and gRNA. Upon induction, we achieved strong repression of the target gene with up to a 40-fold reduction of a reporter protein signal. Graded knockdown was achieved by using gRNAs of different lengths and with mismatches to the target sequence. This leads to weakened binding of the dCas9-gRNA complex to the DNA target sequence (Stukenberg et al., 2024, **Chapter 3.3**).

With NT-CRISPR and graded-CRISPRi, we developed important tools for the establishment of *V. natriegens* as a next-generation SynBio chassis. Furthermore, we applied these tools to investigate potential mechanisms enabling the rapid growth of *V. natriegens*.

Using NT-CRISPR, we succeeded in fusing both chromosomes of *V. natriegens*, resulting in synSC1.0, a strain with a single 5.2 Mbp chromosome. synSC1.0 does not show a major growth defect or phenotypic difference compared to the parental strain. This demonstrates that the bipartite chromosome configuration of *V. natriegens* is not a requirement for its rapid growth (Ramming et al., 2023, **Chapter 3.2**). synSC1.0 is an interesting platform strain for future project, due to the simplified genome configuration and the possibility to use the Ori2 as the basis for synthetic chromosomes.

We used the graded-CRISPRi tool to generate a library of strains with different repression strengths targeting genes essential in minimal medium. By correlating the resulting abundance of the target protein with growth phenotypes, we could show that a strong knockdown is possible without any effect on growth for some genes (*metE*, *argA*), while for other targets

(*metA*, *eno*), growth is severely impaired as soon as protein abundance is reduced significantly (Stukenberg et al., 2024, **Chapter 3.3**).

These results are not sufficient to conclusively explain the rapid growth of *V. natriegens*. However, our results certainly contribute to the growing body of literature in this field. More importantly, our efficient tools will enable others to design and execute ambitious projects focusing either on basic research or on applied science.

Future research to fully establish *V. natriegens* as a SynBio chassis should focus on closing the remaining ability gaps by developing tools for the generation of strain libraries and the integration of large exogenous sequences. Furthermore, the high susceptibility of *V. natriegens* towards metabolic burden will be a major challenge for future ambitious projects and should therefore be addressed with high priority.

6. References

- Adams, B.L., 2016. The Next Generation of Synthetic Biology Chassis: Moving Synthetic Biology from the Laboratory to the Field. *ACS Synth. Biol.* 5, 1328–1330. <https://doi.org/10.1021/acssynbio.6b00256>
- Aguilar Suárez, R., Stülke, J., Van Dijl, J.M., 2019. Less Is More: Toward a Genome-Reduced *Bacillus* Cell Factory for “Difficult Proteins.” *ACS Synth. Biol.* 8, 99–108. <https://doi.org/10.1021/acssynbio.8b00342>
- Aiyar, S.E., Gaal, T., Gourse, R.L., 2002. rRNA promoter activity in the fast-growing bacterium *Vibrio natriegens*. *J. Bacteriol.* 184, 1349–1358. <https://doi.org/10.1128/JB.184.5.1349-1358.2002>
- Anagnostopoulos, C., Spizizen, J., 1961. REQUIREMENTS FOR TRANSFORMATION IN BACILLUS SUBTILIS. *J. Bacteriol.* 81, 741–746. <https://doi.org/10.1128/jb.81.5.741-746.1961>
- Anders, C., Niewoehner, O., Duerst, A., Jinek, M., 2014. Structural basis of PAM-dependent target DNA recognition by the Cas9 endonuclease. *Nature* 513, 569–573. <https://doi.org/10.1038/nature13579>
- Andrianantoandro, E., Basu, S., Karig, D.K., Weiss, R., 2006. Synthetic biology: new engineering rules for an emerging discipline. *Mol. Syst. Biol.* 2, 2006.0028. <https://doi.org/10.1038/msb4100073>
- Aschenbrenner, S., Kallenberger, S.M., Hoffmann, M.D., Huck, A., Eils, R., Niopek, D., 2020. Coupling Cas9 to artificial inhibitory domains enhances CRISPR-Cas9 target specificity. *Sci. Adv.* 6, eaay0187. <https://doi.org/10.1126/sciadv.aay0187>
- Avery, O.T., Macleod, C.M., McCarty, M., 1944. STUDIES ON THE CHEMICAL NATURE OF THE SUBSTANCE INDUCING TRANSFORMATION OF PNEUMOCOCCAL TYPES : INDUCTION OF TRANSFORMATION BY A DESOXYRIBONUCLEIC ACID FRACTION ISOLATED FROM PNEUMOCOCCUS TYPE III. *J. Exp. Med.* 79, 137–158. <https://doi.org/10.1084/jem.79.2.137>
- Baek, J.H., Chattoraj, D.K., 2014. Chromosome I Controls Chromosome II Replication in *Vibrio cholerae*. *PLoS Genet.* 10, e1004184. <https://doi.org/10.1371/journal.pgen.1004184>
- Barrangou, R., Fremaux, C., Deveau, H., Richards, M., Boyaval, P., Moineau, S., Romero, D.A., Horvath, P., 2007. CRISPR Provides Acquired Resistance Against Viruses in Prokaryotes. *Science* 315, 1709–1712. <https://doi.org/10.1126/science.1138140>
- Basan, M., Zhu, M., Dai, X., Warren, M., Sévin, D., Wang, Y., Hwa, T., 2015. Inflating bacterial cells by increased protein synthesis. *Mol. Syst. Biol.* 11, 836. <https://doi.org/10.15252/msb.20156178>
- Benbouzid-Rollet, N.D., Conte, M., Guezennec, J., Prieur, D., 1991. Monitoring of a *Vibrio natriegens* and *Desulfovibrio vulgaris* marine aerobic biofilm on a stainless steel surface in a laboratory tubular flow system. *J. Appl. Bacteriol.* 71, 244–251. <https://doi.org/10.1111/j.1365-2672.1991.tb04455.x>
- Bienick, M.S., Young, K.W., Klesmith, J.R., Detwiler, E.E., Tomek, K.J., Whitehead, T.A., 2014. The Interrelationship between Promoter Strength, Gene Expression, and Growth Rate. *PLoS ONE* 9, e109105. <https://doi.org/10.1371/journal.pone.0109105>
- Bigot, S., Saleh, O.A., Lesterlin, C., Pages, C., El Karoui, M., Dennis, C., Grigoriev, M., Allemand, J.-F., Barre, F.-X., Cornet, F., 2005. KOPS: DNA motifs that control *E. coli* chromosome segregation by orienting the FtsK translocase. *EMBO J.* 24, 3770–3780. <https://doi.org/10.1038/sj.emboj.7600835>
- Blattner, F.R., Plunkett, G., Bloch, C.A., Perna, N.T., Burland, V., Riley, M., Collado-Vides, J., Glasner, J.D., Rode, C.K., Mayhew, G.F., Gregor, J., Davis, N.W., Kirkpatrick, H.A., Goeden, M.A., Rose, D.J., Mau, B., Shao, Y., 1997. The Complete Genome Sequence of *Escherichia coli* K-12. *Science* 277, 1453–1462. <https://doi.org/10.1126/science.277.5331.1453>
- Blokesch, M., Schoolnik, G.K., 2008. The Extracellular Nuclease Dns and Its Role in Natural Transformation of *Vibrio cholerae*. *J. Bacteriol.* 190, 7232 LP – 7240. <https://doi.org/10.1128/JB.00959-08>

6. References

- Bolotin, A., Quinquis, B., Sorokin, A., Ehrlich, S.D., 2005. Clustered regularly interspaced short palindrome repeats (CRISPRs) have spacers of extrachromosomal origin. *Microbiology* 151, 2551–2561. <https://doi.org/10.1099/mic.0.28048-0>
- Bondy-Denomy, J., Pawluk, A., Maxwell, K.L., Davidson, A.R., 2013. Bacteriophage genes that inactivate the CRISPR/Cas bacterial immune system. *Nature* 493, 429–432. <https://doi.org/10.1038/nature11723>
- Borkowski, O., Ceroni, F., Stan, G.-B., Ellis, T., 2016. Overloaded and stressed: whole-cell considerations for bacterial synthetic biology. *Curr. Opin. Microbiol.* 33, 123–130. <https://doi.org/10.1016/j.mib.2016.07.009>
- Bubeck, F., Hoffmann, M.D., Harteveld, Z., Aschenbrenner, S., Bietz, A., Waldhauer, M.C., Börner, K., Fakhiri, J., Schmelas, C., Dietz, L., Grimm, D., Correia, B.E., Eils, R., Niopek, D., 2018. Engineered anti-CRISPR proteins for optogenetic control of CRISPR–Cas9. *Nat. Methods* 15, 924–927. <https://doi.org/10.1038/s41592-018-0178-9>
- Cameron, D.E., Bashor, C.J., Collins, J.J., 2014. A brief history of synthetic biology. *Nat. Rev. Microbiol.* 12, 381–390. <https://doi.org/10.1038/nrmicro3239>
- Ceroni, F., Boo, A., Furini, S., Gorochofski, T.E., Borkowski, O., Ladak, Y.N., Awan, A.R., Gilbert, C., Stan, G.-B., Ellis, T., 2018. Burden-driven feedback control of gene expression. *Nat. Methods* 15, 387–393. <https://doi.org/10.1038/nmeth.4635>
- Cheng, A.A., Lu, T.K., 2012. Synthetic Biology: An Emerging Engineering Discipline. *Annu. Rev. Biomed. Eng.* 14, 155–178. <https://doi.org/10.1146/annurev-bioeng-071811-150118>
- Cho, S., Choe, D., Lee, E., Kim, S.C., Palsson, B., Cho, B.-K., 2018. High-Level dCas9 Expression Induces Abnormal Cell Morphology in *Escherichia coli*. *ACS Synth. Biol.* 7, 1085–1094. <https://doi.org/10.1021/acssynbio.7b00462>
- Cookson, N.A., Mather, W.H., Danino, T., Mondragón-Palomino, O., Williams, R.J., Tsimring, L.S., Hasty, J., 2011. Queueing up for enzymatic processing: correlated signaling through coupled degradation. *Mol. Syst. Biol.* 7, 561. <https://doi.org/10.1038/msb.2011.94>
- Coppens, L., Tschirhart, T., Leary, D.H., Colston, S.M., Compton, J.R., Hervey, W.J., Dana, K.L., Vora, G.J., Bordel, S., Ledesma-Amaro, R., 2023. *Vibrio natriegens* genome-scale modeling reveals insights into halophilic adaptations and resource allocation. *Mol. Syst. Biol.* 19, e10523. <https://doi.org/10.15252/msb.202110523>
- Dai, K., He, L., Chang, Y.-F., Cao, S., Zhao, Q., Huang, X., Wu, R., Huang, Y., Yan, Q., Han, X., Ma, X., Wen, X., Wen, Y., 2018. Basic Characterization of Natural Transformation in a Highly Transformable *Haemophilus parasuis* Strain SC1401. *Front. Cell. Infect. Microbiol.* 8, 32. <https://doi.org/10.3389/fcimb.2018.00032>
- Dalia, A.B., Lazinski, D.W., Camilli, A., 2014. Identification of a Membrane-Bound Transcriptional Regulator That Links Chitin and Natural Competence in *Vibrio cholerae*. *mBio* 5, e01028-13. <https://doi.org/10.1128/mBio.01028-13>
- Dalia, T.N., Hayes, C.A., Stolyar, S., Marx, C.J., McKinlay, J.B., Dalia, A.B., 2017. Multiplex Genome Editing by Natural Transformation (MuGENT) for Synthetic Biology in *Vibrio natriegens*. *ACS Synth. Biol.* 6, 1650–1655. <https://doi.org/10.1021/acssynbio.7b00116>
- David, A., Demarre, G., Muresan, L., Paly, E., Barre, F.-X., Possoz, C., 2014. The Two Cis-Acting Sites, parS1 and oriC1, Contribute to the Longitudinal Organisation of *Vibrio cholerae* Chromosome I. *PLoS Genet.* 10, e1004448. <https://doi.org/10.1371/journal.pgen.1004448>
- De Lorenzo, V., Krasnogor, N., Schmidt, M., 2021. For the sake of the Bioeconomy: define what a Synthetic Biology Chassis is! *New Biotechnol.* 60, 44–51. <https://doi.org/10.1016/j.nbt.2020.08.004>
- de Lemos Martins, F., Fournes, F., Mazzuoli, M.-V., Mazel, D., Val, M.-E., 2018. *Vibrio cholerae* chromosome 2 copy number is controlled by the methylation-independent binding of its monomeric initiator to the chromosome 1 *crtS* site. *Nucleic Acids Res.* <https://doi.org/10.1093/nar/gky790>

6. References

- Deltcheva, E., Chylinski, K., Sharma, C.M., Gonzales, K., Chao, Y., Pirzada, Z.A., Eckert, M.R., Vogel, J., Charpentier, E., 2011. CRISPR RNA maturation by trans-encoded small RNA and host factor RNase III. *Nature* 471, 602–607. <https://doi.org/10.1038/nature09886>
- Doan, A., Chatterjee, S., Kothapalli, R., Khan, Z., Sen, S., Keddi, N., Jha, J.K., Chatteraj, D.K., Ramachandran, R., 2023. The replication enhancer *crtS* depends on transcription factor Lrp for modulating binding of initiator RctB to *ori2* of *Vibrio cholerae*. *Nucleic Acids Res.* gkad1111. <https://doi.org/10.1093/nar/gkad1111>
- Donati, S., Kuntz, M., Pahl, V., Farke, N., Beuter, D., Glatter, T., Gomes-Filho, J.V., Randau, L., Wang, C.-Y., Link, H., 2021. Multi-omics Analysis of CRISPRi-Knockdowns Identifies Mechanisms that Buffer Decreases of Enzymes in *E. coli* Metabolism. *Cell Syst.* 12, 56–67.e6. <https://doi.org/10.1016/j.cels.2020.10.011>
- Eagon, R.G., 1961. Generation Time of Less Than 10 Minutes 1961–1962.
- Ellis, H.M., Yu, D., DiTizio, T., Court, D.L., 2001. High efficiency mutagenesis, repair, and engineering of chromosomal DNA using single-stranded oligonucleotides. *Proc. Natl. Acad. Sci.* 98, 6742–6746. <https://doi.org/10.1073/pnas.121164898>
- Ellison, C.K., Dalia, T.N., Vidal Ceballos, A., Wang, J.C.-Y., Biais, N., Brun, Y.V., Dalia, A.B., 2018. Retraction of DNA-bound type IV competence pili initiates DNA uptake during natural transformation in *Vibrio cholerae*. *Nat. Microbiol.* 3, 773–780. <https://doi.org/10.1038/s41564-018-0174-y>
- Espinosa, E., Barre, F.-X., Galli, E., 2017. Coordination between replication, segregation and cell division in multi-chromosomal bacteria: lessons from *Vibrio cholerae*. *Int. Microbiol. Off. J. Span. Soc. Microbiol.* 121–129. <https://doi.org/10.2436/20.1501.01.293>
- Faber, A., 2020. Entwicklung eines modularen CRISPRi-basierten Systems zur orthogonalen und flexiblen Regulation der Genexpression im schnell-wachsenden Bakterium *Vibrio natriegens*. Philipps-Universität Marburg, Staatsexamensarbeit.
- Farrell, C.M., Grossman, A.D., Sauer, R.T., 2005. Cytoplasmic degradation of *ssrA*-tagged proteins. *Mol. Microbiol.* 57, 1750–1761. <https://doi.org/10.1111/j.1365-2958.2005.04798.x>
- Feng, H., Guo, J., Wang, T., Zhang, C., Xing, X., 2021. Guide-target mismatch effects on dCas9–sgRNA binding activity in living bacterial cells. *Nucleic Acids Res.* 49, 1263–1277. <https://doi.org/10.1093/nar/gkaa1295>
- Fogel, M.A., Waldor, M.K., 2005. Distinct segregation dynamics of the two *Vibrio cholerae* chromosomes. *Mol. Microbiol.* 55, 125–136. <https://doi.org/10.1111/j.1365-2958.2004.04379.x>
- Fontana, J., Dong, C., Ham, J.Y., Zalatan, J.G., Carothers, J.M., 2018. Regulated Expression of sgRNAs Tunes CRISPRi in *E. coli*. *Biotechnol. J.* 13, 1800069. <https://doi.org/10.1002/biot.201800069>
- Fournes, F., Niaux, T., Czarnecki, J., Tissier-Visconti, A., Mazel, D., Val, M.-E., 2021. The coordinated replication of *Vibrio cholerae* 's two chromosomes required the acquisition of a unique domain by the RctB initiator. *Nucleic Acids Res.* 49, 11119–11133. <https://doi.org/10.1093/nar/gkab903>
- Fu, Y., Sander, J.D., Reyon, D., Cascio, V.M., Joung, J.K., 2014. Improving CRISPR-Cas nuclease specificity using truncated guide RNAs. *Nat. Biotechnol.* 32, 279–284. <https://doi.org/10.1038/nbt.2808>
- Garner, K.L., 2021. Principles of synthetic biology. *Essays Biochem.* 65, 791–811. <https://doi.org/10.1042/EBC20200059>
- Gasiunas, G., Barrangou, R., Horvath, P., Siksnys, V., 2012. Cas9–crRNA ribonucleoprotein complex mediates specific DNA cleavage for adaptive immunity in bacteria. *Proc. Natl. Acad. Sci. U. S. A.* 109, E2579–E2586. <https://doi.org/10.1073/pnas.1208507109>
- Griffith, Fred., 1928. The Significance of Pneumococcal Types. *J. Hyg. (Lond.)* 27, 113–159.
- Hamilton, H.L., Dillard, J.P., 2006. Natural transformation of *Neisseria gonorrhoeae*: from DNA donation to homologous recombination. *Mol. Microbiol.* 59, 376–385. <https://doi.org/10.1111/j.1365-2958.2005.04964.x>

- Harris, M.T., Ho, T.C., Fruchtman, H., Garin, M.E., Kubatin, V., Lu, T., Xue, L., Marr, M.T., 2020. Complete Genome Sequences of Two *Vibrio natriegens* Bacteriophages. *Microbiol. Resour. Announc.* 9, e01133-20. <https://doi.org/10.1128/MRA.01133-20>
- Hawkins, J.S., Silvis, M.R., Koo, B.-M., Peters, J.M., Osadnik, H., Jost, M., Hearne, C.C., Weissman, J.S., Todor, H., Gross, C.A., 2020. Mismatch-CRISPRi Reveals the Co-varying Expression-Fitness Relationships of Essential Genes in *Escherichia coli* and *Bacillus subtilis*. *Cell Syst.* 11, 523-535.e9. <https://doi.org/10.1016/j.cels.2020.09.009>
- Hoff, J., 2023. Complexes involved in plastid gene regulation using novel vectors for *E. coli* and *V. natriegens*. Philipps-Universität Marburg, master's thesis.
- Hoff, J., Daniel, B., Stukenberg, D., Thuronyi, B.W., Waldminghaus, T., Fritz, G., 2020. *Vibrio natriegens*: an ultrafast-growing marine bacterium as emerging synthetic biology chassis. *Environ. Microbiol.* 22, 4394-4408. <https://doi.org/10.1111/1462-2920.15128>
- Hoffart, E., Grenz, S., Lange, J., Nitschel, R., Müller, F., Schwentner, A., Feith, A., Lenfers-Lücker, M., Takors, R., Blombach, B., 2017. High substrate uptake rates empower *Vibrio natriegens* as production host for industrial biotechnology. *Appl. Environ. Microbiol.* 83, 1-10. <https://doi.org/10.1128/AEM.01614-17>
- Hoffmann, M.D., Aschenbrenner, S., Grosse, S., Rapti, K., Domenger, C., Fakhiri, J., Mastel, M., Börner, K., Eils, R., Grimm, D., Niopek, D., 2019. Cell-specific CRISPR-Cas9 activation by microRNA-dependent expression of anti-CRISPR proteins. *Nucleic Acids Res.* 47, e75. <https://doi.org/10.1093/nar/gkz271>
- Hui, M.P., Galkin, V.E., Yu, X., Stasiak, A.Z., Stasiak, A., Waldor, M.K., Egelman, E.H., 2010. ParA2, a *Vibrio cholerae* chromosome partitioning protein, forms left-handed helical filaments on DNA. *Proc. Natl. Acad. Sci.* 107, 4590-4595. <https://doi.org/10.1073/pnas.0913060107>
- Huq, A., Small, E.B., West, P.A., Huq, M.I., Rahman, R., Colwell, R.R., 1983. Ecological relationships between *Vibrio cholerae* and planktonic crustacean copepods. *Appl. Environ. Microbiol.* 45, 275-283. <https://doi.org/10.1128/aem.45.1.275-283.1983>
- Ishino, Y., Shinagawa, H., Makino, K., Amemura, M., Nakata, A., 1987. Nucleotide sequence of the iap gene, responsible for alkaline phosphatase isozyme conversion in *Escherichia coli*, and identification of the gene product. *J. Bacteriol.* 169, 5429-5433. <https://doi.org/10.1128/jb.169.12.5429-5433.1987>
- Jakhanwal, S., Cress, B.F., Maguin, P., Lobba, M.J., Marraffini, L.A., Doudna, J.A., 2021. A CRISPR-Cas9-integrase complex generates precise DNA fragments for genome integration. *Nucleic Acids Res.* 49, 3546-3556. <https://doi.org/10.1093/nar/gkab123>
- Jansen, Ruud., Embden, Jan.D.A. van, Gaastra, Wim., Schouls, Leo.M., 2002. Identification of genes that are associated with DNA repeats in prokaryotes. *Mol. Microbiol.* 43, 1565-1575. <https://doi.org/10.1046/j.1365-2958.2002.02839.x>
- Jaskólska, M., Stutzmann, S., Stoudmann, C., Blokesch, M., 2018. QstR-dependent regulation of natural competence and type VI secretion in *Vibrio cholerae*. *Nucleic Acids Res.* <https://doi.org/10.1093/nar/gky717>
- Jiang, Y., Chen, B., Duan, C., Sun, B., Yang, J., Yang, S., Kelly, R.M., 2015. Multigene Editing in the *Escherichia coli* Genome via the CRISPR-Cas9 System. *Appl. Environ. Microbiol.* 81, 2506 LP-2514. <https://doi.org/10.1128/AEM.04023-14>
- Jinek, M., Chylinski, K., Fonfara, I., Hauer, M., Doudna, J.A., Charpentier, E., 2012. A programmable dual-RNA-guided DNA endonuclease in adaptive bacterial immunity. *Science* 337, 816-821. <https://doi.org/10.1126/science.1225829>
- Johnsborg, O., Eldholm, V., Håvarstein, L.S., 2007. Natural genetic transformation: prevalence, mechanisms and function. *Res. Microbiol.* 158, 767-778. <https://doi.org/10.1016/j.resmic.2007.09.004>
- Johnston, C., Martin, B., Fichant, G., Polard, P., Claverys, J.-P., 2014. Bacterial transformation: distribution, shared mechanisms and divergent control. *Nat. Rev. Microbiol.* 12, 181-196. <https://doi.org/10.1038/nrmicro3199>

- Ka, D., Jang, D.M., Han, B.W., Bae, E., 2018. Molecular organization of the type II-A CRISPR adaptation module and its interaction with Cas9 via Csn2. *Nucleic Acids Res.* 46, 9805–9815. <https://doi.org/10.1093/nar/gky702>
- Kemter, F.S., Messerschmidt, S.J., Schallopp, N., Sobetzko, P., Lang, E., Bunk, B., Spröer, C., Teschler, J.K., Yildiz, F.H., Overmann, J., Waldminghaus, T., 2018. Synchronous termination of replication of the two chromosomes is an evolutionary selected feature in *Vibrionaceae*. *PLOS Genet.* 14, e1007251. <https://doi.org/10.1371/journal.pgen.1007251>
- Kim, J., Salvador, M., Saunders, E., González, J., Avignone-Rossa, C., Jiménez, J.I., 2016. Properties of alternative microbial hosts used in synthetic biology: towards the design of a modular chassis. *Essays Biochem.* 60, 303–313. <https://doi.org/10.1042/EBC20160015>
- Kim, S.K., Seong, W., Han, G.H., Lee, D.-H., Lee, S.-G., 2017. CRISPR interference-guided multiplex repression of endogenous competing pathway genes for redirecting metabolic flux in *Escherichia coli*. *Microb. Cell Factories* 16, 188. <https://doi.org/10.1186/s12934-017-0802-x>
- Koch, B., Ma, X., Løbner-Olesen, A., 2010. Replication of *Vibrio cholerae* Chromosome I in *Escherichia coli*: Dependence on Dam Methylation. *J. Bacteriol.* 192, 3903–3914. <https://doi.org/10.1128/JB.00311-10>
- Konieczny, I., Bury, K., Wawrzycka, A., Wegrzyn, K., 2014. Iteron Plasmids. *Microbiol. Spectr.* 2, 10.1128/microbiolspec.plas-0026–2014. <https://doi.org/10.1128/microbiolspec.plas-0026-2014>
- Kunst, F., Ogasawara, N., Moszer, I., Albertini, A.M., Alloni, G., Azevedo, V., Bertero, M.G., Bessières, P., Bolotin, A., Borchert, S., Borriss, R., Boursier, L., Brans, A., Braun, M., Brignell, S.C., Bron, S., Brouillet, S., Bruschi, C.V., Caldwell, B., Capuano, V., Carter, N.M., Choi, S.K., Cordani, J.J., Connerton, I.F., Cummings, N.J., Daniel, R.A., Denziot, F., Devine, K.M., Düsterhöft, A., Ehrlich, S.D., Emmerson, P.T., Entian, K.D., Errington, J., Fabret, C., Ferrari, E., Foulger, D., Fritz, C., Fujita, M., Fujita, Y., Fuma, S., Galizzi, A., Galleron, N., Ghim, S.Y., Glaser, P., Goffeau, A., Golightly, E.J., Grandi, G., Guiseppi, G., Guy, B.J., Haga, K., Haiech, J., Harwood, C.R., Hénaut, A., Hilbert, H., Holsappel, S., Hosono, S., Hullo, M.F., Itaya, M., Jones, L., Joris, B., Karamata, D., Kasahara, Y., Klaerr-Blanchard, M., Klein, C., Kobayashi, Y., Koetter, P., Koningstein, G., Krogh, S., Kumano, M., Kurita, K., Lapidus, A., Lardinois, S., Lauber, J., Lazarevic, V., Lee, S.M., Levine, A., Liu, H., Masuda, S., Mauël, C., Médigue, C., Medina, N., Mellado, R.P., Mizuno, M., Moestl, D., Nakai, S., Noback, M., Noone, D., O'Reilly, M., Ogawa, K., Ogiwara, A., Oudega, B., Park, S.H., Parro, V., Pohl, T.M., Portelle, D., Porwollik, S., Prescott, A.M., Presecan, E., Pujic, P., Purnelle, B., Rapoport, G., Rey, M., Reynolds, S., Rieger, M., Rivolta, C., Rocha, E., Roche, B., Rose, M., Sadaie, Y., Sato, T., Scanlan, E., Schleich, S., Schroeter, R., Scoffone, F., Sekiguchi, J., Sekowska, A., Seror, S.J., Serror, P., Shin, B.S., Soldo, B., Sorokin, A., Tacconi, E., Takagi, T., Takahashi, H., Takemaru, K., Takeuchi, M., Tamakoshi, A., Tanaka, T., Terpstra, P., Togoni, A., Tosato, V., Uchiyama, S., Vandebol, M., Vannier, F., Vassarotti, A., Viari, A., Wambutt, R., Wedler, H., Weitzenegger, T., Winters, P., Wipat, A., Yamamoto, H., Yamane, K., Yasumoto, K., Yata, K., Yoshida, K., Yoshikawa, H.F., Zumstein, E., Yoshikawa, H., Danchin, A., 1997. The complete genome sequence of the gram-positive bacterium *Bacillus subtilis*. *Nature* 390, 249–256. <https://doi.org/10.1038/36786>
- La biologie synthétique, 1912. , Études de biophysique. A. Poinat, Paris.
- Le Rhun, A., Escalera-Maurer, A., Bratovič, M., Charpentier, E., 2019. CRISPR-Cas in *Streptococcus pyogenes*. *RNA Biol.* 16, 380–389. <https://doi.org/10.1080/15476286.2019.1582974>
- Lee, H.H., Ostrov, N., Gold, M.A., Church, G.M., 2017. Recombineering in *Vibrio natriegens*. <https://doi.org/10.1101/130088>
- Lee, H.H., Ostrov, N., Wong, B.G., Gold, M.A., Khalil, A.S., Church, G.M., 2019. Functional genomics of the rapidly replicating bacterium *Vibrio natriegens* by CRISPRi. *Nat. Microbiol.* 4, 1105–1113. <https://doi.org/10.1038/s41564-019-0423-8>
- Lee, H.H., Ostrov, N., Wong, B.G., Gold, M.A., Khalil, A.S., Church, G.M., 2016. *Vibrio natriegens*, a new genomic powerhouse. *bioRxiv* 58487. <https://doi.org/10.1101/058487>

6. References

- Lee, J.H., Sung, B.H., Kim, M.S., Blattner, F.R., Yoon, B.H., Kim, J.H., Kim, S.C., 2009. Metabolic engineering of a reduced-genome strain of *Escherichia coli* for L-threonine production. *Microb. Cell Factories* 8, 2. <https://doi.org/10.1186/1475-2859-8-2>
- Lee, Y.J., Hoynes-O'Connor, A., Leong, M.C., Moon, T.S., 2016. Programmable control of bacterial gene expression with the combined CRISPR and antisense RNA system. *Nucleic Acids Res.* 44, 2462–2473. <https://doi.org/10.1093/nar/gkw056>
- Li, X., Jun, Y., Erickstad, M.J., Brown, S.D., Parks, A., Court, D.L., Jun, S., 2016. tCRISPRi: tunable and reversible, one-step control of gene expression. *Sci. Rep.* 6, 39076. <https://doi.org/10.1038/srep39076>
- Li, X., Liang, Y., Wang, Z., Yao, Y., Chen, X., Shao, A., Lu, L., Dang, H., 2022. Isolation and Characterization of a Novel *Vibrio natriegens*—Infecting Phage and Its Potential Therapeutic Application in Abalone Aquaculture. *Biology* 11, 1670. <https://doi.org/10.3390/biology11111670>
- Libicher, K., Hornberger, R., Heymann, M., Mutschler, H., 2020. In vitro self-replication and multicistronic expression of large synthetic genomes. *Nat. Commun.* 11, 904. <https://doi.org/10.1038/s41467-020-14694-2>
- Lo Scudato, M., Blokesch, M., 2013. A transcriptional regulator linking quorum sensing and chitin induction to render *Vibrio cholerae* naturally transformable. *Nucleic Acids Res.* 41, 3644–3658. <https://doi.org/10.1093/nar/gkt041>
- Long, C.P., Gonzalez, J.E., Cipolla, R.M., Antoniewicz, M.R., 2017. Metabolism of the fast-growing bacterium *Vibrio natriegens* elucidated by (13)C metabolic flux analysis. *Metab. Eng.* 44, 191–197. <https://doi.org/10.1016/j.ymben.2017.10.008>
- Maida, I., Bosi, E., Perrin, E., Papaleo, M.C., Orlandini, V., Fondi, M., Fani, R., Wiegel, J., Bianconi, G., Canganella, F., 2013. Draft Genome Sequence of the Fast-Growing Bacterium *Vibrio natriegens* Strain DSMZ 759. *Genome Announc.* 1. <https://doi.org/10.1128/genomeA.00648-13>
- Makarova, K.S., Wolf, Y.I., Iranzo, J., Shmakov, S.A., Alkhnbashi, O.S., Brouns, S.J.J., Charpentier, E., Cheng, D., Haft, D.H., Horvath, P., Moineau, S., Mojica, F.J.M., Scott, D., Shah, S.A., Siksnys, V., Terns, M.P., Venclovas, Č., White, M.F., Yakunin, A.F., Yan, W., Zhang, F., Garrett, R.A., Backofen, R., Van Der Oost, J., Barrangou, R., Koonin, E.V., 2020. Evolutionary classification of CRISPR–Cas systems: a burst of class 2 and derived variants. *Nat. Rev. Microbiol.* 18, 67–83. <https://doi.org/10.1038/s41579-019-0299-x>
- Mauri, M., Klumpp, S., 2014. A Model for Sigma Factor Competition in Bacterial Cells. *PLoS Comput. Biol.* 10, e1003845. <https://doi.org/10.1371/journal.pcbi.1003845>
- Mehub, M.F., Tanner, J.E., Barnett, S.J., Bekker, J., Franco, C.M.M., Zhang, W., 2018. A controlled aquarium system and approach to study the role of sponge-bacteria interactions using *Aplysilla rosea* and *Vibrio natriegens*. *Sci. Rep.* 8, 11801. <https://doi.org/10.1038/s41598-018-30295-y>
- Meibom, K.L., Blokesch, M., Dolganov, N.A., Wu, C.-Y., Schoolnik, G.K., 2005. Chitin induces natural competence in *Vibrio cholerae*. *Science* 310, 1824–1827. <https://doi.org/10.1126/science.1120096>
- Messerschmidt, S.J., Kemter, F.S., Schindler, D., Waldminghaus, T., 2015. Synthetic secondary chromosomes in *Escherichia coli* based on the replication origin of chromosome II in *Vibrio cholerae*. *Biotechnol. J.* 10, 302–314. <https://doi.org/10.1002/biot.201400031>
- Messerschmidt, S.J., Schindler, D., Zumkeller, C.M., Kemter, F.S., Schallopp, N., Waldminghaus, T., 2016. Optimization and Characterization of the Synthetic Secondary Chromosome synVicII in *Escherichia coli*. *Front. Bioeng. Biotechnol.* 4, 96. <https://doi.org/10.3389/fbioe.2016.00096>
- Meyer, A.J., Segall-Shapiro, T.H., Glassey, E., Zhang, J., Voigt, C.A., 2019. *Escherichia coli* "Marionette" strains with 12 highly optimized small-molecule sensors. *Nat. Chem. Biol.* 15, 196–204. <https://doi.org/10.1038/s41589-018-0168-3>

6. References

- Mojica, F.J.M., Díez-Villaseñor, C., García-Martínez, J., Almendros, C., 2009. Short motif sequences determine the targets of the prokaryotic CRISPR defence system. *Microbiology* 155, 733–740. <https://doi.org/10.1099/mic.0.023960-0>
- Mojica, F.J.M., Díez-Villasenor, C., García-Martínez, J., Soria, E., 2005. Intervening Sequences of Regularly Spaced Prokaryotic Repeats Derive from Foreign Genetic Elements. *J. Mol. Evol.* 60, 174–182. <https://doi.org/10.1007/s00239-004-0046-3>
- Mortier-Barrière, I., Velten, M., Dupaigne, P., Mirouze, N., Piétrement, O., McGovern, S., Fichant, G., Martin, B., Noirot, P., Cam, E.L., Polard, P., Claverys, J.-P., 2007. A Key Presynaptic Role in Transformation for a Widespread Bacterial Protein: DprA Conveys Incoming ssDNA to RecA. *Cell* 130, 824–836. <https://doi.org/10.1016/j.cell.2007.07.038>
- Mosberg, J.A., Lajoie, M.J., Church, G.M., 2010. Lambda Red Recombineering in *Escherichia coli* Occurs Through a Fully Single-Stranded Intermediate. *Genetics* 186, 791–799. <https://doi.org/10.1534/genetics.110.120782>
- Nikolados, E.-M., Weiße, A.Y., Ceroni, F., Oyarzún, D.A., 2019. Growth Defects and Loss-of-Function in Synthetic Gene Circuits. *ACS Synth. Biol.* 8, 1231–1240. <https://doi.org/10.1021/acssynbio.8b00531>
- Okada, K., Iida, T., Kita-Tsukamoto, K., Honda, T., 2005. *Vibrios* Commonly Possess Two Chromosomes. *J. Bacteriol.* 187, 752–757. <https://doi.org/10.1128/JB.187.2.752-757.2005>
- Okano, K., Sato, Y., Hizume, T., Honda, K., 2021. Genome editing by miniature CRISPR/Cas12f1 enzyme in *Escherichia coli*. *J. Biosci. Bioeng.* 132, 120–124. <https://doi.org/10.1016/j.jbiosc.2021.04.009>
- Patange, O., Schwall, C., Jones, M., Villava, C., Griffith, D.A., Phillips, A., Locke, J.C.W., 2018. *Escherichia coli* can survive stress by noisy growth modulation. *Nat. Commun.* 9, 5333. <https://doi.org/10.1038/s41467-018-07702-z>
- Pausch, P., Al-Shayeb, B., Bisom-Rapp, E., Tsuchida, C.A., Li, Z., Cress, B.F., Knott, G.J., Jacobsen, S.E., Banfield, J.F., Doudna, J.A., 2020. CRISPR-CasΦ from huge phages is a hypercompact genome editor. *Science* 369, 333–337. <https://doi.org/10.1126/science.abb1400>
- Pawluk, A., Bondy-Denomy, J., Cheung, V.H.W., Maxwell, K.L., Davidson, A.R., 2014. A new group of phage anti-CRISPR genes inhibits the type I-E CRISPR-Cas system of *Pseudomonas aeruginosa*. *mBio* 5, e00896. <https://doi.org/10.1128/mBio.00896-14>
- Pawluk, A., Davidson, A.R., Maxwell, K.L., 2018. Anti-CRISPR: discovery, mechanism and function. *Nat. Rev. Microbiol.* 16, 12–17. <https://doi.org/10.1038/nrmicro.2017.120>
- Payne, W.J., 1958. Studies on bacterial utilization of uronic acids. III. Induction of oxidative enzymes in a marine isolate. *J. Bacteriol.* 76, 301–307. <https://doi.org/10.1128/JB.76.3.301-307.1958>
- Pfeifer, E., Michniewski, S., Gätgens, C., Münch, E., Müller, F., Polen, T., Millard, A., Blombach, B., Frunzke, J., 2019. Generation of a Prophage-Free Variant of the Fast-Growing Bacterium *Vibrio natriegens*. *Appl. Environ. Microbiol.* 85. <https://doi.org/10.1128/AEM.00853-19>
- Possoz, C., Yamaichi, Y., Galli, E., Ferat, J.-L., Barre, F.-X., 2022. *Vibrio cholerae* Chromosome Partitioning without Polar Anchoring by HubP. *Genes* 13, 877. <https://doi.org/10.3390/genes13050877>
- Pourcel, C., Salvignol, G., Vergnaud, G., 2005. CRISPR elements in *Yersinia pestis* acquire new repeats by preferential uptake of bacteriophage DNA, and provide additional tools for evolutionary studies. *Microbiology* 151, 653–663. <https://doi.org/10.1099/mic.0.27437-0>
- Qi, L.S., Larson, M.H., Gilbert, L.A., Doudna, J.A., Weissman, J.S., Arkin, A.P., Lim, W.A., 2013. Repurposing CRISPR as an RNA-Guided Platform for Sequence-Specific Control of Gene Expression. *Cell* 152, 1173–1183. <https://doi.org/10.1016/j.cell.2013.02.022>
- Ramachandran, R., Ciaccia, P.N., Filsuf, T.A., Jha, J.K., Chatteraj, D.K., 2018. Chromosome 1 licenses chromosome 2 replication in *Vibrio cholerae* by doubling the *crtS* gene dosage. *PLOS Genet.* 14, e1007426. <https://doi.org/10.1371/journal.pgen.1007426>
- Ramachandran, R., Jha, J., Chatteraj, D.K., 2014. Chromosome Segregation in *Vibrio cholerae*. *Microb. Physiol.* 24, 360–370. <https://doi.org/10.1159/000368853>

6. References

- Raman, K., Sinha, H., Vickers, C.E., Nikel, P.I., 2021. Synthetic biology beyond borders. *Microb. Biotechnol.* 14, 2254–2256. <https://doi.org/10.1111/1751-7915.13966>
- Ramming, Daniel Stukenberg, María del Carmen Sánchez Olmos, Anke Becker, Daniel Schindler, 2023. DNA replication is not a limiting factor for rapid growth of *Vibrio natriegens*. *bioRxiv* 2023.05.26.541695. <https://doi.org/10.1101/2023.05.26.541695>
- Rauch, B.J., Silvis, M.R., Hultquist, J.F., Waters, C.S., McGregor, M.J., Krogan, N.J., Bondy-Denomy, J., 2017. Inhibition of CRISPR-Cas9 with Bacteriophage Proteins. *Cell* 168, 150–158.e10. <https://doi.org/10.1016/j.cell.2016.12.009>
- Reisch, C.R., Prather, K.L.J., 2015. The no-SCAR (Scarless Cas9 Assisted Recombineering) system for genome editing in *Escherichia coli*. *Sci. Rep.* 5, 15096. <https://doi.org/10.1038/srep15096>
- Rock, J.M., Hopkins, F.F., Chavez, A., Diallo, M., Chase, M.R., Gerrick, E.R., Pritchard, J.R., Church, G.M., Rubin, E.J., Sasseti, C.M., Schnappinger, D., Fortune, S.M., 2017. Programmable transcriptional repression in mycobacteria using an orthogonal CRISPR interference platform. *Nat. Microbiol.* 2, 16274. <https://doi.org/10.1038/nmicrobiol.2016.274>
- Roncarati, D., Scarlato, V., 2017. Regulation of heat-shock genes in bacteria: from signal sensing to gene expression output. *FEMS Microbiol. Rev.* 41, 549–574. <https://doi.org/10.1093/femsre/fux015>
- Sander, T., Farke, N., Diehl, C., Kuntz, M., Glatter, T., Link, H., 2019. Allosteric Feedback Inhibition Enables Robust Amino Acid Biosynthesis in *E. coli* by Enforcing Enzyme Overabundance. *Cell Syst.* 8, 66–75.e8. <https://doi.org/10.1016/j.cels.2018.12.005>
- Sawabe, Tomoo, Ogura, Y., Matsumura, Y., Feng, G., Amin, A.R., Mino, S., Nakagawa, S., Sawabe, Toko, Kumar, R., Fukui, Y., Satomi, M., Matsushima, R., Thompson, F.L., Gomez-Gil, B., Christen, R., Maruyama, F., Kurokawa, K., Hayashi, T., 2013. Updating the *Vibrio* clades defined by multilocus sequence phylogeny: proposal of eight new clades, and the description of *Vibrio tritonius sp. nov.* *Front. Microbiol.* 4, 414. <https://doi.org/10.3389/fmicb.2013.00414>
- Schellhorn, H.E., 2020. Function, Evolution, and Composition of the RpoS Regulon in *Escherichia coli*. *Front. Microbiol.* 11, 560099. <https://doi.org/10.3389/fmicb.2020.560099>
- Schramm, T., Lubrano, P., Pahl, V., Stadelmann, A., Verhülsdonk, A., Link, H., 2023. Mapping temperature-sensitive mutations at a genome scale to engineer growth switches in *Escherichia coli*. *Mol. Syst. Biol.* n/a, e11596. <https://doi.org/10.15252/msb.202311596>
- Schubert, M.G., Goodman, D.B., Wannier, T.M., Kaur, D., Farzadfard, F., Lu, T.K., Shipman, S.L., Church, G.M., 2021. High-throughput functional variant screens via in vivo production of single-stranded DNA. *Proc. Natl. Acad. Sci.* 118, e2018181118. <https://doi.org/10.1073/pnas.2018181118>
- Schweder, T., Lee, K.-H., Lomovskaya, O., Matin, A., 1996. Regulation of *Escherichia coli* Starvation Sigma Factor (σ) by ClpXP Protease. *J BACTERIOL* 178.
- Schwinn, M.K., Machleidt, T., Zimmerman, K., Eggers, C.T., Dixon, A.S., Hurst, R., Hall, M.P., Encell, L.P., Binkowski, B.F., Wood, K.V., 2018. CRISPR-Mediated Tagging of Endogenous Proteins with a Luminescent Peptide. *ACS Chem. Biol.* 13, 467–474. <https://doi.org/10.1021/acscchembio.7b00549>
- Scott, M., Gunderson, C.W., Mateescu, E.M., Zhang, Z., Hwa, T., 2010. Interdependence of Cell Growth and Gene Expression: Origins and Consequences. *Science* 330, 1099–1102. <https://doi.org/10.1126/science.1192588>
- Seitz, P., Blokesch, M., 2013. Cues and regulatory pathways involved in natural competence and transformation in pathogenic and environmental Gram-negative bacteria. *FEMS Microbiol. Rev.* 37, 336–363. <https://doi.org/10.1111/j.1574-6976.2012.00353.x>
- Seitz, P., Pezeshgi Modarres, H., Borgeaud, S., Bulushev, R.D., Steinbock, L.J., Radenovic, A., Dal Peraro, M., Blokesch, M., 2014. ComEA Is Essential for the Transfer of External DNA into the Periplasm in Naturally Transformable *Vibrio cholerae* Cells. *PLoS Genet.* 10, e1004066. <https://doi.org/10.1371/journal.pgen.1004066>

6. References

- Shachrai, I., Zaslaver, A., Alon, U., Dekel, E., 2010. Cost of Unneeded Proteins in *E. coli* Is Reduced after Several Generations in Exponential Growth. *Mol. Cell* 38, 758–767. <https://doi.org/10.1016/j.molcel.2010.04.015>
- Shin, J., Jiang, F., Liu, J.-J., Bray, N.L., Rauch, B.J., Baik, S.H., Nogales, E., Bondy-Denomy, J., Corn, J.E., Doudna, J.A., 2017. Disabling Cas9 by an anti-CRISPR DNA mimic. *Sci. Adv.* 3, e1701620. <https://doi.org/10.1126/sciadv.1701620>
- Shin, J., Rychel, K., Palsson, B.O., 2023. Systems biology of competency in *Vibrio natriegens* is revealed by applying novel data analytics to the transcriptome. *Cell Rep.* 42, 112619. <https://doi.org/10.1016/j.celrep.2023.112619>
- Silale, A., Lea, S.M., Berks, B.C., 2021. The DNA transporter ComEC has metal-dependent nuclease activity that is important for natural transformation. *Mol. Microbiol.* 116, 416–426. <https://doi.org/10.1111/mmi.14720>
- Sozhamannan, S., Waldminghaus, T., 2020. Exception to the exception rule: synthetic and naturally occurring single chromosome *Vibrio cholerae*. *Environ. Microbiol.* 22, 4123–4132. <https://doi.org/10.1111/1462-2920.15002>
- Specht, D.A., Sheppard, T.J., Kennedy, F., Li, S., Gadikota, G., Barstow, B., 2023. Efficient Natural Plasmid Transformation of *Vibrio natriegens* Enables Zero-capital Molecular Biology (preprint). *Synthetic Biology*. <https://doi.org/10.1101/2023.08.11.553013>
- Srivastava, P., Fekete, R.A., Chatteraj, D.K., 2006. Segregation of the Replication Terminus of the Two *Vibrio cholerae* Chromosomes. *J. Bacteriol.* 188, 1060–1070. <https://doi.org/10.1128/JB.188.3.1060-1070.2006>
- Stouf, M., Meile, J.-C., Cornet, F., 2013. FtsK actively segregates sister chromosomes in *Escherichia coli*. *Proc. Natl. Acad. Sci.* 110, 11157–11162. <https://doi.org/10.1073/pnas.1304080110>
- Stukenberg, D., Faber, A., Becker, A., 2024. graded-CRISPRi, a novel tool for tuning the strengths of CRISPRi-mediated knockdowns in *Vibrio natriegens* using gRNA libraries (preprint). *Synthetic Biology*. <https://doi.org/10.1101/2024.01.29.577714>
- Stukenberg, D., Hensel, T., Hoff, J., Daniel, B., Inckemann, R., Tedeschi, J.N., Nusch, F., Fritz, G., 2021. The Marburg Collection: A Golden Gate DNA Assembly Framework for Synthetic Biology Applications in *Vibrio natriegens*. *ACS Synth. Biol.* 10, 1904–1919. <https://doi.org/10.1021/acssynbio.1c00126>
- Stukenberg, D., Hoff, J., Faber, A., Becker, A., 2022. NT-CRISPR, combining natural transformation and CRISPR-Cas9 counterselection for markerless and scarless genome editing in *Vibrio natriegens*. *Commun. Biol.* 5, 265. <https://doi.org/10.1038/s42003-022-03150-0>
- Suckow, G., Seitz, P., Blokesch, M., 2011. Quorum Sensing Contributes to Natural Transformation of *Vibrio cholerae* in a Species-Specific Manner. *J. Bacteriol.* 193, 4914–4924. <https://doi.org/10.1128/JB.05396-11>
- Thoma, F., Blombach, B., 2021. Metabolic engineering of *Vibrio natriegens*. *Essays Biochem.* 65, 381–392. <https://doi.org/10.1042/EBC20200135>
- Thoma, F., Schulze, C., Gutierrez-Coto, C., Hädrich, M., Huber, J., Gunkel, C., Thoma, R., Blombach, B., 2022. Metabolic engineering of *Vibrio natriegens* for anaerobic succinate production. *Microb. Biotechnol.* 15, 1671–1684. <https://doi.org/10.1111/1751-7915.13983>
- Tietze, L., Mangold, A., Hoff, M.W., Lale, R., 2022. Identification and Cross-Characterisation of Artificial Promoters and 5' Untranslated Regions in *Vibrio natriegens*. *Front. Bioeng. Biotechnol.* 10.
- Tschirhart, T., Shukla, V., Kelly, E.E., Schultzhaus, Z., Newringeisen, E., Erickson, J.S., Wang, Z., Garcia, W., Curl, E., Egbert, R.G., Yeung, E., Vora, G.J., 2019. Synthetic Biology Tools for the Fast-Growing Marine Bacterium *Vibrio natriegens*. *ACS Synth. Biol.* 8, 2069–2079. <https://doi.org/10.1021/acssynbio.9b00176>
- Val, M., Kennedy, S.P., Soler-Bistué, A.J., Barbe, V., Bouchier, C., Ducos-Galand, M., Skovgaard, O., Mazel, D., 2014. Fuse or die: how to survive the loss of DAM in *Vibrio cholerae*. *Mol. Microbiol.* 91, 665–678. <https://doi.org/10.1111/mmi.12483>

6. References

- Val, M.-E., Kennedy, S.P., El Karoui, M., Bonné, L., Chevalier, F., Barre, F.-X., 2008. FtsK-Dependent Dimer Resolution on Multiple Chromosomes in the Pathogen *Vibrio cholerae*. *PLoS Genet.* 4, e1000201. <https://doi.org/10.1371/journal.pgen.1000201>
- Val, M.-E., Marbouty, M., de Lemos Martins, F., Kennedy, S.P., Kemble, H., Bland, M.J., Possoz, C., Koszul, R., Skovgaard, O., Mazel, D., 2016. A checkpoint control orchestrates the replication of the two chromosomes of *Vibrio cholerae*. *Sci. Adv.* 2, e1501914. <https://doi.org/10.1126/sciadv.1501914>
- Val, M.-E., Skovgaard, O., Ducos-Galand, M., Bland, M.J., Mazel, D., 2012. Genome Engineering in *Vibrio cholerae*: A Feasible Approach to Address Biological Issues. *PLoS Genet.* 8, e1002472. <https://doi.org/10.1371/journal.pgen.1002472>
- Vecchione, S., Fritz, G., 2019. CRIMoClo plasmids for modular assembly and orthogonal chromosomal integration of synthetic circuits in *Escherichia coli*. *J. Biol. Eng.* 13, 92. <https://doi.org/10.1186/s13036-019-0218-8>
- Vigouroux, A., Oldewurtel, E., Cui, L., Bikard, D., van Teeffelen, S., 2018. Tuning dCas9's ability to block transcription enables robust, noiseless knockdown of bacterial genes. *Mol. Syst. Biol.* 14, e7899–e7899. <https://doi.org/10.15252/msb.20177899>
- Walton, R.T., Christie, K.A., Whittaker, M.N., Kleinstiver, B.P., 2020. Unconstrained genome targeting with near-PAMless engineered CRISPR-Cas9 variants. *Science* 368, 290 LP – 296. <https://doi.org/10.1126/science.aba8853>
- Wang, H.H., Isaacs, F.J., Carr, P.A., Sun, Z.Z., Xu, G., Forest, C.R., Church, G.M., 2009. Programming cells by multiplex genome engineering and accelerated evolution. *Nature* 460, 894–898. <https://doi.org/10.1038/nature08187>
- Wang, T., Guan, C., Guo, J., Liu, B., Wu, Y., Xie, Z., Zhang, C., Xing, X.-H., 2018. Pooled CRISPR interference screening enables genome-scale functional genomics study in bacteria with superior performance. *Nat. Commun.* 9, 2475. <https://doi.org/10.1038/s41467-018-04899-x>
- Wang, Z., Lin, B., Hervey 4th, W Judson, Vora, G.J., 2013. Draft Genome Sequence of the Fast-Growing Marine Bacterium *Vibrio natriegens* Strain ATCC 14048. *Genome Announc.* 1, e00589-13. <https://doi.org/10.1128/genomeA.00589-13>
- Wang, Z., Tschirhart, T., Schultzhaus, Z., Kelly, E.E., Chen, A., Oh, E., Nag, O., Glaser, E.R., Kim, E., Lloyd, P.F., Charles, P.T., Li, W., Leary, D., Compton, J., Phillips, D.A., Dhinojwala, A., Payne, G.F., Vora, G.J., Johnson, K.N., 2020. Melanin produced by the fast-growing marine bacterium *vibrio natriegens* through heterologous biosynthesis: Characterization and application. *Appl. Environ. Microbiol.* 86, e02749-19. <https://doi.org/10.1128/AEM.02749-19>
- Weaver, S.J., Ortega, D.R., Sazinsky, M.H., Dalia, T.N., Dalia, A.B., Jensen, G.J., 2020. CryoEM structure of the type IVa pilus secretin required for natural competence in *Vibrio cholerae*. *Nat. Commun.* 11, 5080. <https://doi.org/10.1038/s41467-020-18866-y>
- Weinstock, M.T., Heseck, E.D., Wilson, C.M., Gibson, D.G., 2016. *Vibrio natriegens* as a fast-growing host for molecular biology. *Nat. Methods* 13, 849–851. <https://doi.org/10.1038/nmeth.3970>
- Wenning, J., 2023. Modifications of the NT-CRISPR methodology to increase the speed of genetic modifications of the fast growing bacterium *Vibrio natriegens*. Philipps-Universität Marburg, master's thesis.
- Wilkinson, M., Drabavicius, G., Silanskas, A., Gasiunas, G., Siksnys, V., Wigley, D.B., 2019. Structure of the DNA-Bound Spacer Capture Complex of a Type II CRISPR-Cas System. *Mol. Cell* 75, 90-101.e5. <https://doi.org/10.1016/j.molcel.2019.04.020>
- Wu, F., Chen, W., Peng, Y., Tu, R., Lin, Y., Xing, J., Wang, Q., 2020. Design and Reconstruction of Regulatory Parts for Fast-frowning *Vibrio natriegens* Synthetic Biology. *ACS Synth. Biol.* 9, 2399–2409. <https://doi.org/10.1021/acssynbio.0c00158>
- Wu, R., Zhao, M., Li, J., Gao, H., Kan, B., Liang, W., 2015. Direct regulation of the natural competence regulator gene *tfoX* by cyclic AMP (cAMP) and cAMP receptor protein (CRP) in *Vibrios*. *Sci. Rep.* 5, 14921. <https://doi.org/10.1038/srep14921>
- Xie, G., Johnson, S.L., Davenport, K.W., Rajavel, M., Waldminghaus, T., Detter, J.C., Chain, P.S., Sozhamannan, S., 2017. Exception to the Rule: Genomic Characterization of Naturally

6. References

- Occurring Unusual *Vibrio cholerae* Strains with a Single Chromosome. *Int. J. Genomics* 2017, 1–14. <https://doi.org/10.1155/2017/8724304>
- Xin, C., Yin, J., Yuan, S., Ou, L., Liu, M., Zhang, W., Hu, J., 2022. Comprehensive assessment of miniature CRISPR-Cas12f nucleases for gene disruption. *Nat. Commun.* 13, 5623. <https://doi.org/10.1038/s41467-022-33346-1>
- Xu, L., Chen, H., Hu, X., Zhang, R., Zhang, Z., Luo, Z.W., 2006. Average Gene Length Is Highly Conserved in Prokaryotes and Eukaryotes and Diverges Only Between the Two Kingdoms. *Mol. Biol. Evol.* 23, 1107–1108. <https://doi.org/10.1093/molbev/msk019>
- Yamamoto, S., Izumiya, H., Mitobe, J., Morita, M., Arakawa, E., Ohnishi, M., Watanabe, H., 2011. Identification of a Chitin-Induced Small RNA That Regulates Translation of the *tfoX* Gene, Encoding a Positive Regulator of Natural Competence in *Vibrio cholerae*. *J. Bacteriol.* 193, 1953–1965. <https://doi.org/10.1128/JB.01340-10>
- Yang, H., Patel, D.J., 2017. Inhibition Mechanism of an Anti-CRISPR Suppressor AcrIIA4 Targeting SpyCas9. *Mol. Cell* 67, 117-127.e5. <https://doi.org/10.1016/j.molcel.2017.05.024>
- Yura, T., Guisbert, E., Poritz, M., Lu, C.Z., Campbell, E., Gross, C.A., 2007. Analysis of σ^{32} mutants defective in chaperone-mediated feedback control reveals unexpected complexity of the heat shock response. *Proc. Natl. Acad. Sci.* 104, 17638–17643. <https://doi.org/10.1073/pnas.0708819104>
- Zhang, S., Voigt, C.A., 2018. Engineered dCas9 with reduced toxicity in bacteria: implications for genetic circuit design. *Nucleic Acids Res.* 46, 11115–11125. <https://doi.org/10.1093/nar/gky884>
- Zhang, Y., Li, Z., Liu, Y., Cen, X., Liu, D., Chen, Z., 2021. Systems metabolic engineering of *Vibrio natriegens* for the production of 1,3-propanediol. *Metab. Eng.* 65, 52–65. <https://doi.org/10.1016/j.ymben.2021.03.008>
- Zorrilla, S., Monterroso, B., Robles-Ramos, M.-Á., Margolin, W., Rivas, G., 2021. FtsZ Interactions and Biomolecular Condensates as Potential Targets for New Antibiotics. *Antibiotics* 10, 254. <https://doi.org/10.3390/antibiotics10030254>

Erklärung

Ich versichere, dass ich meine Dissertation mit dem Titel

“Establishing the fast-growing bacterium *Vibrio natriegens* as a next-generation chassis for synthetic biology”

selbstständig ohne unerlaubte Hilfe angefertigt und mich dabei keiner anderen als der von mir ausdrücklich bezeichneten Quellen und Hilfsmittel bedient habe.

Diese Dissertation wurde in der jetzigen oder einer ähnlichen Form noch bei keiner anderen Hochschule eingereicht und hat noch keinen sonstigen Prüfungszwecken gedient.

Marburg, den 31.01.2024

Daniel Stukenberg

Danksagung

Die vergangenen vier Jahre waren für mich eine spannende, anstrengende und teilweise auch frustrierende Zeit. Auf dieser Reise hatte ich viel Unterstützung, ohne die ich nie so weit gekommen wäre. Dafür bin ich unendlich dankbar.

Mein größter Dank gilt Anke Becker. Durch Ihre Unterstützung hatte ich die Möglichkeit während meiner Promotion an meinen eigenen Projekten zu arbeiten. Dabei hat sie mich darin ermutigt meine eigenen Ideen, die guten wie auch die schlechten, auszutesten. Ihre Betreuung meiner Promotion hat mich sicherlich als Wissenschaftler nachhaltig geprägt.

Die Arbeit an meinem eigenen Projekt war nur durch die Förderung durch die IMPRS möglich. Ich möchte mich für die Unterstützung und das damit verbundene Vertrauen in mein wissenschaftliches Potential bedanken.

Bedanken möchte ich mich außerdem bei Victor Sourjik, Martin Tanbichler und Lennart Randau für Ihre Bereitschaft Teil meiner Prüfungskommission zu sein.

Außerdem danke ich den aktuellen und ehemaligen Mitgliedern unserer Arbeitsgruppe. Hervorheben möchte ich alle Personen, die das Labor am Laufen halten, egal ob es um defekte Geräte oder das Bestellen von Enzymen geht. Danke dafür an Javier Serrania, Patrick Manz, Andreas Kautz, Bernadette Boomers und Jutta Gade. Darüber hinaus möchte ich mich bei Bettina Happel für Ihre großartige Unterstützung bedanken, egal ob es um ein offenes Ohr für private Probleme oder um den Versand von Paketen rund um die Welt ging.

Bedanken möchte ich mich außerdem bei den Postdocs, Doktoranden und Studenten, mit denen ich in den vergangenen Jahren zusammenarbeiten durfte. Es war für mich immer schön offen über gescheiterte Experimente, aber auch über spannende neue Daten reden zu können. Speziell hervorheben möchte ich unsere „Mensa Gruppe“. Die vielen Gespräche in der Mittagspause werden mir in guter Erinnerung bleiben.

Ich möchte mich bei meinen Kollaborationspartnern bedanken, die wesentlich zum Erfolg meines Promotionsprojektes beigetragen haben. An dieser Stelle möchte ich Daniel Schindler, Lea Ramming, Josef Hoff und Anna Faber besonders hervorheben.

Zuletzt möchte ich mich bei meinem privaten Umfeld bedanken. Bei meinen Eltern Ute und Horst und meiner Schwester Nicole, die mich nicht nur in den letzten vier Jahren, sondern über meinen kompletten bisherigen Lebensweg unterstützt. Außerdem danke ich meiner Partnerin Aline Masson für ihr große Unterstützung und vor allem für ihr Verständnis, wenn sie wegen langer Tage und kurzen Wochenenden auf mich verzichten musste.